Performance and Emission Analysis an RCCI engine fueled with Gasoline-n-Butanol and Biodiesel-Diesel Blends

Negasa Tesfaye Tefera

A Dissertation Submitted to
The Department of Mechanical Engineering
College of Mechanical, Chemical, and Materials Engineering

Presented in Partial Fulfillment of the Requirement for the Degree of Doctor of Philosophy in Automotive Engineering

School of Postgraduate Studies
Adama Science and Technology University

February 2026
Adama, Ethiopia

Performance and Emission Analysis an RCCI engine fueled with Gasoline-n-Butanol and Biodiesel-Diesel Blends

Negasa Tesfaye Tefera

Main Supervisor: Dr. Ramesh Babu Nallamothu (Associate professor)

Co-Supervisor: Dr. Getachew Alemayehu (Assistant professor)

A Dissertation Submitted to

The Department of Mechanical Engineering

College of Mechanical, Chemical, and Material Engineering

Presented in Partial Fulfillment of the Requirement for the Degree of Doctor of Philosophy in Automotive Engineering

School of Postgraduate Studies

Adama Science and Technology University

February 2026

Adama, Ethiopia

DECLARATION

I declare that this dissertation entitled **"Performance and Emission Analysis an RCCI engine fueled with Gasoline-n-Butanol and Biodiesel-Diesel Blends"** is my original work. That is, it has not been submitted for the award of any academic degree, diploma, or certificate in any other university. All sources of materials used for the dissertation have been duly acknowledged through appropriate citations.

_____	_____	_____
Name of student	Signature	Date

RECOMMENDATION

We, the supervisors of this dissertation, hereby certify that we have read and revised the dissertation **"Performance and Emission Analysis an RCCI engine fueled with Gasoline-n-Butanol and Biodiesel-Diesel Blends"** prepared under our guidance by **Negasa Tesfaye** submitted in partial fulfillment of the requirements for the degree of Doctor of Philosophy in Automotive Engineering, Therefore, we recommend the submission of the dissertation to the department for further review and defense.

Dr. Ramesh Babu Nallamothu		
Major Advisor/Supervisor	Signature	Date
Dr. Getachew Alemayehu		
Co-advisor/Co-supervisor	Signature	Date

APPROVAL PAGE FOR DISSERTATION

We hereby certify that the recommendation and suggestion given by the board of examiners are appropriately incorporated into the final dissertation entitled **"Performance and Emission Analysis an RCCI engine fueled with Gasoline-n-Butanol and Biodiesel-Diesel Blends"** by **Negasa Tesfaye.**

Dr. Ramesh Babu Nallamothu	_____	_____
Major Advisor/Supervisor	Signature	Date
Dr. Getachew Alemayehu	_____	_____
Co-advisor/ Co-supervisor	Signature	Date

We, the undersigned, members of the board of examiners of the dissertation open defense by Negasa Tesfaye have read and evaluated the dissertation entitled *"Performance and Emission Analysis an RCCI engine fueled with Gasoline-n-Butanol and Biodiesel-Diesel Blends"* and examined the candidate during open defense. This is, therefore, to certify that the dissertation is accepted for fulfillment of the requirement of the degree of Doctor of Philosophy in Automotive Engineering.

Dr. Deresse Firew	_____	_____
Chairperson	Signature	Date
Dr. Addisu Bekele	_____	_____
Internal Examiner	Signature	Date
Dr. Rajendiran Gopal	_____	_____
External Examiner 1	Signature	Date
Dr. J. Isaac Joshua Ramesh Lalvani	_____	_____
External Examiner 2	Signature	Date

Finally, approval and acceptance of the dissertation is contingent upon submission of its final copy to the School of Postgraduate Studies (SPGS) through the candidate's Department Graduate Council (DGC) and School Graduate Committee (SGC)

_____	_____	_____
Department Head	Signature	Date
_____	_____	_____
College Dean	Signature	Date
_____	_____	_____
School of Postgraduate Studies, Dean	Signature	Date

ACKNOWLEDGEMENTS

First and foremost, I would to express my deepest gratitude to GOD for his countless blessing, guidance, and strength throughout this journey. Without his divine support, this achievement would not have been possible. Next, I extend my heartful appreciation to my supervisor, **Dr. Ramesh Babu**, for his invaluable guidance, continuous support and constructive guidance throughout my research. His mentorship has been pivotal in shaping the direction and quality of this dissertation. My heartfelt gratitude also goes to my co-supervisor, **Dr. Getachew Alemayehu,** for his invaluable supervision, continuous encouragement, and professional guidance throughout the entire research. His expertise, thoughtful insights, and unwavering support have greatly enriched my work.

I would like to sincerely thank to my doctoral committee members, **Dr. Deresse Firew**, **Dr. Zelalem Tumsa**, and **Dr. Amanuel Gabisa**, for their valuable feedback, critical critiques, and insightful suggestions that have greatly enhanced the quality and depth of this dissertation. Additionally, I am profoundly grateful to **Dr. Habtamu Deresso** for his senior guidance, encouragement, and wise counsel, which significantly contribute to my academic growth and development. I am deeply thankful to Adama Science and Technology University for providing financial support and resources for this work with grant research number **ASTU/SP-R/223/23**. I would like to express my gratitude to **Jimma Institute of Technology** for providing the necessary laboratory facilities, which played a crucial role in successful completion of my experiments and analysis. I would like to express my genuine gratitude to my friends **Yohannes Kefale**, **Fitsum Fekedu**, and **Teshome Kumsa** for their valuable encouragement and support throughout this research. Their constructive discussions and constant motivation were truly appreciated. I am thankful for their friendship and collaborative spirit during this journey.

Last but not least, a special note of appreciation goes to my beloved mother **Elsabeth Molla** and dear siblings for their unwavering encouragement, support, and understanding throughout my doctoral studies. Their faith in me has been a constant source of inspiration and motivation.

TABLE OF CONTENTS

Contents **Page**

LIST OF TABLES

LIST OF FIGURES

LIST OF ACRONYMS AND ABBREVIATIONS

AARE	Absolute average relative error
AASTU	Addis Ababa Science and Technology University
ABE	Acetone-butanol-ethanol
Adj-R^2	Adjusted coefficient of determination
A/F	Air fuel ratio
ANOVA	Analysis of variance
ASTM	American Society for testing and materials
B0	Pure diesel
B5	5% of biodiesel and 95 % of diesel
B20	20% of biodiesel and 80 % of diesel
B100	Pure biodiesel
BBD	Box-Behnken design
BMEP	Brake mean effective pressure
BP	Brake power
BSFC	Brake-specific fuel consumption
BT	Brake torque
BTE	Brake thermal efficiency
CCD	Central composite design
CDC	Conventional diesel combustion
CDE	Conventional diesel engine
CI	Compression engine
CN	Cetane number
CNG	Compressed natural gas
CO	Carbon monoxide
CP	Cylinder pressure
CRDI	Common rail direct injection
CSO	Cottonseed oil
CR	Compression ratio
CO_2	Carbon dioxide

CSOME	Cottonseed oil methyl ester
CT	Cylinder temperature
DAS	Data acquisition system
DI	Direct injection
DOE	Design of experiment
EGA	Exhaust gas analyzer
EGR	Exhaust gas recirculation
EGT	Exhaust gas temperature
EN	European norm
EPSE	Ethiopian petroleum supply enterprise
FAAE	Fatty acid alkyl esters
FAME	Fatty acid methyl ester
FFA	Free fatty acids
FFD	Full factorial design
FTIR	Fourier transform infrared spectroscopy
G25n-b75	25% of gasoline and 75 % of n-butanol
G50n-b50	50% of gasoline and 50 % of n-butanol
G75n-b25	75% of gasoline and 25 % of n-butanol
GC-MS	Gas chromatograph-mass spectroscopy
GCI	Gasoline compression ignition
HC	Hydrocarbon
HCI	Hydrochloric acid
HCCI	Homogeneous charge compression ignition
HECC	High-efficiency clean combustion
HRF	High reactivity fuel
HRR	Heat release rate
ICE	Internal combustion engine
IMEP	Indicated mean effective pressure
ITE	Indicated thermal efficiency
JIT	Jimma Institute of Technology
KOH	Potassium hydroxide

LHV	Latent heat of vaporization
LPG	Liquefied petroleum gas
LRF	Low reactivity fuel
LTC	Low-temperature combustion
MAP	Manifold absolute pressure
MPRR	Maximum pressure rise rate
MSE	Mean square error
NaOH	Sodium hydroxide
$Na_2S_2O_3$	Sodium thiosulphate
NOx	Nitrogen oxides
OMEx	Oxymethylene dimethyl ether
PCCI	Premixed charge compression ignition
PI	Port injection
PM	Particulate matter
PODE	Polyoxymethylene dimethyl ether
R^2	Coefficient of determination
RCCI	Reactivity-controlled compression ignition
RMSE	Root mean square error
RON	Research octane number
rpm	Revolution per minute
RSM	Response surface methodology
SD	Standard deviation
SCCI	Stratified charge compression ignition
SI	Spark ignition
SOI	Start of injection
SSE	Sum square of the errors
TDC	Top dead center
UHC	Unburnt hydrocarbons
VCR	Variable compression ratio
VVC	Variable valve control

ABSTRACT

Conventional compression ignition engines are widely used due to their high thermal efficiency and reliability; however, they remain major contributors to nitrogen oxides (NOx), particulate matter, and carbon dioxide (CO_2), which contribute to air pollution and global climate change. Growing concerns over fossil fuel depletion and environmental degradation intensified the search for cleaner, renewable, and more sustainable fuel alternatives. Although reactivity-controlled compression ignition (RCCI) combustion has emerged as a promising strategy for improving engine efficiency and reducing emissions, several research gaps persist. These include challenges in achieving stable combustion at higher loads, limited fuel flexibility, and insufficient exploration of oxygenated biodiesel-alcohol fuel combinations. Moreover, there is a scarcity of optimization-based studies for determining optimal blends and operating conditions in RCCI combustion mode. In response to these issues, the present study integrates Response surface methodology (RSM) and Artificial neural networks (ANN) to optimize biodiesel production and its application in a RCCI engine, using biodiesel-diesel blend as a high reactivity fuel and a gasoline-n-butanol blend as a low reactivity fuel. Biodiesel was produced from cottonseed oil through the transesterification process using methanol and a KOH catalyst, with RSM optimization identifying optimal conditions that yielded of 94.80% biodiesel. The fuel's chemical composition was validated through GC-MS analysis. The RCCI engine experiments were carried out on a modified single-cylinder CI engine at varying engine speeds and of gasoline- n-butanol blend ratios. The results demonstrated that the B20+G50n-b50 blend produced the maximum cylinder pressure of 92.25 bar at 2800 rpm, significantly outperforming the baseline fuel's 57.24 bar. This blend also delivered the maximum brake power of 4.35 kW. In contrast, the lowest NOx (150 ppm) and CO_2 (3.7 vol%) emissions were achieved using the B20+G25n-b75 blend at the same speed, while HC and CO emissions were minimized with the B20+G75n-b25 blend. The RSM and ANOVA analysis confirmed strong predictive capability for performance and emissions, with R^2 values exceeding 97% for all key parameters. The optimal operating condition was identified to be 2523 rpm with a 51.78% n-butanol ratio. Overall, this study demonstrates the effectiveness of RCCI combustion in reducing emissions and enhancing performance, offering a viable pathway toward cleaner and more sustainable engine technologies.

Keywords: n-butanol, biodiesel, ANOVA, emissions, cylinder pressure, RCCI

CHAPTER ONE

INTRODUCTION

1.1. Background of the study

The agricultural, industrial, and transportation sectors, which are rapidly growing, rely heavily on nonrenewable fuel sources. In 2020, the transport of goods and people was accounted for 30% of the global total final energy consumption. Road and rail transport utilized 81% of transport-related energy (Cardama et al., 2023). Fossil fuels supplied 95.9% of the energy consumed in the transport sector, while renewables only 4.1% (Couzin et al., 2023). Due to its almost total reliance on fossil fuels and the increasing demand for transportation, the transport sector was responsible for 20.7% of global carbon dioxide (CO_2) emissions from fossil fuels in 2022 (Cardama et al., 2023). At present, over 98% of the transportation sector is powered by combustion engines. Petroleum diesel is commonly used in engines for vehicles, ships, trains, and various industrial machines due to its higher thermal efficiency and energy density. However, despite its efficiency, diesel combustion still produces significant CO_2 emissions. Additionally, diesel engines are responsible for significant emissions of pollutants including carbon monoxide (CO), particulate matter (PM), unburned hydrocarbons (UHC), and nitrogen oxides (NOx), which are detrimental to both human health and the environment. Despite these drawbacks, diesel engines remain popular due to their affordability and superior fuel efficiency compared to gasoline engine, making them the preferred choice in the transportation industry (Fan et al., 2023; T. Li et al., 2025).

In CDC the auto-ignition and subsequent oxidation reactions are closely influenced by fuel-spray breakup and the effectiveness of fuel-air mixing. The presence of locally fuel-rich zones inside the combustion chamber significantly affects combustion behavior and promotes NO_x and PM formation. Hence, diesel combustion has become a major source of harmful emissions released into the environment (Cao et al., 2024). As a result, several main strategies have been extensively established to address stringent emission regulations and the growing demand for fossil fuels by enhancing the combustion process. These strategies include modifying engine design, utilizing alternative fuels, implementing exhaust after-treatment systems, and presenting Low-Temperature Combustion techniques to resolve the PM and NOx trade-off in CDC while meeting emission standards (Ma et al., 2024; Pachiannan et al., 2019).

In diesel combustion, it is crucial to avoid high temperature stoichiometric and fuel-rich regions at the same time to minimize both NOx and PM emissions. Low-Temperature Combustion (LTC) can be defined as an advanced combustion strategy for cleaner and more efficient operation of the engine, based on early fuel-air mixture preparation and low peak in-cylinder temperatures. LTC suppresses NOx and PM formation through the restriction of high temperature zones (Srivatsa et al., 2024). One effective approach, LTC, enhances mixture preparation, fuel atomization, lowers local equivalence ratios, and reduces combustion temperatures. These enhancements raise the possibility of lowering PM and NOx emissions at the same time while preserving greater thermal efficiency to satisfy emission regulations. However, a common challenge with Low- Temperature Combustion engines is the increased emissions of CO and HC, which can be mitigated by using oxygenated fuels (Ramalingam et al., 2024). Low- Temperature Combustion can be achieved through various methods, including GCI, HCCI, PCCI, and RCCI (Rameez & Ibrahim, 2024).

HCCI has been extensively studied due to its potential to significantly reduce NOx and soot emissions from CDC while maintaining higher thermal efficiency. However, HCCI hasn't been extensively used in manufacturing engines, primarily due to challenges in controlling combustion timing and managing the rate of peak pressure rise, especially at high loads. To address this, several advanced techniques have been developed that use direct fuel injection (DI) to regulate the fuel concentration and reactivity distribution within the cylinder, leading to improved combustion control (Duan et al., 2021).

A PCCI has been developed to offer more precise control over the combustion process. These methods are derivatives of HCCI and aim to broaden the operating range and improve stability by injecting part or all of the fuel directly into the cylinder, creating a stratified fuel charge, and adjusting the equivalence ratio. This stratification results in varying ignition delays across the cylinder, which extends the combustion duration and reduces the overall rate of pressure rise. PCCI, which utilizes split injection, involves premixing a portion of the fuel to form a homogeneous charge, while the remaining fuel is directly injected to optimize combustion by controlling the injection timing. Mostly, high cetane fuels, which ignite easily under compression, are used for PCCI mode. To achieve the premixed fuel-air mixture, either early direct injection or port fuel injection can be employed.

In PCCI mode, similar to HCCI, minimal NOx and soot emissions are produced, with part of the charge being homogeneous. Nevertheless, operating at high torque in PCCI can lead to knocking, limiting its effectiveness to low-torque conditions. This issue arises because high cetane fuels burn more quickly at high torque, causing knocking. Both HCCI and PCCI have limitations, including challenges in operating at higher loads, controlling HC and CO emissions, and managing combustion. To address these issues, a new approach known as RCCI has been developed, which mitigates the weaknesses of both PCCI and HCCI modes (Dwarshala et al., 2023).

Among the advanced combustion technologies, RCCI has drawn a lot of interest because of its potential to achieve higher thermal efficiency and lower PM and NOx emissions. RCCI operates by using two fuels with distinct reactivity levels: a high reactivity fuel (HRF) and a low reactivity fuel (LRF). With more control over the combustion process, this dual-fuel approach increases efficiency and lowers emissions (Agarwal, Singh, et al., 2022). One of the major challenges in RCCI implementation is selecting suitable fuel combinations that optimize performance while minimizing emissions. Traditionally, diesel has been used as the HRF, while gasoline has served as the LRF. However, increasing interest in renewable and oxygenated fuels has prompted the investigation of biodiesel as a substitute HRF and alcohols such as ethanol and n-butanol as a substitute LRF. Biodiesel derived from renewable sources, exhibits oxygen content and high cetane number, which can attribute to complete combustion and lower CO and HC emissions (Cai et al., 2024). Conversely, n-butanol, an oxygenated alcohol, has been considered a promising LRF due to its higher energy density, better miscibility with gasoline, and lower hygroscopicity compared to ethanol (Lapuerta et al., 2017).

Numerous studies have examined the impact of biodiesel-diesel blends as HRF and gasoline-alcohol blends as LRF in RCCI engines. Research indicates that using biodiesel blends as HRF enhances oxidation characteristics and reduces PM emissions due to the higher oxygen content (Fırat et al., 2022). Meanwhile, incorporating n-butanol in gasoline has been reported to enhance combustion stability and lower NOx emissions by altering the reactivity stratification within the cylinder. Despite these advantages, limited investigations have been conducted on the combined effect of gasoline-n-butanol and biodiesel-diesel blends in RCCI engines.

The RCCI engine's performance is typically evaluated based on key parameters such as BP, BTE, and BSFC. The emission characteristics, including CO, CO_2, NOx, HC, and smoke opacity,

provide insights into the environmental impact of the fuel blends. The inclusion of n-butanol in gasoline is expected to influence combustion phasing and efficiency, while the addition of biodiesel to diesel is likely to enhance combustion completeness due to its oxygen content. However, achieving the optimal fuel blend ratio that balances performance and emissions remains an area requiring further investigation (Wang et al., 2021; Zhao et al., 2021). Given the increasing demand for sustainable energy solutions and stringent emission regulations, investing in the impact of n-butanol-gasoline blends as LRF and biodiesel-diesel blends as HRF in RCCI engines holds significant scientific and practical importance. This study aims to analyze the combustion, performance, and emission characteristics of RCCI engines fueled with these blends, contributing to the existing body of knowledge offering the potential to advance RCCI technology and encouraging the use of renewable fuel sources in modern engine applications.

1.2. Statement of the problem

Due to the fast growth of the transportation, industrial, and agricultural sectors, fossil fuels are now essential. However, the increasing demand for these fuels has led to their depletion and reduced availability. Additionally, the combustion of fossil fuels releases harmful emissions including NOx, CO, CO_2, HC, and PM, which contribute to environmental degradation. CI engines are extensively used in transportation due to their higher fuel efficiency and power output, but they are also major contributors to NOx and PM emissions. These challenges have driven the development of alternative strategies to meet stringent emission standards for exhaust gas emissions. Among these LTC has emerged as one of the most advanced combustion techniques, offering significant potential for reducing emissions while also improving fuel efficiency. RCCI is one of the most promising LTC strategies, offering higher thermal efficiency and lower PM and NOx emissions. However, RCCI combustion is often associated with high CO and HC emissions, which can negatively impact engine performance and durability. To address these challenges, the use of alternative fuels with different physicochemical properties has been proposed as an effective solution to optimize RCCI combustion.

In this study, the combination of gasoline and n-butanol as LRF and a diesel–biodiesel blend as HRF presents a promising solution. n-butanol offers improved reactivity control and oxygen content compared to pure gasoline, while biodiesel contributes a higher cetane number and additional oxygen for more complete combustion. However, the combined effects of these fuel

blends on RCCI combustion characteristics, engine performance, and emission behavior remain insufficiently understood and require further investigation. Therefore, this study investigates the impact of using a gasoline-n-butanol blend as LRF and a diesel-biodiesel blend as HRF on the combustion behavior, performance, and emissions of an RCCI engine, aiming to address the key operational challenges associated with this advanced combustion mode.

1.3. Objectives

1.3.1. General Objective

The general objective of this study is to examine the impacts of using an n-butanol-gasoline blend as a low reactivity fuel and a biodiesel-diesel blend as a high reactivity fuel on the performance, combustion, and emission characteristics of reactivity-controlled combustion ignition engine.

1.3.2. Specific Objectives

The specific objectives of this study are:

- To develop an optimized biodiesel production framework-using cottonseed oil as a renewable feedstock.
- To evaluate the fuel quality characteristics and compositional profile of the produced biodiesel in order to assess its suitability for compression ignition engines.
- To assess the impact of biodiesel-diesel blends and n-butanol-gasoline blends on the performance, combustion behavior, and emission characteristics of an RCCI engine.
- To identify the optimal LRF blend ratio that enhances engine efficiency while minimizing exhaust emissions under RCCI operation.

1.4. Significance of the study

This study investigates the impacts of an n-butanol-gasoline blend as an LRF and a biodiesel-diesel blend as an HRF on the performance, combustion and emission characteristics of RCCI engine. The incorporation of n-butanol in gasoline improves oxygenation and volatility, potentially enhancing combustion efficiency, while diesel-biodiesel blend as HRF offers improved ignition characteristics and reduced emissions. By optimizing these fuel blends, this study addressed the key limitations of RCCI combustion and contributed to its practical implementation in ICEs. The results of this study provided valuable insights into alternative fuel applications in RCCI engines, facilitating the development of more sustainable and environmentally friendly ICE technologies.

Additionally, the study supported reducing dependence on fossil fuels, complying with stringent emission regulations, and advancing the transition toward cleaner energy solutions in the transport sector.

1.5. Scope of the study

The scope of this study focuses on the impact of an n-butanol-gasoline blend as an LRF and a biodiesel-diesel blend as an HRF on the performance, combustion, and emission characteristics of an RCCI engine. In this work, the HRF is fixed at B20 based on established recommendations, while only the LRF blend ratio is varied to assess its influence on RCCI engine behavior. It examines key performance parameters, including BT, BP, and BSFC under different engine speeds and constant load. The combustion analysis focuses on key factors such as CP and HRR. Additionally, the emissions of NO_X, CO_2, CO, and HC are evaluated to determine the environmental impacts of the blends. The experimental work is conducted using a single-cylinder CI engine test setup, with accurate diagnostics for exhaust gas analysis and performance measurements. The study did not consider various factors associated with combustion, performance, and emissions, including the ignition delay, mechanical efficiency, start of combustion, friction power, and the emissions of smoke and particulate matter, due to specific constraints. This investigation focuses exclusively on the alteration of the engine's intake manifold, excluding any changes to other engine components. The main goal of this investigation is to enhance fuel blend optimization for RCCI engines, thereby promoting the development of cleaner combustion technologies within the automotive sector.

1.6. Limitations of the study

The current study faced some limitations that affected the scope and accuracy of the research output. One of the major limitations was not being able to measure and analyze the PM emissions, which was because the requisite PM measurement device was not available. Also, the in-cylinder temperature measurement was not possible since the engine cylinder did not have an inbuilt temperature sensor, which further restricted the accuracy of thermal analysis. In spite of these challenges, the research methodology was adapted to be optimal for the equipment and resources available; all measures feasible under the circumstances were taken to ensure the reliability, consistency, and validity of the experimental results presented here.

1.7. Organization of the Dissertation

This dissertation is divided into five chapters that contain the major components.

Chapter One: This chapter presents the background of the study, problem statement, objective, significance, scope, and limitations of the study. The background of the study provides an overview of issues with CI engines, fossil fuels, and low temperature combustion, along with, the advantage of LTC. The problem statement establishes the study's content and outlines the general analytic approach. The research explores the blending of diesel with biodiesel and gasoline with n-butanol as a strategy to enhance performance and minimize emissions of RCCI engine. Furthermore, it highlights the primary goal of the study, which is to examine the impact of using n-butanol-gasoline LRF and biodiesel-diesel blend on the performance, combustion, and emission characteristics of RCCI engine.

Chapter Two: This chapter presents the findings, key considerations, and discussions of previous studies on the RCCI engine, along with identified research gaps. It also highlights the gaps observed by the researcher, providing insights into areas that require further investigation. Low temperature combustion methods, biodiesel production, factors affecting biodiesel production, n-butanol as an alternative fuel and optimization techniques are included in this section.

Chapter Three: This chapter outlines the various materials, equipment, and fuels utilized in the experimental process. It also provides a concise overview of the methodological approaches employed to conduct the research effectively.

Chapter Four: This chapter explains the experimental results along with a scientific analysis and interpretation of the findings.

Chapter Five: Finally, this chapter includes the conclusions derived from the experimental results and provides recommendations for potential extensions of the study. It also outlines future research directions in the field.

CHAPTER TWO

LITERATURE REVIEW

2.1. Introduction

CI engines are recognized as the most fuel-efficient machines ever developed in the history of engine technology and have gained widespread adoption in the market. Due to their durability and superior fuel efficiency, CI engines are extensively used in trucks, heavy-duty vehicles (HDV), small to medium-sized transport vehicles, and electric generators (Dahham et al., 2022). Conventional diesel combustion engines operate in the principle of compression ignition, which burns high reactivity fuel such as diesel at elevated temperatures, regulated by the mixing process. This method often results in significant emissions of NOx and PM. Meanwhile, petroleum diesel becoming increasingly insufficient and scarce due to the rise in global fuel consumption. Furthermore, the high levels of harmful gases emitted from burning fuel contribute to a range of environmental concerns.

The primary focus in CI engine development today is on minimizing fuel consumption and reducing NOx and PM emissions (Riyadi et al., 2023). For over two decades, research has been dedicated to exploring more efficient, cleaner, and alternative combustion techniques. CDC engines have evolved significantly, incorporating advancements such as pre-main and post-main injection strategies, high-pressure common rail DI, enhanced EGR with improved cooling, and turbocharging technologies. Furthermore, CI engines are enabling some degree of downsizing by increasing specific output. Significant attention is given to exhaust treatment systems, which utilize oxidation catalytic converters and particulate filters to reduce emissions of PM, NOx, CO, and HC. For HDVs, selective catalytic reduction with urea injection presents an effective solution for emission control.

The are multiple development pathways for both gasoline and diesel engines aimed at enhancing performance while reducing emissions, fuel consumption, and noise. Current advancement is focused on lowering fuel consumption, decreasing emissions (CO, CO_2, HC, NOx, and PM), improving driving dynamics, reducing friction, increasing specific power, dampening oscillations, and minimizing energy consumption. Modern engines are equipped with mechatronic components to support greater variability and advanced control functions (Dahham et al., 2022). Low-

temperature combustion (LTC) represents a sophisticated approach that significantly diminishes both soot and NOx emissions when compared to traditional combustion techniques. This method improves the fuel atomization and the preparation of the fuel-air mixture, while also maintaining lower local equivalence ratios and reducing combustion temperatures. These enhancements lead to a decrease in PM and NOx emissions, all while ensuring higher thermal efficiency to comply with rigorous emission standards. Nonetheless, a notable challenge associated with LTC engines is the elevated emissions of CO and HC, which can be addressed through the implementation of oxygenated fuels and advanced after-treatment technologies (Gupta & Anand, 2018). Various techniques can facilitate LTC, including gasoline compression ignition, HCCI, PCCI, and RCCI (Pachiannan et al., 2019).

2.2. Limitations of conventional CI engine

The CI engine utilizes a fuel utilization system that adjusts the engine's fuel supply based on mass regulation to accommodate changes in operating conditions. In this system, the fuel-air mixture is formed in the cylinder. Specifically, as the piston approaches TDC, the fuel injection system delivers fuel at high pressure within a narrow crank angle, enabling the mixture of fuel with air. However, due to the brief mixing period, the mixture in the CI engine tends to be non-uniform. The combustion process in such engines is governed by the mixing and diffusion of fuel and air. Since a chemical reaction rate during combustion is significantly faster than the rate of mixing and diffusion, the overall combustion speed is determined by the rate of mixing and diffusion. As a result, although multiple ignition points occur simultaneously during compression, the uneven distribution of mixture concentration and temperature within the cylinder leads to the formation of NOx in localized high-temperature zones and carbon particles in high-temperature, oxygen-deficient areas. In essence, traditional combustion methods in CI engines are characterized by non-uniform temperature distribution and an uneven combustion process, making it challenging to achieve both high efficiency and low emissions simultaneously. Consequently, there is a need to develop new combustion strategies that build upon traditional methods to enhance efficiency and decrease the emissions of ICEs (Hao, 2023).

2.3. Low temperature combustion methods

High-temperature conditions with excess oxygen promote the formation of NOx and lowering the combustion temperature (CT) can efficiently reduce NOx levels. Nevertheless, lowering the CT

also hinders the oxidation of soot, leading to increased soot emissions. This means that simply lowering the combustion temperature is not a viable solution. Nevertheless, if the temperature is maintained below a certain threshold, combustion can avoid the primary zones where NOx and soot are generated. LTC is a method that avoids high CT in the cylinder while also altering the fuel-air mixture before combustion. By improving the uniformity of the mixture, LTC efficiently reduces emissions of both NOx and PM, while also providing higher thermal efficiency. This approach addresses the limitations of traditional combustion methods. LTC is primarily achieved through a high EGR ratio reduction (Rahman et al., 2021).

A higher EGR rate increases the specific heat capacity of the in-cylinder mixture, which lowers the CT and avoids the temperature range where significant NOx is produced. Additionally, EGR alters the fuel-air mixture before combustion, improving its uniformity and reducing localized areas of high fuel concentration, thereby minimizing soot formation. However, if the CT is too low, it can reduce combustion efficiency and negatively impact fuel economy. Therefore, the key to successfully implementing LTC technology lies in achieving an optimum balance between combustion efficiency, fuel economy, and emission reduction (Rajendran et al., 2023). Achieving low CT involves the application of specific techniques that regulate fuel consumption mechanisms. This can be accomplished through various processes, including SCCI, HCCI, HECC, charge PCCI, and RCCI (Singh et al., 2020). Fig.2.1 demonstrates how various LTC methods have developed.

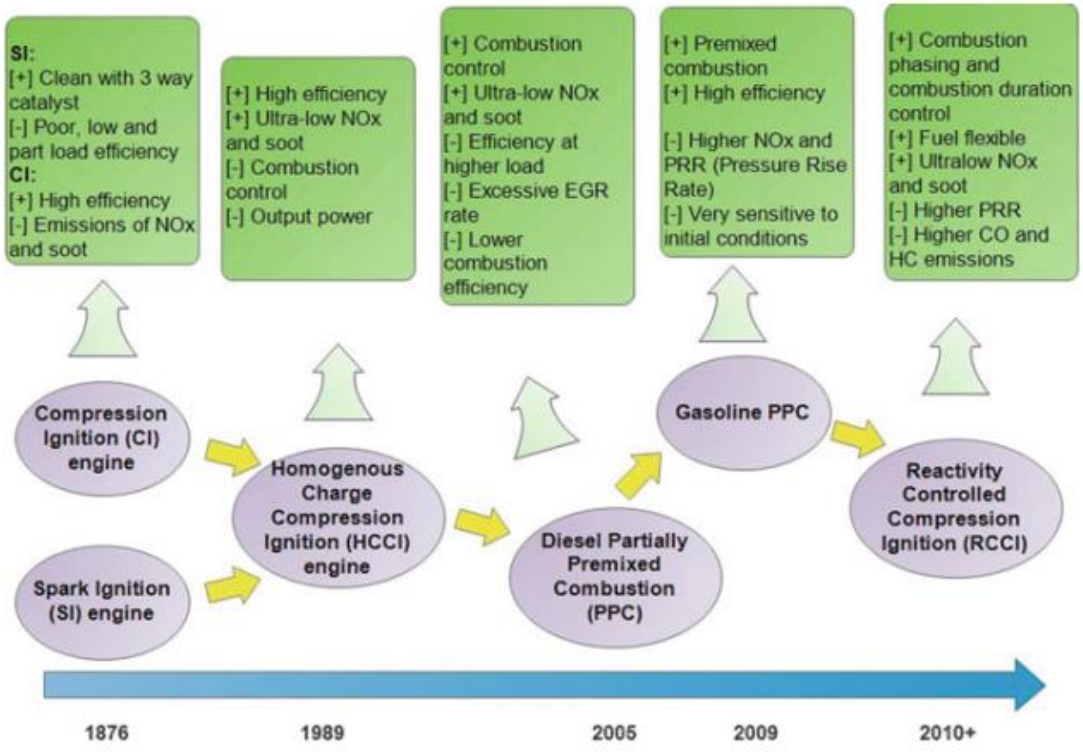

Figure 2.1 LTC method Evolution and their Pros [+] and Cons [-] (Agarwal, et al., 2022)

2.3.1. HCCI combustion method and its characteristics

HCCI mode was first introduced by Noguchi, Najt, and Onishi in the late 1970s and early 1980s. This concept is characterized by two fundamental features: a homogeneous mixture and compression ignition, effectively combining the strengths of both SI and CI engines. Nevertheless, due to technical challenges at the time, HCCI did not gain significant attention until recent years. After decades of study by scholars worldwide, HCCI has emerged as a novel combustion method for ICEs. HCCI combustion builds on the principles of homogeneous charge (gasoline engines) and stratified charge (diesel engines), integrating their advantages into an innovative design. While HCCI appears to blend the homogeneous premixed SI engines with the CI of diesel engines, its combustion mechanism is fundamentally distinct from traditional SI and CI methods (Maurya & Akhil, 2017).

In an SI engine, fuel is injected during the intake stroke to form a homogeneous fuel-air mixture, and combustion is initiated by a spark, propagating through flame spread. In a diesel engine, fuel is injected through mass regulation, and combustion occurs through compression ignition, relying

on flame propagation during the expansion phase and diffusion of the combustible mixture during the slower combustion period. HCCI, however, is not merely a combination of these two traditional methods. It does not rely on flame propagation or diffusion combustion. Instead, similar to an SI engine, the combustion chamber in an HCCI engine is filled with a uniformly mixed, critical combustible gas before combustion begins. Like a diesel engine, the mixture is further compressed during the piston's compression stroke, raising the pressure and temperature in the cylinder until multiple ignition points simultaneously ignite the mixture.

The HCCI combustion process is governed by chemical kinetics and occurs in two stages: the initial stage involves low-temperature oxidation (LTO), followed by the second stage of high-temperature oxidation (HTO). This unique approach distinguishes HCCI from conventional combustion methods and offers a promising pathway for enhancing engine efficiency and lowering emissions (Mohammed Elbanna et al., 2022). Various methods are employed to regulate the combustion process in HCCI engines (see Fig 2.2).

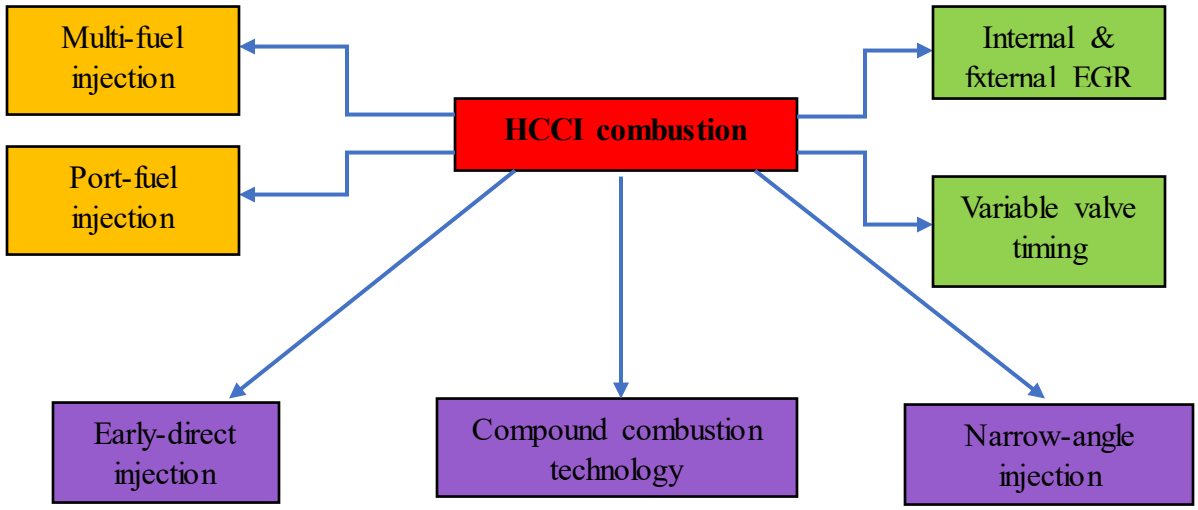

Figure 2.2 Control methods the combustion in HCCI (Agarwal, Martínez, et al., 2022)

2.3.1.1. Advantage of HCCI combustion mode

High thermal efficiency

HCCI modes are typically achieved using EGR. By incorporating a high proportion of EGR, the combustible mixture in each cycle includes not only fuel and fresh air but also exhaust gases from the previous cycle. This alters the mixture's concentration and increases its total specific heat

capacity, significantly lowering the CT within the cylinder. Hence, heat transfer losses to the cylinder walls are effectively reduced. Additionally, HCCI engines employ a quality regulation method similar to CI engines, eliminating throttling losses. During combustion, multiple ignition points occur simultaneously without noticeable flame propagation, further minimizing heat losses. HCCI engines operate at a higher CR, and the compression ignition process is characterized by a short, continuous combustion duration, which enhances thermal efficiency. Moreover, HCCI engines can utilize a lean fuel-air mixture while still delivering relatively high-power output. This combination of features makes HCCI a promising approach for improving engine efficiency and performance (Sakthivel et al., 2019).

Low NOx and carbon soot particle emissions

In an HCCI mode, the combustible mixture is uniformly mixed before undergoing compression and ignition. The use of EGR further dilutes the fuel-air mixture, reducing its concentration. Because the mixture is both homogeneous and lean, soot emissions from HCCI engines are exceptionally low. Additionally, HCCI engines employ a quality regulation control method similar to CI engines to inject fuel, which is then compressed and ignited simultaneously at multiple points. The uniform mixture burns rapidly, enhancing fuel utilization efficiency. The lean fuel-air mixture also lowers the peak temperature within the cylinder. As a result, while the average temperature in the cylinder increases, the maximum temperature is reduced, leading to a substantial reduction in NOx emissions. This combination of features allows HCCI to achieve low emissions and high efficiency simultaneously (Hao, 2023).

Fuel flexibility

The HCCI engine exhibits fuel flexibility, distinguishing it from SI and CI engines that require specific fuel types for optimal performance. This innovative engine design is capable of utilizing a diverse range of fuels, including high-octane fuels and propane, thereby enhancing its adaptability and efficiency in various operational contexts (Charitha et al., 2019).

2.3.1.2. Drawbacks of HCCI combustion mode

Emissions of carbon monoxide and hydrocarbons

The HCCI method effectively addresses the emission issues of NOx and soot, however, it results in higher emissions of CO and HC compared to conventional combustion methods. This is mostly

due to the high ratio of EGR, which lowers the peak in-cylinder CT. Therefore, some fuel remains incompletely burned during the combustion process, and hydrocarbons are not fully oxidized, ultimately being expelled with the exhaust gases. Additionally, the LTC characteristic of HCCI increases the concentration of the cylinder wall quenching effect, where the flame is extinguished near the cooler cylinder walls. This further contributes to the rise in HC emissions. While HCCI offers significant advantages in reducing NOx and soot, managing CO and UHC emissions remains a challenge (Hao, 2023).

Difficulty in cold starting

Due to the low-temperature, lean combustion nature of HCCI engines, the cylinder wall and mixture temperatures are often too low under cold start conditions. This can prevent the engine from achieving normal compression and ignition, negatively impacting startup and combustion performance. To address this issue, researchers have explored several solutions. One approach is to initiate the engine using a conventional combustion mode and then transition to HCCI combustion once operating conditions are stable. Another method involves adjusting the intake air temperature by heating the incoming air to facilitate startup. A third solution is to employ VCR or VVC technology, which increases the compression ratio. This not only enhances the cold start performance of HCCI engines but also expands their load range, improving overall flexibility and efficiency (Vallinayagam et al., 2018) .

Combustion phase control

Two critical parameters in the combustion of an engine are fuel ignition and injection timing. Unlike SI engines, which use spark plugs to directly control ignition timing, HCCI engines rely on compression to ignite the fuel-air mixture. This means that the ignition timing in HCCI engines is entirely dependent on the pressure and temperature inside the combustion chamber, as well as the chemical and physical properties of the fuel. Since there is no physical mechanism to exactly control the moment of spontaneous combustion, managing the combustion phase in HCCI engines becomes challenging, directly impacting their combustion performance. As a result, controlling the combustion phase in HCCI mode has emerged as one of the most significant and challenging aspects of current HCCI combustion research. Achieving precise control over this process is essential for optimizing engine performance and efficiency (Khandal et al., 2019).

Small operating range

Since HCCI operates as a low-temperature, lean-burn system, it can function efficiently only within a low-load range. At low loads, there is a risk of misfire, while at high loads, the fuel-air mixture is prone to premature auto-ignition due to cylinder compression, potentially leading to engine knocking. As a result, HCCI engines struggle to perform reliably under a broad range of operating conditions, unlike traditional CI and SI engines, which limits the broader adoption of HCCI mode technology (Vallinayagam et al., 2018).

2.3.2. PCCI combustion method and its characteristics

The development of PCCI combustion stems from the limitations of HCCI, which is primarily governed by chemical reaction kinetics, making it challenging to control combustion timing and rate across a wide operating condition range. PCCI engines offer a broader range of mixture concentrations and have the potential to expand operating conditions more easily than HCCI (Elbanna et al., 2023). PCCI typically employs multi-stage fuel injection strategies, where a portion of the fuel (ranging from 10% to 70% of the total fuel volume) is injected into the intake manifold or cylinder during the early intake or compression stages. Additionally, fuel is directly injected into the cylinder near TDC during the compression stroke (Mei et al., 2021).

The initial premixed charge is relatively lean and not easily ignitable. However, after the main injection, the mixture's concentration increases, and once it reaches the auto-ignition temperature, combustion occurs. The two critical factors influencing PCCI performance are the volume of premixed fuel and the timing of the main injection. Compared to HCCI, PCCI offers a more practical and cost-effective method for optimizing in-cylinder combustion parameters. The PCCI combustion process relies on multi-stage injection techniques such as advanced or delayed injection and EGR to regulate the combustion phase. Based on injection timing, PCCI can be categorized into two types: one involves early fuel injection (90° to 120° crank angle before TDC) to allow sufficient time for thorough mixing, resulting in a lean, homogeneous mixture; the other involves late fuel injection, where fuel is introduced closer to TDC (Singh et al., 2020).

2.3.2.1. Advantage of PCCI combustion mode

Combustion control

Compared to conventional CI engines, PCCI combustion emphasizes enhanced fuel-air premixing prior to ignition, significantly reducing the dominance of diffusion combustion. By enabling simultaneous multi-point ignition, this approach ensures that most fuel is fully burned during the premixed combustion phase, effectively minimizing or even eliminating the diffusion combustion stage. This strategy not only improves combustion efficiency but also offers greater control over the process of combustion compared to HCCI, overcoming HCCI's challenges in managing ignition timing and combustion stability. The result is a more optimized combustion process with reduced emissions and better performance predictability (Hao, 2023).

Operating conditions

Unlike HCCI mode, PCCI mode utilizes a mixture that is not fully homogeneous. Instead, it creates a charge gradient in both temperature and concentration, allowing regions with varying concentration levels to ignite at different times within the cylinder. This staggered combustion helps regulate the combustion speed and lowers the HRR. As a result, the PCCI mode is suitable for medium to high load conditions (Park et al., 2019).

Emission performance

PCCI combustion operates under a low-temperature regime, though its overall combustion temperature is higher than HCCI yet remains lower than traditional combustion modes. This intermediate thermal profile results in PM and NOx emissions that are higher than HCCI but still notably lower than conventional engines. Emissions in PCCI are closely tied to the timing of the main fuel injection. When fuel is injected early (under low in-cylinder temperature and density), incomplete fuel vaporization can increase UHC emissions and reduce combustion efficiency. Conversely, late injection near TDC, combined with high EGR rates, allows precise control over ignition timing and mixture preparation. This approach optimizes air-fuel mixing duration, limits localized rich zones, and reduces soot formation by operating under low oxygen concentration conditions. Thus, PCCI strategically balances temperature, mixing, and emissions to enhance combustion quality while mitigating environmental trade-offs (Elkelawy et al., 2022).

2.3.2.2. Drawbacks of PCCI combustion mode

Carbon monoxide (CO) and hydrocarbons (HC) emissions

(Shim et al., 2020) A comparison of engine emission and performance characteristics among HCCI and PCCI combustion modes in heavy-duty CI engines revealed that, at an average indicated pressure of 0.45 MPa, HC and CO emissions are higher in HCCI and PCCI modes compared to conventional combustion. Additionally, the PCCI mode produces more HC and CO emissions than HCCI. This elevated emission level is one of the key factors limiting the practicality of these advanced combustion technologies.

Reduced thermal efficiency

PCCI mode typically employs two-stage or multi-stage fuel injection. In the case of a two-stage high-pressure injection, the fuel injected during the initial stage can ignite during the compression process. This approach helps control the rate of pressure rise and the peak CT. However, it also increases the negative work during compression and causes an earlier onset of cyclic combustion due to incomplete oxidation. As a result, heat transfer losses rise, leading to a reduction in thermal efficiency (Pan et al., 2020).

2.3.3. RCCI mode and its characteristics

RCCI is a type of LTC that controls the combustion process by utilizing the ignition properties of different fuels. Unlike HCCI and PCCI, the key distinction of RCCI mode is the use of two fuels with significantly different reactivity and physical and chemical characteristics. A low-reactivity fuel, such as alcohol or gasoline, is injected through the intake, while a high-reactivity fuel is directly injected into the cylinder near the end of the compression stroke. By creating reactivity stratification and varying the concentration of the fuel mixture within the cylinder, RCCI effectively manages the combustion phase, heat release rate, and premixing ratio. This approach helps optimize combustion, enhance thermal efficiency, and lower emissions (Wang et al., 2019). The RCCI mode diagram is illustrated in Fig. 2.3.

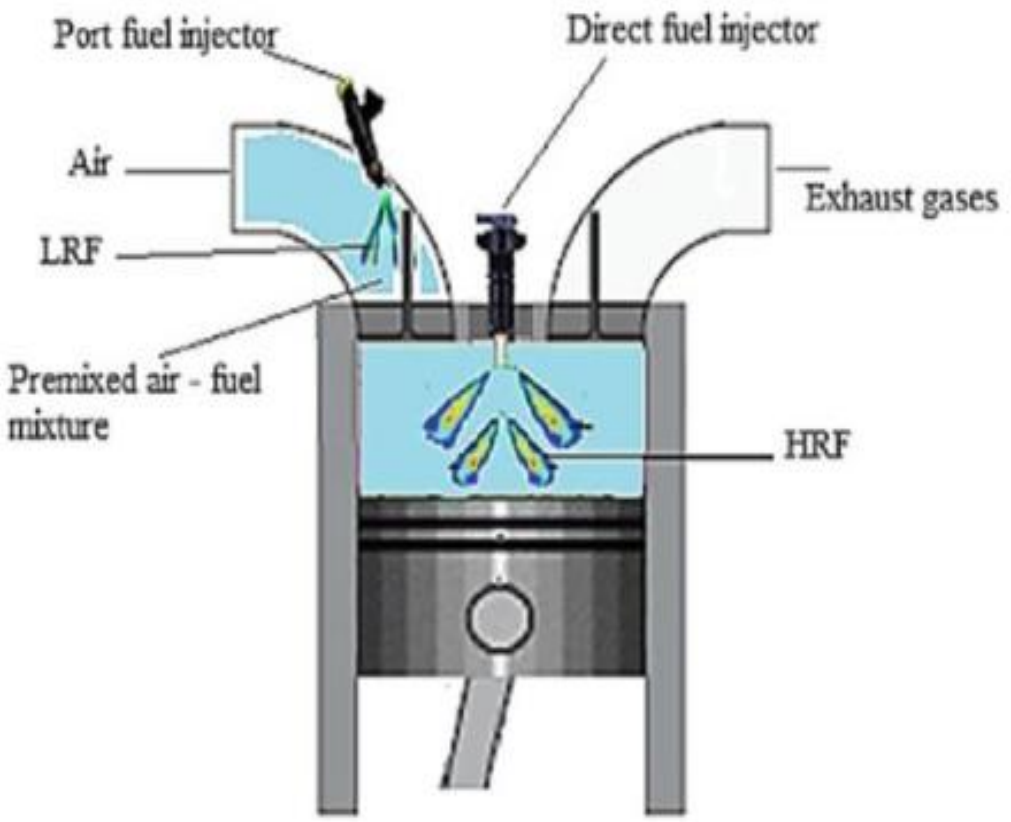

Figure 2.3 Schematic on RCCI engine (Fakhari et al., 2023)

2.3.3.1. Advantage of RCCI mode

Controlled combustion phase

The main challenge with HCCI is the inability to control the combustion phase. RCCI has made significant progress in addressing this issue by regulating the reactivity of the fuel mixture through the blending ratio of two fuels with different reactivity levels. This approach allows precise control over the ignition timing and the overall combustion process, while also helping to mitigate the peak pressure rise rate effectively (Li et al., 2017).

Wider operating conditions

Due to the in-cylinder stratification of reactivity, equivalence ratio, and temperature in RCCI combustion, effectively controlling these factors can significantly reduce engine knocking. This enhances the stability of the combustion process, allowing RCCI to operate efficiently across a wider range of conditions (Sattarzadeh et al., 2022).

High thermal efficiency

In RCCI mode, the working fluid is more uniformly mixed, resulting in a more consistent temperature distribution. This leads to a lower peak temperature, although the overall average temperature remains relatively high. In contrast, traditional diesel engine combustion features uneven mixing and a wide range of equivalence ratio stratification, causing extremely high peak combustion temperatures, often near the cylinder wall. This increases heat transfer losses, However, the average temperature is not higher overall than when RCCI combustion occurs (Xu et al., 2019).

2.3.3.2. Drawbacks of RCCI mode

High carbon monoxide and hydrocarbons emissions

RCCI mode, like other premixed combustion strategies, faces challenges with elevated CO and HC emissions due to the premixed fuel-air mixture entering narrow crevice regions (e.g., between cylinder wall and piston) where combustion flames cannot propagate. This results in unburned fuel trapped in these gaps, reducing combustion efficiency compared to traditional methods. To mitigate this issue, two existing solutions are employed: (1) reintroducing unburned exhaust gases into the cylinder via EGR to promote secondary combustion, and (2) using catalytic after-treatment systems to oxidize residual HC and CO emissions in the exhaust stream. These approaches help address incomplete combustion while maintaining RCCI's efficiency and emission advantages (Hao, 2023).

Harsh engine operation at high load

The RCCI mode strategy addresses the limited operational load range of HCCI by enabling high-load operation, though combustion stability at these loads remains a significant challenge. While RCCI achieves near-zero soot and NOx emissions with high thermal efficiency at low-to-medium loads without requiring EGR, high-load conditions demand increased intake-port fuel injection to maintain emission control. This excess fuel intensifies in-cylinder compression ignition of high-reactivity direct-injected fuel, triggering phenomena akin to gasoline engine knock. The resultant rapid pressure rise rate, coupled with pronounced pressure fluctuations, leads to rough engine operation and unstable combustion, highlighting the trade-off between load expansion and combustion robustness in RCCI systems (Zheng et al., 2018). Table 2.1 shows the primary distinctions between PCCI, HCCI, and RCCI.

Table 2.1 Primary distinctions between PCCI, HCCI, and RCCI modes (Chauhan et al., 2021).

	HCCI	PCCI	RCCI
Type of fuel	Use blends containing multiple gaseous and liquid fuel types.	Use blends containing multiple gaseous and liquid fuel types.	Uses PF injection of high octane and DI of high cetane fuel types
Power output	Fuel flow is regulated by charge dilution or the equivalency ratio ($\Phi \leq 1$).	Fuel flow is regulated by high charge dilution or the equivalence ratio ($1 \leq \Phi \leq 2$)	A/F ratio stratification and fuel reactivity stratification typically without charge dilution
Mechanism of fuel consumption control	Chemical kinetics	Chemical kinetics and injection timing	Chemical kinetics and fuel reactivity
Control of ignition timing	Temperature and pressure	Injection timing	Injection timing
Type of combustion	Premixed volumetric dominated by chemical kinetics	Premixed and diffusion combustion	Premixed and diffusion combustion
Flame front	No flame propagation (homogenous oxidation)	Diffusion flame propagation	Diffusion flame propagation
Emission	Higher CO and HC Lower PM, NOx, and CO_2	Higher CO and HC Lower PM, NOx, and CO_2	Very high CO and HC Ultra-low PM, NOx, and CO_2

2.4. Thermodynamic Principles of RCCI Combustion

Reactivity-Controlled Compression Ignition (RCCI) is a dual-fuel combustion approach that exploits the different reactivities of two fuels to achieve controlled auto-ignition timing, lower

peak temperatures, and stratified combustion (Dempsey, 2013). In RCCI, a low-reactivity fuel, LRF, is port-injected to achieve a premixed homogeneous mixture with air, while a high-reactivity fuel, HRF, is directly injected (DI) near top dead center during the compression stroke. This stratification in reactivity produces a more gradual and controlled heat release that mitigates harsh combustion, reduces local hot spots, and thus suppresses NO_x and soot formation (Harari et al., 2020). Thermodynamically, the result of premixing the low-reactivity fuel is to extend the ignition delay, providing more time for mixing with air and creating a homogeneous charge. The higher-reactivity fuel, being injected late, provides ignition in a more controlled manner, leading to a moderated pressure-rise rate and a lower peak in-cylinder temperature. These features are helpful in meeting the emission regulations in particular: the lower peak temperature reduces NO_x generation, while better premixing reduces the rich zones where soot is formed (Dwarshala et al., 2023).

2.5. Effect of operating parameters on RCCI

2.5.1. Effects of various types of LRF on RCCI

Numerous researchers have explored alternative fuels within the RCCI engine framework, focusing on fuel reactivity management. The combustion, performance, and emission characteristics results of the engine differ when low-reactivity fuels (LRFs) including natural gas, biogas, gasoline, and alcohol fuels like ethanol and methanol are utilized. A key benefit of RCCI mode is its adaptability to a broad range of fuel combinations.

2.5.1.1. Gasoline

(Harari et al., 2020) examined the performance and emission characteristics of a RCCI engine fueled with gasoline and biodiesel revealed that higher gasoline proportions in blends such as gasoline+B100, gasoline+B20, and gasoline-diesel led to increased specific fuel consumption. Conversely, elevated gasoline content correlated with reduced emissions of CO_2, NOx, and soot. Nevertheless, HC and CO emissions were observed to rise with greater gasoline inclusion in the fuel mixtures. Additionally, Figures 2.4 and 2.5 illustrate that in-cylinder pressure and heat release rate for the RCCI engine running at 80% load are significantly affected by fuel properties and operation mode. The diesel–gasoline operation gave higher peak pressure and heat release rate compared with the biodiesel–gasoline mode because of better ignition quality and lower viscosity

of diesel fuel. On the other hand, the biodiesel–gasoline operation resulted in lower values due to higher viscosity, poor ignition quality, and less premixed combustion phase.

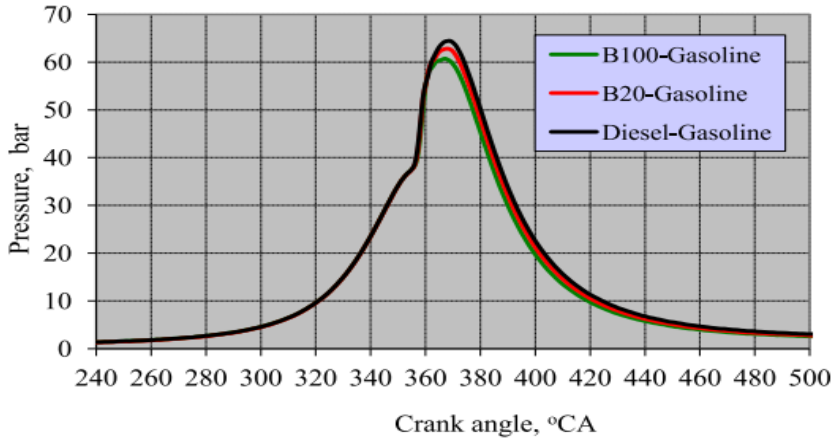

Figure 2.4 In-cylinder pressure verses crank angle at 80% load.

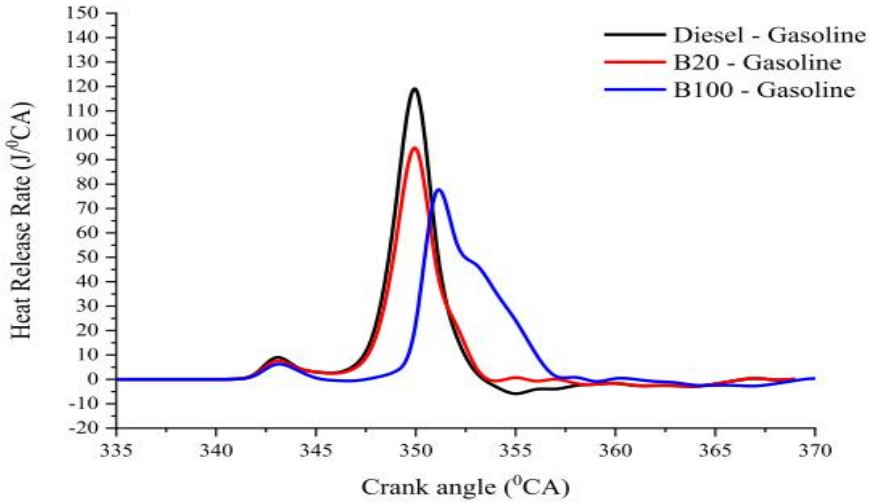

Figure 2.5 Heat Release Rate verses crank angle at 80% load

(Pan et al., 2020) studied the combustion and emissions of diesel/iso-butanol on RCCI under low loads compared its performance with diesel/gasoline RCCI. The results showed that cylinder pressure gradually enhanced with a higher gasoline content in port fuel injection (PFI) when using a 6-cylinder turbocharged CI engine fueled with both diesel/iso-butanol and diesel/gasoline blends (see Figure 2.6). IMEP for diesel/gasoline rose from 40% to 60% with an increased premixed fuel ratio. However, the IMEP of the diesel/gasoline blend was lower than both of conventional combustion and that of diesel/iso-butanol at the same ratio of premixed fuel. This difference is

attributed to gasoline's lower octane rating and latent heat compared to iso-butanol, which shortened the fuel-air mixing time before ignition. Enhancing the premixed fuel ratio in both diesel/iso-butanol and diesel/gasoline RCCI modes led to reduced CO emissions, primarily influenced by combustion chamber temperature and fuel mixture uniformity. Moreover, a higher proportion of LRF extended ignition delay, enhancing fuel-air mixing, which contributed to lower NOx emissions and reduced CO formation during combustion.

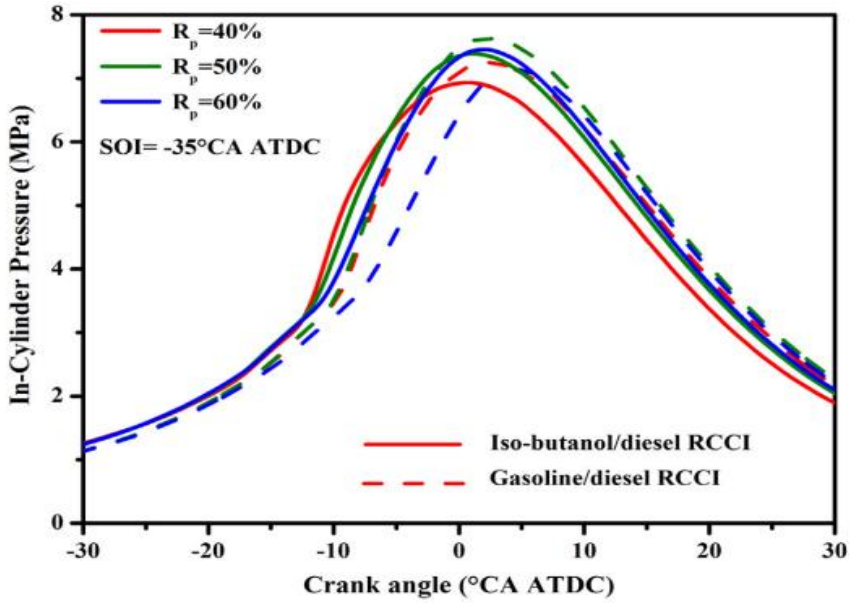

Figure 2.6 In-cylinder pressure of iso-butanol/diesel and gasoline/diesel RCCI combustion mode.

(Habtamu, et al., 2023) investigated a PI ethanol/gasoline blended RCCI engine, revealing that the G25E75-RCCI configuration achieved a maximum cylinder pressure of 91 bar and an HRR of 64 J/CA at 3000 rpm, while the baseline diesel fuel (D100G0E0) showed a lowest cylinder pressure of 58 bar and HRR of 12 J/CA at 2600 rpm. The G25E75-RCCI blend also resulted minimum CO_2 and NOx emissions. Notably, UHC and CO, common RCCI issues, were significantly reduced at intermediate speeds with G50E50-RCCI. Brake power in RCCI mode slightly exceeded that of diesel at higher speeds, and brake torque remained consistently higher across 2000–3000 rpm, peaking at 2400 rpm for G50E50-RCCI. Additionally, RCCI mode demonstrated comparable or superior brake thermal efficiency (BTE) to conventional diesel, with G25E75 performing better at higher speeds and G50E50 showing greater efficiency at lower speeds. Overall, RCCI operation improved performance at high speeds and optimized emissions at intermediate speeds,

highlighting the need for further research to determine optimal conditions by adjusting the port-injected fuel blend ratio and other variables.

2.5.1.2. Alcohols

Alcohol-based fuels like methanol, butanol, and ethanol are viable substitutes for gasoline due to their renewable nature. Both fuels possess higher octane numbers compared to gasoline, which helps prevent engine knocking.

(García et al., 2021) investigated the impact of OMEx and methanol in dual-mode combustion. Their study revealed that in RCCI operation; methanol/diesel mixtures exhibit delayed combustion across varying load conditions compared to gasoline/diesel blends. This delay is attributed to the different reactivity of methanol and gasoline; gasoline's lower research octane number (RON) causes earlier combustion, whereas methanol's higher RON allows for prolonged combustion, promoting a more homogeneous fuel-air mixture. When methanol replaced gasoline in port fuel injection (PFI), cylinder peak pressure significantly decreased from medium to high loads. Although peak pressure fluctuated at low and high loads, the high-reactivity fuel (HRF) influenced combustion phasing. At lower loads, methanol's CP behavior was similar to that of a blend of gasoline/diesel.

(Duraisamy et al., 2020) investigated the impact of high-reactivity fuels, specifically diesel and PODE, alongside methanol-based dual-fuel RCCI operation on combustion characteristics. The experiments were performed at 1500 rpm and 3.4 bar BMEP, with an energy input of 21 kW, while maintaining a constant CA50 of 10° CA a TDC by modifying the start of injection (SOI) of the direct-injected fuel. As illustrated in Figure 2.7, PODE necessitated a slightly delayed SOI in comparison to diesel to achieve the same CA50, attributable to its elevated cetane number, oxygen content, and volatility. In the context of dual-fuel RCCI operation utilizing methanol, the SOI had to be advanced with an increasing methanol premixed ratio (PRm) to counteract the cooling effect induced by methanol's higher latent heat of vaporization, which results in a reduction of in-cylinder temperature and a delay in the commencement of combustion.

An analysis of cylinder pressure and crank angle-resolved data, averaged over 100 cycles, demonstrated the effect of methanol PRm on ignition delay and combustion duration during dual-fuel RCCI operation (Figure 2.8). Both Methanol/Diesel and Methanol/PODE dual-fuel configurations exhibited prolonged ignition delays relative to conventional operation, due to the

high-octane nature of methanol, which resists auto-ignition and absorbs compression heat. The ignition delay for Methanol/PODE was shorter than that for Methanol/Diesel, owing to PODE's superior cetane number, oxygen content, and volatility, which facilitate earlier combustion. An increase in methanol PRm further prolonged ignition delay while simultaneously reducing combustion duration, indicative of methanol's rapid burning characteristics.

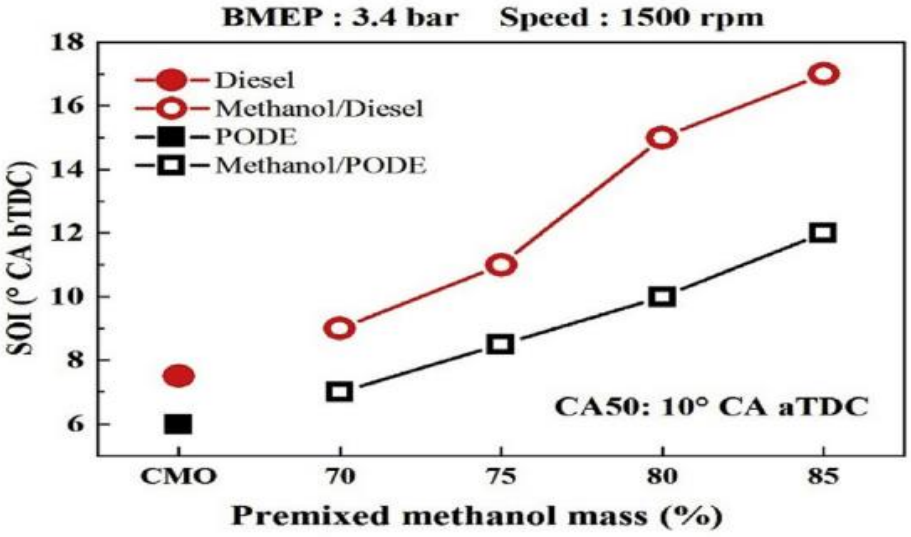

Figure 2.7 Effect of SOI of high reactivity fuel on CA50

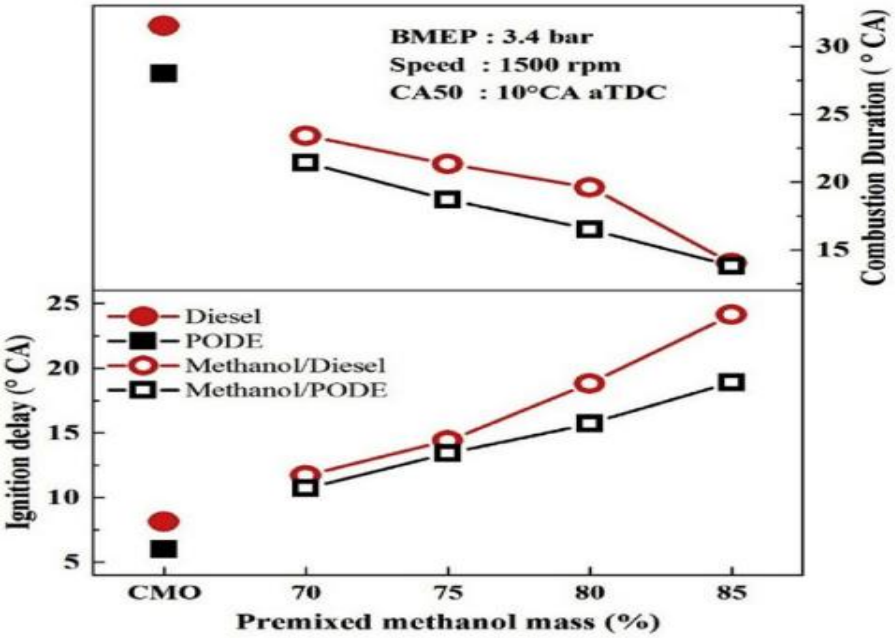

Figure 2.8 Ignition delay and combustion duration at different premixed mass %

(Zheng et al., 2018) compared biodiesel/n-butanol-fueled RCCI and blended combustion modes in a single-cylinder engine under varying injection timings, n-butanol ratios (20%, 50%, 80%). EGR rates (0%, 30%, 50%), and engine loads (low, medium, high). The findings showed that the ignition delay in blended mode is longer and more sensitive to EGR rate and n-butanol ratio compared to RCCI mode. An optimal EGR rate of 30% was identified for balancing efficiency and emissions in both modes. Blended mode maintained high efficiency across all n-butanol ratios and loads, achieving a maximum ITE of 47.5%, while RCCI showed comparable efficiency only at high loads. The issue of high MPRR in blended mode can be mitigated by retarding combustion phasing. Overall, blended mode exhibited lower HC, soot, and CO emissions, with slightly higher NOx emissions than RCCI. While blended mode offers superior performance when MPRR is controlled, RCCI demonstrates potential for load extension due to its lower MPRR and flexible fuel split and injection timing.

(Han et al., 2021) examined the use of n-butanol as LRF and n-heptane as an HRF to attain high thermal efficiency with low NOx and soot emissions in a single-cylinder heavy-duty CI engine. Experimental findings reveal that single direct injection leads to either excessively early combustion phasing or elevated HC and CO emissions. While increasing intake boost pressure improves thermal efficiency, it significantly worsens CO and HC emissions. A double direct injection strategy effectively optimizes combustion phasing, achieving high gross indicated efficiency with minimal CO emission penalties. Furthermore, a high EGR rate is crucial for controlling combustion phasing due to n-butanol's relatively high reactivity. The n-butanol/n-heptane RCCI system operates efficiently from low to medium loads, with the sensitivity of combustion phasing to DI timing decreasing as load increases. However, at medium-high loads, combustion cannot be effectively phased after TDC, resulting in high peak pressures and pressure rise rates. Despite this, the system consistently produces extremely low NOx and PM emissions, with gross indicated efficiency exceeding 50% from low to medium loads.

(Wang et al., 2021) explored a novel approach to enhance combustion stability and reduce harmful emissions in methyl oleate/n-butanol dual-fuel RCCI engines operating at high loads. Experiments were carried out on a single-cylinder engine at rated speed and 90% full load, using n-butanol as the LRF for port PFI and a methyl oleate/n-butanol blend for DI. The impact of varying PFI and DI ratios on combustion and emission characteristics was analyzed. Findings showed that increasing the n-butanol PFI and DI ratios led to higher cylinder pressure and HRR, while reducing

soot and NOx emissions. However, this also caused a rise in CO and HC emissions. The optimal balance was achieved at a PFI ratio of 40% and a DI ratio of 20%, minimizing NOx and soot emissions without significantly increasing peak cylinder pressure or fuel consumption. Further optimization through pilot injection adjustments demonstrated that appropriate pilot injection ratios and timing intervals effectively reduced peak CP and NOx emissions, with minimal effect on CO, soot, and HC emissions.

2.5.2. Effects of various types of HRF on RCCI

(Harari et al., 2020) the investigation revealed that utilizing diesel as a high-replacement fuel and subsequently examining a diesel/gasoline blend demonstrated a superior BTE when compared to a diesel/gasoline mixture. It was noted that the BTE progressively diminished with the increased injection of gasoline into the system. The enhanced BTE associated with diesel fuel can be attributed to the effective mixing of fuel and air, which facilitates a greater conversion of thermal energy into mechanical work, owing to the higher calorific value of diesel and lower viscosity. Additionally, the diesel/gasoline dual fuel combination exhibited elevated cylinder pressure and a more rapid HRR relative to the gasoline/B100 and gasoline/B20 blends. Furthermore, experiments involving a blend of biodiesel and gasoline as an HRF at a constant speed indicated that NOx emissions decreased as the gasoline proportion in the PFI system increased, with the biodiesel/gasoline blend producing minimum NOx than the diesel/gasoline combination.

(Dalha et al., 2020) conducted an experimental assessment of how biogas port injection at the intake valve influences the combustion behavior of a B5/biogas RCCI engine, with the key results illustrated in Figure 2.9. The study showed that valve-based biogas injection significantly reduced the combustion duration compared with the traditional premixed method (Figure 2.9b), primarily because less biogas participated in LTC, improving the oxidation of directly injected diesel under in-cylinder mixing conditions. In contrast, premixed biogas led to a longer burning duration due to the early involvement of the low-reactivity biogas mixture. Also noted that variability in burning duration at 5-6 bar IMEP (Figure 2.9a, b) could be influenced by differences in direct-injection quantity or improved atomization when biogas was premixed. Regarding ignition delay, Figure 2.9c shows that biogas injection at the valve produced an almost constant ignition delay across load ranges, although the delay was higher at 5.5-6.5 bar IMEP due to advanced injection promoting diesel spray diffusion toward the cylinder wall, creating poorer reactivity distribution.

Meanwhile, premixed biogas consistently exhibited the longest ignition delay (Figure 2.9d), as early combustion of low-reactivity biogas suppressed the onset of ignition. Overall, Figure 2.9 demonstrates that biogas injection at the valve effectively shortens burning duration and mitigates the excessive ignition delay associated with the premixed biogas approach.

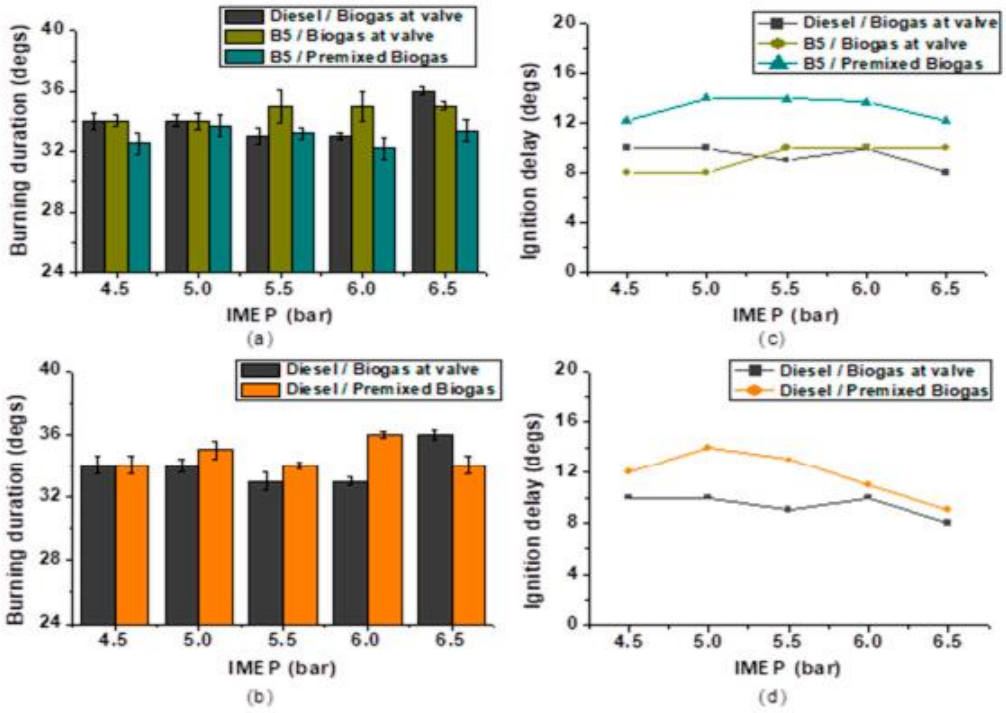

Figure 2.9 Variation of (a) burning duration for B5/biogas RCCI combustion, (b) burning duration for biogas injection approaches in RCCI, (c) ignition delay period for B5/biogas RCCI combustion, and (d) ignition delay for biogas injection approaches in RCCI

(Lin et al., 2021) investigated the effects of polyoxymethylene dimethyl ether 3 (PODE3) and injection pressure on combustion and performance of CI engine reveals significant insights. PODE, along with biodiesel, emerges as a promising renewable fuel alternative to diesel in dual fuel RCCI engines, primarily due to its high cetane number, which enhances ignition characteristics compatible with diesel combustion. The unique properties of PODE, including its higher viscosity and reduced vapor pressure compared to Petrodiesel, contribute to the mitigation of vapor lock within the fuel system. Experimental results indicated that the incorporation of PODE into RCCI dual fuel engines led to a more gradual enhance in the HRR of diesel fuel,

particularly at a PODE/Diesel ratio of 3:7, suggesting that the addition of PODE facilitates advanced ignition during the combustion process.

(Duraisamy et al., 2020) indicated that the usage of PODE as a high-replacement fuel necessitates a postponement of the start of injection (SOI) in comparison to diesel fuel, primarily due to its elevated cetane number and oxygen content. Furthermore, an increase in the mass of methanol within the port fuel enhances the dual fuel operation of both diesel/methanol and PODE/methanol systems, affecting the SOI. The presence of a greater mass of methanol in the premixed fuel results in a reduction of CT, attributable to methanol's higher LHV, which allows it to effectively absorb heat generated during compression. To ensure optimal engine performance, it is essential to maintain engine load, which necessitates an earlier injection of direct injection (DI) fuel, thereby further delaying the SOI.

(Wang et al., 2021) examined the impact of different ratios of n-butanol PFI (RNBPI) and methyl oleate DI (RNBDI) on the duration of combustion in a dual-fuel RCCI engine. Their findings revealed that elevated levels of RNBPI (40% and 60%) significantly decreased combustion duration in comparison to 20% RNBPI (see Figure 2.10). This phenomenon was linked to the lower methyl oleate DI, which enhanced the premixed fuel fraction and prolonged the ignition delay, thus facilitating quicker premixed combustion. Furthermore, at RNBPI = 60% and RNBDI = 30%, the combustion duration was markedly reduced due to improved atomization and evaporation of methyl oleate during the extended ignition delay. In summary, increasing n-butanol PFI and modifying the DI methyl oleate ratios effectively accelerated premixed combustion, leading to a reduction in total combustion duration.

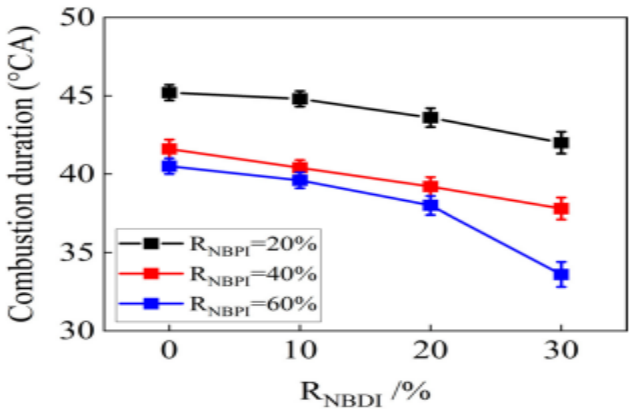

Figure 2.10 Combustion durations of various RNBPI and RNBDI

In summary, when the HRF is kept constant, LRFs derived from natural gas and alcohol exhibit a greater tendency for reactivity compared to those derived from gasoline. Natural gas and alcohol fuels possess higher octane ratings than gasoline, which contributes to a reduction in NOx emissions by facilitating a cooler combustion environment. Additionally, these alternative fuels have elevated oxygen content. Nevertheless, optimizing engine parameters such as adjusting the injection timing, employing high-pressure injectors, and modifying the fuel spray angle can enhance the performance of gasoline as an LRF. The application of high injection pressure leads to better fuel atomization and a more uniform fuel mixture, thereby increasing combustion efficiency. Furthermore, the integration of pilot injection with multiple injection pulses has been shown to elevate pressure rise rates and advance combustion timing compared to single injection techniques. This approach results in a more uniform and reactive fuel mixture, enhancing the cetane number of the dual-fuel blend through improved in-cylinder mixing.

2.5.3. Premixing Ratio

The proportion of the mass of LRF to the total mass of both LRF and HRF is referred to as the premixed ratio. The premixed ratio (PR) is a key factor that influences the performance and emissions of RCCI engines. (Duraisamy et al., 2020) conducted on the CDC and RCCI modes at a rotational speed of 1500 rpm. Diesel and PODE were utilized as HRF, while CH_3OH served as an LRF. The PRs employed were 70, 75, 80, and 85, with an injection pressure set at 3 bar. Throughout all trials, the EGR rate was maintained at 26%. Figure 2.11a illustrates the pressure and HRR achieved with PODE as the HRF at 3.4 bar brake mean effective pressure (BMEP). The solid line indicates the CDC operation using PODE as the fuel. It is observed that the compression pressure is elevated during CDC operation. Conversely, the introduction of LRF in the RCCI operation results in a reduction of compression pressure, attributed to the vaporization of the LRF. As the PR increases, the quantity of heat extracted by the LRF for vaporization from the in-cylinder gas mixture also rises. Consequently, both the compression pressure and temperature diminish with increasing PR. This phenomenon also contributes to an increase in the ignition delay (ID) as the PR escalates. The peak values of HRR rise with higher PRs; however, the crank angle at which these peaks occur shifts away from the top dead center (TDC), resulting in lower in-cylinder gas temperatures.

Figure 2.11b illustrates that the concentration of NOx diminishes as the pressure ratio (PR) rises from 70 to 85. This phenomenon can be attributed to a decrease in the average gas temperature associated with the increase in PR. At this specific load point, it is noted that the formation of soot does not significantly depend on the PR. Conversely, hydrocarbon (HC) and carbon monoxide (CO) emissions are observed to escalate with the rising PR. Additionally, tests were conducted using diesel as the high-reactivity fuel (HRF). It was found that the heat release rate (HRR) and in-cylinder pressure recorded with diesel were lower compared to those obtained with PODE. Unstable engine performance was detected when the PR exceeded 85%.

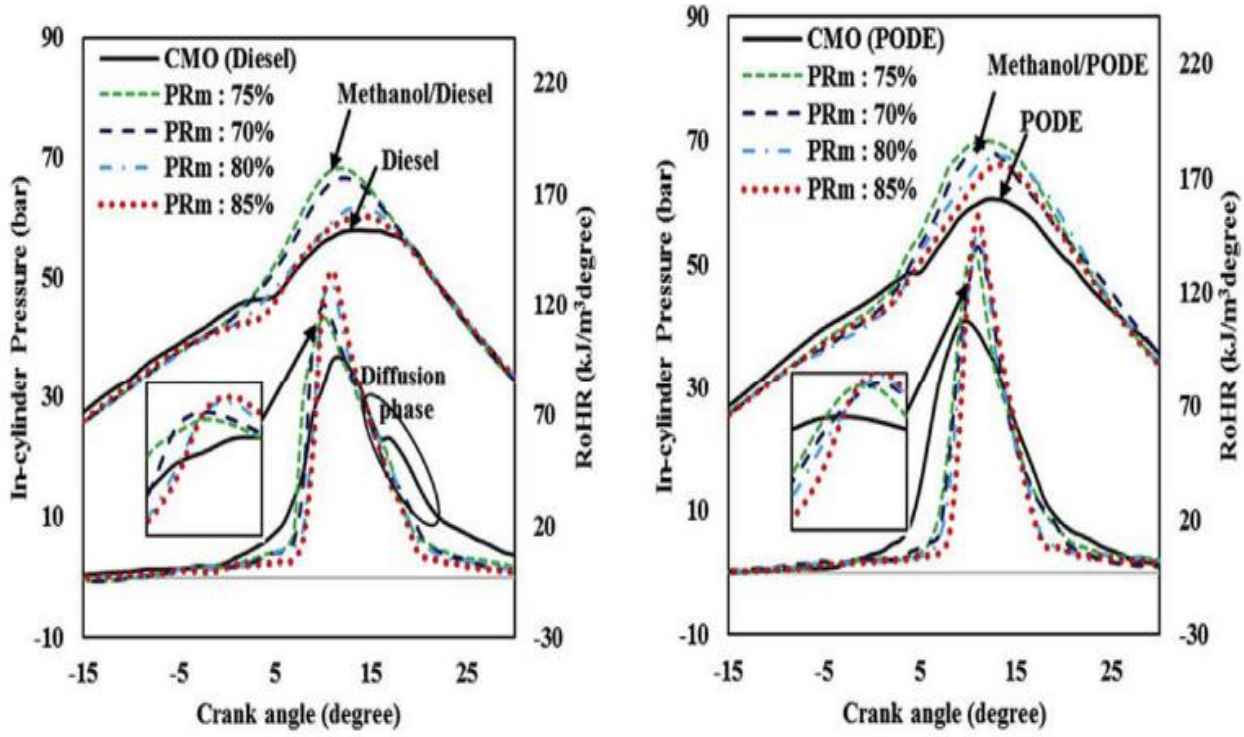

(a) (b)

Figure 2. 11 (a) Effects of premixing ratios Methanol/Diesel (b) Methanol/PODE dual fuel RCCI combustion

A comparable study was conducted by (Okcu et al., 2021) at 2400 RPM on a single-cylinder engine. In this investigation, a blend of isopropanol, butanol, and ethanol in a volumetric ratio of 3:6:1 was utilized as the low-reactivity fuel (LRF), while diesel and biodiesel served as the HRFs. The injection pressure for the HRF was approximately 300 bar, whereas that for the LRF was around 5 bar. Engine performance metrics and emission data were collected for PR values of 0, 15, 30, 45, and 60, along with the corresponding HRR for a load of 15.42 Nm. As the PR increases,

both the in-cylinder pressure and HRR exhibit an upward trend. Due to the vaporization of the LRF, an increase in PR leads to a reduction in pressure and temperature towards the end of the compression phase. This enhancement in mixing and ID results in the majority of the LRF combusting during the premixing stage. Consequently, the HRR, in-cylinder pressure, and rate of pressure rise all increase with a higher PR. Under the 60% load condition, an increase in PR from 15 to 60 resulted in a 43% rise in NOx emissions, while smoke emissions decreased by 93%. However, both HC and CO emissions saw increases of 75% and 9.6%, respectively.

2.6. Theoretical Foundation for Gasoline–n-Butanol and Biodiesel-Diesel RCCI Combustion

RCCI represents a dual-fuel combustion approach that leverages variations in fuel reactivity to manage ignition timing, heat-release rates, and the dynamics of combustion within the cylinder. Traditional studies on RCCI typically employ diesel as the HRF and gasoline as the LRF (Pan et al., 2020). The use of diesel facilitates rapid autoignition due to its elevated cetane number, while gasoline, with its higher-octane rating, delays combustion, thereby allowing for enhanced premixing of the charge and a more gradual heat release. Nevertheless, conventional diesel-gasoline mixtures present certain trade-offs: although there is a reduction in NOx and soot emissions attributed to improved premixing, there is often an increase in HC and CO emissions, particularly when higher gasoline fractions are utilized. Furthermore, elevated in-cylinder pressure and heat-release rates may pose challenges to combustion stability, especially under conditions of increased load (Harari et al., 2020).

Among others, alcohol fuels like n-butanol, methanol, and ethanol have emerged as strong alternatives for LRF in RCCI. Compared to gasoline, all these fuels have a higher-octane number, which extends the ignition delay and allows ample opportunity for better mixing of air and fuel (Duraisamy et al., 2020). Among alcohols, n-butanol has several thermodynamic and chemical-kinetic advantages: owing to the higher latent heat of vaporization, its charge cooling lowers in-cylinder temperatures, thereby reducing NOx formation; with slower autoignition kinetics compared to diesel, n-butanol allows longer premixing time, which enables a more homogeneous combustion process (Han & Somers, 2020). The port injection of n-butanol as LRF enables the engine to make a well-mixed low-reactivity zone, while direct injection of biodiesel-diesel as HRF triggers-controlled ignition.

Biodiesel–diesel blends provide a suitable HRF with enriched oxygen supply and better ignition quality. The oxygen atoms in biodiesel molecules promote more complete combustion, thus resulting in lower CO and unburned hydrocarbons (Zheng et al., 2018). Furthermore, the high cetane number of biodiesels will ensure proper ignition of the stratified premixed charge. In comparison with conventional diesel–gasoline RCCI, the biodiesel–diesel HRF increases the oxidation of intermediate species coming from LTC in order to enhance thermal efficiency and reduce soot formation. Experimental results have demonstrated that biodiesel–diesel as HRF and n-butanol/gasoline as LRF could enable higher in-cylinder pressures, a smoother heat-release rate, and improved IMEP while keeping NOx and soot low for different engine loads (Han et al., 2021).

The root of the performance advantages for gasoline-n-butanol and biodiesel-diesel combinations lies in thermodynamic and chemical-kinetic principles. The port-injected LRF vaporizes and mixes with air, absorbing heat from compression and, in so doing, reduces peak cylinder temperatures and mitigates NOx formation. The subsequent direct injection of HRF near TDC produces controlled autoignition, limiting the local hotspots and pressure spikes seen. This two-stage heat-release profile, a hallmark of RCCI, provides a smoother pressure rise rate and lower mechanical stresses on the engine (Harari et al., 2020).

Chemically, reactivity-controlled combustion phasing is enabled by the difference in reactivity between the fuels. Slower radical formation from the n-butanol/gasoline LRF delays the start of combustion for better premixing, while fast-reacting biodiesel-diesel HRF will ensure instant ignition and thus rapid radical chain propagation. This balance between delayed ignition and rapid propagation smooths the heat-release rate and stabilizes combustion under varying loads. Moreover, the oxygenated nature of biodiesel accelerates oxidation reactions through the high-temperature phase, thereby reducing CO and HC formation, whereas n-butanol contributes to more uniform fuel-air distribution and minimizes soot precursors (Wang et al., 2021). In this system, the premixing ratio (PR) is a critical factor. According to various studies, increasing the fraction of LRF prolongs the ignition delay, enhances fuel-air mixing, and shifts HRR peaks away from TDC, causing in-cylinder temperature and NOx emissions to decrease (Okcu et al., 2021).

In summary, the combination of gasoline/n-butanol as the fuel LRF and biodiesel/diesel as the HRF provides several advantages for RCCI combustion. The LRF promotes enhanced premixing and extended ignition delay, which improves heat-release control, while the HRF ensures reliable

ignition and oxygen-assisted combustion, reducing soot and CO_2 formation. This fuel pairing allows flexible optimization of the premixing ratio to balance NOx, CO, and HC emissions while maintaining high thermal efficiency. Additionally, it is compatible with LTC strategies, effectively minimizing peak cylinder temperatures and sustaining high brake thermal efficiency.

2.7. Optimization Techniques

Optimization is the process of selecting the process parameter to produce the desired result. Under a variety of restrictions, optimization determines the optimal result for the given aim. Single-objective and multi-objective optimization are both possible. Two approaches can be used for optimization. First, the global minima or maxima in the plotted result can be located using the graphical method. The latter is the gradient approach, which determines the maximum or lowest gradient by utilizing the gradient of the objective function. In the design space of the design vector, the two approaches locate the maxima or minima. a number of forecasts and optimization strategies were used to look at the emissions and engine performance. One tool for optimization and prediction used to examine engine characteristics is response surface methodology (Sakthivel et al., 2021).

2.7.1. Response Surface Methodology (RSM)

RSM serves as a widely utilized experimental design approach for the exploration and modeling of processes. It stands out as an exceptionally effective method for the multivariate analysis of responses, offering enhanced error management across various conditions. This robust statistical method enables the examination of how different input factors affect output variables. Consequently, through the optimization process, RSM significantly minimizes the time, materials, and costs associated with performing multiple trials (Abdullahi et al., 2023).

RSM is a sophisticated statistical and mathematical approach employed in the design of experimental studies. Its primary goal is to enhance the output variable that is influenced by several independent factors. The 2^{nd}-order polynomial equation presented in Equation (2.1) serves as a predictive model for the output response, incorporating the various input variables into its formulation. (Veza et al., 2023).

$$Y = b_0 + \sum_{i=1}^{k} b_i x_i + \sum_{i=1}^{k} b_{ii} x_i^2 + \sum_{i<1}^{k} b_{ij} x_{ixj} + e \quad (2.1)$$

Where Y is the output; x_i and x_j are variables; b_i and b_{ii} are the 1^{st} order and the 2^{nd} order

coefficients, respectively; b_0 denotes the intercept; b_{ij} is the model linear coefficients (for the i and j variables); k is the number of factors studied in the experiment and e is the error related with output.

The initial and most crucial phase in the application of RSM involves the careful selection of input or independent variables, as these elements play a pivotal role in influencing the entire process, including the resultant outputs. A review of existing literature on the implementation of RSM in ICEs operating on alternative fuels reveals that the independent variables typically encompass operational variables such as engine speed, load, compression ratio, and blending ratio. It is essential to judiciously determine the ranges for these selected factors, which are generally informed by prior experimental findings. Inadequate selection of the independent variables and their corresponding ranges can lead to results that are both inaccurate and of limited utility. Furthermore, it is imperative to identify desirable responses that significantly affect engine performance, combustion efficiency, and emission profiles. Consequently, the foremost task prior to employing the RSM technique is to methodically establish the independent variables and the desired outputs in a manner that is both logical and effective (Alhassan et al., 2016).

2.7.2. Response surface design for RSM

Response surface design (RSD) encompasses a collection of sophisticated DOE methods aimed at optimizing specific responses. Following the identification of factors and responses, the subsequent essential phase involves the strategic design of experiments, which entails selecting the experimental points where the anticipated responses can be accurately predicted and assessed. After determining the number of variables involved, several DOE approaches can be articulated to construct a response surface. These designs are classified according to their important characteristics, such as total number of experiments and variance (Ahmad et al., 2024). The selection of a suitable design strategy is essential to the overall experimental process. Nevertheless, it is noteworthy that many previously published studies inadequately justify their choice of response surface design, often providing only cursory explanations. Response surface design encompasses three primary categories: FFD, CCD, and BBD. In the context of experimental design, a variable is defined as a factor that can affect the system's response. The ranges of a variable denote the various values or settings applied during the experiment. Understanding the

concept of levels is essential, as it enables scholars to systematically investigate the interplay between variables and outputs across a spectrum of conditions.

The selection of ranges for a variable is contingent upon the specific objectives of the experiment and the anticipated range of influence on the response. By strategically choosing these ranges, researchers can examine how temperature, for instance, affects the output variable at various points within the designated range. It is vital to select suitable levels for each variable to confirm that the experiment yields relevant data and valuable insights. The levels should encompass a range that accurately reflects practical operating conditions. Furthermore, the number of ranges selected for each variable can significantly influence the accuracy and precision of the experimental outcomes, necessitating a careful determination of an adequate number of levels to efficiently capture the output variable's behavior across the factors range (Karchiyappan & Karri, 2021).

2.7.2.1. Full factorial design (FFD)

A response surface methodology experiment utilizing an FFD examines every possible combination of factor level. This approach necessitates that at least one trial is conducted for each conceivable combination of factors and their respective levels, thereby ensuring that all interactions among factors are accounted for. The total number of trials or repetitions is a pivotal aspect of the experimental design, influenced by various elements such as the required accuracy of the results, the inherent variability of the data, and the resources available, including time and materials. By increasing the number of trials, researchers can mitigate the effects of random variation, leading to a more accurate estimation of the factors' true effects. It is crucial to document the number of trials employed in the study, as this information reflects the robustness and reliability of the experimental outcomes. However, practical limitations may restrict the ability to perform a large number of repetitions, necessitating an acknowledgment of these constraints and their potential impact on the precision and generalizability of the results. Consequently, the implementation of FFD can be relatively costly and time-intensive, particularly as the number of variables and levels escalates (Veza et al., 2023).

2.7.2.2. Central composite design (CCD)

RSM employing a CCD is widely recognized as a predominant approach in experimental design. CCD is particularly advantageous for sequential experimental investigations, as it allows for the enhancement of earlier factorial experiments by incorporating additional center and axial points.

This design facilitates the actual approximation of both first and second-order terms, enabling the modeling of an output variable that exhibits curvature through the integration of axial and center points into a factorial framework. The curvature of the response surface can be assessed by utilizing points situated at the midpoint of the experimental domain alongside "star" points placed outside this domain. In a factorial design, the levels of the points are set at ±1, whereas the "star" points are designated at ±α, where |α| is greater than or equal to 1. The value of the α parameter is determined based on the computational capabilities and the desired accuracy of the response surface estimation. The efficacy of predictions is influenced by the spatial arrangement of these points, highlighting the significance of the α value and the number of trials conducted at the center of the domain in determining the precision of the estimations (Veza et al., 2023).

2.7.2.3. Box-Behnken design (BBD)

Another variant of RSM is referred to as BBD. This design type is distinct from factorial designs, as it does not rely on either fractional or full factorial approaches. The BBD is predominantly advantageous for estimating first and second-order coefficients due to its typically reduced number of design points, which can lead to significant savings in both time and cost. However, it is vital to note that BBD lacks the inherent factorial structure found in CCD, making it less suitable for experiments that require a chronological approach. Despite its limitations in covering the corners of the nonlinear design space, BBD is often regarded as more effective than other RSM, such as three-level FFD and CCD. It allows for the exploration of higher-order outputs with fewer experimental runs compared to traditional factorial methods. Like CCD, BBD is designed to maintain a higher-order surface by strategically selecting runs and is characterized by its rotatability and the necessity for three levels per factor, enabling it to fit a full quadratic model of the response surface (Veza et al., 2023).

2.8. Butanol as an alternative fuel

Like methanol and ethanol, butanol is an alcohol-based fuel. The most commonly utilized alternative fuel in ICEs is ethanol. Some countries, such as Brazil, have fully embraced ethanol as an ICE fuel. Research indicates that butanol, which can be utilized in ICEs, has more advantageous properties than ethanol. Although butanol isn't currently used in the automotive industry for commercial purposes, studies have shown that it is a renewable alternative fuel with numerous promising applications for internal combustion engines. One typical method for making butanol is

the fermentation of biomass feedstock. The isomers of butanol are n-butanol (1-butanol), s-butanol (2-butanol), iso-butanol, and tert-butanol. Nowadays, it's likely that the isomers isobutanol and n-butanol are used as biofuels. Because the butanol isomer degrades much more slowly than the other fuels, its use is not widely recognized.

The most advantageous fuel among all the butanol isomers is n-butanol since it blends well and is simple to combine with gasoline. Additionally, because butanol is an alcohol fuel with an oxygen concentration that is highly useful in lowering smoke formation a significant concern of CI engines. it offers a chance to utilize it in CI engines with diesel as a blend. Lowering the combustion temperature can also address the problem of NOx emissions in diesel engines. The enthalpy of evaporation of butanol is greater than that of ethanol, which lowers the ignition temperature and provides a chance to regulate the emission of NOx. In SI engines, bio-butanol can be used as fuel and as an oxygen enhancer in mixtures with gasoline. Blends of diesel and n-butanol can also be utilized in CI engines because their different properties especially their cetane number are found to be close to those of pure diesel. With all these advantages over other alcohols, butanol is a contender for the role of alternative fuel of the future (Gwalwanshi et al., 2022).

2.9. Characteristics of n-butanol

Due to its superior qualities over other alcohols, n-butanol has the potential to be the next generation of alternative biofuel. Table 2.2 illustrates the key characteristics of n-butanol, other alcohols, and fossil fuels to help with understanding of the substance's qualities. Table 2.3 shows the key characteristics of conventional fuels like petrol and diesel as well as unconventional biofuels like methanol, ethanol, and n-butanol. This table can be used to support the following claims. Because n-butanol is more viscous than other alcohols, it is a fuel with greater resistance to friction. During engine operations, certain sections of the engines' cylinders come into direct contact with engine fuel. The engine's fuel can lessen the impact of friction between its various components if it has a high enough viscosity. Additionally, the low enthalpy of vaporization of n-butanol may make the cold start problem less significant. Because it contains a higher carbon content than other alcohol fuels, n-butanol is less volatile and therefore safer to use in transportation. Additionally, n-butanol has a significantly greater energy density than other alcohol fuels, which means it will probably exhibit better fuel efficiency (Gwalwanshi et al., 2022).

Table 2.2 Properties of conventional fuels and various alcohol (Feroskhan & Gobinath, 2024; Okcu et al., 2021; Sánchez et al., 2022)

Parameter	Diesel	Gasoline	n-butanol	Methanol	Ethanol
Molecular formula	C_{12}-C_{15}	C_4-C_{12}	C_4H_9OH	CH_3OH	C_2H_5OH
Density (kg/m^3) at 20^{o}C	810-890	720-780	808-810	790-796	785-794
Molecular weight	198.4	111.19	74.11	32.04	46.06
Auto-ignition temp (^{o}C)	210-250	300	343-385	463-470	423-434
Viscosity (mm^2/s) at 40^{o}C	1.9-4.10	0.4-0.8	2.2-3.70	0.58-0.59	1.08-1.20
Cetane number	40-55	0-10	15-25	3-5	5-8
Octane number	20-30	80-99	96	111	108
Oxygen content (weight %)	-	-	21.6	50	34.8
Lower heating value (MJ/kg)	42-45	42-46	33-34.5	19.5-20.0	26-29
Energy density (MJ/L)	35.86	32	29.2	16	19.6

2.10. Biodiesel as an alternative fuel

According to ASTM specifications, biodiesel (designated as B100) refers to mono-alkyl esters of long-chain fatty acids derived from a range of sources, such as waste, edible, and non-edible oils. It is synthesized through transesterification, a process where triglycerides in oils or fats react with alcohol (like methanol or ethanol) in the existence of a catalyst to form alkyl esters. Feedstocks for these fatty acid alkyl esters (FAAE) commonly include animal fats, cooking oils, and vegetable oils (both edible and non-edible varieties). Biodiesel provides numerous advantages, including a higher flash point (improved safety), superior lubricity, enhanced cetane number (better combustion efficiency), biodegradability, prolonged engine component lifespan, renewability, non-toxic properties, and environmental benefits: notably reduced carbon monoxide emissions compared to diesel fuels (Malik et al., 2024).

Transesterification serves as the primary technique for biodiesel production, involving a reaction between triglycerides and short-chain alcohols to produce biodiesel (alkyl esters) and glycerol. This process is executed through two approaches: conventional and in-situ transesterification. In the conventional method, refined oil is first extracted from feedstocks before undergoing the reaction. Conversely, the in-situ method simplifies the process by directly using raw materials like whole seeds, bypassing the oil extraction step. However, the in-situ approach demands

significantly higher methanol volumes, raising operational costs compared to the conventional method. Additionally, conventional transesterification enables tighter regulation of variables such as alcohol-to-oil ratios, temperature, and pressure, which enhances process efficiency and maximizes biodiesel yield (Amirthavalli et al., 2022).

A variety of feedstocks is used in the synthesis of biodiesel, which encompasses plant, animal fats, microbial, waste, and algae oils. Biodiesel generated from unrefined vegetable oils exhibits characteristics similar to those of petroleum diesel, allowing it to serve as a direct substitute for conventional fuels. The vegetable oils frequently employed in biodiesel production include palm, castor, soybean, cottonseed, rapeseed, pongamia, jatropha, mahua, linseed, and rice bran oils. Specifically, cottonseed oil, which is a byproduct of the cotton processing industry, has a density ranging from 0.917 to 0.933 g/cm³ at 15°C, a viscosity of 34.79 cSt at 40°C, and a calorific value of 39,500 kJ/kg. The oil content in cotton seeds varies between 17% and 25%, and it is particularly rich in fatty acids, including oleic acid (19.2% to 23.26%), linoleic acid (55.2% to 55.5%), and palmitic acid (11.66% to 20.1%) (Singh et al., 2019).

Catalysts are required for the transesterification process and are selected based on the feedstock's properties. In the production of biodiesel, both acid and base (alkali) catalysts are employed. These catalysts facilitate the reaction between oils with alcohols, resulting in the formation of biodiesel. The presence of catalysts not only accelerates the reaction rates but also enhances the quality of the resulting methyl esters. Generally, base catalysts are favored over their acid counterparts due to their quicker reaction times, lower operational temperatures, and superior conversion efficiencies. Potassium hydroxide (KOH), a widely utilized base catalyst, is effective at reduced temperatures, requires short reaction durations, operates under atmospheric pressure, does not generate intermediate compounds, and achieves high conversion rates. Nonetheless, alkali catalysts exhibit sensitivity to feedstocks with elevated FFA content, as they are prone to producing soap instead of biodiesel, thus making them more appropriate for oils with lower FFA concentrations (Neupane, 2022).

2.10.1. Transesterification process

Biodiesel generated through the transesterification process exhibits properties comparable to those of petroleum diesel fuel, making it an economically advantageous method for commercial production. In this process, triglycerides, which are organic fats and oils, react with alcohol to

produce methyl esters and glycerol. The transesterification reaction, illustrated in Figure 2.13, involves the conversion of triglycerides into FFAs through hydrolysis. These FFAs subsequently react with alcohol, resulting in the formation of esters, specifically methyl or ethyl fatty acid esters, alongside glycerol. This reaction of free fatty acids with alcohol is often referred to as alcoholysis. Upon completion of the transesterification process, the resulting products are separated, with biodiesel rising to the top and glycerol settling at the bottom due to gravitational forces. It is crucial that this separation occurs rapidly to prevent any reverse reactions from taking place (Osman et al., 2024).

The transesterification process commonly employs methanol and ethanol as key reactants. When FFAs react with methanol, the process is referred to as methanolysis. During methanolysis, a mixture consisting of 10-20% methanol and 80-90% oil is subjected to heat, along with a minimal amount of catalyst. Effective mixing of FFAs and methanol is crucial due to the limited solubility of methanol in oil. The biodiesel generated through this methanolysis process is classified as FAME (Banga & Pathak, 2023). In the transesterification process, methanol is often favored due to its superior reactivity and lower cost compared to other alcohols. When free fatty acids are involved, ethanol is utilized in a reaction termed ethanolysis. This method not only slightly enhances the fuel's heat content and cetane number but also presents a lower toxicity profile relative to alternative alcohols. However, ethanolysis faces two primary challenges: the high energy requirement for the reaction and the difficulties associated with separating the resulting ester from glycerol, which contributes to the rising costs of biodiesel produced through this method.

The biodiesel generated from ethanolysis is classified as fatty acid ethyl ester. Biodiesel obtained from the transesterification process offers several advantages over pure plant oil. One critical property of fuel is viscosity, which significantly impacts performance of engine. Pure plant oil exhibits a higher viscosity than methyl ester. Elevated viscosity adversely affects fuel injection timing, atomization, and injection pressure in CI engines. The characteristics of biodiesel closely resemble those of petroleum diesel, allowing it to be utilized in CI engines with minimal modifications (Singh et al., 2020).

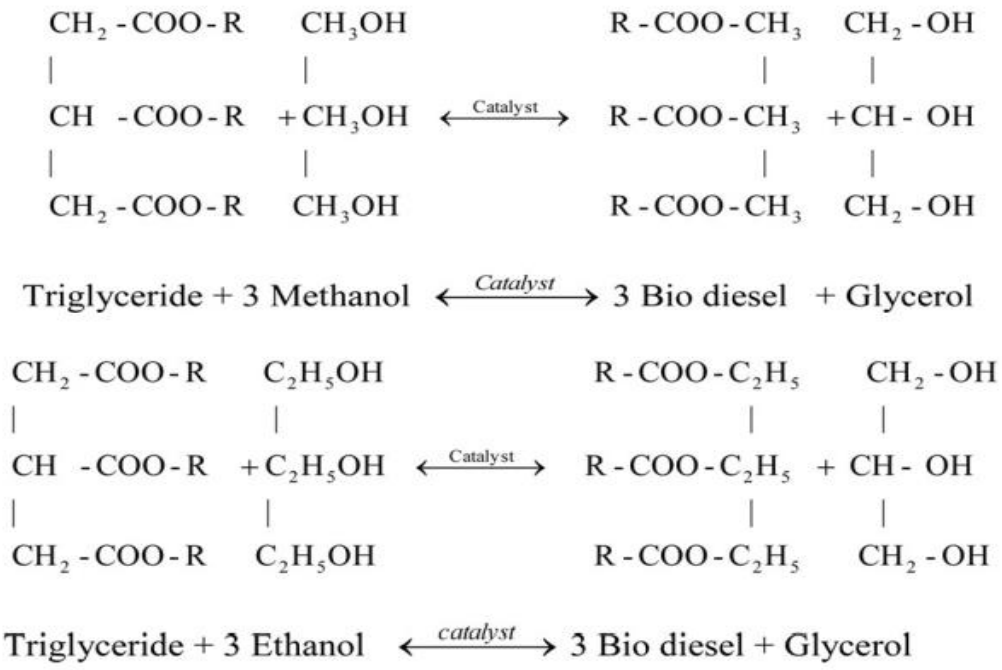

Figure 2.12 Transesterification reaction for biodiesel production (Subramaniam et al., 2013)

2.10.2. Key factors affecting the transesterification reaction

The transesterification process involved in biodiesel production is influenced by a variety of factors. Key elements that impact this process include the duration of the reaction, the molar ratio of alcohol to oil, the temperature and pressure at which the reaction occurs, the type of catalyst used, as well as the levels of water and FFAs existing in the feedstock (Vilas Bôas & Mendes, 2022).

2.10.2.1. Reaction temperature

The temperature at which a reaction occurs plays a significant role in determining its rate. In this context, reactions are typically performed near the boiling point of methanol, which ranges from 60 to 70 ºC, under atmospheric pressure for a designated duration. While the alkaline alcoholysis of vegetable oils is generally executed at temperatures near to the boiling point of the alcohol, it is also feasible to conduct this reaction at room temperature. However, if the temperature surpasses the boiling point of the alcohol, vaporization occurs, leading to the formation of large bubbles that can obstruct the reaction process. This obstruction may result in a reduced yield of biodiesel, as elevated temperatures can enhance the saponification of triglycerides (Demisu, 2021).

2.10.2.2. Ratio of alcohol to oil

The molar ratio of alcohol to vegetable oil is a critical factor influencing conversion efficiency, biodiesel yield, and production costs. The stoichiometric ratio for transesterification is established at 3:1; however, due to the reversible nature of the reaction, a higher molar ratio is necessary to improve miscibility and facilitate better interaction between alcohol molecules and triglycerides. Transesterification operates as an equilibrium-controlled process, where utilizing an excess of alcohol can lead to complete conversion, and the alcohol can be readily recovered. Furthermore, increasing the alcohol-to-oil ratio enhances both the yield and purity of biodiesel, resulting in a more efficient conversion of alkyl esters in a reduced timeframe. The optimal molar ratio is also contingent upon the type of catalyst employed; for alkali-catalyzed transesterification, a ratio between 5:1 and 12:1 is typically recommended to achieve maximum ester conversion. In contrast, when utilizing an acid catalyst, the ideal conversion is achieved with sulfuric acid at a molar ratio of 30:1. The findings related to various vegetable oils, where a 6:1 molar ratio is commonly adopted in industrial processes to yield biodiesel exceeding 98%. Notably, variations in the alcohol to oil ratio do not significantly impact the acid, saponification, or iodine values of the resulting esters (Naseef & Tulaimat, 2025).

2.10.2.3. Catalyst concentration

A catalyst plays a vital role in enhancing the transesterification process and increasing the yield of the reaction. Among the various types of catalysts, alkali metal alkoxides have demonstrated superior effectiveness in facilitating transesterification compared to their acidic counterparts. Specifically, KOH and NaOH are recognized as the most prevalent and efficient catalysts employed in biodiesel production. Research indicates that a catalyst concentration ranging from 0.5% to 1% (w/w) can achieve conversion rates of 94% to 99% into vegetable oil esters. Notably, increasing the catalyst concentration beyond this range does not significantly improve conversion rates; rather, it incurs additional costs due to the necessity of removing the catalyst from the reaction mixture post-reaction. Consequently, when dealing with oils that have low FFA and moisture content, the transesterification process utilizing base catalysts is considerably faster than that using acid catalysts, making it the preferred choice for commercial applications on an industrial scale (Mandari & Devarai, 2022).

2.10.2.4. Mixing intensity

During the transesterification process, the initial formation of a biphasic liquid system occurs due to the limited miscibility of oils and alcohols, necessitating dynamic mixing to enhance the contact area between these two immiscible phases. The efficiency of the alcoholysis reaction can be significantly improved by increasing the agitation intensity within the reactor. A critical aspect of this process is the mass transfer of biodiesel from the oil phase to the alcohol-oil interface, which can be a limiting factor in the rate of the alcoholysis reaction due to its heterogeneous nature. Research has indicated that the mixing effect is a crucial determinant of the reaction's slow kinetics. Once phase separation is no longer present, the importance of mixing diminishes. Understanding the influence of mixing on the kinetics of the transesterification process is essential for scaling up and designing the process; thus, enhanced mixing speeds facilitate transesterification reactions, and variations in mixing intensity are anticipated to alter the kinetics of these reactions (Mandari & Devarai, 2022).

2.10.2.5. Effect of FFA and moisture

Impurities present in oil play a significant role in influencing the efficiency of converting crude oil into biodiesel. The primary factors that determine the suitability of vegetable oils for the transesterification process are the levels of FFA and moisture content. An increase in moisture within the oil can lead to a rise in FFA levels. For the transesterification reaction to proceed effectively, it is essential that the FFA content remains below 3%. A higher acidity in the oil correlates with reduced conversion efficiency. Even a minimal presence of 3% water in the reaction mixture can diminish glycerol yield by depleting the catalyst. Other researchers have emphasized the necessity of utilizing oil that is nearly devoid of moisture and contains less than 0.5% FFA. Oils with elevated FFA concentrations are typically treated with an immiscible basic glycerol phase, which serves to neutralize the FFAs, allowing them to migrate into the glycerol phase (Chozhavendhan et al., 2020).

2.10.3. Characteristics and attributes of biodiesel

The characteristics and attributes of biodiesel must conform to established international standards. These standards encompass the ASTM D6751 and EN 14214 regulations for biodiesel. The defining features of biodiesel are primarily determined by its physicochemical properties, which include calorific value, density, viscosity, cetane number, copper corrosion, pour point, sulfur

content, flash point, ash content, cloud point, acid value, water content, carbon residue, distillation range, phosphorus, glycerin, and oxidation stability. The physical and chemical properties of biodiesel are fundamentally influenced by the type of feedstock used and the composition of their fatty acids (Singh et al., 2019).

2.10.3.1 Density

Density is a significant property, as it is closely linked to other essential fuel characteristics, including cetane number and calorific value. The density of a fuel is heavily influenced by factors such as storage conditions, fatty acid composition, and water content. Furthermore, since the volume of fuel injected into a diesel engine's combustion chamber is determined by its density, any variations in density will have a direct impact on engine performance and fuel consumption. Moreover, density plays a crucial role in determining injection onset, injection pressure, and the characteristics of the fuel spray, all of which influence combustion efficiency and emissions (Sarin et al., 2021).

2.10.3.2. Viscosity

Biodiesel viscosity is a critical fuel property in that it determines the ease at which the fuel can flow, particularly at lower temperatures, and it has a strong impact on injection performance and atomization. Biodiesel's kinematic viscosity can be profoundly higher compared to conventional diesel because its larger and more complex fatty acid methyl ester molecules impede the fuel's fluidity when cold and can compromise the spray behavior in fuel injectors, such as longer droplet breakup times and a less effective atomization process. The acceptable kinematic viscosity for biodiesel in standard specifications generally falls within a range of 1.9-6.0 mm^2/s according to ASTM D445 or 3.5 to 5.0 mm^2/s under EN ISO 3104 conditions (Feng et al., 2025).

2.10.3.3. Flash point (FP)

Flash point is the minimum temperature at which biodiesel evaporates to produce a flammable mixture of vapour and air, and it is a critical safety-related parameter that determines how fuel can be stored, handled, and transported. In general, biodiesel exhibits a much higher flash point compared with conventional diesel, generally within a range of 145–175 °C, owing to its higher molecular weight and lower volatility, which make it safer during storage and reduce the likelihood of accidental ignition (Boichenko et al., 2025). Some works have reported that the flash point for

biodiesel from palm oil was approximately 157.9 °C, as obtained by the ASTM D93 method, which shows its relatively lower flammability (Balfas et al., 2024).

2.10.3.4. Cold flow properties

The cold flow properties of biodiesel refer to the behaviors or characteristics exhibited by biodiesel when subjected to low-temperature conditions. These properties are typically represented by the parameters of pour point, cloud point, and cold filter plugging point. The pour point (PP) is a physical property that measures the lowest temperature at which the fuel can still flow from one location to another. At this temperature and below, crystalline solids begin to agglomerate, resulting in the formation of a gel phase; consequently, the fuel loses its fluidity and ceases to flow. This property is often associated with the freezing or melting point of a fluid mixture. The international standard testing methods for the pour point parameter are ASTM D97 and EN ISO 3016 (Pradana et al., 2024).

Cloud Point is the temperature at which wax crystals begin to appear in the biodiesel and the fuel starts to become cloudy. CP is a vital cold-flow property because crystals may obstruct the flow of fuel, which seriously influences engine performance under low temperatures. Biodiesels prepared from feedstocks that have a high proportion of saturated fatty acids have higher cloud points, while unsaturated fatty acids have the effect of lowering the CP value, thereby enhancing operability in cold conditions (Bouaid et al., 2024). The Cold Filter Plugging Point is defined as the lowest temperature at which a biodiesel can pass through a standard filtration device under cooling conditions. CFPP has become a common basis for the practical use of biodiesel in engines under winter conditions. High values indicate that filter clogging and flow problems may be inevitable, whereas in contrast, a low CFPP guarantees undisturbed fuel delivery. Many factors such as fatty acid composition of the biodiesel, source of feedstock, and cold-flow improvement additives largely contribute to CP and CFPP (Bouaid et al., 2024).

2.10.3.5. Cetane number

The cetane number (CN) serves as a crucial measure of the ignition quality for both diesel and biodiesel fuels, indicating the time lag between the injection of fuel and the initiation of combustion. An elevated CN is associated with a reduced ignition delay, resulting in more efficient engine performance and improved combustion completeness, which in turn minimizes the emission of unburned hydrocarbons and smoke. Biodiesel generally displays CN values that

surpass those of traditional diesel, attributable to its oxygen-rich composition and the inclusion of long-chain fatty acid methyl esters, which improve its auto-ignition properties (Boichenko et al., 2025).

2.10.3.6. Heating value and carbon residue

One of the essential characteristics employed to assess the viability of using a fuel for internal combustion engines is the fuel's heating or calorific value, as this property directly influences the engine's power output. Typically, the calorific value of a fuel depends on its chemical composition, including elements such as carbon (C), hydrogen (H), and oxygen (O). The constituents of biodiesel, known as fatty acid methyl esters (FAMEs), exhibit variations in their chemical compositions and, as a result, their heating values can differ significantly. An increased heating value indicates a greater energy output, which has a direct effect on engine performance, fuel usage, and thermal efficiency. Biodiesel typically possesses a marginally lower heating value compared to traditional diesel because of its elevated oxygen content; however, it still delivers adequate energy for effective engine functioning. (Pham et al., 2020). The carbon residue of biodiesel, which is indicative of a deposit-forming tendency, is noticeably higher compared to conventional diesel due to a strong correlation with free fatty acids, higher unsaturated fatty acids, glycerides, soaps, polymers, and inorganic impurities (Thangaraj & Solomon, 2020).

2.10.3.7. Oxidation stability

Oxidation stability denotes the ability of biodiesel to resist chemical degradation when subjected to oxygen over an extended period. Throughout storage, biodiesel may interact with oxygen, resulting in the production of peroxides, acids, and polymers, which can lead to increased viscosity, sediment formation, and potential injector blockages in engines. Generally, biodiesel exhibits lower oxidation stability compared to petroleum diesel due to the presence of unsaturated fatty acid methyl esters, which are more susceptible to autoxidation. Various factors, including feedstock composition, the degree of unsaturation, the presence of natural antioxidants, and storage conditions, significantly affect oxidation stability. It is essential to maintain sufficient oxidation stability to guarantee long-term fuel quality, engine dependability, and adherence to standards such as EN 14214 (Rashed et al., 2015).

2.10.3.8. Lubrication properties

Biodiesel demonstrates enhanced lubrication properties in comparison to conventional diesel, which can improve engine efficiency. Nevertheless, these attributes may also result in the buildup of deposits, challenges with cold flow, and filter obstructions, significantly affected by elements such as degradability, glycerol concentration, and the existence of various impurities. The elevated lubricity linked to biodiesel can diminish friction losses, consequently enhancing brake effective power (Rajendran et al., 2023).

2.10.3.9 Acid value (AV)

Acid value, also known as neutralization number, describes the amount of free fatty acids in a fuel. Free fatty acids are naturally occurring saturated or unsaturated mono-carboxylic acids not attached to glycerol. The higher the AV, the greater the quantity of FFA; it is usually expressed as milligrams of KOH needed to neutralize one gram of FAME. An increase in acid value in diesel or biodiesel could result in serious corrosion in the engine fuel-supply system (Thangaraj & Solomon, 2020).

2.11. Research Gap

Despite the promising potential of RCCI engines in achieving high thermal efficiency and significantly reducing PM and NOx emissions, there are still research gaps.

1. Lack of studies using gasoline-n-butanol blends as LRF and biodiesel-diesel blends as HRF in RCCI.

- Gap: Research focuses mainly on gasoline-diesel and gasoline-biodiesel combinations; very few studies have been conducted with fuel combinations including both oxygenated alcohol (n-butanol) and biodiesel. (Addressed in the present work)

2. Limited investigation RCCI operation at medium to high engine speeds (1800-2800 rpm) and 80% load using alterative oxygenated fuels.

- Gap: Most RCCI research focuses on lower speeds and partial load, with very limited works at higher loads where combustion instability and phasing challenges are more severe. (Addressed in the present work)

3. Insufficient application of optimization methods such as Response Surface methodology for RCCI engine using alternative fuel blends.

- Gap: Most RCCI studies rely on trial and error experimentation and do not employ statistical optimization techniques to determine optimal fuel ratios and operating conditions. (Addressed in the present work)

4. limited long-term analysis of injector durability and deposit formation when using oxygenated alcohols and biodiesel blends at higher loads.

- Gap: Long-term effects such as injector fouling, carbon deposition, and material compatibility 80% load with oxygenated fuels remain largely unexplored. (Recommended for future work)

CHAPTER THREE

MATERIAL AND METHODS

This research is primarily focused on experimental investigations. To achieve the objectives of the study, a structured methodology was adopted, encompassing activities such as biodiesel production and optimization, biodiesel characterization, development of a control mechanism for the port injection system, modification of the CI to RCCI mode, and experimental testing on the RCCI engine. Various materials, including consumables and non-consumables, as well as equipment and instruments were utilized at different stages of the methodology. This chapter outlines the materials and equipment used and provides a concise description of the step-by-step procedure followed. The activities undertaken at each stage are illustrated in the flowchart provided below (Fig.3.1).

3.1. Materials

Materials play a pivotal role in any experimental investigation, as they provide the essential data required for thorough analysis. Before embarking on an experimental study, it is imperative to acquire a comprehensive understanding of the materials necessary for the experiment, including their operational principles, range, and accuracy. This section delineates the various tools employed in the experimental inquiry, accompanied by appropriate illustrations. The primary objectives of this research include a CI engine modification, the synthesis and optimization of biodiesel, and the implementation of a modified engine. The materials utilized in this study encompass an Arduino board, fuel injector, potentiometer, electronic fuel pump, n-butanol, gasoline, funnel separators, diesel, beakers, and analytical instruments such as a GC-MS analyzer and FTIR analyzer. Detailed listings of the materials and equipment employed for biodiesel production and experimental testing can be found in Tables 3.1 and 3.2. Additionally, Minitab software was utilized for numerical analysis.

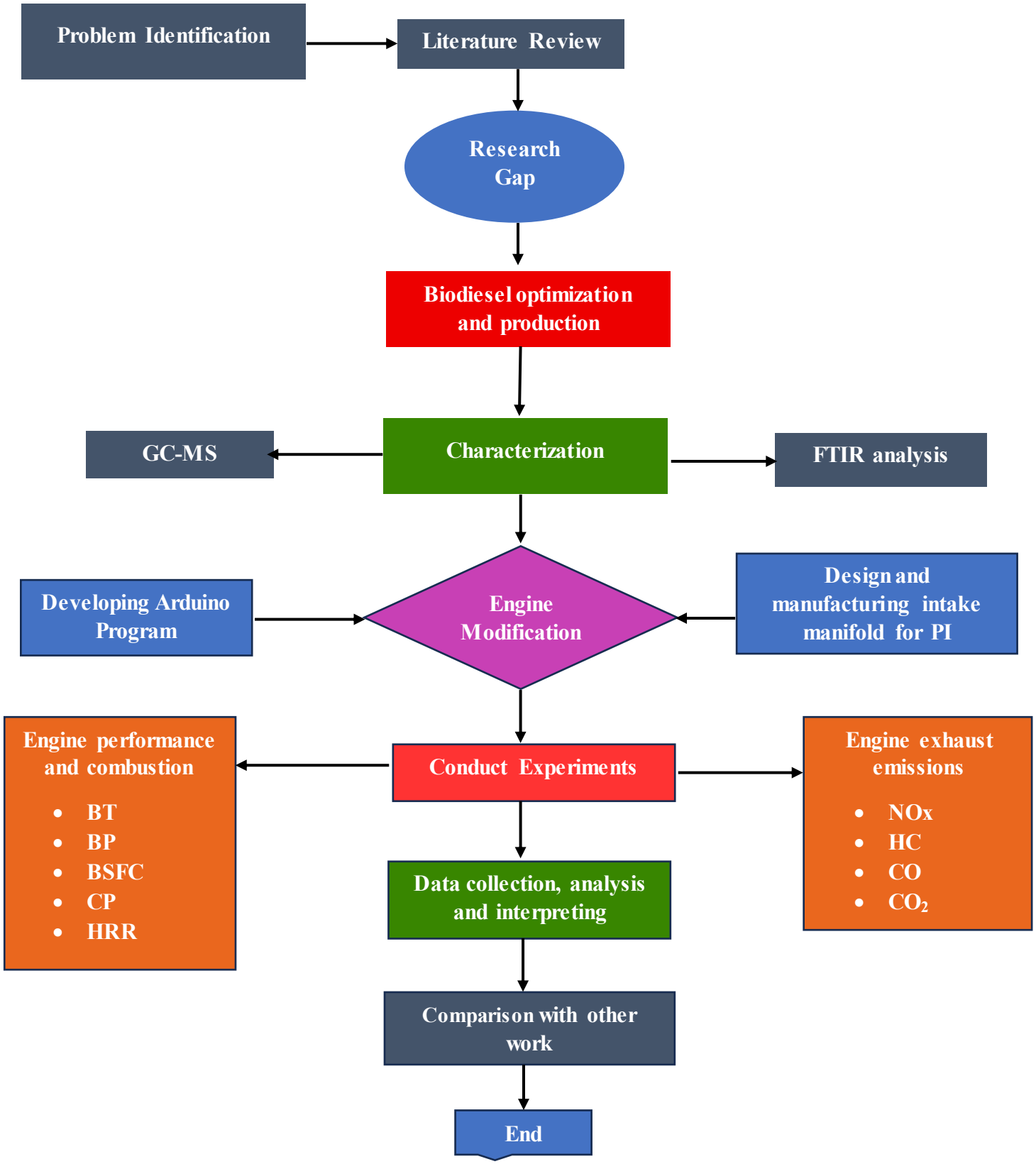

Figure 3.1 Flowchart illustrating the steps of the methodology

Table 3.1 Equipment and material list for producing and characterizing biodiesel

No.	Items	No.	Items
1	Cottonseed oil	11	Aluminum foil
2	Potassium hydroxide	12	Beakers with different size
3	Methanol	13	Thermometer
4	Absolute ethanol	14	Conical flasks
5	Sodium thiosulfate	15	Hot plate with magnetic stirrer
6	phenolphthalein	16	Digital balance
7	Chloroform	17	Funnel separators
8	Hydrochloric acid	18	Measuring cylinder
9	Starch soluble	19	Burette
10	Distill water	20	Glove

Table 3.2 Equipment and material list used in experimental test

No.	Items	No.	Items
1	Biodiesel	7	Electronic fuel pump
2	Diesel	8	Gasoline fuel injector
3	Gasoline	9	Engine test rig
4	n-butanol	10	Exhaust gas analyzer
5	Ultrasonicator	11	Data acquisition system
6	Arduino board with assembly		

3.2. Biodiesel production and optimization

3.2.1. Biodiesel production

Biodiesel was produced from CSO and methanol using KOH as an alkali catalyst (KOH) via the transesterification process. Before the transesterification reaction, the acid value of the feedstock was determined by a standard titration method with 0.1 M KOH solution and phenolphthalein as the indicator, to quantify the FFA content. This pre-test made sure the FFA level was within acceptable limits for a direct base-catalyzed transesterification to avoid excessive saponification. Transesterification is a chemical reaction employed to synthesize biodiesel through the interaction of triglycerides, which are derived from vegetable oils or animal fats, with an alcohol, typically

methanol or ethanol, facilitated by a catalyst such as KOH or NaOH. This reaction effectively transforms triglycerides into FAMEs, widely recognized as biodiesel, while simultaneously producing glycerol as a secondary product (Naseef & Tulaimat, 2025). This procedure was conducted in the laboratory of the chemistry department at Adama Science and Technology University, located in Adama, Ethiopia. The general procedures for biodiesel production across all experimental runs were outlined as follows:

- A precise quantity of CSO was measured and transferred to a beaker.
- The oil was preheated to 60 °C (see Fig.3.2).
- A specified amount of KOH was weighed and dissolved in the measured volume of methanol.
- The prepared KOH-Methanol solution was added to the pre-heated oil in a beaker.
- The beaker was positioned on the hot plate with a magnetic stirrer maintained at 60 °C, operating steadily at a speed of 500 rpm (see Fig.3.3).
- The reaction was allowed to proceed for predetermined time.
- After the reaction, the mixture was left in a separator funnel for 24 hours to enable phase separation: the upper phase consisted of biodiesel while the bottom layer contained glycerol (see Fig. 3.4).
- Subsequently, the methyl ester was washed multiple times with hot distilled water to remove impurities such as glycerol, methanol, and residual catalyst.
- Finally, the washed biodiesel was dried at 130 °C for one hour to eliminate any remaining water. After drying, the pure biodiesel was collected and biodiesel yield was determined using Eq. (3.1) (Razzaq et al., 2022). Fig. 3.5 shows the final collected pure biodiesel for each experimental run. Figure 3.6 & 3.7 presents a visual and schematic depiction of the process used to produce biodiesel from CSO.

$$(\%)\ \text{CSO Biodiesel yield} = \frac{\text{Volume of biodiesel obtained}}{\text{Volume of cottoseed oil comsumed}} \times 100 \qquad (3.1)$$

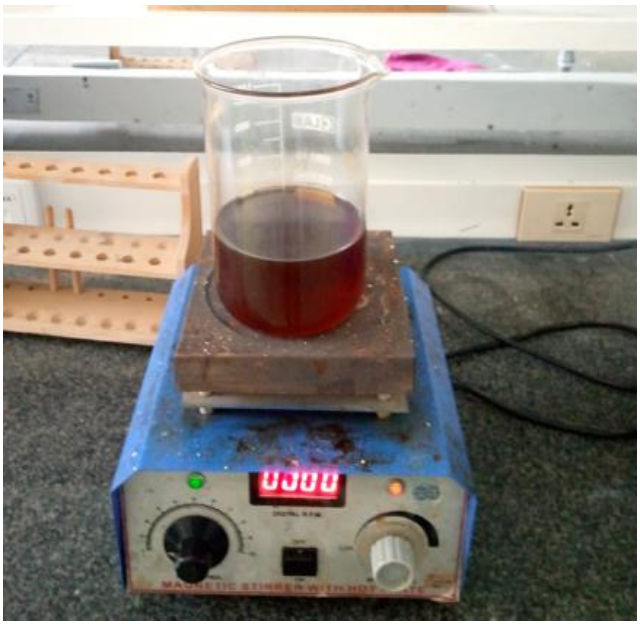

Figure 3.2 Preheating of oil

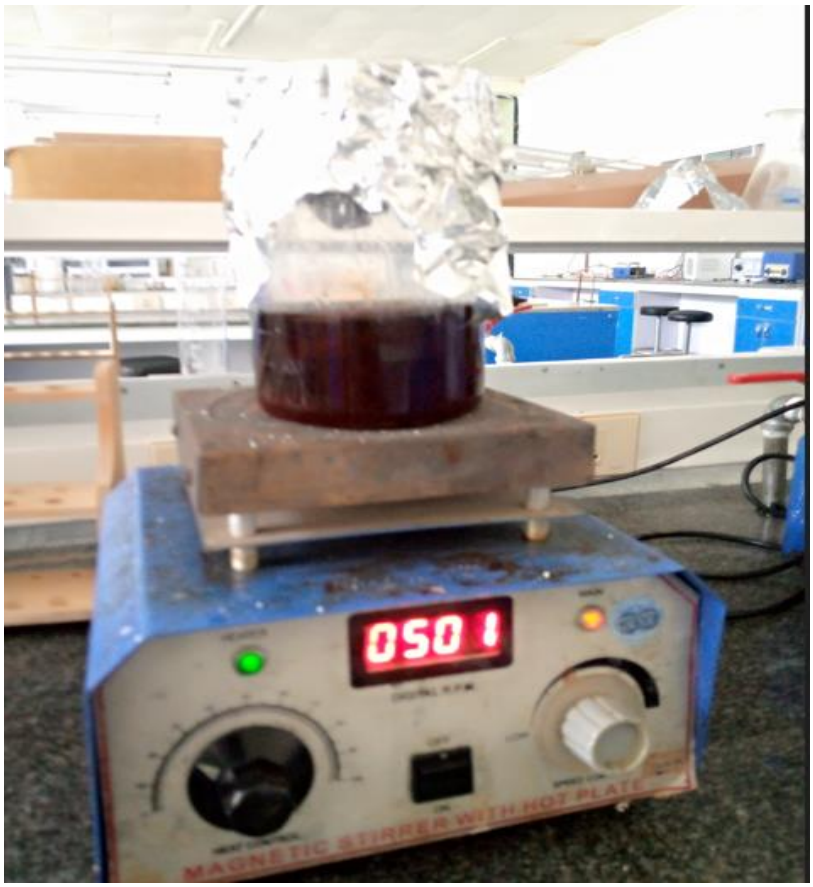

Figure 3.3 Heating the mixture of methanol and KOH along with oil

Figure 3.4 Glycerol and biodiesel separation in a separator funnel

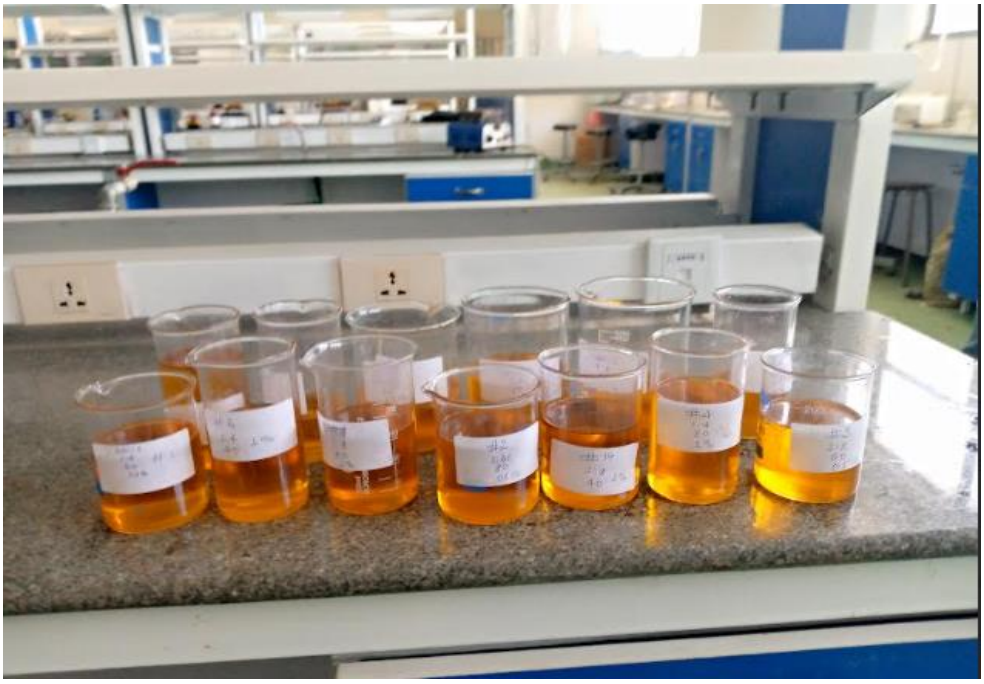

Figure 3.5 Final collected pure biodiesel samples obtained for each experimental run generated by the RSM design

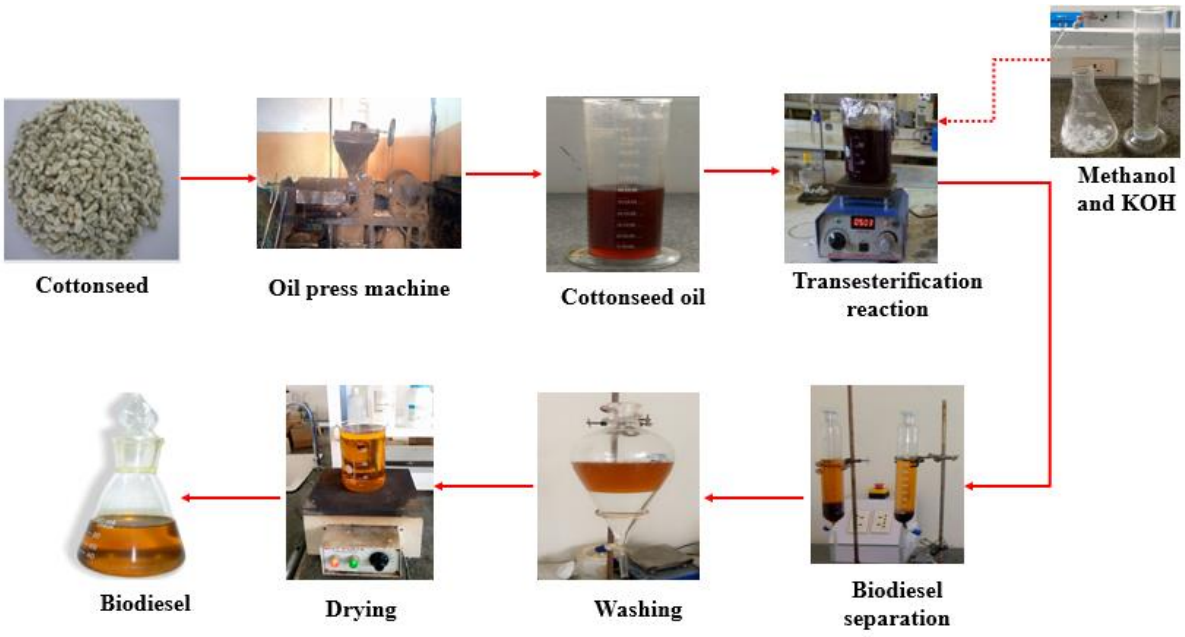

Figure 3.6 Pictorial view of biodiesel production process from CSO

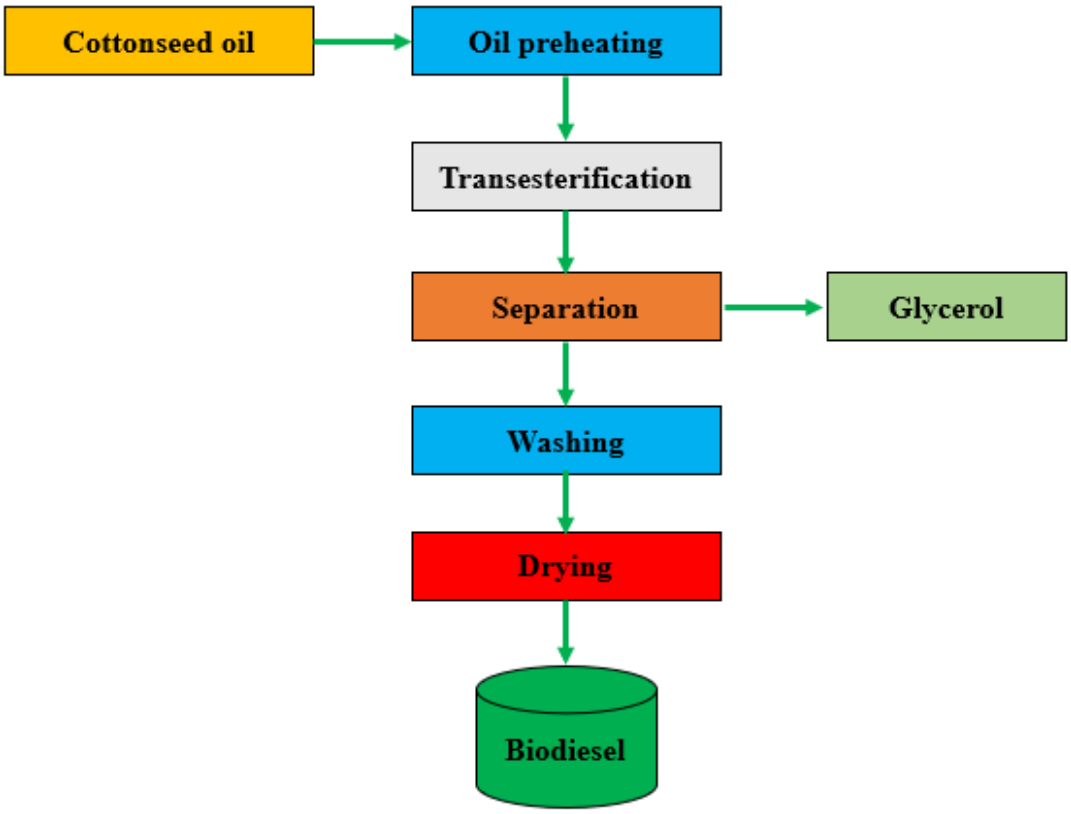

Figure 3.7 Schematic biodiesel production process from CSO

3.2.2. Optimization of biodiesel using RSM

RSM comprises a set of statistical and mathematical tools used to model and analyze processes where multiple variables influence one or more outputs, with a goal of optimizing these responses. In this study, a Box-Behnken Design under RSM with three independent variables was utilized to evaluate the response and identify the optimal combinations of parameters. The percentage yield of CSO biodiesel yield was primarily influenced by the selected process variables. Significant changes in methyl ester were observed when all three factors were varied. By optimizing these parameters, it is possible to reduce both time and energy consumption, while achieving maximum biodiesel yield. Therefore, RSM was employed to improve methyl ester yield production from CSO. The input variables examined in this analysis were reaction time, methanol to oil ratio, and catalyst concentration, all of which significantly influenced the output response. Drawing from earlier investigations (Elango et al., 2019; Razzaq et al., 2022; Sambasivam et al., 2023), appropriate ranges for these process variables were established. Table 3.3 outlines the selected ranges for the transesterification process, and the flowchart in Fig. 3.8 illustrates the steps involved in the RSM analysis. Eq. (3.2) was used to determine the biodiesel yield under varying operational conditions.

$$Y = X_0 + \sum_{i=1}^{k} X_i A_i + \sum_{i=1}^{k} X_{ii} B^2 i + \sum_{j=i+1}^{k} . \sum_{i=1}^{k} X_{ij} C_{ij} \quad (3.2)$$

Where Y is biodiesel yield; A_i, B_i, and C_i are the input variables; X_0 and X_i represent intercept and first-order regression coefficient, respectively; k is the total number of experiments and X_{ii} is the quadratic regression coefficient.

Table 3.3 Range of process variables used in Box Behnken design

Input variables	Coded	High	Average	Low
Reaction duration (min.)	A	80	60	40
Concentration of catalyst (wt.%)	B	1.5	1	0.5
Methanol to oil ratio (vol/vol)	C	1:8	1:6	1:4

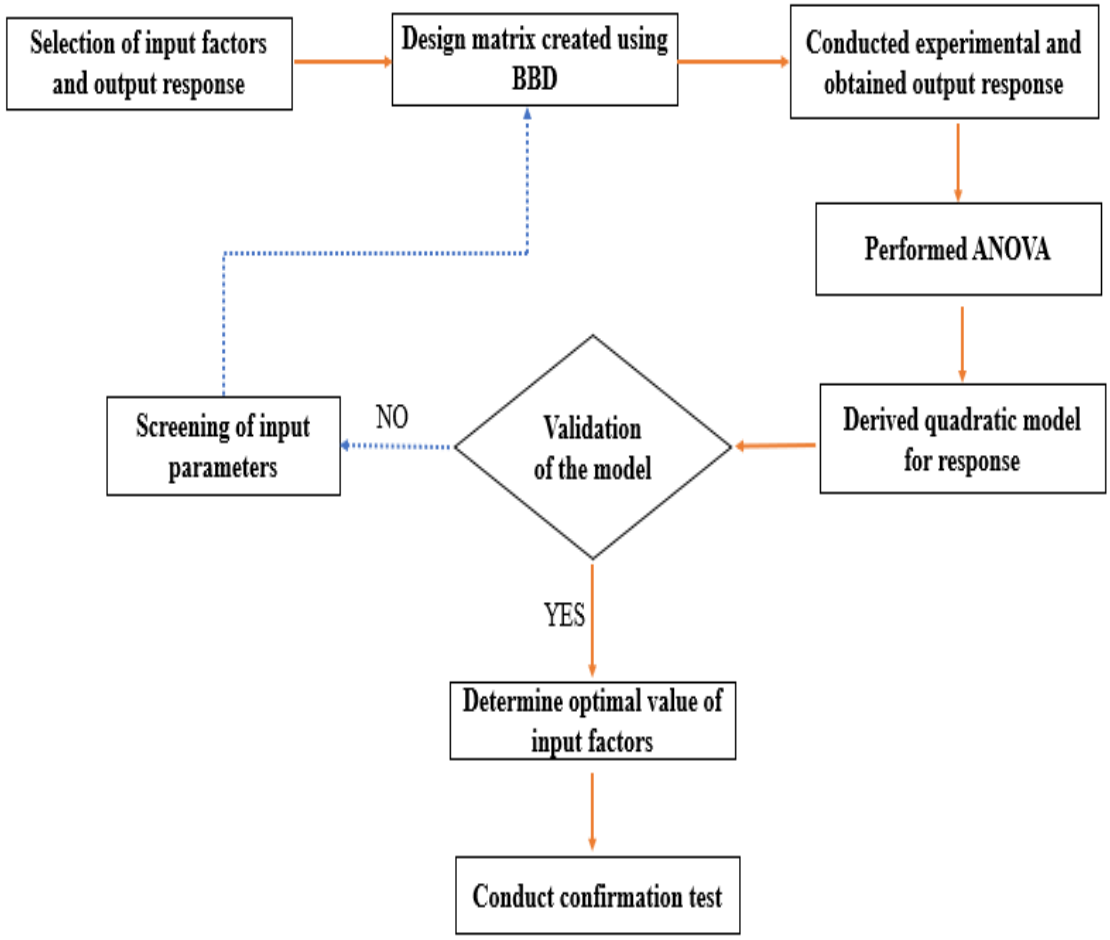

Figure 3.8 Response surface methodology flowchart

3.2.3. Artificial neural network (ANN) framework for modelling

ANN serves as a fundamental element in machine learning frameworks, adept at capturing complex relationships within data to facilitate predictions and decision-making processes. Within the ANN, neurons are interconnected through synaptic weights, which enable the storage of information (Selvan et al., 2018). In this study, catalyst concentration, reaction time, and the methanol to oil ratio were utilized as independent input variables, derived from a dataset comprising 15 samples. Building on insights from prior research (Agu et al., 2022; Razzaq et al., 2023), the investigation employed the TRAINLM training function, LEARNGDM adaptation learning function, and mean squared error (MSE) as the performance metric, utilizing a feed-forward back-propagation network. The ANN model, structured with three input layers, ten hidden layers, and a single output layer, was trained using the Levenberg-Marquardt algorithm, incorporating the TANSIG transfer function across the layers. The output response, representing

biodiesel yield, was determined based on the results of the 15 experimental input factors, with the ANN implemented using MATLAB software version R2020a. Fig.3.9 depicts the structure of the artificial ANN employed for forecasting biodiesel production. In the present study, biodiesel yields obtained from experimental work were compared with the predicted yields generated by RSM and ANN models in order to assess their predictive capability. Various statistical metrics have been employed to evaluate the performance of RSM and ANN models. These include the sum of squared errors (SSE), mean squared error (MSE), root mean squared error (RMSE), average absolute relative error (AARE), standard deviation (SD), and the coefficient of determination (R^2). These are standard quantitative metrics that are widely used to evaluate the accuracy and precision as well as the generalization capability of regression-based and neural-network-based models. These are defined by Equations (3.3) to (3.8) (Agu et al., 2024; Muhammad et al., 2022; Selvan et al., 2018). A flowchart showing the steps involved in creating and refining an ANN model is shown in Fig.3.10.

$$\mathrm{SSE} = \sum_{i=1}^{n}\left(X_{ei} - X_{pi}\right)^2 \tag{3.3}$$

$$\mathrm{MSE} = \frac{1}{n}\sum_{i=1}^{n}\left(X_{ei} - X_{pi}\right)^2 \tag{3.4}$$

$$\mathrm{RMSE} = \sqrt{\frac{1}{n}\sum_{i==1}^{n}\left(X_{ei} - X_{pi}\right)^2} \tag{3.5}$$

$$\mathrm{AARE} = \frac{1}{n}\sum_{i=1}^{n}\left|\frac{X_{ei} - X_{pi}}{X_{ei}}\right| \tag{3.6}$$

$$\mathrm{SD} = \sqrt{\frac{1}{n-1}\sum_{i=1}^{n}\left(X_{pi} - \overline{X}_p\right)^2} \tag{3.7}$$

$$R^2 = 1 - \left(\frac{\sum_{i=1}^{n}\left(X_e - X_{pi}\right)^2}{\sum_{i=1}^{n}\left(X_{ei} - X_{av}\right)^2}\right) \tag{3.8}$$

Where n is the total number of experiments and X_p and X_e; the predicted and observed values, respectively, X_{av} is an average value and $\overline{X}_p$ is mean of predicted value.

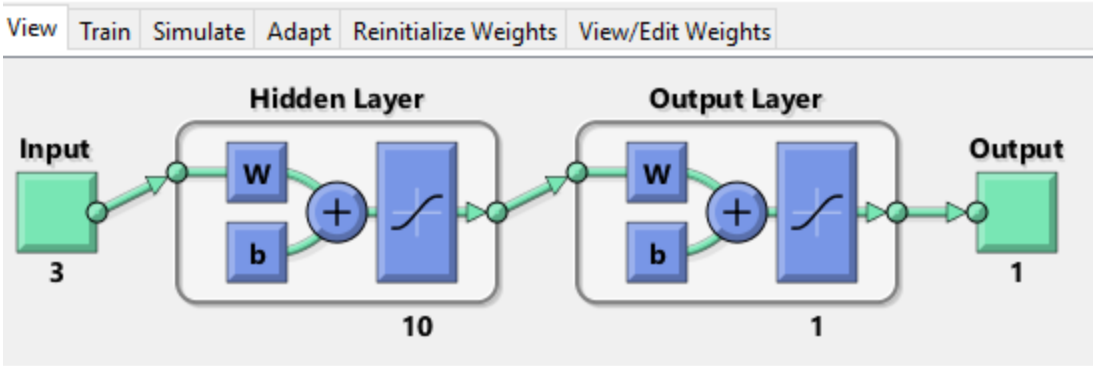

Figure 3.9 ANN structure for predicting biodiesel production

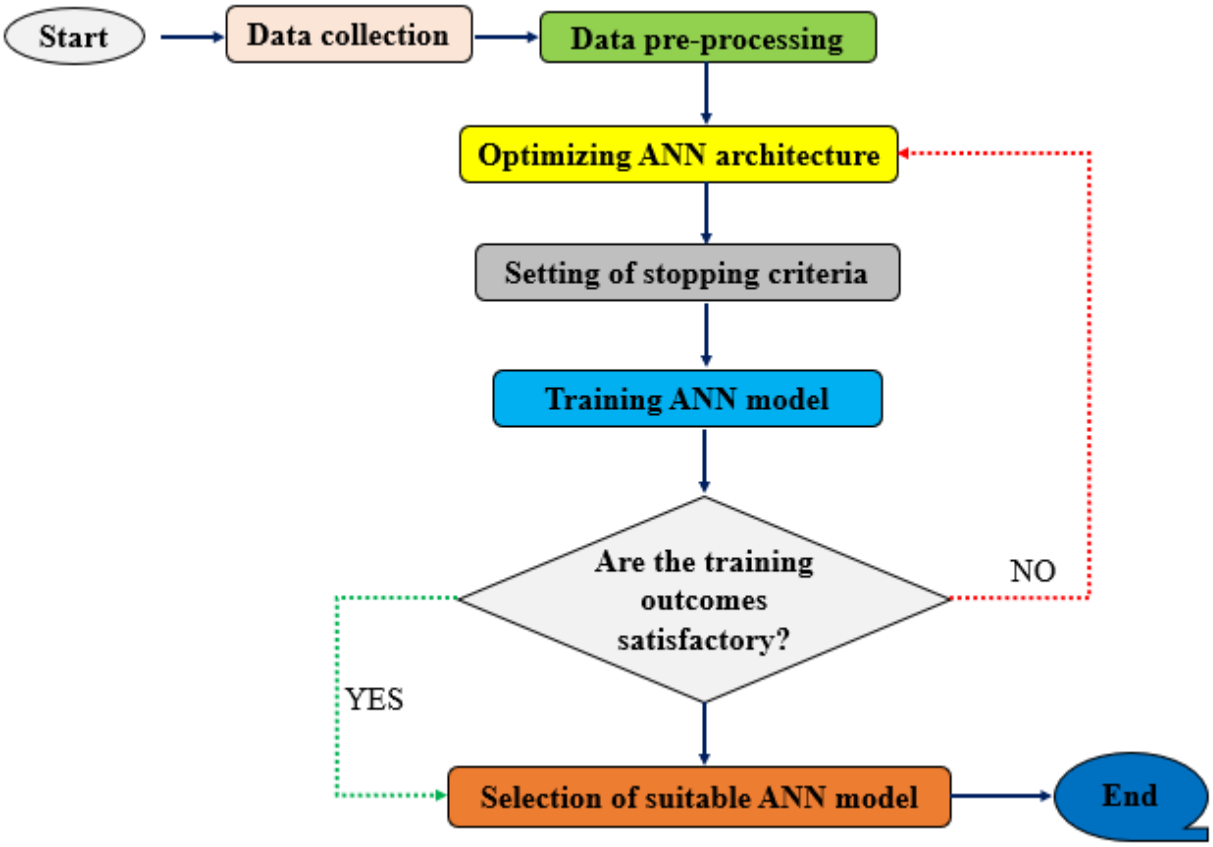

Figure 3.10 A typical flowchart of the ANN model

3.3. Characterization of physicochemical property of biodiesel

Characterization involves the assessment of the physical and chemical properties of both conventional fuels and alternative fuels, such as biodiesel and its blends with Petrodiesel. Prior to evaluating the combustion, performance, and exhaust emissions of the engine, it is crucial to

analyze the physicochemical attributes of biodiesel and its blends with diesel. The characterization of CSO and produced biodiesel was performed following European and ASTM standards. Physicochemical properties including moisture content, density, saponification value, cloud point, acid value, flash point, iodine value, and viscosity, were experimentally measured. The analysis of the percentages and varieties of FAMEs in produced biodiesel from CSO was conducted utilizing a GC-MS analyzer. In the course of the GC-MS analysis, each peak identified in the chromatogram corresponds to a specific FAME found in the sample. The process of identifying particular FAMEs is enhanced by examining the retention times in conjunction with the mass spectra generated during the GC-MS analysis. The calculation of each FAME percentage detected in the produced biodiesel was performed using Eq. (3.9). Fig. 3.11 shows the apparatus used for GC-MS analysis. Additionally, FTIR analysis was conducted to examine the chemical structure found in the produced biodiesel. These characterizations were conducted at EPSE, AASTU, and ASTU in Ethiopia.

$$\text{Percentage of FAME} = \left(\frac{\text{Specific FAME area}}{\text{Area of total FAME}}\right) \times 100 \tag{3.9}$$

Figure 3.11 GC-MS analyzer with data system

3.3.1. Determination of Acid value (AV)

A 25ml mixture of ethanol and diethyl ether was added to 5g of oil or biodiesel sample in a 250ml conical flask. The resulting solution was titrated with 0.1N ethanolic KOH, using five drops of phenolphthalein indicator. Titration was carried out with continuous shaking until a stable pink color appeared, signaling the endpoint. The volume of 0.1N ethanolic KOH consumed during titration was recorded, and the AV was determined using Eq. (3.10).

$$\text{Acid Value } \left({}^{\text{mg KOH}}/_{\text{g}}\right) = \frac{\text{N}\times\text{V}\times 56.1}{\text{W}} \quad (3.10)$$

Where, V is volume of 0.1N ethanolic KOH solution used (mL); N is normality of KOH; W is weight of sample (g); 56.1 is molecular mass of KOH.

3.3.2. Determination of saponification value (SV)

A 2g of oil or biodiesel sample was accurately weighed and placed in a conical flask, followed by the addition of 25 mL of 0.1N ethanolic KOH solution. The mixture was continuously stirred and heated to 70 ^{o}C for 60 min., with a reflux condenser attached. After heating, five drops of phenolphthalein indicator were added to the warm solution. The mixture was then titrated with 0.5M HCl until the pink color disappeared, and the volume of HCl used (Vs) was recorded. A blank test was carried out using the same procedure, and the volume of HCL for the blank (Vb) was also noted. The SV was determined using the Eq. (3.11).

$$\text{Saponification Value (SV)} = \frac{56.1\times\text{N}\times(\text{Vb}-\text{Vs})}{\text{W}} \quad (3.11)$$

Where, Vb is volume of HCl used in the blank (mL); Vs is volume of HCl solution used in the sample (mL); N is normality of HCl; 56.1 is molecular mass of KOH; W is weight of the sample (g).

3.3.3. Determination of iodine value (IV)

0.25 g of oil or biodiesel sample was weighed into a 250 mL conical flask, followed by the addition of 10 mL of chloroform and 30 mL of Hanus solution. The flask was sealed with parafilm and the contents were shaken continuously for 30 min. After this, 10 mL of 15% potassium iodide and 100 ml of distilled water were added, and the mixture was shaken thoroughly. The solution was then titrated with 0.1N $Na_2S_2O_3$ until it turned yellow. At this stage, three drops of starch indicator were added, resulting in blue coloration. Titration continued until the blue color disappeared, and the volume of $Na_2S_2O_3$ used for the sample (Vs) was recorded. A blank was prepared using the same

procedure without a sample, and the volume of $Na_2S_2O_3$ used (Vb) was noted. The IV was determined using the equation below.

$$\text{Iodine Value (IV)} = \frac{12.69 \times N \times (Vb - Vs)}{W} \quad (3.12)$$

Where, N is normality of $Na_2S_2O_3$; W is weight of the sample (g); 12.96 is milliequivalent weight of iodine; Vs is volume of $Na_2S_2O_3$ used for sample (mL); Vb is volume of $Na_2S_2O_3$ used for the blank (mL).

3.3.4. Determination of Moisture content

The empty dish was weighed both with and without the kernel sample, then placed in an oven at 105°C for 7 hours. The weight was measured every 2 hours until constant weight was achieved. Finally, the final weight was recorded and compared with the initial weight. The moisture content was determined using the Eq. (3.13).

$$(\%)\ \text{Moisture content} = \frac{\text{Initial weight of the sample} - \text{Final weight of the sample}}{\text{Initial weight of the sample}} \times 100\% \quad (3.13)$$

3.3.5. Determination of Density

Density is a key property used to characterize both light and heavy fractions of petroleum products and is essential for converting measured volumes to standard temperatures, typically 15ºc or 25ºc. the digital density analyzer, depicted in Fig.3.12, was utilized to measure density. The digital density analyzer consists of a U-shaped oscillating sample tube, an electronic excitation system, and a frequency counting and display unit. It is designed to measure sample temperature accurately during analysis. To perform a measurement, introduce a small sample (approximately 1 to 2 mL) into the clean, dry sample tube using a suitable syringe. Ensure the sample tube is properly filled and free from gas bubbles. The sample should be homogeneous and completely devoid of any bubbles, even small ones. Once the instrument displays a stable reading with four significant figures of density, record the result. If the two measurements differ by more than 0.0002 g/mL, calculate their average. If the difference exceeds this limit, discard both measurements and repeat the analysis with two new test specimens until the specified criteria are meet.

Figure 3.12 Digital density analyzer

3.3.6. Determination of Kinematic viscosity

The viscosity of biodiesel was assessed in accordance with ASTM D445, which outlines the standard procedure for evaluating the viscosity of both transparent and opaque liquids. This assessment utilized a Cannon Fenske glass capillary viscometer tube, as depicted in Fig. 3.13, within a SETA KV-8 viscometer bath. The bath was maintained at a temperature of 40°C, into which the sample fuel was introduced into the capillary viscometer tube. After insertion, the setup was allowed to equilibrate for 30 min. to ensure uniform temperature throughout the bath. The time (t) required for a predetermined volume of liquid to flow through the capillary under the influence of gravity was recorded. Subsequently, the kinematic viscosity was computed by multiplying the recorded time (t) in seconds by the calibration constant (K) specific to the viscometer tube, as specified in the ASTM standard test method for viscosity of transport and opaque liquids (Designation: 71/1/97 D445-06).

$$\text{Viscosity} = K \times t \tag{3.14}$$

Where: k is the viscometer calibration constant (mm^2/s); t is time (s)

Figure 3.13 Kinematic viscosity apparatus

3.3.7. Cloud point (CP) determination

The CP of a petroleum product refers to the specific temperature at which wax crystals become discernible as the fuel is subjected to cooling. To achieve temperature reduction, several mixtures are typically employed, including a combination of ice and water effective up to 10ºC, crushed ice mixed with sodium chloride for temperatures as low as -12ºC, and crushed ice combined with calcium chloride, which can lower temperatures to -26ºC. The determination of the cloud point was conducted through visual inspection for haze in the otherwise clear fuel, while the sample was cooled under meticulously controlled conditions. Continuous monitoring of the sample allowed for the precise recording of the temperature (ºC) at which the initial cloud formation occurred in the fuel.

3.3.8. Determination of Flash point

The determination of the flash point of fuel was conducted utilizing the open cup method. In this procedure, the biodiesel was poured into the cup until it reached a volume of approximately 75 ml, after which the cup was subjected to heating via a Bunsen burner. An external natural gas supply was used to sustain a small open flame, which was periodically moved across the surface of the biodiesel. The moment the flash temperature caused the vapors above the oil to ignite, the corresponding temperature was recorded and designated as the flash point temperature.

3.4. Biodiesel blend preparation

Several studies have been carried out to explore the utilization of biodiesel, both in its pure state and in various blended forms. Research indicates that while pure biodiesel can be employed as fuel, blended options are generally preferred due to their enhanced performance characteristics. Biodiesel can be mixed in varying proportions, with blends such as B5 (95% diesel and 5% biodiesel) and B20 (80% diesel and 20% biodiesel) being among the most prevalent. Many scholars have noted that biodiesel blends at B20 and lower concentrations can operate in engines without necessitating modifications. In the context of this study, cottonseed oil biodiesel was blended with diesel fuel in a B20 formulation, as illustrated in Fig.3.14b. The blending process involved the following steps. First, 800 mL of diesel was measured using a beaker, followed by 200 mL of biodiesel (20% of biodiesel in total volume) measured. The diesel was then poured into a 1-liter container, and the biodiesel was added to the same container. The mixture was shaken for at least wo minutes to ensure proper blending. Finally, the prepared sample was blended using an ultrasonicator cleaner operated at a high-frequency level for 30 min. to achieve uniform suspension. Fig.3.15 below illustrates the process of blending diesel and biodiesel using an ultrasonicator. The same procedure was followed for blending gasoline and n-butanol.

(a) (b)

Figure 3.14 (a) Measured biodiesel and diesel, (b) Biodiesel-diesel blend

Figure 3.15 Photograph of the ultrasonicator used for mixing the fuel blends

3.5. Fuels used for experimental study

ICEs can operate on various fuels depending on their design and intended purposes. This study utilized fuels including gasoline, diesel, n-butanol, and biodiesel, all of which met the required quality standards. In the baseline experiments, diesel fuel was used as primary. With advancement to the RCCI engine mode, a blend of gasoline and n-butanol fuels is utilized for port injection, while B20 (20% biodiesel and 80% diesel) is used for direct injection. For advanced RCCI engine experiments, a consistent fuel ratio of 80% of HRF and 20% of LRF is maintained. The physicochemical characteristics of these fuels are outlined in Table 3.4.

Table 3.4 Physicochemical Characteristics of fuels, properties of biodiesel needed for comparison

Parameter	Gasoline	Diesel	n-butanol	B20
Density @20°C (kg/m^3)	720	840	810	840.5
Viscosity @ 40°C (mm^2/s)	0.7	3.15	2.22	3.4
Cetane number	13	52	15	53.1
Flash point (°C)	-45	69	35	78
Self-ignition temperature (°C)	300	210	342.7	-
Low heating value (MJ/kg)	42.4	42.5	33.8	41.42

3.6. Development of port injection control mechanism

This study employed a direct fuel injection system for diesel-biodiesel blend (B20) delivery, while the intake system was redesigned using CATIA modeling software. Additionally, an injector mounting sleeve was fabricated on a lathe machine to accommodate a supplementary port fuel injector for system integration. The CAD design of the injector mounting sleeve, developed in CATIA, is illustrated in Appendix F. The development of a control mechanism for a port injection was achieved using Arduino and Proteus software. The Arduino was utilized to manage the precise timing and duration of the injector pulses, directly influencing the volume of fuel delivered. Through the generation of pulse width modulation (PWM) signals, the Arduino controlled the injector's open duration during each cycle. The Arduino program is designed to produce PWM signals with variable duty cycles, ensuring synchronization to achieve the accurate volume of fuel delivered. Proteus was employed to simulate and validate the control mechanism prior to its implementation on physical hardware. It enabled the creation of virtual circuits, including microcontroller programming, an actuator (injector), MOSFET, and a potentiometer. By simulating the control system, proteus tested the functionality of the injector, ensuring precise timing and debugging potential issues without risking damage to physical hardware. Fig. 3.16 presents the schematic layout of the port injection control circuit designed in Proteus. Additionally, a photograph of actual port fuel injection system is provided in Appendix F. The MOSFET and potentiometer played key roles enhancing in control and interactivity. The MOSFET functioned as a switch, allowing Arduino to manage the injector by handling currents and voltage beyond the microcontroller's capabilities. Meanwhile, the potentiometer served as a variable resistor, providing real-time input control by generating adjustable voltage signals. It was calibrated with engine speed to determine the appropriate fuel volume for injection. Table 3.5 lists all the components and materials used in the development of the port injection system.

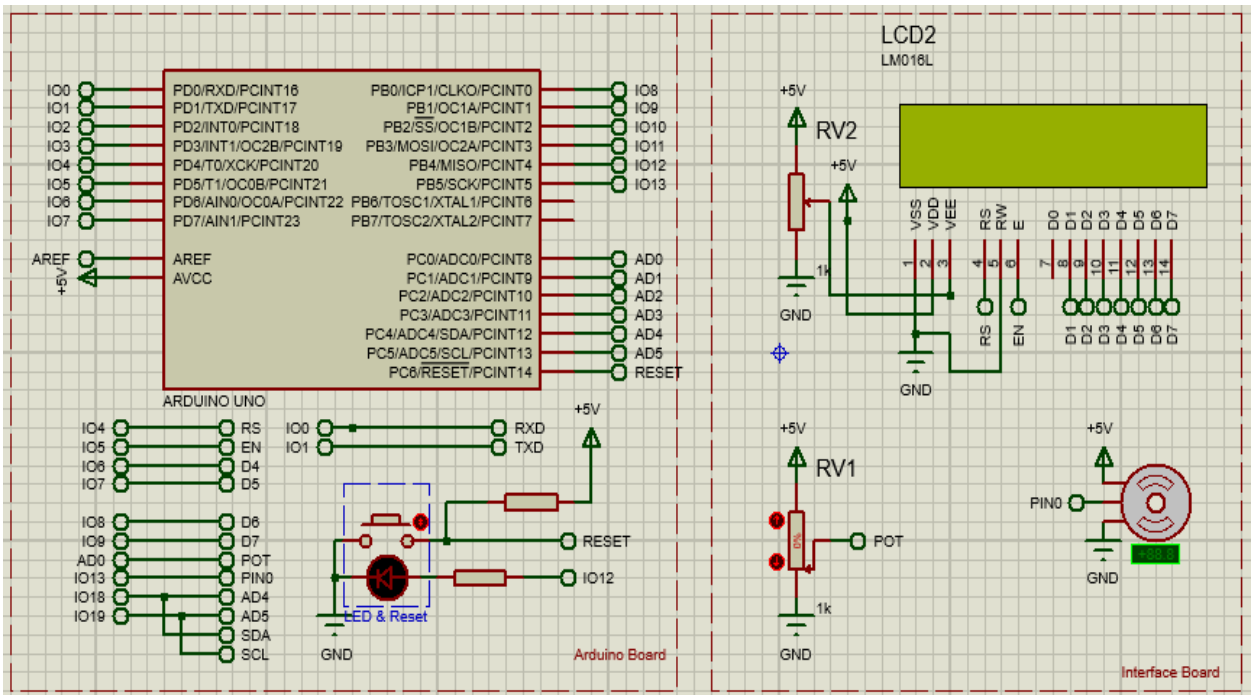

Figure 3.16 Schematic control circuit created by Proteus

Table 3.5 The components and material used in the development of the PI system.

No.	Items	No.	Items
1	Arduino UNO	7	Iron bar
2	Potentiometer	8	Lathe machine
3	MOSFET	9	Fuel hose
4	Gasoline injector	10	Clamps
5	Electric fuel pump	11	Battery
6	Verner caliper		

3.7. Configuration matrix for experimental evaluation

Configuration test matrix outlines the number of tests conducted and serve as guide for carrying out experimental procedures. Table 3.6 presents the experimental test matrix configuration.

Table 3.6 Configuration matrix for experimental evaluation

Engine condition	Fuel used for reference	Fuel for RCCI mode	Parameters
Load (80%) Speed (varying) Compression ratio: (23:1)	Diesel	B20+G25n-b75 B20+G50n-b50 B20+G75n-b25 B20+G85n-b15 B20+G15n-b85	**Combustion parameters** ❖ HRR ❖ CP **Engine performance** ❖ BP ❖ BT ❖ BSFC **Exhaust emissions** ❖ CO ❖ CO_2 ❖ NOx ❖ HC

3.8. Experimental test setup

Engine performance and exhaust emissions tests were carried out at the workshop of the Mechanical Engineering department of Jimma Institute of Technology, using the CT 110 test stand. This system includes a small combustion engine with a single-cylinder, air-cooled CI engine connected to an asynchronous motor, which functions as a dynamometric brake for load application. Table 3.7 presents the technical specifications of the CT 110 test stand used for small combustion engine. Additionally, specification of the asynchronous motor for CT 110 test stand is provided in Table 3.8.

The setup enables the evaluation of engine performance parameters such as BP, BT, and BSFC, along with exhaust emissions analysis. The CT 110 test stand is designed for combustion engine experiments, including air and fuel consumption measurements, as well as assessing engine load and speed behavior. Additionally, the experimental setup requires at least one engine, such as the CT 100.23. The CT 100.15 model pressure transducer, designed for the CT 100.23 engine, utilizes a quartz pressure transducer with a measurement range of 0-100 bar and a maximum allowable pressure of 250 bar. This cylinder pressure transducer is essential for monitoring engine

combustion conditions by measuring cylinder pressure relative to the crank angle. The CT 110 unit includes an electric motor that facilitates both engine startup and deceleration. Additionally, the cooling water circulation system comprises a temperature sensor, flow meter, and circulating pump. The braking unit is connected using an elastic claw coupling, while an intake pressure connector and an exhaust gas temperature sensor are also integrated into the system. Once the engine is installed on the test stand, experiments can be conducted to assess engine performance. The engine is connected to a synchronous motor that functions as a dynamometric brake. The braking unit consists of an air-cooled asynchronous motor equipped with a regenerative feedback system. Torque and speed are controlled via a frequency converter, and braking energy is efficiently fed back into the system for energy-efficient operation. Torque is measured using a suspended brake unit and force sensor. The engine is mounted on a vibration-insulated base plate, which, along with the soft bearing support, minimizes vibrations and eliminates the need for a solid foundation.

The asynchronous motor is initially used to start the engine before transitioning into a braking unit to apply load. The braking power is regenerated into the electrical system. The lower section of the mobile frame houses fuel tanks and a quietening vessel for intake air. Air flow is measured using a nozzle-type flow meter to determine the volumetric flow rate of the intake air, while fuel consumption is monitored by tracking the change in fuel level in a calibrated vertical pipe, allowing accurate measurement of the fuel flow during engine operation. The switch cabinet features digital displays for speed, torque, and various temperature readings, including engine cooling water inlet and outlet, exhaust gas, fuel, and intake air. Pressure gauges provide readings for negative intake pressure and air consumption. All measured data is transmitted directly to a desktop computer via USB, with included data acquisition software. Well-structured instructional material provides fundamental concepts and a step-by-step guide for conducting experiments. Beyond fuel and combustion air consumption measurements, the test stand is used to measure engine torque and speed, with relevant data displayed on digital screens. A photographic of the CT 110 test stand engine test rig setup can be found in Fig.3.17.

Table 3.7 The CT 110 Test Stand for small combustion engine specification

S.no	Parameter	Specification
1	Engine Company, Model	GUNT, CT110
2	No. of cylinder	Single- cylinder
3	Methods of ignition	CI
4	Cooling system	Water-cooled
5	No. of stroke	4-stroke
6	Engine displacement	309 cm^3
7	Compression ratio	23:1
8	Bore*stroke	75 mm*70 mm
9	Power (maximum)	7.50 kW@3000 min^{-1}

Table 3.8 Specification of the Asynchronous motor for CT 110 Test Stand

S.no	Parameter	Specification
1	Motor type	Asynchronous
2	Power output	7.5 kW at 2900 rpm
3	Torque measuring range	-50 to 50 Nm
4	Speed measuring range	0 to 5000 rpm
5	Dimensions (L×W×H)	1450 x 850 x 1880 mm
6	Electrical connection	400V, 50/60Hz, 3 phases

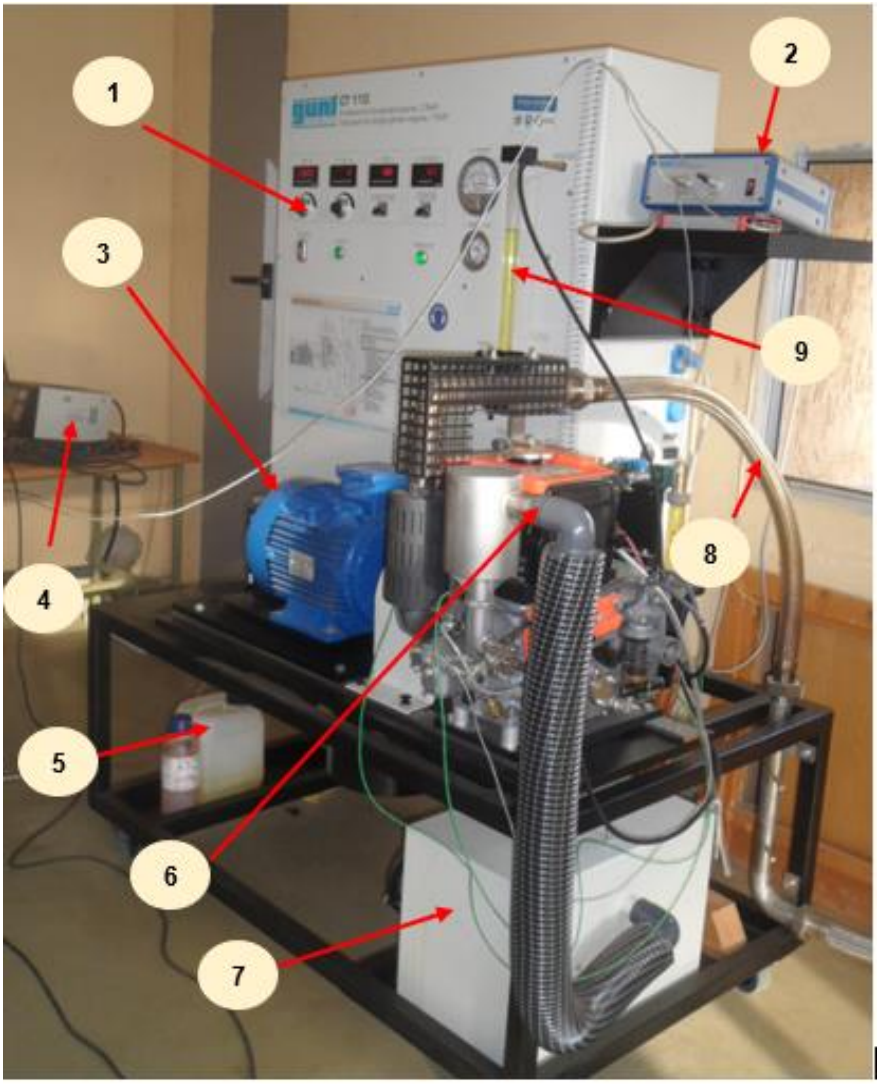

1	Control panel	2	MAP: TDC sensor	3	Dynamometer
4	Exhaust gas analyzer	5	Fuel tank	6	Intake air connection
7	Air stabilization tank	8	Exhaust gas line	9	Fuel flow meter

Figure 3.17 Engine test rig setup

The CI engine has been modified into an RCCI engine, as illustrated in Fig. 3.18. In this RCCI configuration, a gasoline/n-butanol fuel blend is supplied through PI using a separate fuel tank, an electronic fuel pump, and an electronic port injector, while a biodiesel–diesel blend (B20) is delivered via DI. The port-injected fuel mixture consisted of three volume-fraction combinations of gasoline and n-butanol: 25% gasoline and 75% n-butanol (G25n-b75), 50% gasoline and 50% n-butanol (G50n-b50), and 75% gasoline and 25% n-butanol (G75n-b25). These percentages refer

only to the composition of the fuel supplied through the intake port, whereas the DI fuel remained fixed as B20 under all test conditions. The LRF mixtures were blended and made up 20% of the total fuel, while the remaining 80% was the biodiesel-diesel blend (B20) used in direct injection for RCCI engine mode investigation. The blended LRF fuel was supplied to the PI by an in-tank electronic fuel pump, with injection volume controlled by the programmed Arduino board microcontroller. The investigations were conducted at steady load, with varying engine speed, and different LRF ratios in RCCI mode. For the baseline tests, the engine operated at a constant load, with speed variations, and using only diesel fuel. The tests were conducted within a speed range of 1800 to 2800 rpm. In all experiments, the start of injection timing for biodiesel-diesel blend fuel was consistently set at 14°CA before TDC. The premixed ratio (rp) is defined as the proportion of energy contributed by the port-injected fuel to the total fuel energy, as described in Eq. 3.15.

$$rp = \frac{m \times LHV_{G-nb}}{M \times LHV_{B20} + m \times LHV_{G-nb}} \tag{3.15}$$

Where: LHV is the lower heating value fuel; M is the mass flow rates of HRF; m is the mass flow rates of LRF and G-nb for the gasoline/n-butanol blend.

The cylinder pressure data recorded during the compression and expansion strokes of the engine cycle offered quantitative insights into the combustion process. This data was utilized to determine the heat release rate (HRR) during the combustion, which was calculated by applying the first law of thermodynamics applied to a single-zone model, as expressed in Eq.3.16 (Gad et al., 2021).

$$HRR(\theta) = \left(\frac{\gamma}{\gamma-1} \times P(\theta) \times \frac{dV(\theta)}{d\theta}\right) + \left(\frac{1}{\gamma-1} \times V(\theta) \times \frac{dP(\theta)}{d\theta}\right) \tag{3.16}$$

Where: HRR is heat release rate, γ is the specific heat ratio (Cp/Cv), θ is crank angle, P is instantaneous cylinder pressure, V is instantaneous cylinder volume, $\frac{dV(\theta)}{d\theta}$ is rate of change of cylinder volume with respect to crank angle, and $\frac{dP(\theta)}{d\theta}$ is rate of change of cylinder pressure with respect to crank angle

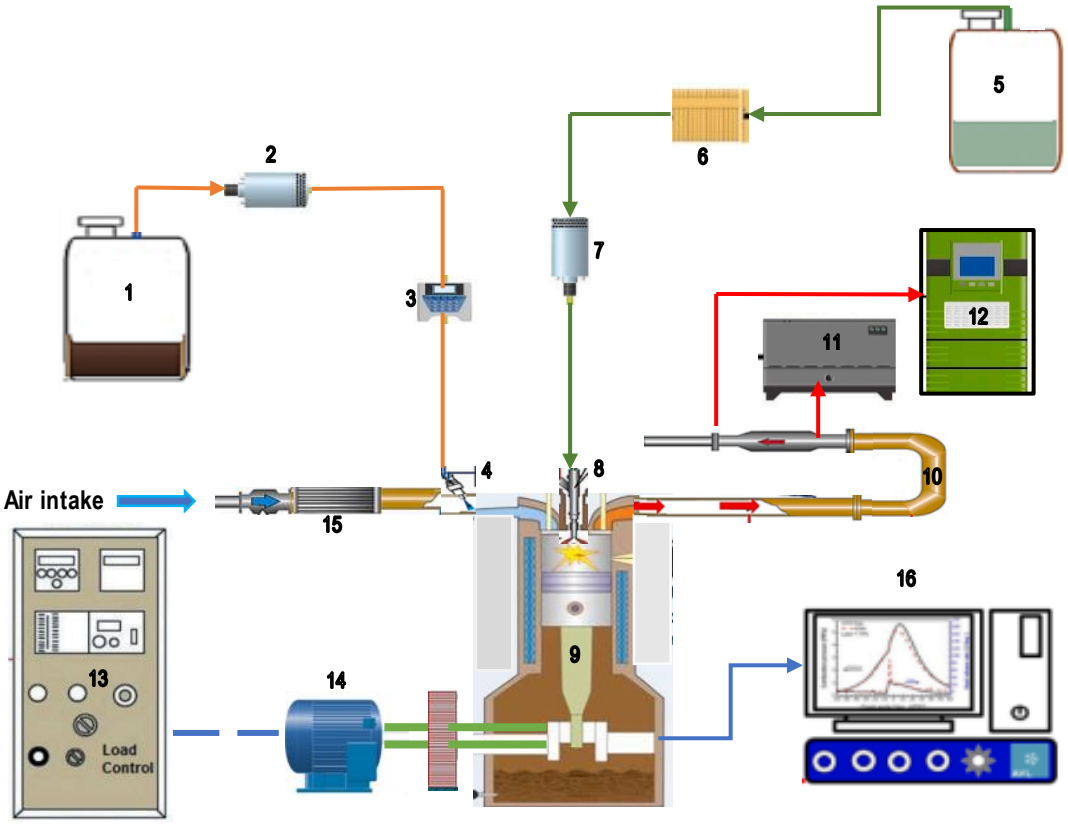

1	Fuel tank for LRF	2	Electronic fuel pump	3	Arduino microcontroller
4	Port injector	5	Fuel tank for HRF	6	Fuel filter
7	High-pressure fuel pump	8	Direct injector	9	Test Engine
10	Exhaust manifold	11	NOx gas analyzer	12	Exhaust emissions analyzer
13	Control panel	14	Dynamometer	15	Air filter
16	Data acquisition				

Figure 3.18 Schematic diagram of RCCI engine

3.9. Exhaust gas analyzers

An exhaust gas analyzer (Infralyt smart) was employed to measure and assess the composition of gases emitted from the engine's exhaust. This device provides crucial data on pollutant levels in the exhaust, aiding in the assessment of engine emissions and compliance with regulatory standards. The analyzer operates using infrared absorption to detect gas components such as CO, CO_2, and HC, represented as regular hexane. Additionally, its individual components are designed for easy access, allowing for convenient cleaning and replacement (see Fig 3.19a). The gas analyzers depicted in Figure 3.19b are designed for portability and user-friendly operation, making

them ideal for applications such as tuning, fault diagnosis, and pre-MOT testing. These devices are suitable for both dynamic and static testing environments. They are capable of measuring CO, HC, CO_2, and O_2, while the EGA illustrated in Fig.3.19b specifically measures NOx through the use of electrochemical sensors. The measurement of hydrocarbons is particularly beneficial for identifying fuel flow and misfire problems, making these analyzers excellent tools for roadside compliance testing and pre-compliance assessments. It is important to note that the EGA should be brought to the vehicle rather than transporting the vehicle to the analyzer, allowing for testing under real-world driving conditions. The analyzers can measure lambda and air-fuel ratios, which are crucial for enhancing engine efficiency and optimizing fuel consumption, with lambda or air-fuel ratio values ranging from 0.8 to 1.2 and NOx levels from 0 to 5000 ppm. Furthermore, they are capable of measuring emissions from gasoline, CNG, LPG, and diesel engines. The detailed specification of exhaust gas analyzers was shown in Table 3.9 and Table 3.10.

Table 3.9 Specification of CT 159.02 Infralyt smart exhaust gas analyzer

S.no	Feature	Specification
1	Gases measured	CO, CO_2, HC and O_2
2	Carbon dioxide range	0 - 20% vol
3	Carbon monoxide range	0 - 10% vol
4	Hydrocarbon range	0 – 2500 ppm
5	Lambda	0 – 999
6	Accuracy classes	1 and 0
7	Operating voltage and frequency	230V, 50/60Hz, 1 phase or 120V, 60Hz, 1 phase
8	Weight approx.	7 kg
9	Dimensions (L×W×H)	330 x 260 x 205mm

Table 3.10 Specification of Portable Exhaust Gas Analyzer (Kane Type-EGA5)

S.no	Feature	Specification
1	Gases measured	CO, CO_2, NOx, HC and O_2
2	Carbon dioxide range	0 - 20% vol
3	Carbon monoxide range	0 - 10% vol
4	Hydrocarbon range	0 – 5000 ppm
5	NOx range	0 – 5000 ppm
6	Oxygen range	0 – 25%
7	Operating range	5°C to 50°C
8	Weight	1.2 kg
9	Dimensions (L×W×H	240mm×165mm×65mm

a) EGA (Infralyt Smart) b) EGA(KANE-EGA5)

Figure 3.19 Exhaust gas analyzers employed to assess the levels of emissions

3.10. Experimental procedure for adjusting and testing the CT 110 CI engine

Procedure 1: Preparation and initial checks

- Gather all materials required for the test and adjustment of the CT 110 test stand.
- Ensure that the airflow, lubricating oil levels, and all connections between the test stand and engine are properly checked and secured prior to starting the engine.

Procedure 2: Setup and Connections

- Connect the CT 110 test stand to the main electricity supply.
- Ensure the air and exhaust hoses are properly connected, with the exhaust hose outlet positioned outdoors.

Procedure 3: Temperature Sensor Installation

- Attach a cable of temperature sensor to the engine to measure ETG.
- Connect the engine to the asynchronous motor, which acts as a braking during testing.
- Conduct all tests under 80% of load conditions

Procedure 4: Fuel System Preparation

- Prior to starting, make sure the fuel line and measuring tube on the test stand are properly filled.

Procedure 5: Engine Start-Up

- Start the engine utilizing braking device, which functions by operating the asynchronous motor as a starter.
- Press the corresponding buttons on the test stand to switch the ignition and engage the asynchronous motor.
- Let the engine idle without load for about 5 min. to achieve warm-up and stable operating conditions.

Procedure 6: Fuel Testing Procedure

- Begin testing with pure diesel fuel (B0).
- Sequentially modify the CI engine to RCCI, add biodiesel-diesel blend (B20) into the HRF and LRF (G75n-b25, G50n-b50, and G25n-b75) to fuel tank, ensuring accurate recording of output results.

Procedure 7: Speed and Torque Adjustment

- Adjust the speed of the asynchronous motor and set the torque using the knobs on the test stand.

Procedure 8: Switching to Load Conditions

- After starting the CI engine, deactivate the asynchronous motor using the "starter/brake" button.
- Recor curves of load characteristic for the engine.

Procedure 9: Data Collection

- Allow approximately 10 seconds of load operation at each measurement point for speed stabilization and result recording.
- Document experimental results using a desktop computer interfaced with the exhaust analyzer.

Procedure 10: Fuel Line Flushing

- Run the engine on diesel fuel for a few minutes when changing between diesel-biodiesel blend samples to flush the fuel lines.

3.11. Experimental uncertainty analysis

Experimental investigations are inherently influenced by uncertainty arising from various factors, including human error, the state of measuring devices, methods of data collection, and fluctuating environmental conditions. The precision of measurements is vital for obtaining reliable study results. In this study, the identification of error sources was essential for assessing uncertainty, and calibration of the measuring apparatus employed was considered. To enhance the accuracy of the analysis, three readings were recorded and averaged, thereby minimizing potential measurement discrepancies. The total uncertainty associated with the engine output variables was calculated utilizing the root-mean-square method. The overall uncertainty of the experiment was calculated via Eq. (3.17). The percentage of uncertainty for each parameter is shown in Table 3.11.

$$\Delta U = \sqrt{\left\{\left(\frac{\partial U}{\partial X_1}\,\Delta X_1\right)^2 + \left(\frac{\partial U}{\partial X_2}\,\Delta X_2\right)^2 + . \;.\;. + \left(\frac{\partial U}{\partial X_n}\,\Delta X_n\right)^2\right\}} \tag{3.17}$$

$$\Delta U = \sqrt{\{(BT)^2 + (BP)^2 + \ (BSFC)^2 + (NOx)^2 + (CO)^2 + (CO_2)^2 + (HC)^2\}}$$

$$\Delta U = \sqrt{\{(1.24)^2 + (1.19)^2 + \ (1.55)^2 + (1.93)^2 + (1.36)^2 + (1.48)^2 + (1.86)^2\}}$$

$$\Delta U = 4.07$$

Table 3.11 Uncertainty of the responses in percentage

Parameter	Unit	Accuracy (%)	Uncertainty (%)
BP	kW	±0.1	±1.19
BT	Nm	±0.2	±1.24
BSFC	kg/kWh	±0.05	±1.55
CO	%vol.	±0.06	±1.36
CO_2	%vol.	±0.1	±1.48
HC	ppm	±3	±1.86
NOx	ppm	±12	±1.93

CHAPTER FOUR

RESULTS AND DISCUSSIONS

The data gathered during this research was meticulously analyzed, resulting in a detailed discussion of notable observations and findings. This analysis primarily emphasized the following critical aspects:

- RSM analysis of cottonseed oil biodiesel
- Characterization of cottonseed oil and cottonseed oil biodiesel
- GC-MS and FTIR analysis of cottonseed oil biodiesel
- Combustion analysis of RCCI engine mode
- Performance analysis of RCCI engine mode
- Exhaust gas emissions analysis of RCCI engine mode
- Optimization of performance and emissions of RCCI Engine

4.1. Optimization and characterization of biodiesel

4.1.1. RSM analysis of CSO Methyl ester

To optimize the production of biodiesel from cottonseed oil, a total of 15 experimental runs were systematically developed using the RSM, specifically employing the Box-Behnken design as detailed in Table 4.1. This statistical approach allows for efficient exploration of the relationships among multiple process variables while minimizing the number of required experimental trials. The selected independent variables in this study were reaction time (denoted as A), catalyst concentration (B) and methanol to oil ratio (C), all of which are known to significantly influence the transesterification process. Both the individual (main) effects and the interactive (combined) effects of these parameters on biodiesel production from CSO were thoroughly investigated using RSM. The application of this method not only facilitates the identification of optimal conditions but also enables a deeper understanding of the complex interactions among the variables.

To mathematically model and predict the biodiesel yield based on the process parameters, a quadratic polynomial regression model was constructed. This second-order model captures the nonlinear behavior of the system and serves as a predictive tool for estimating the CSOME under various conditions. The general form of this model is provided in Eq. (4.1), which incorporates

linear, quadratic, and interaction terms of the variables A, B, and C. In this equation, positive coefficients signify a synergistic effect: indicating that the increase in the corresponding variables enhances the yield when acting alone or in combination with others. Conversely, a negative coefficient denotes an antagonistic effect, implying that increasing the variable may reduce the yield or counteract the positive influence of the factors (Razzaq et al., 2022).

$$\%\ \text{Biodiesel yield} = 23.9 + 0.553A + 64B + 10.4C - 0.00535A^2 - 35.43B^2 - 1.123C^2 - 0.0001A \times B + 0.0007A \times C + 0938B \times C \quad (4.1)$$

The adequacy and predictive capability of the developed regression model were evaluated using several metrics, namely the R^2, Adj-R^2, F-value, and P-value. These parameters are crucial in determining how well the model fits the experimental data and how reliably it can be used for predictive purposes. A high-quality regression model is typically characterized by a high R^2 value, indicating that a significant proportion of the variability in the response variable is accounted for by the model, as well as a minimal difference between R^2 and Adj-R^2 values. The Adj-R^2 is particularly important as it corrects for the number of predictors that are meaningful and contribute to the accuracy of the model rather than merely inflating its performance (Yusuff et al., 2022).

In this study, the regression model developed to predict biodiesel yield from cottonseed oil achieved an R^2 value of 0.97 (97%) and an Adj-R^2 of 0.968 (96.8%). These values indicate that the model accounts for approximately 97% of the total variation observed in the biodiesel yield, leaving only 3% attributable to random error. The minimal difference between the R^2 and Adj-R^2 values confirms the robustness and reliability of the model. These findings are in close agreement with the results of (Onukwuli et al., 2017), reported R^2 and Adj-R^2 values of 97.05% and 96.29%, respectively, in a similar study on biodiesel production modeling. Such consistency across studies underscores the effectiveness of the RSM in modeling complex chemical processes like transesterification. The high R^2 value obtained in this study suggests a strong correlation between the selected process parameters (methanol to oil ratio, reaction time, and catalyst concentration) and the output (biodiesel yield). This implies that variations in these input variables are reliably reflected in the output, thereby validating the suitability of the model for prediction and optimization purposes.

Table 4.1 RSM-based experimental design with the biodiesel yield results

Run	Variables						Outcomes		
	A		B		C		Biodiesel yield (%)		
	Coded	Actual	Coded	Actual	Coded	Actual	Experimental	ANN	RSM
1	1	80	-1	0.5	0	1:6	84.16	83.8651	82.73
2	0	60	-1	0.5	1	1:8	75.25	76.8679	75.9525
3	0	60	0	1.0	0	1:6	94.66	94.65	94.66
4	0	60	0	1.0	0	1:6	94.66	94.65	94.66
5	1	80	0	1.0	-1	1:4	90.0	90.622	91.3225
6	0	60	1	1.5	-1	1:4	85.50	85.4403	85.2275
7	0	60	0	1.0	0	1:6	94.66	94.65	94.66
8	0	60	1	1.5	1	1:8	78.75	78.75	77.6425
9	-1	40	1	1.5	0	1:6	83.75	84.7751	84.180
10	-1	40	0	1.0	1	1:8	86.00	85.6195	87.6775
11	1	80	1	1.5	0	1:6	80.00	80.0443	80.38
12	-1	40	-1	0.5	0	1:6	87.33	87.259	87.95
13	-1	40	0	1.0	-1	1:4	93.62	93.6168	94.8925
14	1	80	0	1.0	1	1:6	82.50	83.2133	82.6475
15	0	60	-1	0.5	-1	1:4	85.75	85.7602	86.8575

The statistical validation of the developed model for predicting biodiesel yield from cottonseed oil was performed through an ANOVA, with the results demonstrating the model's robustness and predictive reliability. The close agreement between the predicted and actual values, as revealed in Fig. 4.1, confirms a strong correlation, further substantiated by the high R^2 of 97 %. Diagnostic plots of residuals, provided in Fig. 4.2, offer additional insights into the model's adequacy. The normal probability plot of residuals suggests that the residuals are approximately normally distributed, thereby validating one of the core assumptions in regression analysis. Furthermore, the plots of residuals versus fitted values display a random scatter with no apparent pattern or systematic trend. These homoscedastic behavior-where residuals are evenly distributed across level of predicted values, confirms that the model maintains constant variance and does not suffer from heteroscedasticity, which could otherwise bias the predictions.

ANOVA results for the quadratic model are presented in Table 4.2 and further confirm the model's statistical significance. A model is generally considered statistically significant when it exhibits a high F-value and a low P-value, typically below the threshold of 0.05 (Ngige et al., 2023). In this study, the model achieved an F-value of 16.28 and a corresponding P-value of 0.003. these values indicate that the probability of the observed results occurring due to random variations is extremely low, affirming that the model provides a meaningful representation of the relationship between the input factors and biodiesel yield. Additionally, the high model F-value and statistically significant P-value (typically $P<0.05$) further reinforce the validity of the model, indicating that the observed relationship between the variables is not due to random chance, overall, the statistical evaluation confirms that the developed model is both statistically and practically valuable for optimizing cottonseed oil biodiesel production.

A more granular evaluation of the model terms reveals that several variables exert a statistically significant influence on biodiesel production. specifically, A, C, B^2, and C^2 were found to be highly significant contributors. In contrast, the linear effect of B, as well as the interaction terms AB, BC, and AC, were less significant or contributed minimally to the overall biodiesel yield. The importance of each term is further quantified by their P-values. The response F-value for the overall model was 16.28, indicating a strong signal to noise ratio. Among the linear terms, factor C exhibited the highest influence with an F-value of 37.69, followed by factor A, which recorded an F-value of 6.52. For the squared terms, B^2 showed the strongest effect with an F-value of 83.33, while C^2 also contributed significantly with an F-value of 21.43. These values suggest that methanol to oil ratio and the squared term for catalyst concentration (B^2) are the most influential variables in the transesterification process. Their high F-values indicate a strong effect on the conversion efficiency of cottonseed oil to biodiesel, emphasizing the importance of precisely optimizing the factors to maximize yield. In summary, the ANOVA results not only validated the statistical strength of the model but also provided valuable insights into the relative importance of individual process variables. This highlights the efficiency of the quadratic regression model in capturing the complex interactions among parameters and underscores its utility in guiding process optimization for biodiesel production from cottonseed oil.

Table 4.2 ANOVA of CSOME yield surface quadratic model

Source	DF	Adj-MS	Adj-SS	F-Value	P-Value
Model	9.0	56.569	509.1180	16.280	0.0030
Reaction duration (A)	1.0	22.646	22.6460	6.520	0.0410
Catalyst concentration (B)	1.0	3.213	3.2130	0.920	0.380
Methanol to oil ratio (C)	1.0	130.977	130.9770	37.690	0.0020
A*A	1.0	16.890	16.8900	4.8600	0.0790
B*B	1.0	289.599	289.5990	83.330	0.0000
C*C	1.0	74.479	74.4790	21.430	0.0000
A*B	1.0	0.000	0.000	0.00	1.00
A*C	1.0	0.004	0.004	0.00	0.976
B*C	1.0	3.516	3.516	1.01	0.361
Error	5.0	3.475	17.376		
Lack-of-Fit	3.0	5.92	17.376		
Pure Error	2.0	0.00	0.00		
Total	14.0		526.494		

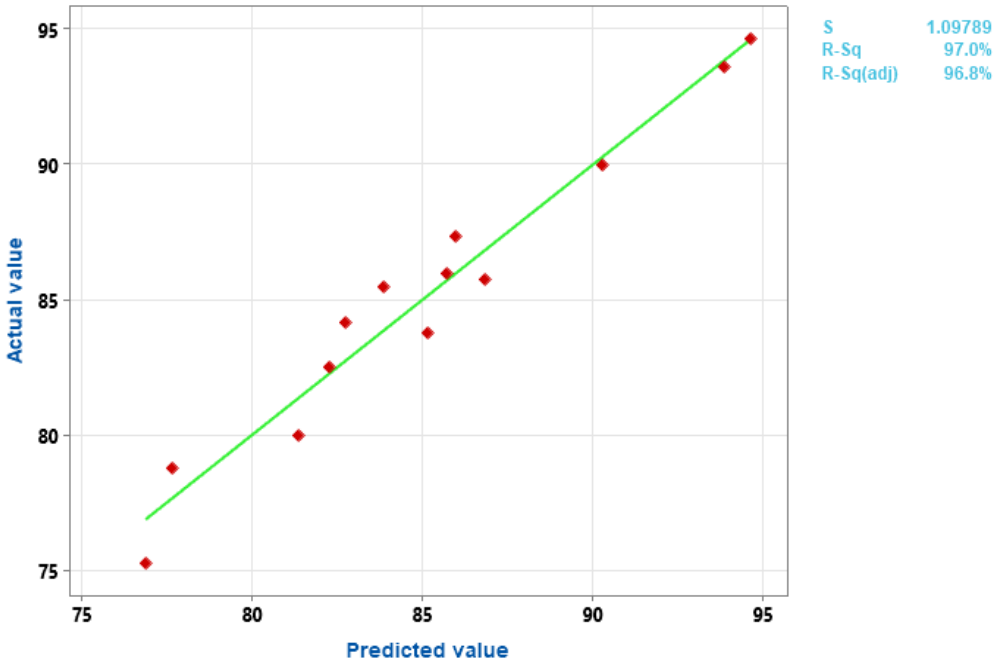

Figure 4.1 Actual vs predicted value

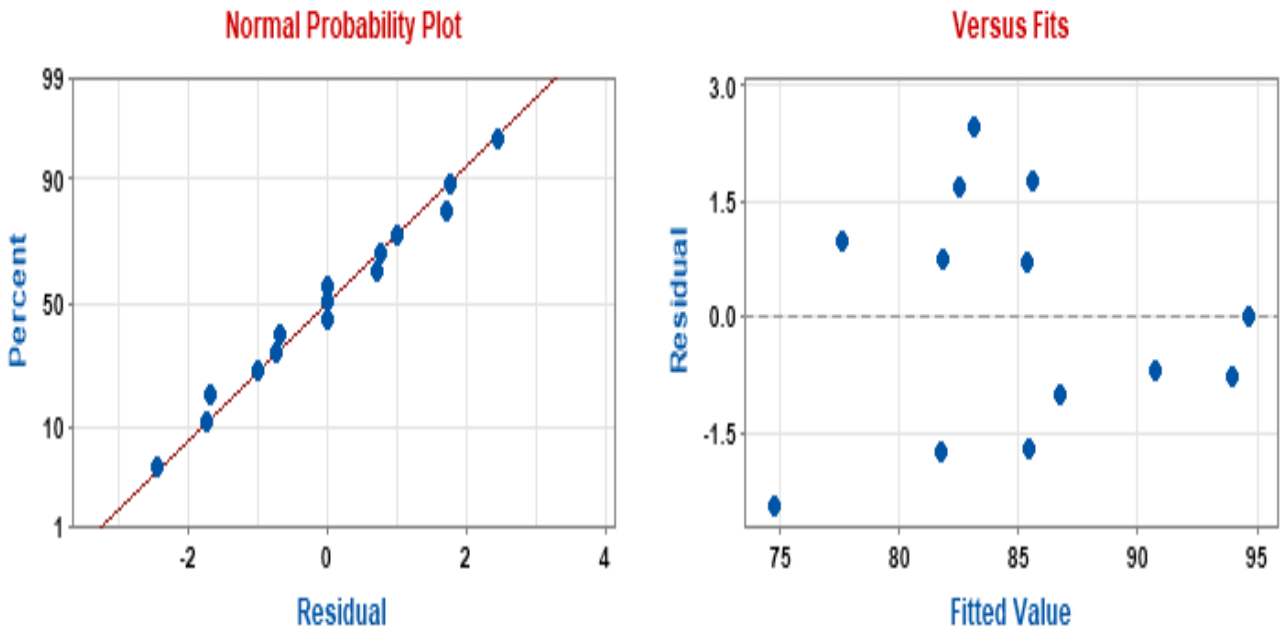

Figure 4.2 Residual plots for biodiesel yield

4.1.2. Effects of experimental variables on biodiesel yield

The experimental investigation examined the effects of three key parameters: methanol to oil ratio, reaction time, and catalyst concentration on the yield of cottonseed oil biodiesel. The study considered methanol to oil ratio at levels of 1:4, 1:6, and 1:8, reaction time of 40, 60, and 80 min., and catalyst concentrations of 0.5, 1, and 1.5 wt.%. To better understand the interactions between these variables, surface and contour plots were generated under specific conditions particularly at an affixed catalyst concentration of 1 wt.%, as shown in Fig.4.3 and Fig.4.4. The graphical representations reveal a clear trend: biodiesel yield increases as methanol to oil ratio increases and longer reaction time. However, this trend holds only up to a certain threshold. Beyond the optimal level, a further increase in both variables leads to a decline in biodiesel yield. The maximum yield of 94.66% was recorded at a methanol to oil ratio of 1:6, a reaction time of 60 min., and a catalyst concentration of 1 wt.%. This combination appears to strike a balance between providing sufficient methanol for complete transesterification and allowing enough reaction time for the process to proceed efficiently. The observed reduction in yield beyond these optimal conditions can be attributed to two primary factors. First, extended reaction times may promote undesirable side reactions or the reversal of the transesterification process, reducing overall yield. Second, using a methanol to oil ratio beyond the optimal level can lead to dilution effects and increased difficulty in separating the glycerol phase, which interferes with the purity and recovery of biodiesel.

Moreover, insufficient methanol results in incomplete conversion of triglycerides, further lowering the yield (Jimoh et al., 2023a).

The study also examined the combined effects of methanol to oil ratio and catalyst concentration while maintaining the reaction time at constant at 60 min. The corresponding surface and contour plots are presented in Fig.4.5 and 4.6. These plots show that while moderate increases in both methanol to oil ratio and catalyst concentration initially enhance the biodiesel yield, excessive levels of either variable lead to a decline in biodiesel yield. This drop is primarily attributed to the formation of soap, a side product of the separation, particularly at higher catalyst concentrations. The presence of excess methanol intensifies this effect, as it promotes the saponification of free fatty acids in the cottonseed oil, reducing the efficiency of the transesterification reaction (Vinoth Arul Raj et al., 2021). This phenomenon not only reduces biodiesel yield but also complicates the downstream purification process by creating emulsions that hinder the separation of biodiesel and glycerol. Therefore, maintaining catalyst concentration within an optimal range is essential to prevent such adverse effects. The findings underscore that while higher reactant concentrations generally favor conversion, exceeding optimal levels results in diminishing returns or negative consequences due to secondary reactions. Overall, these results highlight the delicate balance required among methanol to oil ratio, reaction time, and catalyst concentration to achieve maximum biodiesel yield, fine-tuning these parameters is essential not only for maximizing output but also for ensuring process efficiency and product quality. This reinforces the importance of employing statistical optimization tools such as RSM, which are instrumental in identifying ideal process conditions while accounting for complex variable interactions.

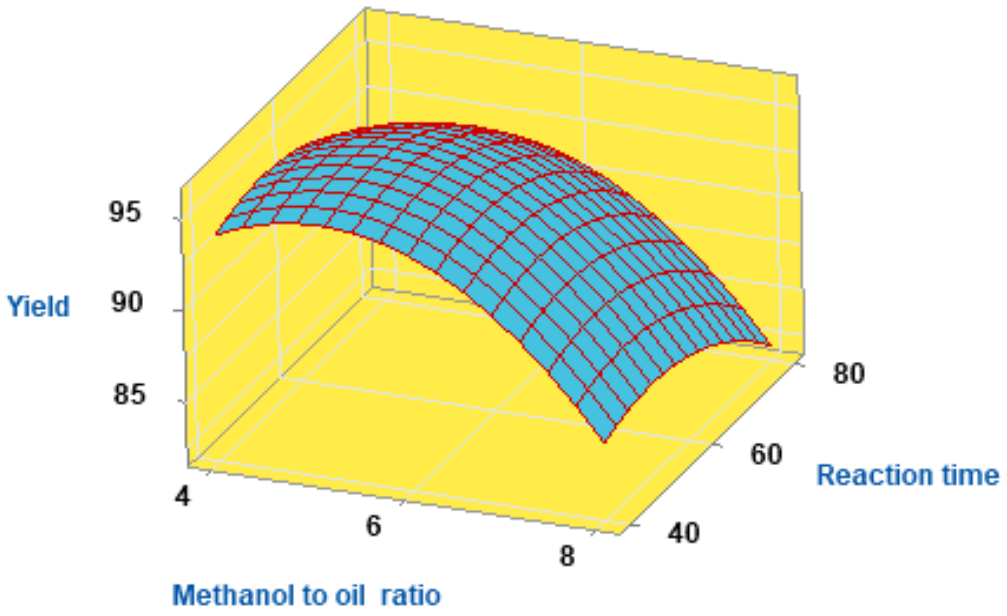

Figure 4.3 Yield as a function of methanol ratio and reaction time

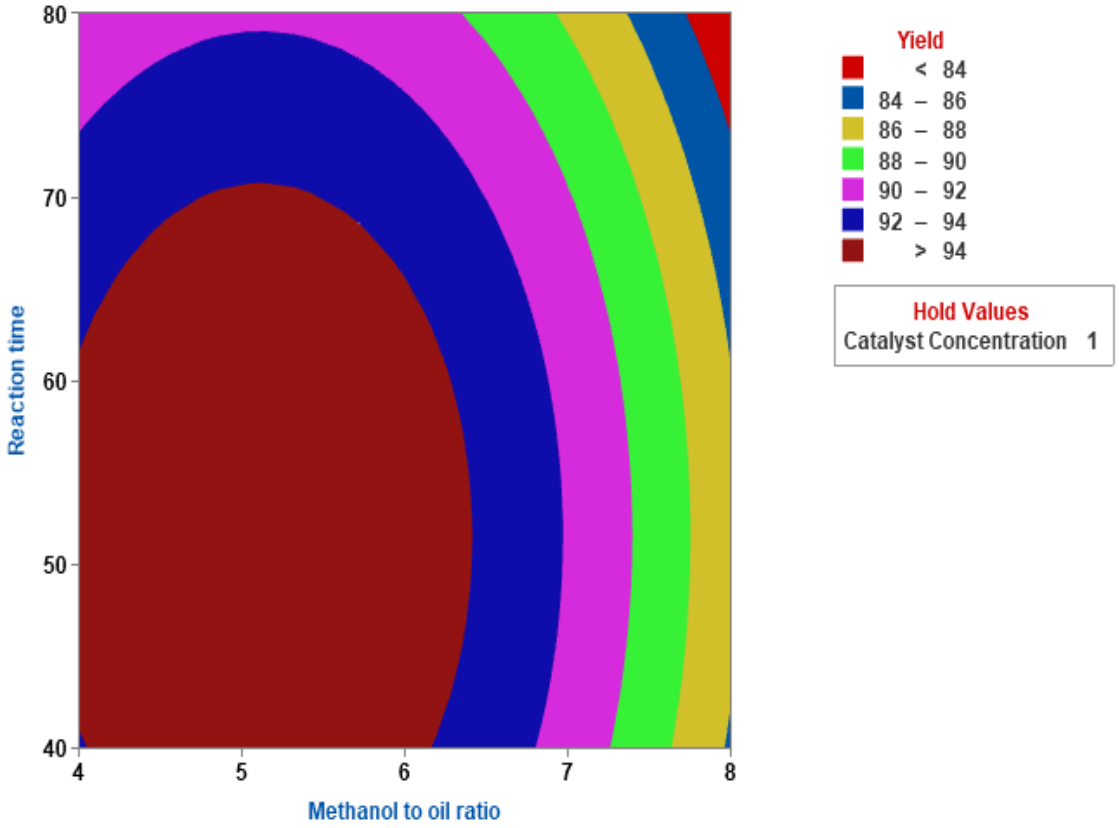

Figure 4.4 Yield as a function of methanol ratio and reaction time in form of contour plot

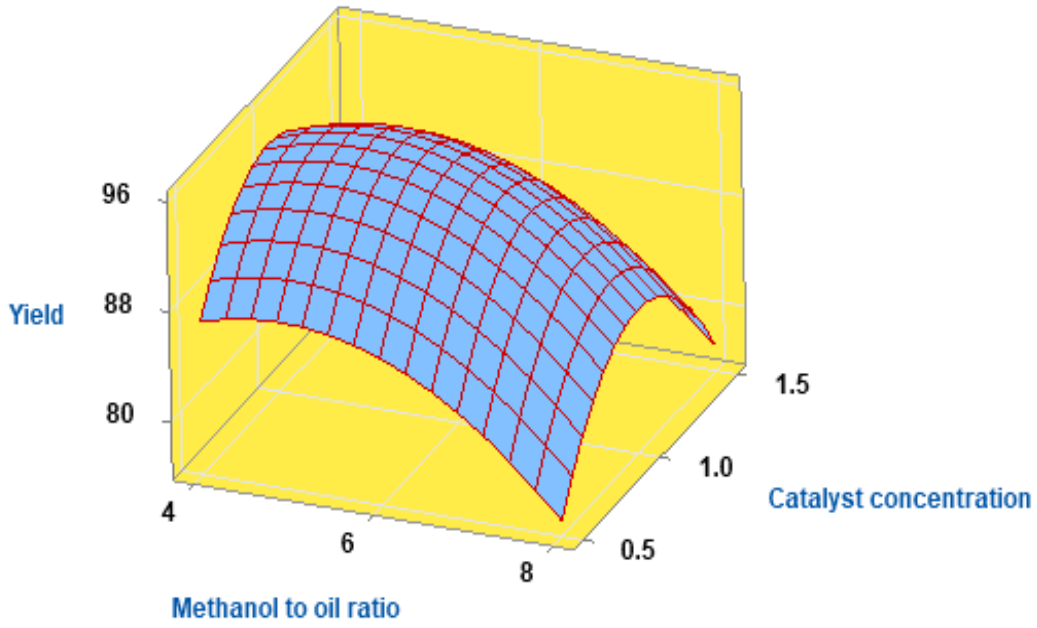

Figure 4.5 Yield as a function of catalyst and methanol to oil ratio in form of surface plot

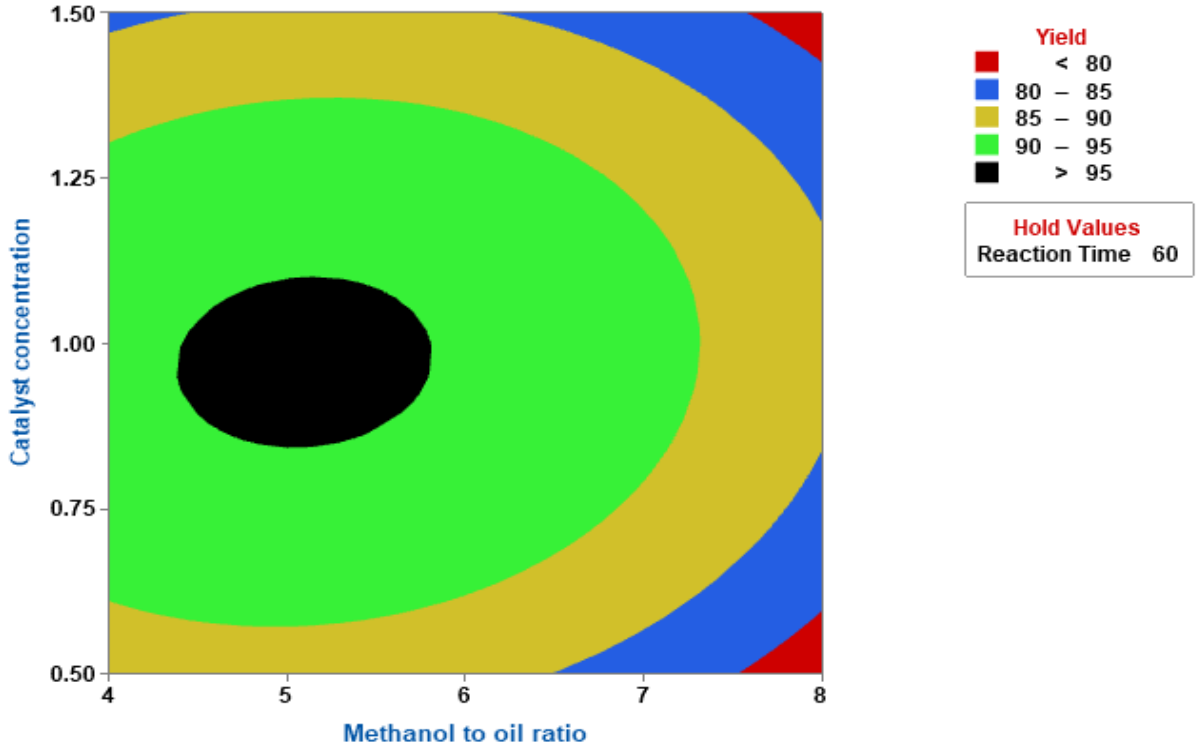

Figure 4.6 Yield as a function of catalyst and methanol to oil ratio in form of contour plot

4.1.3. Optimum conditions for cottonseed oil biodiesel yield

Numerical optimization of the transesterification process in this study identified the optimum conditions: a ratio of methanol to oil of 1:6, a reaction time of 52.2 min., and a catalyst concentration of 0.985 wt. %. These optimized conditions are in close concordance with the results revealed by (Onukwuli et al., 2017), reinforcing their validity within the broader research context. Under these specified conditions, the model predicted a biodiesel yield of 95.04%, while the experimental procedure yielded a slightly lower but comparable value of 94.80%, as detailed in Table 4.3. The marginal discrepancy of only 0.24% between the numerical predicted and experimental results underscores the robustness and predictive reliability of the employed numerical model. This close agreement between computational predictions and experimental outcomes not only validates the model but also emphasizes the importance of integrating numerical optimization into biodiesel production. RSM significantly reduces the reliance on conventional trial and error experimentation, thereby saving both time and resources. Additionally, the findings suggest that the model effectively captures the complex interactions among process variables: methanol to oil ratio, catalyst loading, and reaction time which are well known to influence transesterification efficiency and biodiesel purity.

Table 4.3 Optimal conditions and verification of the model

Process variables	Unit	Results
Reaction time	Min.	52.2
Catalyst concentration	wt.%	0.985
Methanol to oil ratio	vol/vol	1:6
Numerical obtained yield	%	95.04
Experimental obtained yield	%	94.80
Deviation	%	0.24

4.1.4. Artificial neural networks for statistical analysis

In the context of Artificial Neural Network (ANN) modeling, the selection of an appropriate training function, the number of neurons, and the type of network is essential for accurately predicting experimental outcomes. Additionally, ANN can be applied to second-order polynomial regression. In this study, the ANN architecture was configured with three input layers, ten hidden layers, and a single output layer (3-10-1). The first three neurons correspond to reaction duration,

concentration of catalyst, and methanol ratio, while the output layer represents the biodiesel yield (see Fig 4.7). The model's accuracy was assessed using R values, which were recorded as 1 for validation, 0.9934 for training, and 1 for testing. Previous research conducted by (Razzaq et al., 2022) indicated R values of 1, 0.967, and 0.996 for validation, training, and testing, respectively, in predicting biodiesel yield from a mixture of palm and CSO. Furthermore, Selvan et al. reported R values of 0.9989, 0.9977, and 0.9968 for training, validation, and testing in their investigation. The validation outputs versus target plots yielded a linear regression equation of $Y=1*T+5.5\times10^{-9}$, which was utilized to forecast the ANN model's values, where Y represents the ANN model's predictions and T signifies the experimental results that informed these predictions.

Overall, there was a strong correlation between the predicted and actual values, as indicated by the R-values obtained from these experiments. Figure 4.8 presents the training performance of the ANN model in terms of mean squared error. The best validation performance, reached with the model, is approximately $4.96\times10-18$ at epoch 0, which shows that the network could learn the underlying relationship of the data with very high precision from the very beginning of training. The rapid convergence, along with very low values of error for the training, validation, and testing curves, are indicative of the fact that the structure of the ANN architecture was appropriate and did not lead to overfitting or underfitting.

Figure 4.9 presents the regression analysis between the ANN outputs and the corresponding experimental target data for training, testing, validation, and combined datasets. All four regression plots have slopes close to unity with R^2 approaching 1.0 confirms that there is a strong linear relationship between predicted and actual values. In particular, the validation and testing sets fall perfectly on the target line, which shows that the developed ANN model has high generalization capability. In summary, the regression results confirm that ANN reliably captures the nonlinear interaction of input parameters and provides highly accurate predictions.

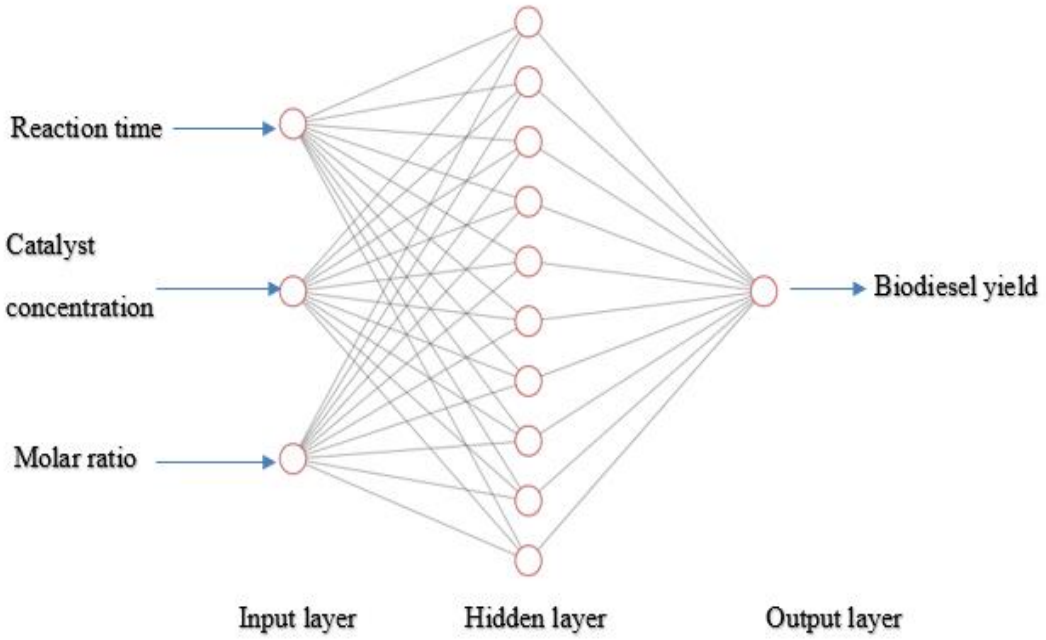

Figure 4.7 ANN model designed for the prediction of biodiesel yield

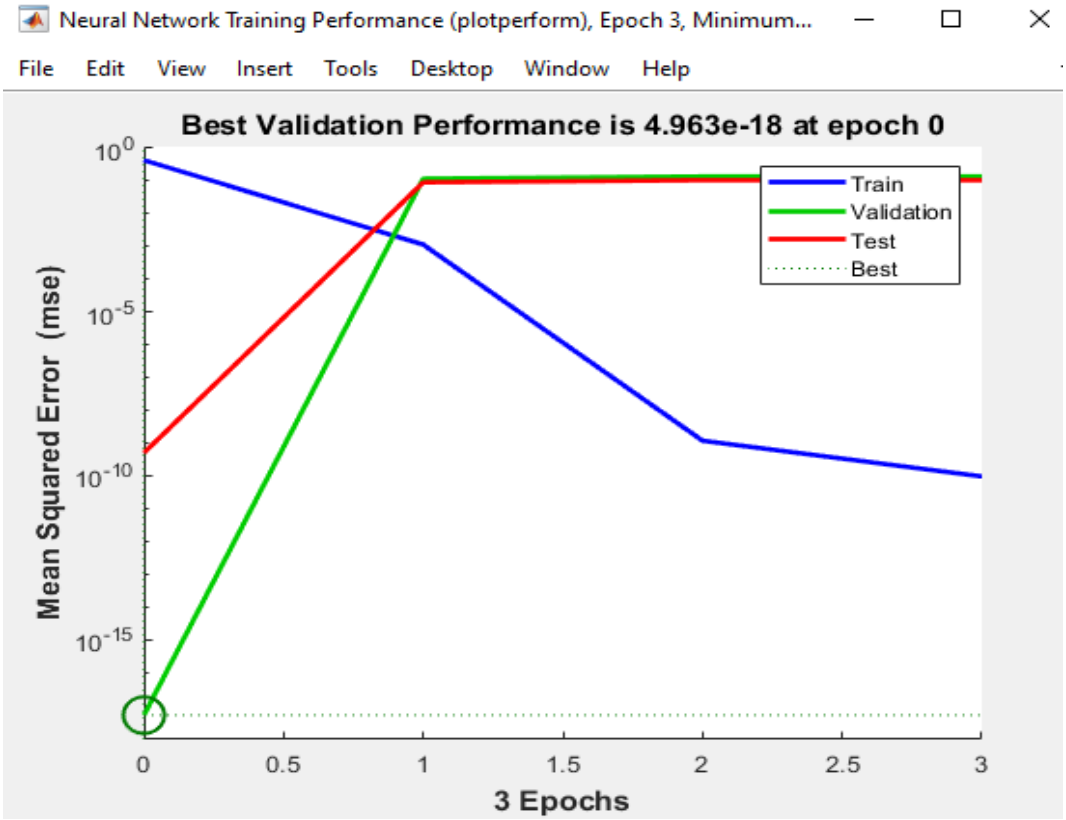

Figure 4.8 Performance of ANN model

Figure 4.9 Regression analysis of ANN for training, testing and validation

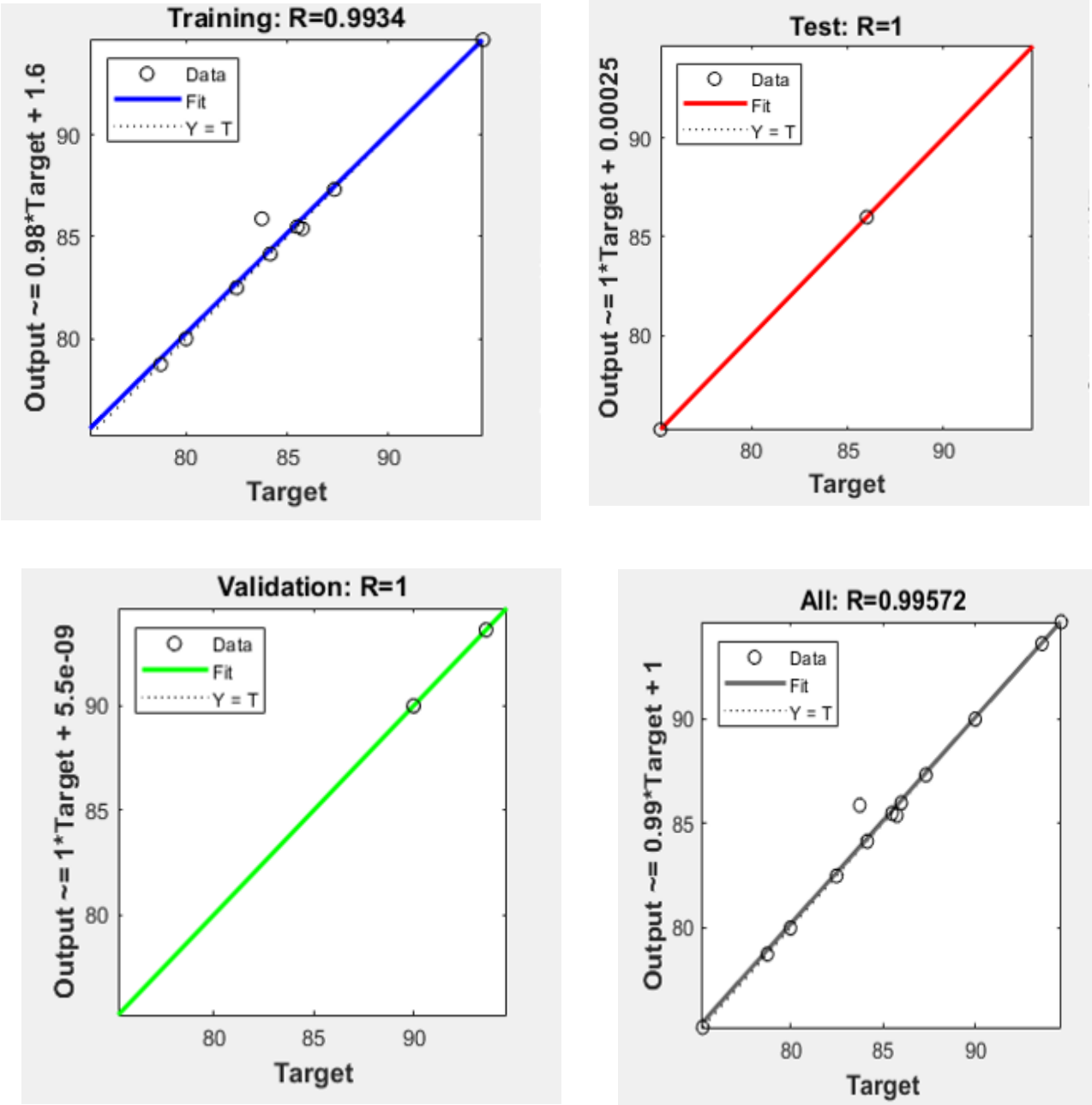

4.1.5. Comparison of RSM and ANN in Optimization Parameter Prediction

The regression coefficient and various error functions were utilized to construct and evaluate the predictive capabilities of RSM and ANN models. Table 4.4 summarizes key statistical indicators namely the standard deviation (SD), coefficient of determination (R^2), root mean square error (RMSE), mean square error (MSE), absolute average relative error (AARE), and sum of squared error (SSE) for both models. These metrics were computed using Equations (3.3–3.8). The R^2

value reflects how effectively each model captures the variability in the experimental data. A value closer to 1 indicates a better fit. The ANN model attained a high R^2 of 0.9957, outperforming the RSM model, which recorded an R^2 of 0.97, both indicating good predictive capabilities. MSE evaluates the average squared differences between predicted and observed values, where lower values indicate improved model accuracy. RMSE, which retains the same units as the output variable, serves as a complementary measure of prediction accuracy. The ANN model achieved lower MSE and RMSE values of 0.348 and 0.590, respectively, compared to 0.80 and 0.895 for the RSM model. Additionally, AARE and SSE were employed to further assess model performance. The ANN model demonstrated superior precision, yielding AARE and SSE values of 0.004 and 5.226, respectively, while the RSM model showed higher values of 0.008 and 12.003. A reduced SSE indicates that the model effectively minimizes overall prediction error across the dataset.

Overall, the ANN model outperformed the RSM model in predicting biodiesel yield, as evidenced by its lower error metrics and higher R^2. Furthermore, the standard deviation of the ANN predictions (5.88) was lower than that of the RSM (6.34), reinforcing the ANN's enhanced accuracy. These findings are consistent with previous studies that underscore the superior predictive performance of ANN in biodiesel modeling. For instance, (G. Ahmad et al., 2023) found ANN to be more accurate than RSM for biodiesel derived from waste cooking oil, reporting a higher R^2 (0.993) and lower MSE (0.072) and RMSE (0.268), compared to RSM (0.986, 0.081, and 0.285, respectively). Likewise, (Muhammad et al., 2022) reported improved predictive accuracy using ANN for biodiesel production from wet microalgae, with an R^2 of 0.94 and RMSE of 0.38. (Bajwa et al., 2024) also confirmed ANN's superior performance in predicting biodiesel yields from waste cooking and sesame oils. Fig.4.10 presents a visual comparison between the experimentally found yield and the values predicted by both RSM and ANN models.

Table 4.4 A statistical comparison of the ANN and RSM models

Variable	RSM	ANN
Coefficient of determination	0.97	0.9957
Sum of squared errors	12.003	5.226
Mean square error	0.80	0.348
Root mean square error	0.895	0.590

Absolute average relative error	0.008	0.004
Standard deviation	6.34	5.88

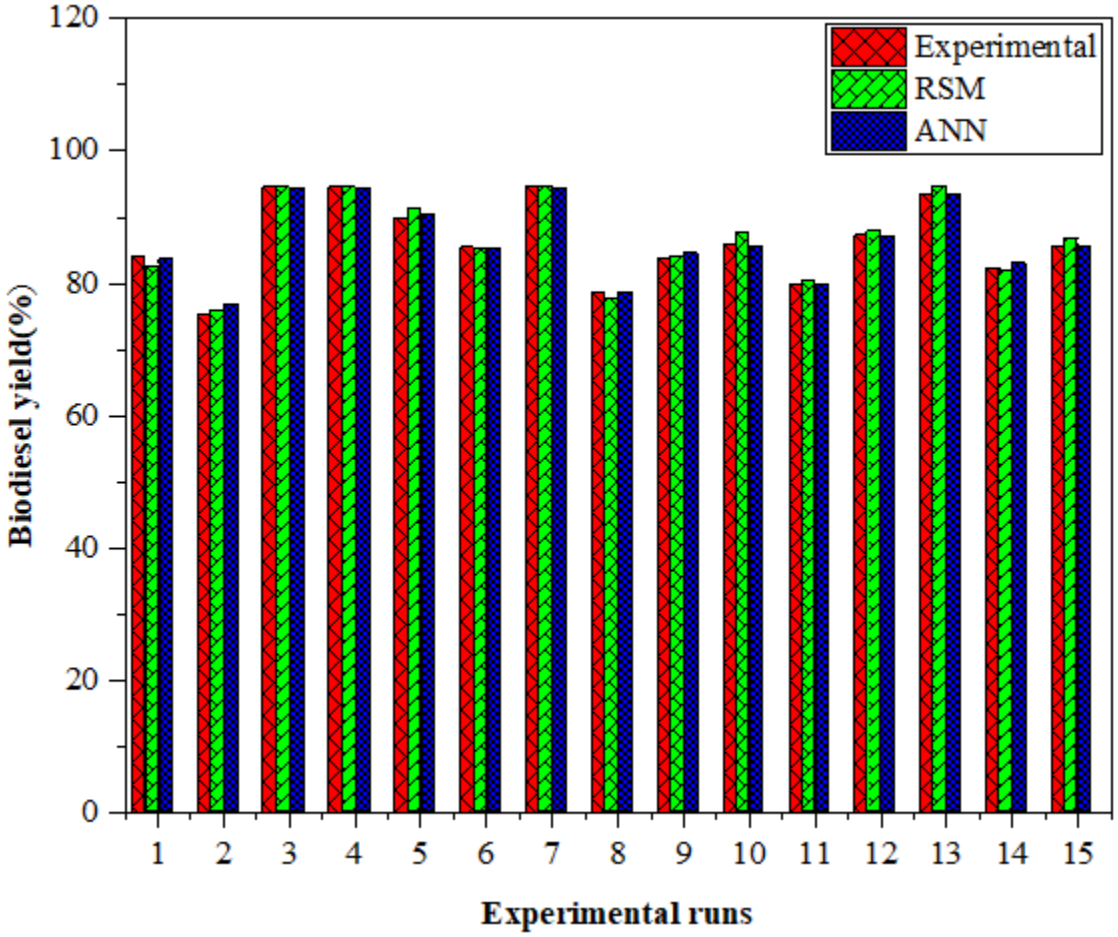

Figure 4.10 Comparing the experiment yield using the ANN and RSM models

4.1.6. GC-MS analysis of CSO biodiesel from optimal conditions

The analysis of cottonseed oil methyl ester (CSOME) using GC-MS demonstrated a wide variety of FAMEs, as depicted in the chromatogram (Fig.4.11). The predominant fatty acids found in the biodiesel include hexadecanoic acid ME (C16:0), methyl 9-cis 11-trans-octadecadienoate (C18:2), 11,14-octadecadienoic acid ME (C18:2), myristic acid ME (C14:0), and methyl 8,9-octadecadienoate ME (C18:2). GC-MS analysis revealed that the biodiesel derived from cottonseed oil contains a significant proportion of both saturated and unsaturated fatty acids. Specifically, Methyl 9-cis 11-trans-octadecadienoate (linoleic) is accounts for 24.76%,

Hexadecanoic acid ME (palmitic acid) is constituting 22.77%, 11,14-Octadecadienoic acid methyl ester (linoleic) comprises 18.44 %, 11-Octadecenoic acid ME (oleic) is found at 16.04 %, Methyl 8,9-octadecadienoate ME (linoleic) represents 3.5%, and myristic acid ME makes up 2.56 %. The results align with the fatty acid profiles documented by (Seal et al., 2015; Shankar et al., 2017) both noted similar distributions in biodiesel derived from cottonseed. The fatty acids C16-C18 range offer advantages for the storage of biodiesel, such as high oxidative stability, low viscosity, and improved engine start-up performance (Muhammad et al., 2022).

The GC-MS analysis revealed a total of 46 unique chemical compounds within the biodiesel sample, encompassing not only methyl esters but also various bioactive substances, including sterols, tocopherols, terpenes, and aldehydes. The existence of these secondary compounds may provide additional functional advantages, such as enhanced lubricity or mild antioxidant effects; however, their specific contributions necessitate further research. This varied molecular profile stands in contrast to the results of (Jimoh et al., 2023a), identified only 34 compounds in biodiesel derived from used cottonseed oil, a discrepancy that may be attributed to variations in feedstock purity, processing conditions, or the resolution of analytical techniques employed. Table 4.5 provides a summary of the identified compounds, detailing their retention times and associated peak intensities. Additionally, the mass spectra for the ten most significant fatty acid methyl esters are illustrated in Fig. 4.12 to 4.23. This thorough profiling serves to confirm the transesterification process and deepens the understanding of the physical and chemical properties of biodiesel, which are crucial for compliance with fuel quality specifications like ASTM D6751 and EN 14214.

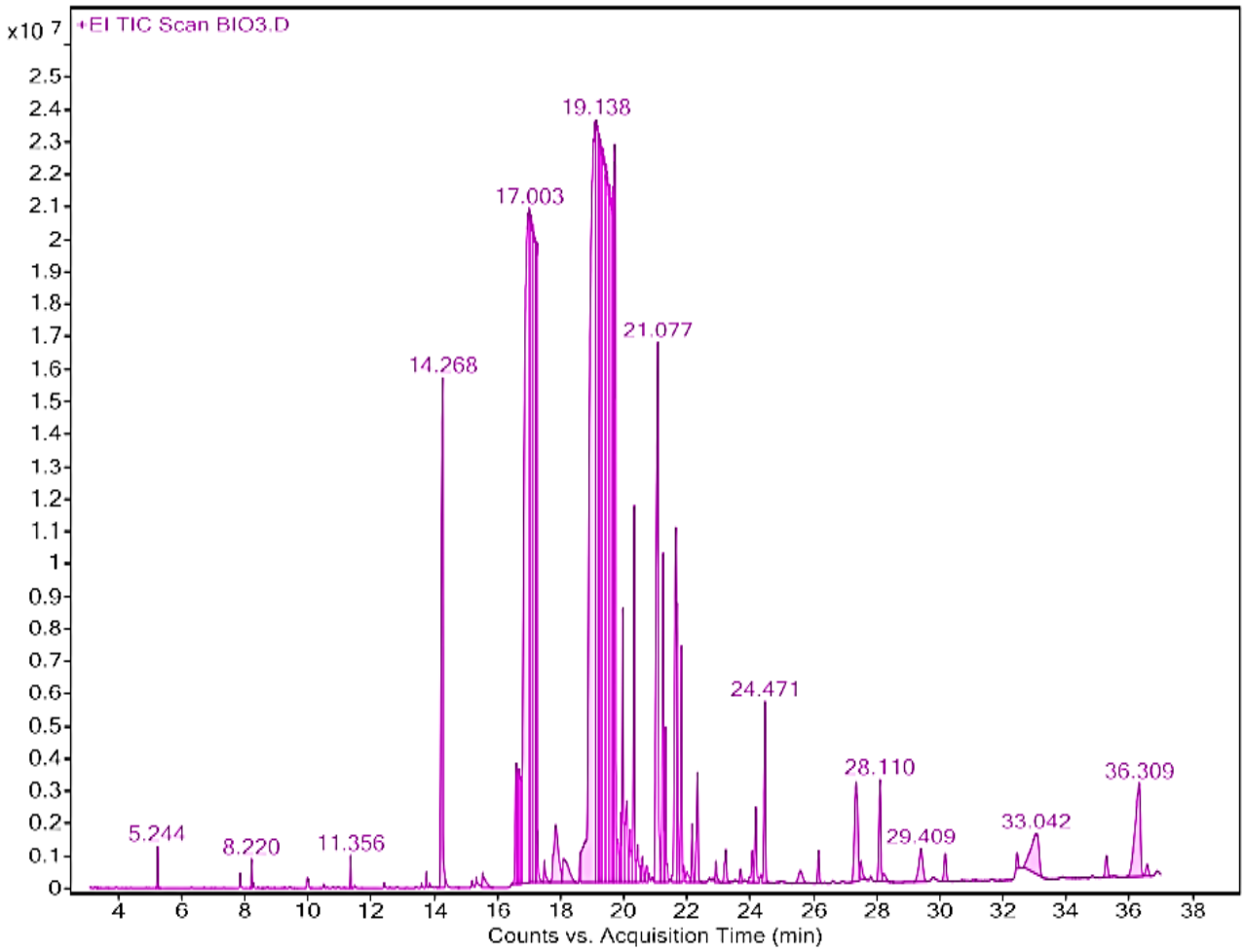

Figure 4.11 Gas Chromatogram of cottonseed oil biodiese1

Figure 4.12 presents the results obtained from GC-MS analysis for the compound identified as Octanoic acid, methyl ester. The findings reveal a distinct, symmetrical chromatographic peak occurring at a retention time of 5.244 minutes, indicating the presence of a pure compound. The mass spectrum is defined by a base peak at m/z 87.0, along with a series of significant fragment ions at m/z 101.0, 115.1, and 127.1, which correspond to the anticipated fragmentation pattern of a saturated medium-chain fatty acid methyl ester. Figure 4.13 illustrates the GC-MS analysis of the compound that elutes at a retention time of 8.22 minutes, which has been identified as 2,4-Decadienal, (E, E). The chromatogram presents a distinct, well-defined peak, indicating a high-purity compound with effective chromatographic separation. The mass spectrum displays a typical fragmentation pattern for this conjugated aldehyde, with a significant molecular ion peak noted at m/z 152.

Table 4.5 GC-MS analysis of cottonseed oil biodiesel

No.	Retention time	Specified esters	Molecular mass	Chemical formula	Weight (%)
1	5.22	Octanoic acid ME	158.090	$C_9H_{18}O_2$	0.1%
2	8.22	2,4-Decadienal, (E, E)	152.110	$C_{10}H_{16}O$	0.11%
3	9.988	Isocaryophyllene	204.150	$C_{15}H_{24}$	0.03%
4	11.356	Lauric acid ME P448	214.130	$C_{13}H_{26}O_2$	0.07%
5	14.268	Myristic acid ME	377.150	$C_{15}H_{30}O_2$	2.56%
6	16.626	Methyl 11-hexadecenoate	268.170	$C_{17}H_{32}O_2$	1.86%
7	17.003	Hexadecanoic acid ME	270.170	$C_{17}H_{34}O_2$	22.77%
8	19.138	Methyl 9-cis,11-transoctadecadienoate	294.190	$C_{19}H_{34}O_2$	24.76%
9	19.55	11,14-Octadecadienoic acid ME	465.190	$C_{19}H_{34}O_2$	18.44%
10	19.687	13-Octadecenoic acid ME	296.190	$C_{19}H_{36}O_2$	3.4%
11	19.801	11,14-Octadecadienoic acid ME	465.190	$C_{19}H_{34}O_2$	0.45%
12	20.436	Octadecane P630	254.180	$C_{18}H_{38}$	0.3%
13	21.077	Methyl 8,9-octadecadienoate	294.190	$C_{19}H_{34}O_2$	3.5%
14	21.993	Methyl 2-octylcyclopropene-1-octanoate	308.200	$C_{20}H_{36}O_2$	0.50%
15	22.817	Linoleic acid @P785	280.180	$C_{18}H_{32}O_2$	0.16%
16	24.471	Methyl 20-methyl heneicosanoate	354.230	$C_{23}H_{46}O_2$	0.81%
17	28.110	Tetracosanoic acid ME	382.250	$C_{25}H_{50}O_2$	0.56%
18	29.409	dl-. alpha. -Tocopherol	430.290	$C_{29}H_{50}O_2$	0.39%
19	33.042	Hentriacontane	436.310	$C_{31}H_{64}$	0.98%
20	36.309	(24R)-Stigmast-5-en-3. beta. -ol	414.290	$C_{29}H_{50}O$	1.46%

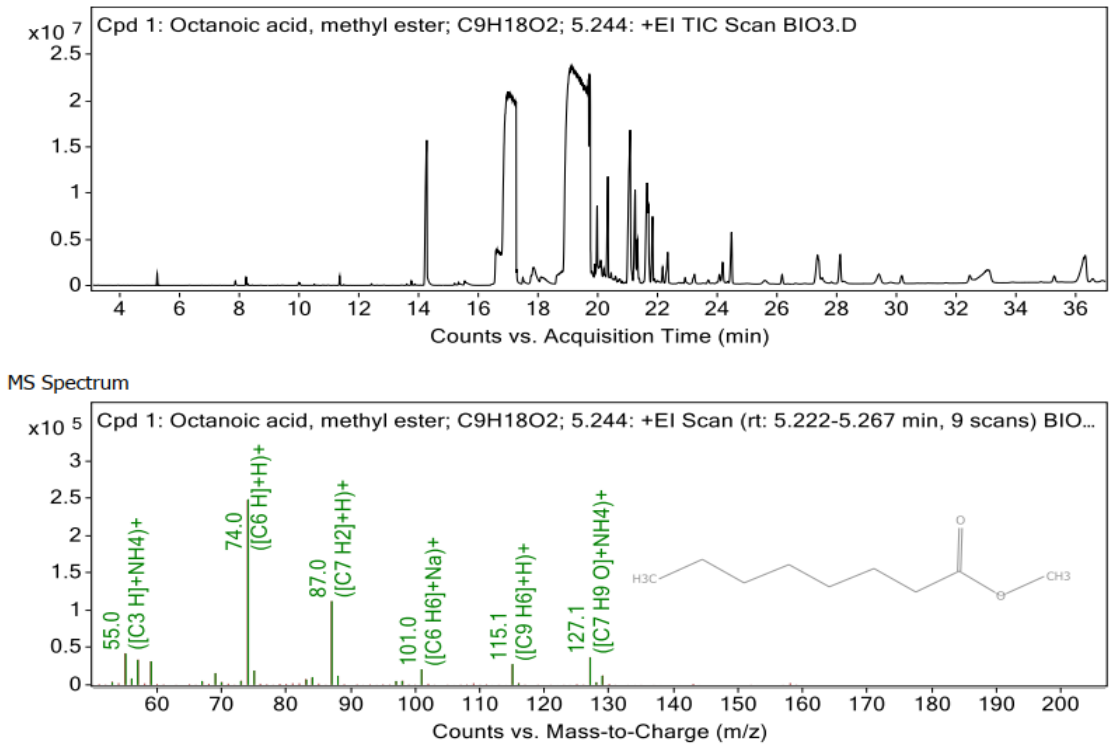

Figure 4.12 Spectrum distribution of Octanoic acid, ME

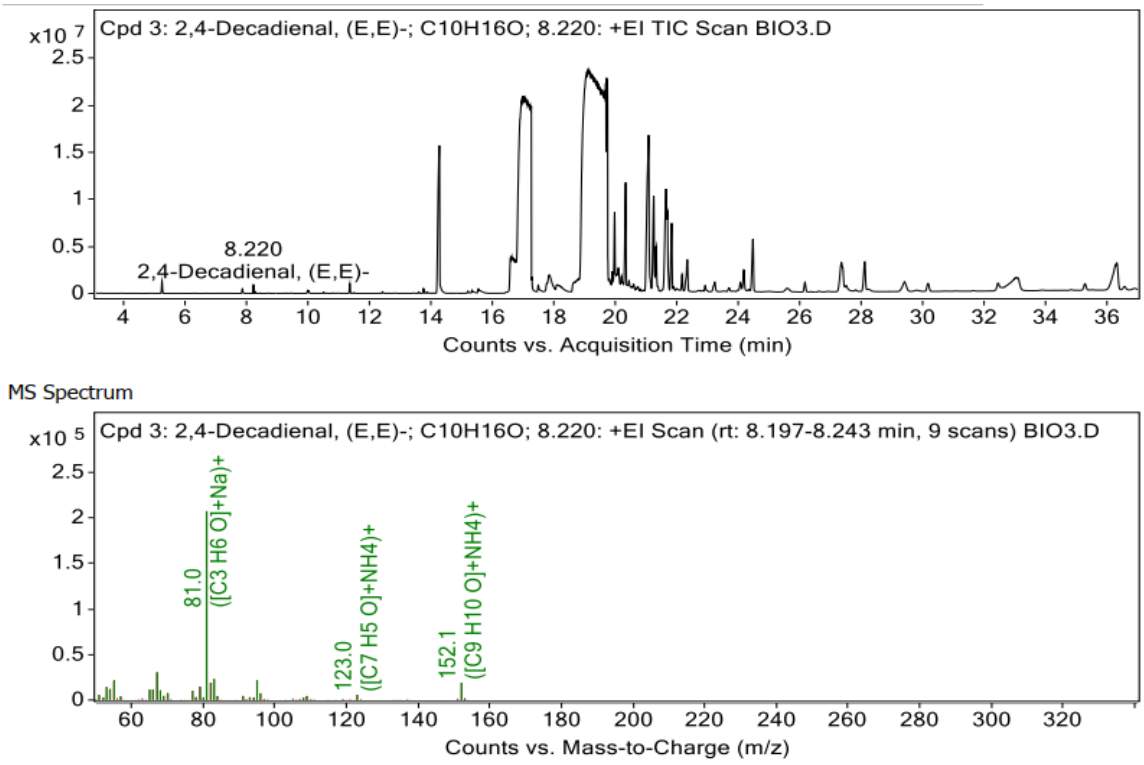

Figure 4.13 Spectrum distribution of 2,4-Decadienal, (E, E)

Figure 4.14 illustrates the GC–MS spectrum distribution for Lauric ME, identified as P448, with a molecular formula of $C_{13}H_{26}O_2$ and retention time of 11.356 minutes. As seen from the top chromatogram, at this retention time, there is a well-defined peak that confirms Lauric acid ME is indeed present in the sample. The fragmentation pattern illustrated in the lower mass spectrum also confirms, through distinctive fragment ions, that it is a fatty acid methyl ester. The highly noticeable m/z peaks include 74.0, 87.0, 143.1, 171.1, 183.2, and 214.2, usually assigned to methyl esters, which reinforce the confirmation of the compound.

Figure 4.15 shows the GC–MS spectrum distribution of Myristic acid ME, identified as compound $C_{15}H_{30}O_2$ with a retention time of 14.268 minutes. The chromatogram in the upper panel has a well-defined peak at this retention time, indicating that Myristic acid ME exists in this biodiesel sample. A representative mass spectrum exhibits characteristic fragmentation patterns typical of long-chain fatty acid methyl esters. Diagnostic fragment ions appear at m/z 74.1, 87.1, 101.1, 129.1, 143.1, 157.1, 185.1, 199.2, and 242.2. In general, combined retention behavior and diagnostic mass fragments provide strong confirmation of the presence and purity of Myristic acid methyl ester in the analyzed sample.

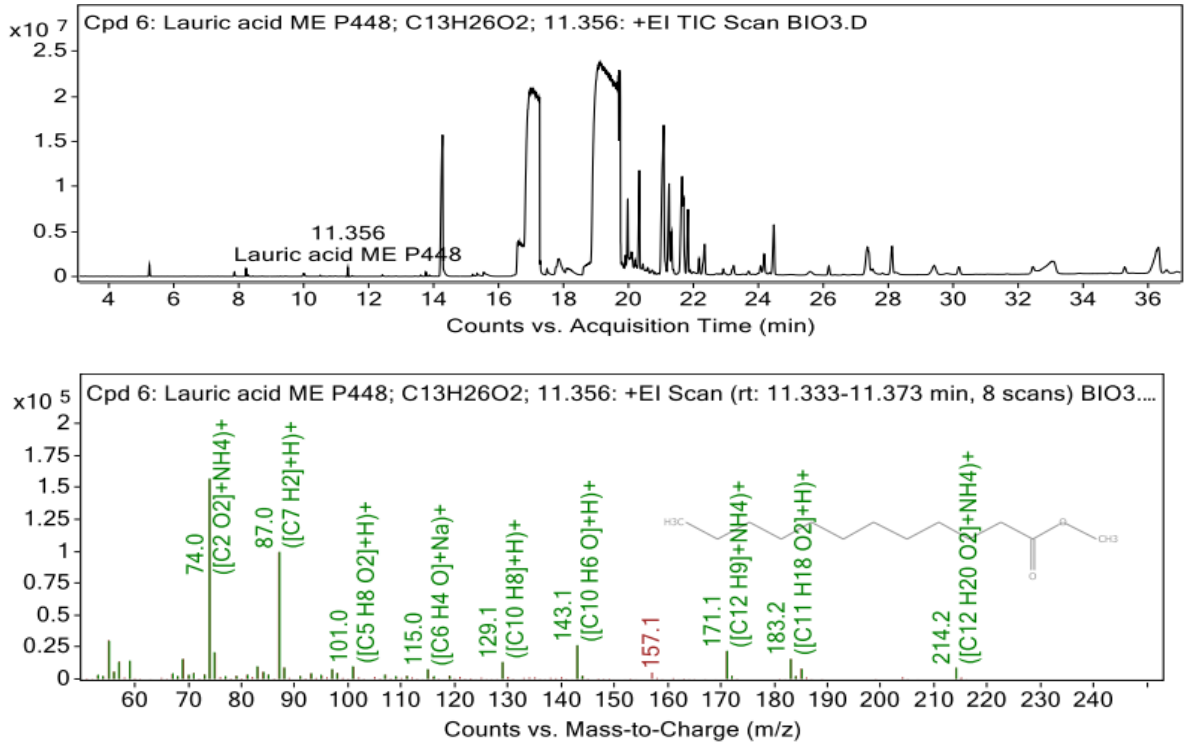

Figure 4.14 Spectrum distribution of Lauric acid ME P448

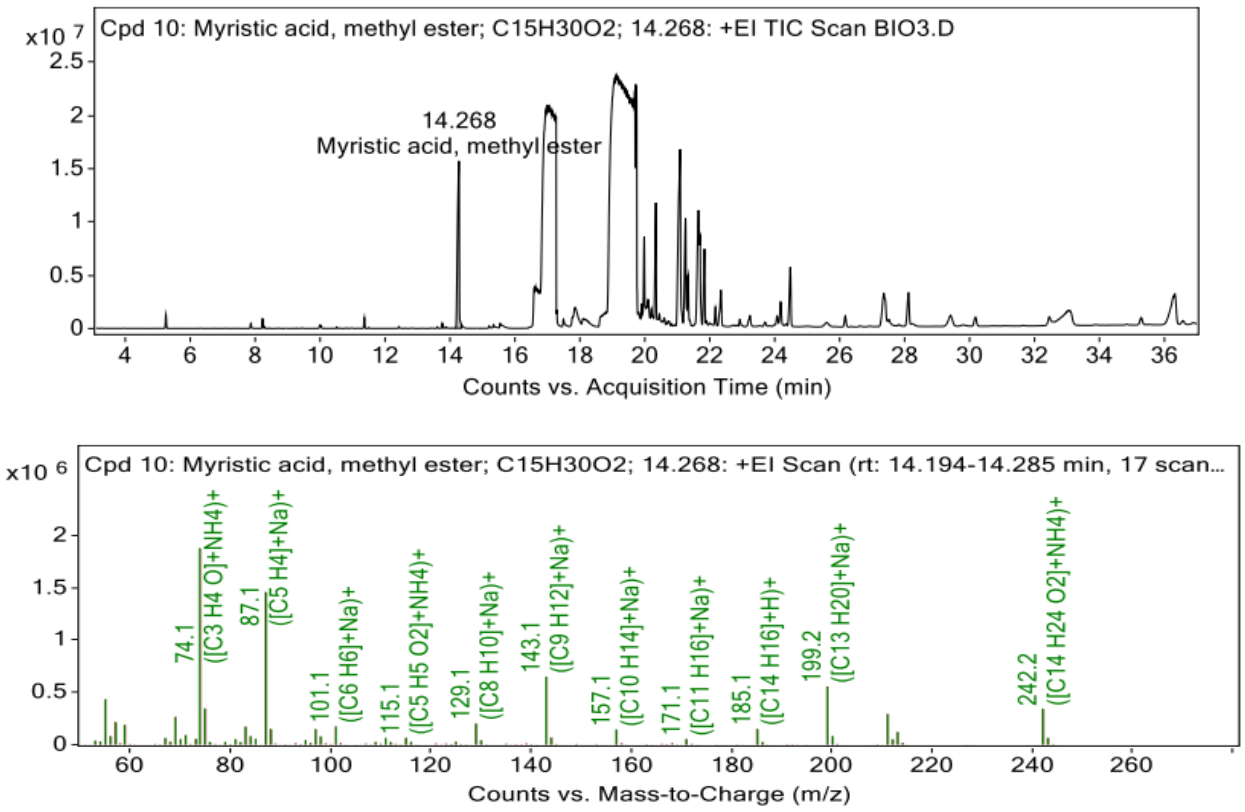

Figure 4.15 Spectrum distribution of Myristic acid, ME

Figure 4.16 represents the GC-MS identification of a common FAME, Hexadecanoic acid, methyl ester ($C_{17}H_{34}O_2$), which eluted at 17.003 minutes. The chromatogram presents a sharp symmetrical peak that indicated a pure compound with good separation. The mass spectrum also shows the typical fragmentation pattern of a long-chain saturated FAME. In addition, very prominent m/z peaks, including 74.1, 84.1, 111.1,129.1,143.1, 171.1, 199.2, and 213.2, commonly associated with methyl esters, reinforce the confirmation of this compound.

Figure 4.17 shows the GC-MS detection and identification of Methyl 9-cis,11-trans-octadecadienoate ($C_{19}H_{34}O_2$), a conjugated linoleic acid methyl ester (C18:2) isomer that eluted at 19.138 minutes. The mass spectrum showed a very distinctive fragmentation pattern for a di-unsaturated fatty acid methyl ester with key fragment ions at m/z 67.1, 95.1, 123.1, 150.1, 178.2, 220.2, 263.3, and 293.3. Based on all spectral data, this is a specific conjugated linoleic acid methyl ester isomer.

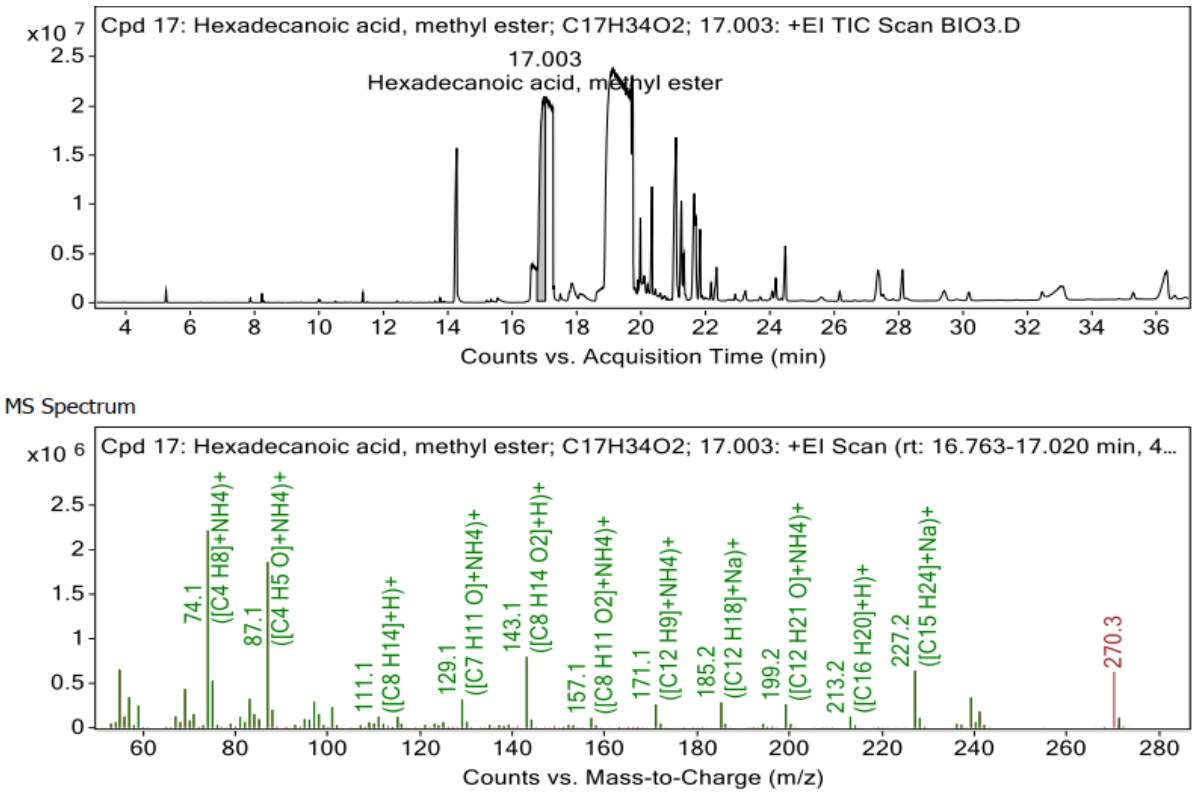

Figure 4.16 Spectrum distribution of Hexadecanoic acid, ME

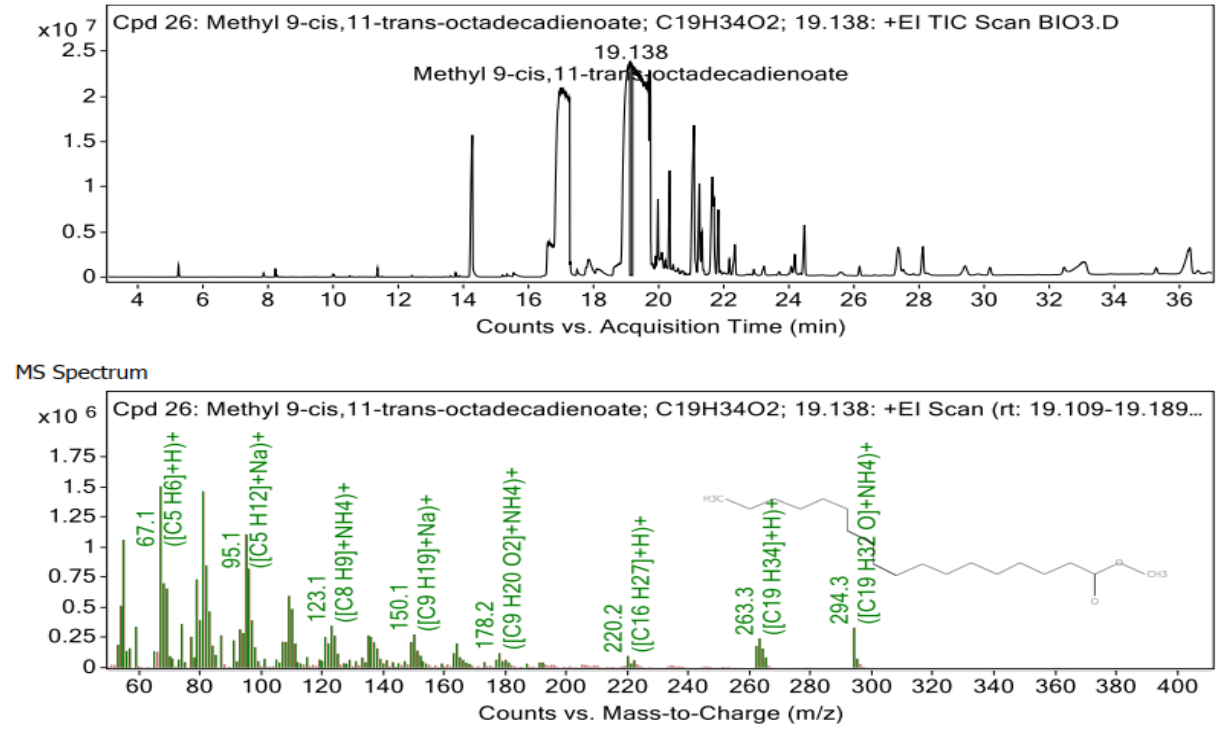

Figure 4.17 Spectrum distribution of Methyl 9-cis,11-transoctadecadienoate

Figure 4.18 presents the GC-MS detection and identification of the non-conjugated linoleic acid methyl ester (C18:2) isomer, Methyl 8,9-octadecadienoate ($C_{19}H_{34}O_2$), which eluted slightly later, at 21.077 minutes. The mass spectrum revealed a fragmentation pattern typical of a di-unsaturated fatty acid methyl ester. Indeed, this methyl ester of a di-unsaturated fatty acid exhibited a very characteristic fragmentation pattern, with fragment ions at m/z 81.1, 121.1, 164.1, 207.1, 235.2, and 279.2, among others. Thus, from both its retention time and spectral data, the compound was with high confidence identified as this particular methyl octadecadienoate isomer.

Figure 4.19 represents the GC-MS detection and identification of Methyl 20-methyl-heneicosanoate ($C_{23}H_{46}O_2$), a branched-chain fatty acid methyl ester that eluted at 24.471 minutes. The fragmentation pattern represented in the lower mass spectrum also confirms, through characteristic fragment ions, that it is a fatty acid methyl ester. The highly noticeable m/z peaks include 74.0, 97.1, 143.1, 171.1, 227.2, and 255.2, usually assigned to methyl esters, which reinforce the confirmation of the compound.

Figure 4.20 illustrates GC-MS detection and identification of Tetracosanoic acid, methyl ester ($C_{25}H_{50}O_2$); this is a long-chain saturated fatty acid methyl ester that eluted at 28.110 minutes. Its mass spectrum demonstrates a classic fragmentation pattern for a saturated FAME. Besides, it shows very prominent m/z peaks at 74.1, 143.1, 171.1,199.1,143.1, 241.1, 283.2, and 311.2 commonly associated with methyl esters, supporting the confirmation of this compound. Additionally, Figures 4.21, 4.22, and 4.23 illustrate the GC–MS detection and characterization of dl-α-Tocopherol, Hentriacontane, and (24R)-Stigmast-5-en-3β-ol, respectively. The identification of these compounds was achieved through a close examination of their retention times and mass spectral fragmentation patterns. Such consistency between spectra and established molecular signatures provides high confidence in the accuracy of the compound identification.

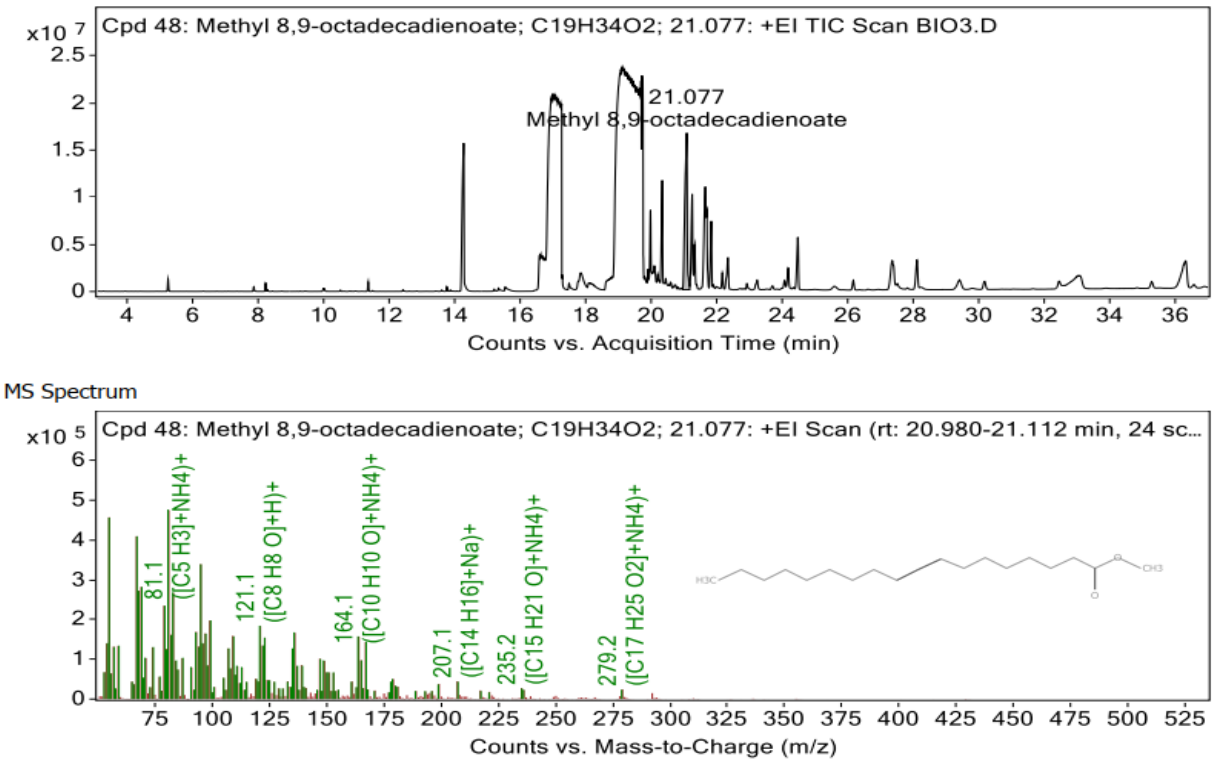

Figure 4.18 Spectrum distribution of Methyl 8,9-octadecadienoate

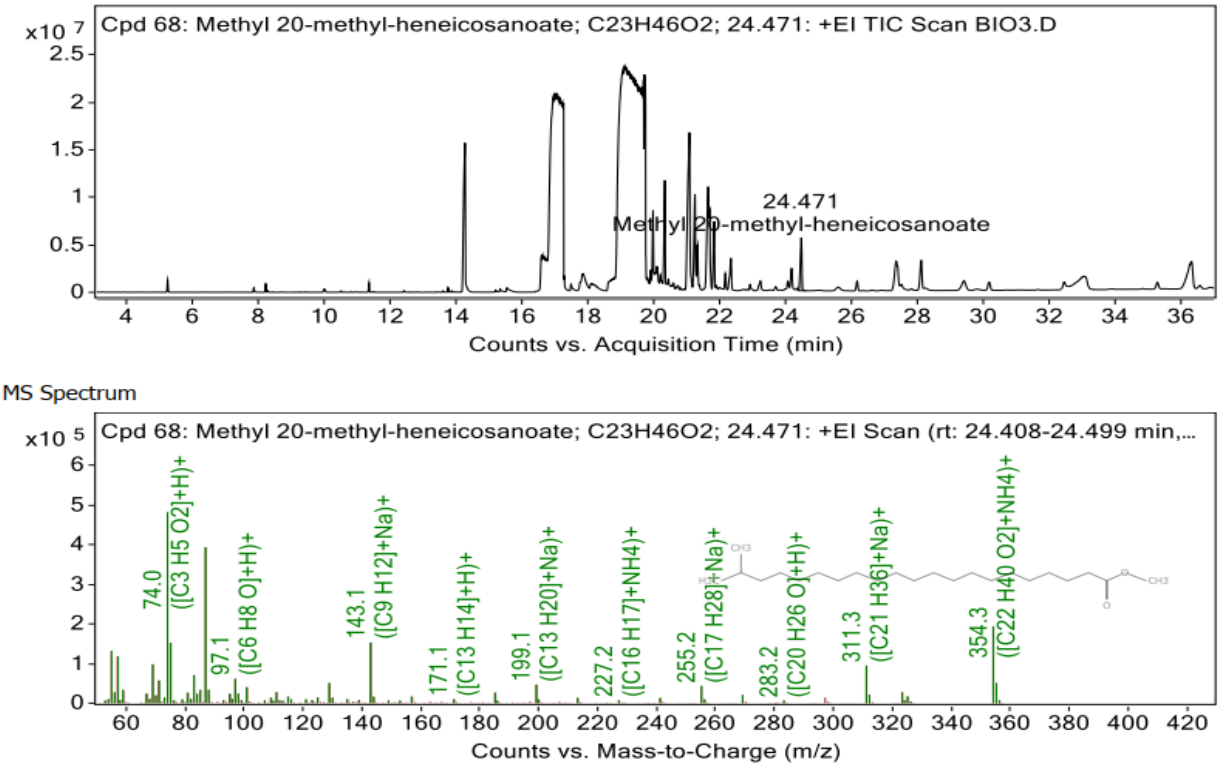

Figure 4.19 Spectrum distribution of Methyl 20-methyl heneicosanoate

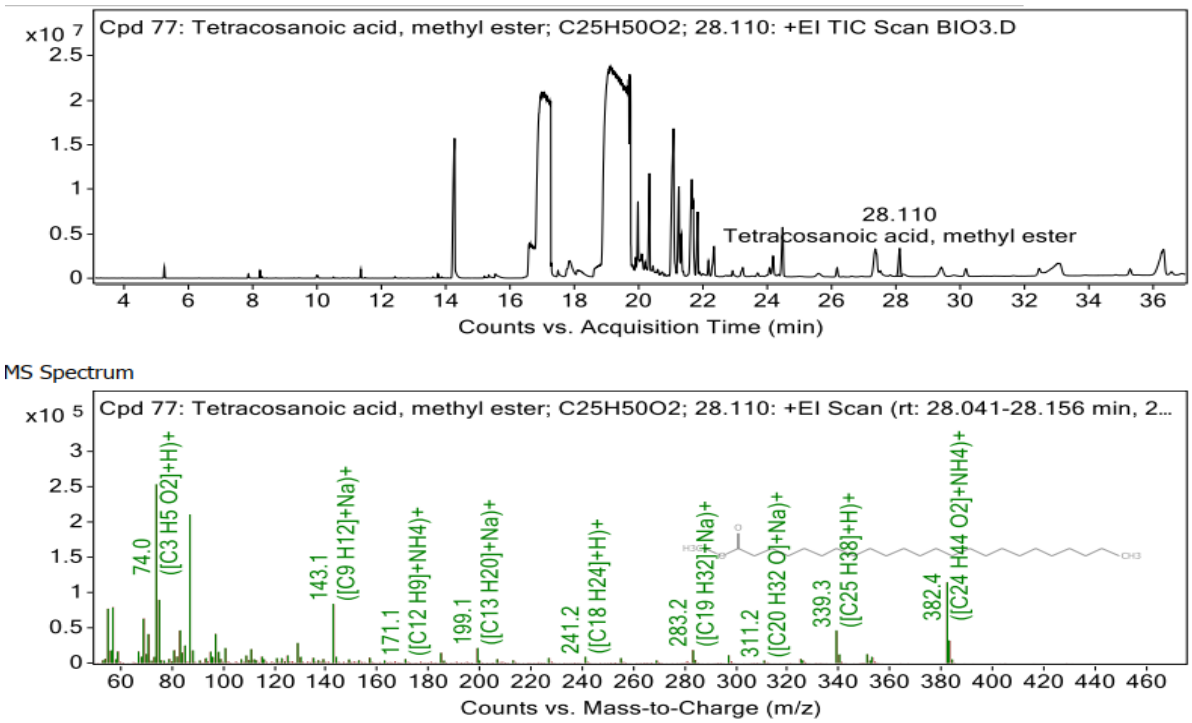

Figure 4.20 Spectrum distribution of Tetracosanoic acid, methyl ester

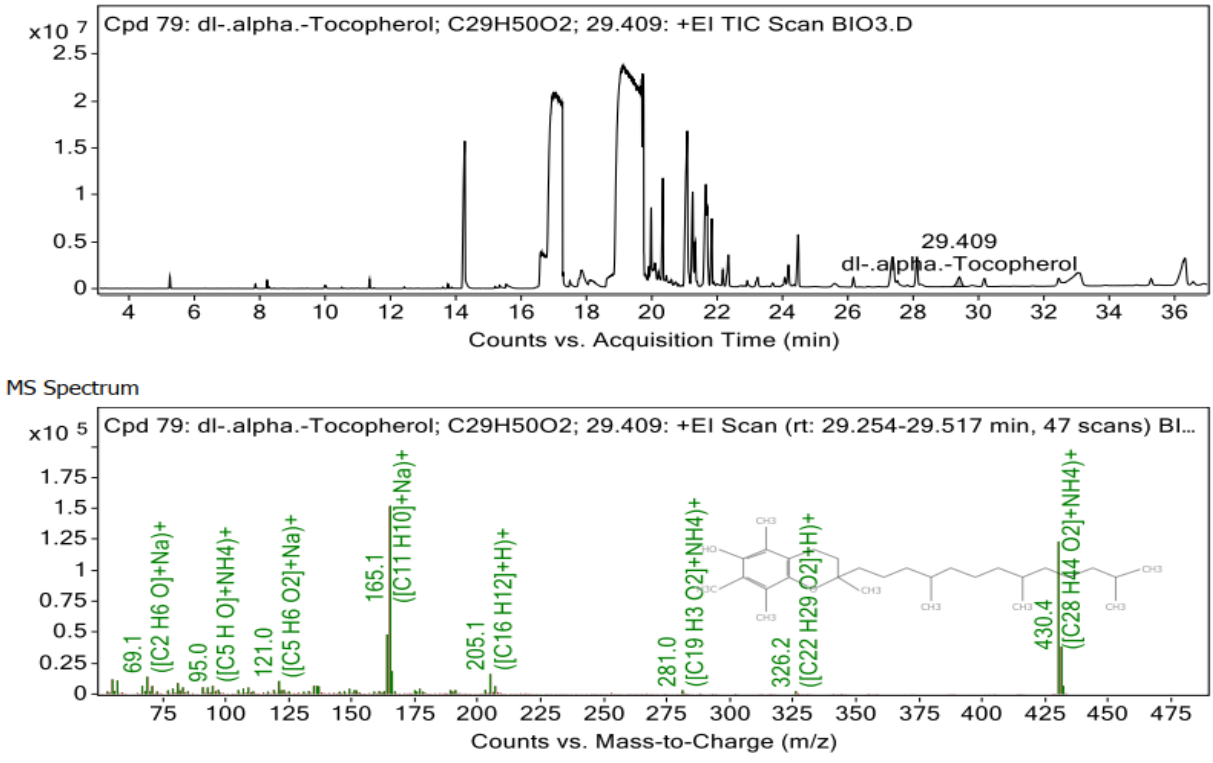

Figure 4.21 Spectrum distribution of dl-. alpha. -Tocopherol

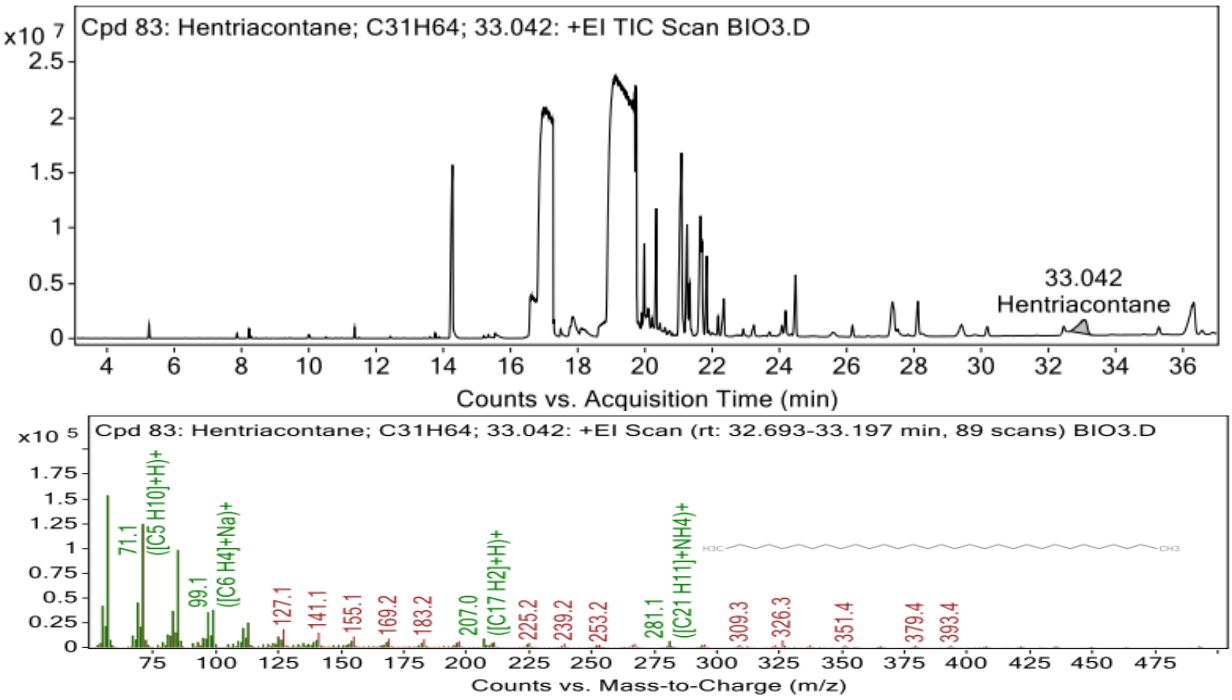

Figure 4.22 Spectrum distribution of Hentriacontane

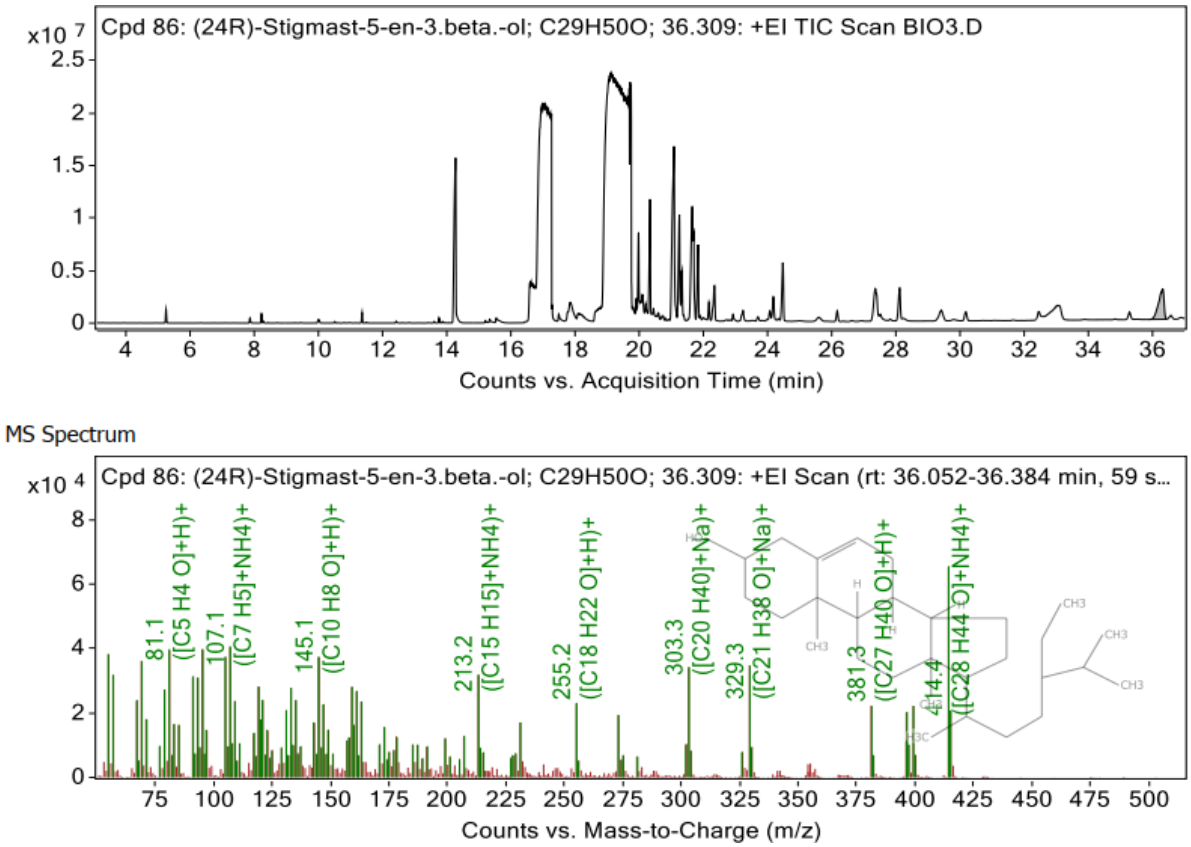

Figure 4.23 Spectrum distribution of (24R)-Stigmast-5-en-3.beta.-ol

4.1.7. FTIR analysis of cottonseed oil biodiesel

The Fourier Transform Infrared (FTIR) spectroscopy analysis, presented in Fig.4.24, was performed to investigate the functional groups present in the biodiesel synthesized via the transesterification of cottonseed oil. The FTIR spectrum revealed both prominent and subtle absorption bands within the wavenumber range of 3500 to 700 cm^{-1}, which reflects the complex molecular structure of the biodiesel sample. A notable peak observed at 3008.7 cm^{-1} was linked to the stretching vibrations of C–H bonds, suggesting the presence of carboxylic acids and alkenes. Additional peaks at 2923.00 cm^{-1} and 2853.94 cm^{-1} were also related to C–H stretching, reinforcing the identification of aliphatic chains typical of alkanes, along with potential residual carboxylic acid groups (Jimoh et al., 2023b). Furthermore, absorption bands at 2160.49 cm^{-1} and 2019.93 cm^{-1} were associated with C≡C stretching, indicating the presence of alkyne functionalities, which may originate from minor unsaturated intermediates or degradation products. The spectrum's most significant feature was the pronounced absorption peak at 1742.72 cm^{-1}, indicative of the C=O stretching vibration found in ester functional groups, thereby confirming the effective transformation of triglycerides into fatty acid methyl esters (FAMEs).

Another important peak at 1653.21 cm^{-1} was attributed to C=C stretching, highlighting the preservation of unsaturated double bonds characteristic of alkenes. Additionally, the band at 1459.35 cm^{-1} was linked to C–H bending vibrations, a common trait in long-chain alkanes. Molecular analysis revealed significant peaks at 1361.98 cm^{-1} and 1242.51 cm^{-1}, which correspond to C–H bending and C–O stretching vibrations, respectively. These peaks are indicative of esterified compounds and play a crucial role in validating the quality of biodiesel. Additionally, absorption bands observed at 1194.85 cm^{-1}, 1106.6 cm^{-1}, and 1015.68 cm^{-1} were linked to C–O stretching vibrations, commonly found in alcohols, ethers, and amine derivatives, suggesting the presence of residues or by-products from the transesterification process. Furthermore, the peak at 846.03 cm^{-1}, associated with C=C bending, reinforces the existence of unsaturated alkenes, while the signal at 721.59 cm^{-1}, resulting from C–H stretching modes, confirms the structural characteristics of long-chain alkanes. The spectral characteristics observed align closely with those documented in previous studies (Clay et al., 2023; Jimoh et al., 2023a; Venkatesan et al., 2017), collectively reinforcing the notion that the biodiesel produced maintains the fundamental

molecular traits of fatty acid methyl esters, while also exhibiting the natural variability associated with feedstocks derived from plant oils.

In a wider scientific framework, Fourier Transform Infrared (FTIR) spectroscopy is recognized as a swift and non-invasive method for tracking the biodiesel production process and evaluating fuel quality. The detection of ester bonds and the assessment of unsaturation levels are crucial for forecasting fuel performance, which encompasses aspects such as oxidative stability, combustion efficiency, and cold flow behavior. A high concentration of esters, indicated by pronounced C=O stretching, is directly linked to effective conversion efficiency, whereas the presence of unsaturated bonds affects the biodiesel's reactivity and its performance during long-term storage. Consequently, FTIR not only confirms the efficacy of the transesterification process but also offers essential insights for enhancing fuel properties to comply with international standards like ASTM D6751 and EN 14214.

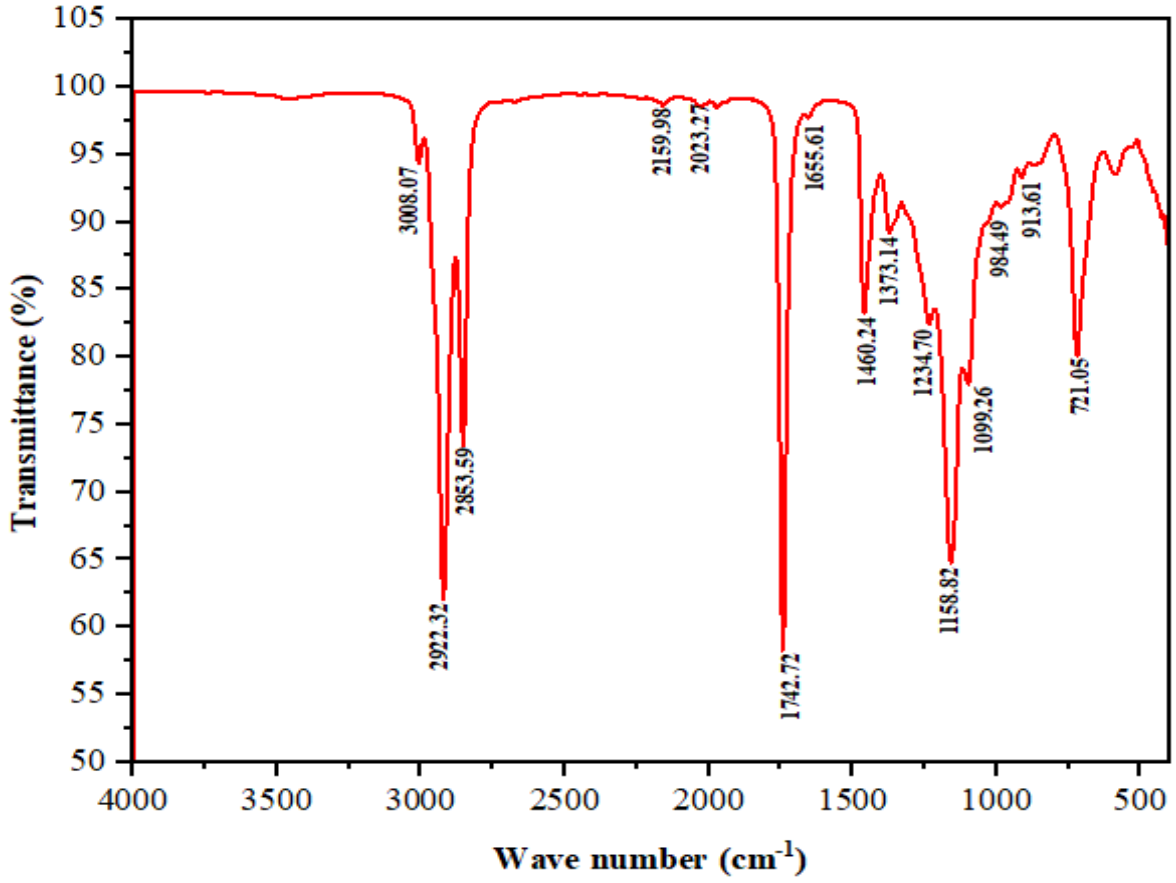

Figure 4.24 FTIR spectrum of cottonseed oil biodiesel

4.1.8. Analysis of the physicochemical characteristics of oil and biodiesel

Table 4.6 presents the physicochemical characteristics of raw cottonseed oil and its transesterified biodiesel (CSO biodiesel), evaluated against the biodiesel quality specifications set by EN 14214 and ASTM D6751. The analyzed parameters, which include viscosity, density, acid value, and iodine value, indicate that the produced biodiesel satisfies the necessary requirements for safe and effective use in engines. The CSO biodiesel exhibited a density of 880 kg/m^3 at 20°C and a viscosity of 4.4 mm^2/s at 40°C. These measurements are well within the acceptable limits defined by ASTM D6751 and EN 14214, highlighting the biodiesel's compatibility with diesel engines regarding fuel atomization and flow characteristics. These factors are essential, as the correct viscosity is vital for optimal fuel injection and combustion, while density affects the energy content per unit volume, thereby influencing both engine performance and emissions. The biodiesel demonstrated a flash point of 178°C and a cloud point of 5°C, both of which comply with the safety and cold flow standards established by ASTM D6751.

The flash point serves as an indicator of the fuel's flammability, suggesting that the biodiesel can be handled and stored safely under standard operating conditions. In contrast, the cloud point signifies its effectiveness in cold weather, which is particularly important for biodiesel use in temperate regions. The acid value, indicative of the concentration of FFAs, was measured at 0.22 mg KOH/g, significantly lower than the maximum allowable limit of 0.5 mg KOH/g set by EN 14214. A lower acid value is advantageous as it reduces the likelihood of corrosion and the formation of deposits within fuel systems. Additionally, the iodine value, which assesses the level of unsaturation, was found to be 82.2 g I_2/100 g, well within the EN 14214 limit of 120 g I_2/100 g. Keeping the iodine value in this range is crucial for ensuring oxidative stability, thereby preventing rancidity and the development of polymers during extended storage.

The biodiesel's saponification value was measured at 137.45 mg KOH/g, which is lower than the saponification value of the original cottonseed oil, recorded at 184.6 mg KOH/g. While the saponification value is not explicitly mentioned in the standards set by ASTM D6751 or EN 14214, it serves as a valuable indicator of the average molecular mass of the fatty acids present. The observed decrease in this value following transesterification indicates an effective transformation of triglycerides into methyl esters, leading to a reduction in molecular complexity. Furthermore, the moisture content for both the unrefined oil and the final biodiesel was found to be 0.04%,

which is within the acceptable limit of 0.05% as per ASTM D6751. It is crucial to maintain a low moisture level to prevent issues such as microbial growth, fuel degradation, and phase separation, all of which can adversely impact engine performance. The physicochemical properties evaluated indicate that the CSO biodiesel produced is of superior quality, confirming its adherence to international fuel standards and highlighting its potential as a sustainable alternative to petroleum-derived diesel. This finding supports the increasing agreement within biofuel research that cottonseed oil, which is non-edible and readily accessible, can be effectively converted into high-quality biodiesel that is appropriate for both commercial use and environmental sustainability.

Table 4.6 Oil and biodiesel's physicochemical properties in relation to diesel fuel

Property	Oil	Biodiesel	Diesel	Standards	
				ASTM D 6751	EN 14214
Acid value (mgKOH/g)	0.39	0.22	-	0.5 max	0.5 max
Cloud point (°C)	+10	+5	Max +5	-3 to 12	-
Density at 20 °C (kg/m^3)	920	880	830-860	-	860-890
Flash point (°C)	289	178	69	130 min	>101
Iodine value (g I/100 g)	102.4	82.2	-	-	120
Moisture content (%)	0.04	0.04	-	0.05 max	-
Saponification value (mgKOH/g)	184.6	137.45	-	-	-
Viscosity at 40 °C (mm^2/s)	30.8	4.41	3.15	1.9-6.0	3.5-5

4.2. Analysis of RCCI Engine Characteristics

4.2.1. Combustion analysis

Engine combustion analysis is generally defined by essential parameters like CP and HRR, which together provide a comprehensive understanding of the thermodynamic and chemical dynamics of the fuel-air mixture throughout the ignition and combustion processes. In this research, the combustion properties of the baseline fuel were first assessed using a conventional compression ignition engine configuration, establishing a foundational reference for comparison with the

advanced RCCI engine modes. The data obtained from the baseline fuel acted as a control benchmark, facilitating the detection of enhancements in performance and alterations in combustion characteristics brought about by the RCCI approach.

4.2.1.1 Cylinder pressure

The combustion characteristics of both the modified RCCI engine and the standard baseline diesel engine were evaluated. The RCCI modes were analyzed through a dual-fuel methodology. This method involved the use of various ratios of gasoline/n-butanol mixtures in the premixed charge, complemented by the direct injection of a B20 biodiesel blend. The objective was to investigate the combined effects of oxygenated alcohol additives and biodiesel on the development of in-cylinder pressure across three distinct engine speeds: 1800, 2200, and 2800 rpm. The findings indicated that at the maximum engine speed of 2800 rpm, the peak cylinder pressures recorded for the baseline diesel and the various fuel blends: B20+G75n-b25, B20+G50n-b50, and B20+G25n-b75, were 59.39 bar, 67.89 bar, 92.25 bar, and 68.42 bar, respectively. At 2200 rpm, the lowest peak cylinder pressures were noted, with the baseline registering 57.24 bar, while the blends showed pressures of 64.65 bar, 72.32 bar, and 63.93 bar. Similarly, at 1800 rpm, the average peak pressures for the baseline fuel reached 58.05 bar, whereas the B20+G75n-b25, B20+G50n-b50, and B20+G25n-b75 blends achieved pressures of 65.34 bar, 76.29 bar, and 65.23 bar, respectively.

As depicted in Fig. 4.25–4.27, the B20+G50n-b50 blend consistently achieved the highest peak cylinder pressure across all tested engine speeds. Although the combustion of the blend of B20 + G50n-b50 was more vigorous and energetically efficient because of improved oxygen availability and enhanced volatility, the RCCI strategy simultaneously mitigated knock tendencies. The much higher-octane contribution from n-butanol and the stratified dual-fuel combustion mode substantially delayed autoignition. In contrast, the B20+G25n-b75 and B20+G75n-b25 blends exhibited a more moderate increase in pressure, suggesting a slower and more controlled combustion process. The maximum cylinder pressure for B20+G50n-b50 is higher than in the cases of B20+G75n-b25 and B20+G25n-b75 due to its more balanced reactivity and optimal oxygenation level. This blend provides superior volatility, better mixture preparation, and a more favorable ignition delay, thus improving the premixed energy release with a slightly higher peak pressure compared to other blends, either rich in gasoline or n-butanol. The comparative evaluation underscores the beneficial impact of incorporating n-butanol, an oxygenated alcohol, on

combustion dynamics. This inclusion fosters better atomization, superior air-fuel mixing, and increased in-cylinder reactivity, owing to n-butanol's lower autoignition temperature and enhanced evaporative qualities compared to conventional gasoline. Specifically, the fuel blends B20+G75n-b25, B20+G50n-b50, and B20+G25n-b75 demonstrated peak pressure increases of 13.27%, 36.40%, and 11.66%, respectively, when compared to baseline diesel operation. These findings are consistent with findings reported in (X. Wang et al., 2021), which indicate that the combination of biodiesel and oxygenated alcohols enhances combustion stability and peak pressure through increased oxygen availability and modified ignition delay characteristics.

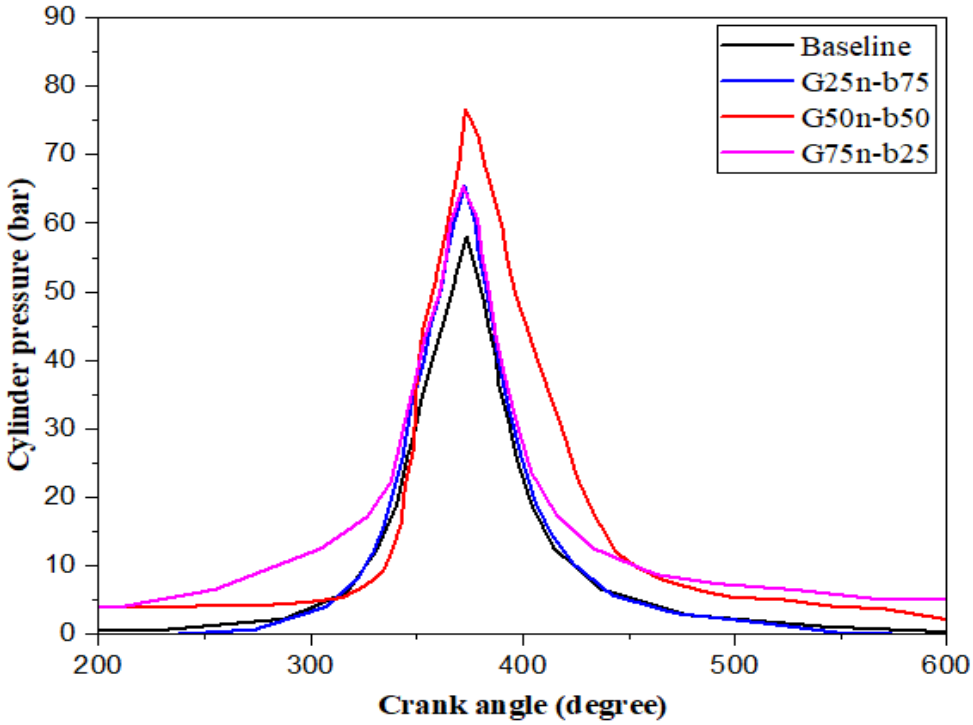

Figure 4.25 Cylinder pressure @1800 rpm

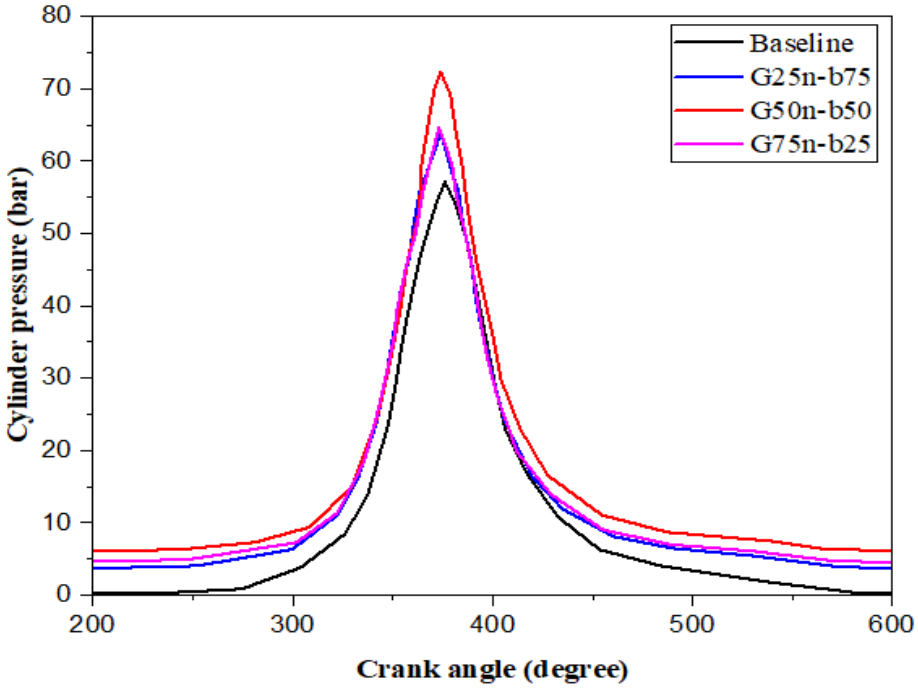

Figure 4.26 Cylinder pressure @2200 rpm

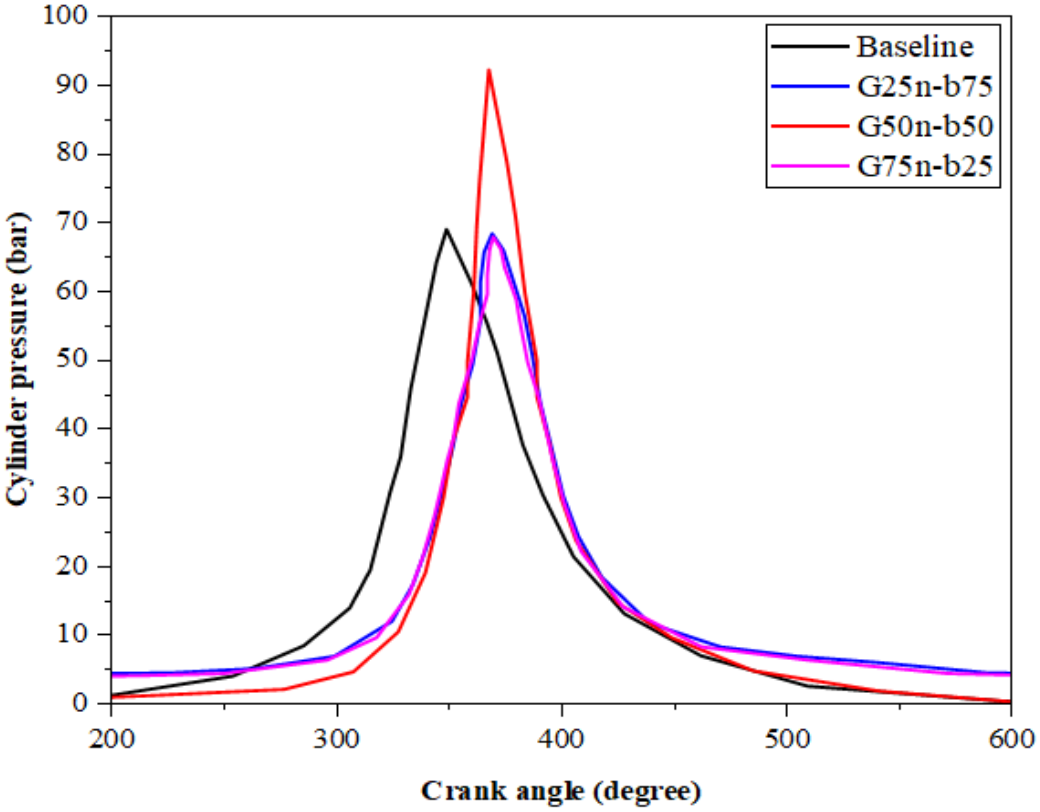

Figure 4.27 Cylinder pressure @2800 rpm

4.2.1.2. Heat release rate

The heat release rate (HRR), a crucial metric for understanding combustion behavior, was derived from in-cylinder pressure measurements by utilizing the first law of thermodynamics within a single-zone combustion model, as outlined in Eq 3.16. This evaluation was conducted for both the standard baseline engine and the modified RCCI engine, which operated using a multi-fuel approach that integrated B20 biodiesel with different proportions of gasoline and n-butanol in the premixed charge. Experimental results obtained at engine speeds of 1800, 2200, and 2800 rpm demonstrated significant variations in HRR profiles among the different fuel blends. At the maximum speed of 2800 rpm, the peak HRR values recorded for the baseline diesel fuel and the blends B20+G25n-b75, B20+G50n-b50, and B20+G75n-b25 were 39.26, 45.16, 62.25, and 43.98 J/°CA, respectively. In contrast, the lowest HRR values were observed at 2200 rpm, with measurements of 28.32, 29.86, 39.59, and 29.96 J/°CA for the corresponding fuels. At 1800 rpm, the baseline fuel exhibited an average HRR of 38.72 J/°CA, while the blends B20+G25n-b75, B20+G50n-b50, and B20+G75n-b25 achieved higher average values of 43.54, 45.88, and 43.75 J/°CA, respectively.

As depicted in Fig.4.28-4.30, the HRR for the baseline fuel consistently remained lower than that of all the RCCI multi-fuel blends tested throughout the entire range of engine speeds. Among these blends, the B20+G50n-b50 exhibited the highest peak HRR, suggesting a more rapid and complete combustion process, likely facilitated by the optimal oxygenation and enhanced volatility of n-butanol at a 50% substitution level. In comparison to the baseline fuel, the B20+G25n-b75, B20+G50n-b50, and B20+G75n-b25 blends showed increases in HRR of 10.95%, 33.99%, and 9.39%, respectively. These results are consistent with earlier research (Disassa, Ancha, & Nallamothu, 2023), supporting the notion that the inclusion of oxygenated fuels, such as n-butanol and biodiesel, enhances combustion thermodynamics by increasing the oxygen availability, shortening ignition delays, and fostering a more uniform release of energy. Importantly, the improved HRR observed in blends with a higher proportion of n-butanol also highlights the advantageous physical properties of n-butanol, such as its lower cetane number and elevated latent heat of vaporization, which aid in achieving better charge stratification and more effective mixing under RCCI operational conditions.

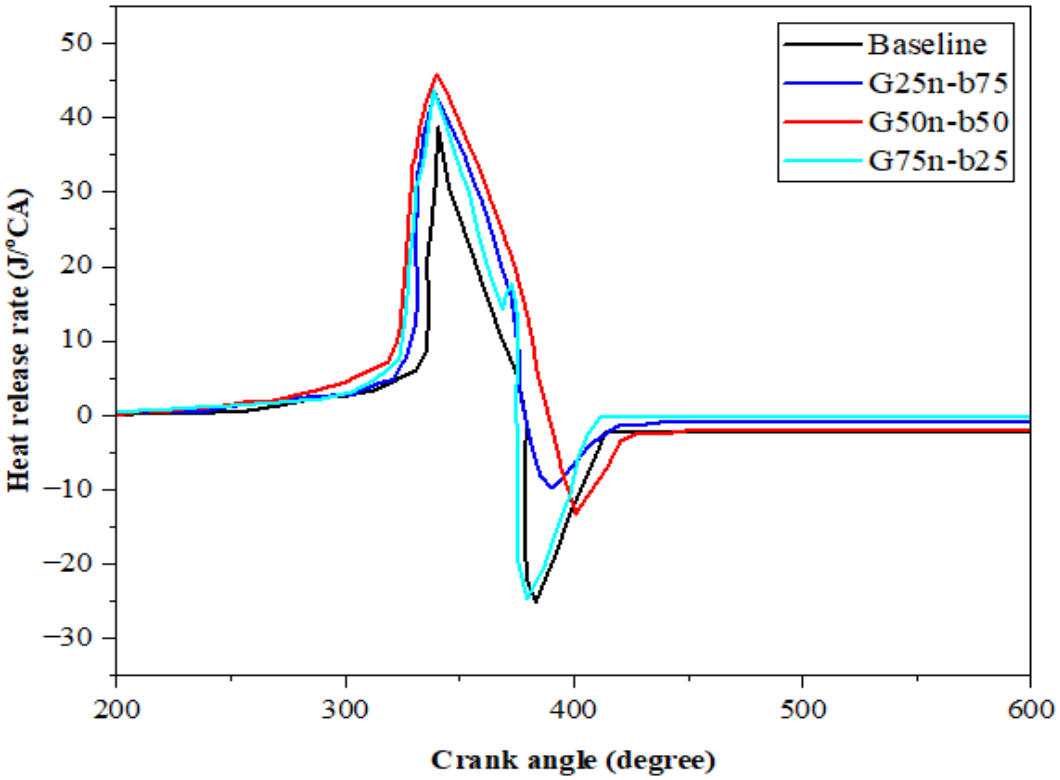

Figure 4.28 Heat release rate @1800 rpm

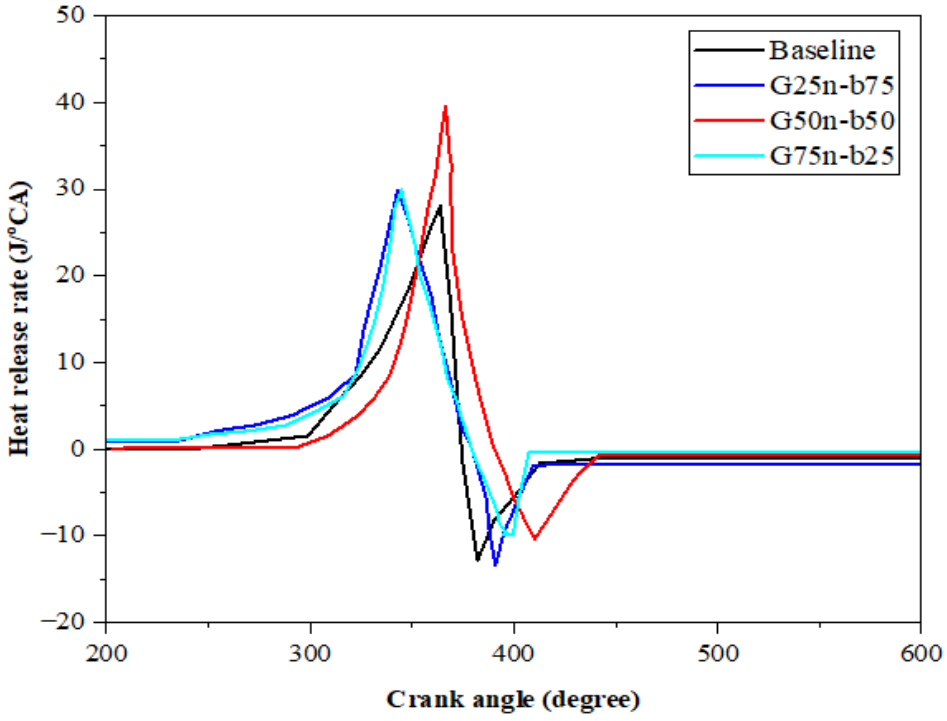

Figure 4.29 Heat release rate @2200 rpm

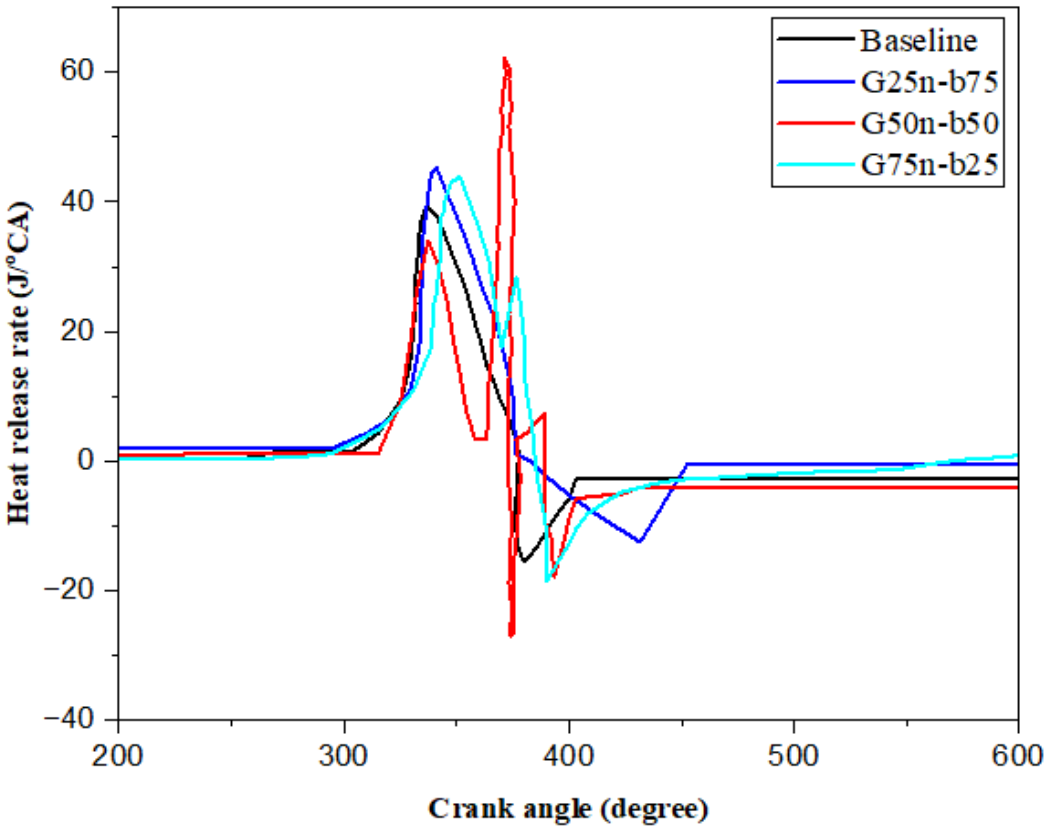

Figure 4.30 Heat release rate @2800 rpm

4.2.2. Engine performance

Engine performance is typically evaluated using key indicators such as BT, BP, and BSFC, which together reflect the mechanical efficiency and fuel utilization behavior of internal combustion engines. In this study, the performance characteristics of the baseline fuel were first assessed under CDC engine conditions, establishing a foundational reference point for subsequent comparative analysis against the various operational modes employed in the RCCI engine.

4.2.2.1. Brake power (BP)

Fig. 4.31 depicts the relationship between BP and engine speed, spanning from 1800 to 2800 rpm. The experimental findings reveal that the BP for all fuel blends tested generally aligns with the trend observed in the baseline fuel, with the B20+G50n-b50 demonstrating superior performance compared to the other blends, especially at higher engine speeds. This improvement underscores the beneficial impact of an optimized gasoline-n-butanol ratio on both combustion efficiency and power output. Throughout the entire range of engine speeds, BP exhibited a steady increase,

peaking at 2800 rpm for all fuel types. This pattern is typically linked to higher number of power strokes per unit time and the corresponding rise in mechanical output. Nevertheless, within the lower speed range of 1800 to 2400 rpm, all port-injected (PI) fuel blends showed a slight decrease in BP relative to the baseline. This reduction may be attributed to factors such as incomplete atomization or diminished in-cylinder turbulence at lower speeds, which can hinder fuel-air mixing and delay the ignition process.

Among the various fuel blends tested, the B20+G50n-b50 mixture achieved the highest BP output, reaching a peak of 4.35 kW at 2800 rpm. This finding indicates that an optimal ratio of gasoline to n-butanol enhances both combustion stability and energy release, particularly under conditions of high load and speed. In contrast, the B20+G25n-b75 blend, which has a greater proportion of n-butanol, consistently yielded lower BP values, averaging a reduction of about 3% compared to the baseline fuel, with the most significant differences observed at lower engine speeds. This decrease in performance can be linked to n-butanol's lower cetane number and its higher latent heat of vaporization, which can hinder ignition and diminish combustion efficiency at reduced temperatures and speeds. On the other hand, the B20+G75n-b25 blend, which contains a larger share of gasoline, showed a slight enhancement in BP at elevated speeds, with an average decrease of 1.83% compared to the baseline.

The notable performance of the B20+G50n-b50 blend, which exhibited an average BP increase of 2.8% across the tested speed range, highlights the critical role of achieving a precise balance between the oxygen content and volatility characteristics of the premixed low-reactivity fuel to optimize power output in RCCI engines. The results of this study support the notion that refining the composition of the fuel blend, particularly the ratio of gasoline to n-butanol, is essential for improving combustion efficiency. This is especially evident at elevated speeds, where better charge stratification and optimum ignition timing lead to increased brake power.

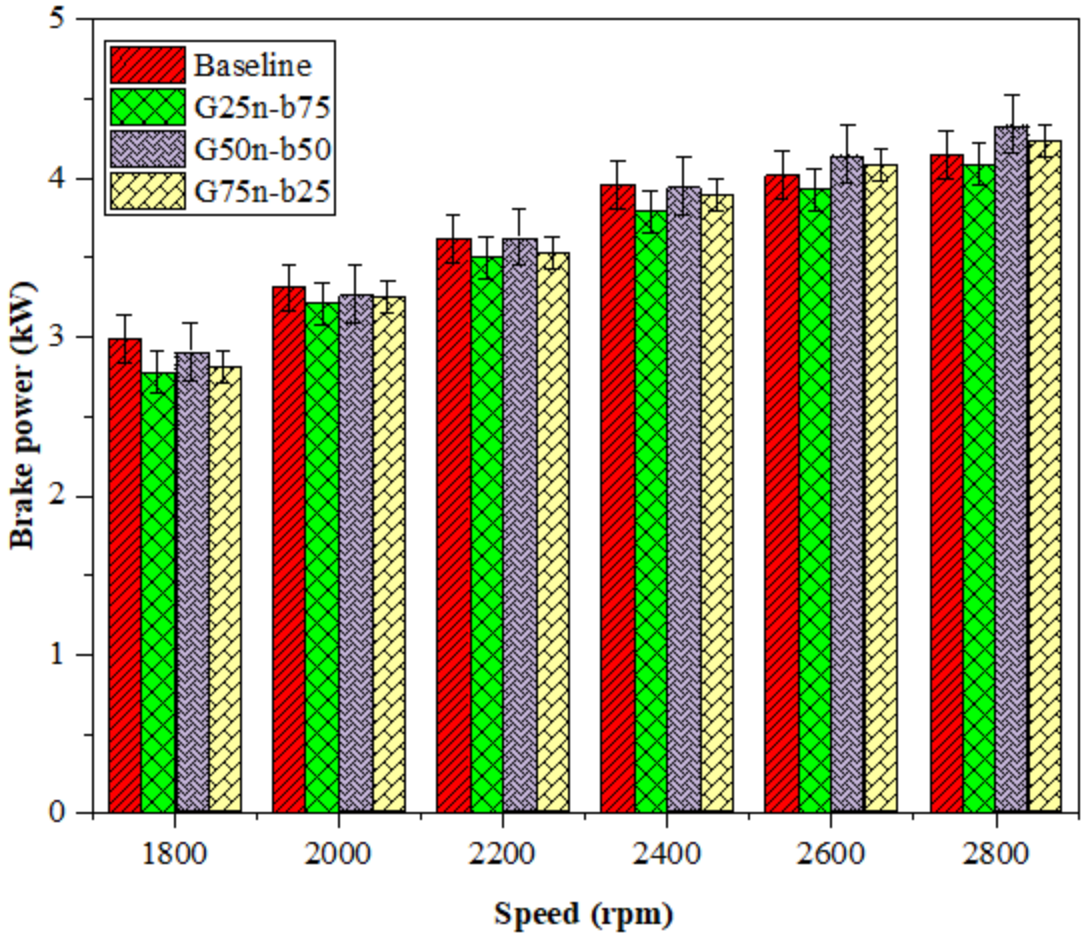

Figure 4.31 Brake power of the engine

4.2.2.2. Brake torque (BT)

The data illustrated in Figure 4.32 reveals the fluctuations in brake torque (BT) across engine speeds from 1800 to 2800 rpm for various fuel blends tested. It was noted that the RCCI engine utilizing the B20+G75n-b25, B20+G50n-b50, and B20+G25n-b75 blends consistently surpassed the baseline diesel configuration in torque output at all evaluated speeds. Notably, the B20+G50n-b50 blend, which comprises an equal mix of gasoline and n-butanol, exhibited the most significant enhancement in BT, followed by B20+G75n-b25 and B20+G25n-b75 in that order. Across all fuel blends, BT reached its maximum around 2400 rpm, subsequently declining as engine speed increased. This trend is characteristic of CI engines, where optimum air-fuel mixing, injection timing, and in-cylinder thermodynamic conditions align at mid-range speeds to enhance combustion efficiency and torque production.

The G50n-b50 blend's superior performance, with an average BT increase of about 3% over the baseline, indicates that this specific gasoline-n-butanol ratio strikes an optimal balance among volatility, oxygen content, and energy density, thereby facilitating improved combustion timing and pressure development within the cylinder. The B20+G75n-b25 blend also demonstrated a significant torque improvement, though slightly less than that of B20+G50n-b50, likely due to its reduced n-butanol content, which enhances evaporative cooling and ignition readiness compared to blends with higher n-butanol proportions. Conversely, the B20+G25n-b75 blend, characterized by a higher n-butanol content, showed only marginal increases in BT compared to the baseline. This limited performance can be linked to n-butanol's lower cetane number and elevated latent heat of vaporization, which tend to delay ignition timing and diminish the rate of pressure increase, particularly at lower engine loads and speeds.

The results align with the well-accepted notion that a moderate incorporation of oxygenated fuels, like n-butanol, improves the uniformity of combustion within the cylinder and facilitates more thorough oxidation of the fuel, leading to enhanced torque performance. Nevertheless, an overabundance of n-butanol may negatively impact combustion stability and the efficiency of energy release, particularly under specific engine operating scenarios.

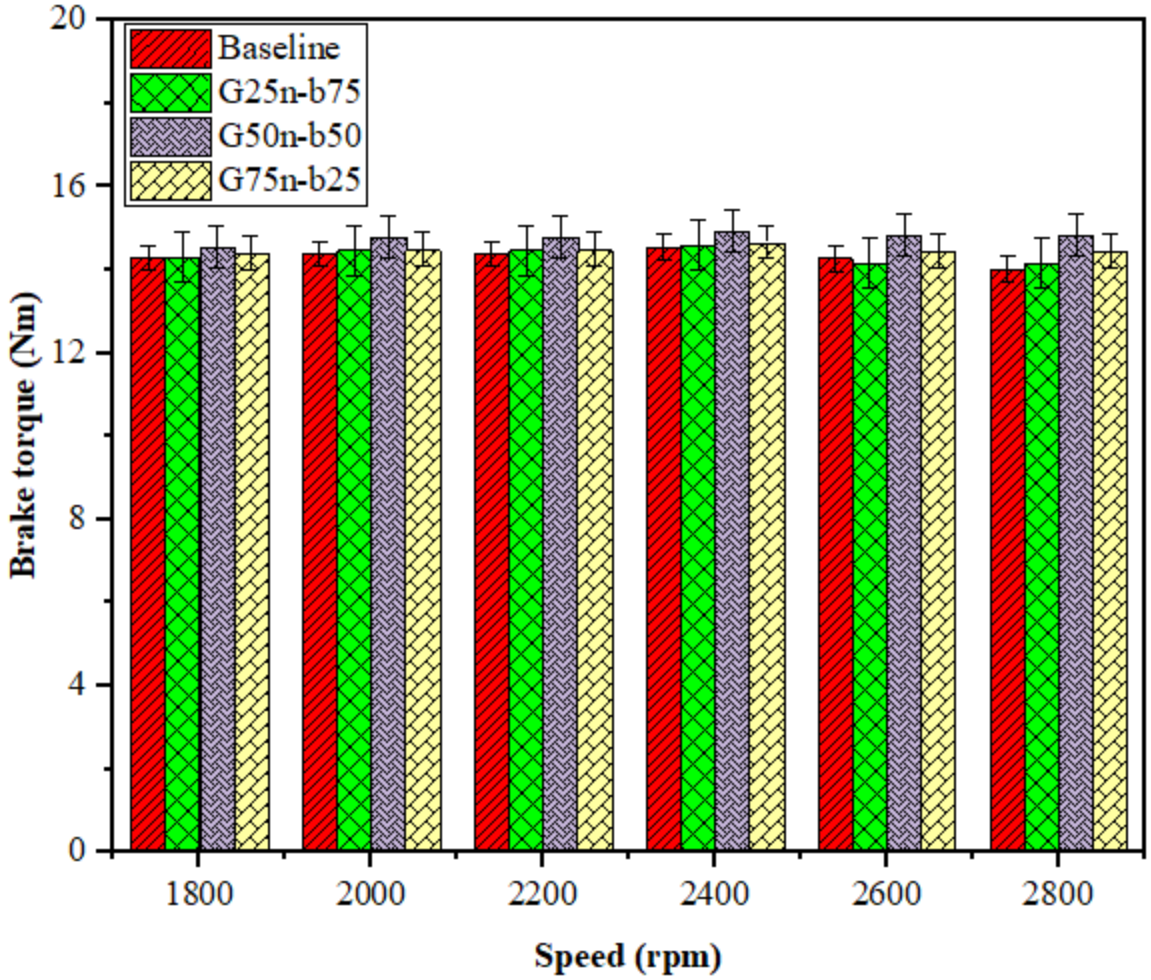

Figure 4.32 Brake torque of the engine

4.2.2.3. Brake specific fuel consumption (BSFC)

Figure 4.33 illustrates the analysis of BSFC, revealing that all tested PI fuel blends demonstrate higher BSFC values compared to the baseline across all engine speeds. On average, the B20+G25n-b75 blend shows an increase in BSFC of approximately 4% relative to the baseline, with the most significant rise occurring at lower speeds. The B20+G75n-b25 blend exhibits a moderate increase of about 2.83%, while the B20+G50n-b50 blend records the smallest increase, averaging around 1.54%. The smaller BSFC increase for B20+G50n-b50 can be attributed to a balanced amount of gasoline and n-butanol, which is more favorable for combustion compared to other blends. During combustion, this blend has moderate volatility and oxygen content that improves fuel-air mixture and energy release characteristics, ensuring relatively better fuel utilizations and hence, a relatively lower increase in BSFC when compared to the B20+G25n-b75

and B20+G75n-b25 blends. The peak BSFC values are noted at 1800 rpm, with a downward trend as the speed increases. These trends suggest that a higher concentration of n-butanol is associated with increased fuel consumption, which can be attributed to its lower energy density. In contrast, an optimal n-butanol to gasoline ratio improves combustion efficiency, leading to a decrease in BSFC at higher speeds compared to other fuel blends.

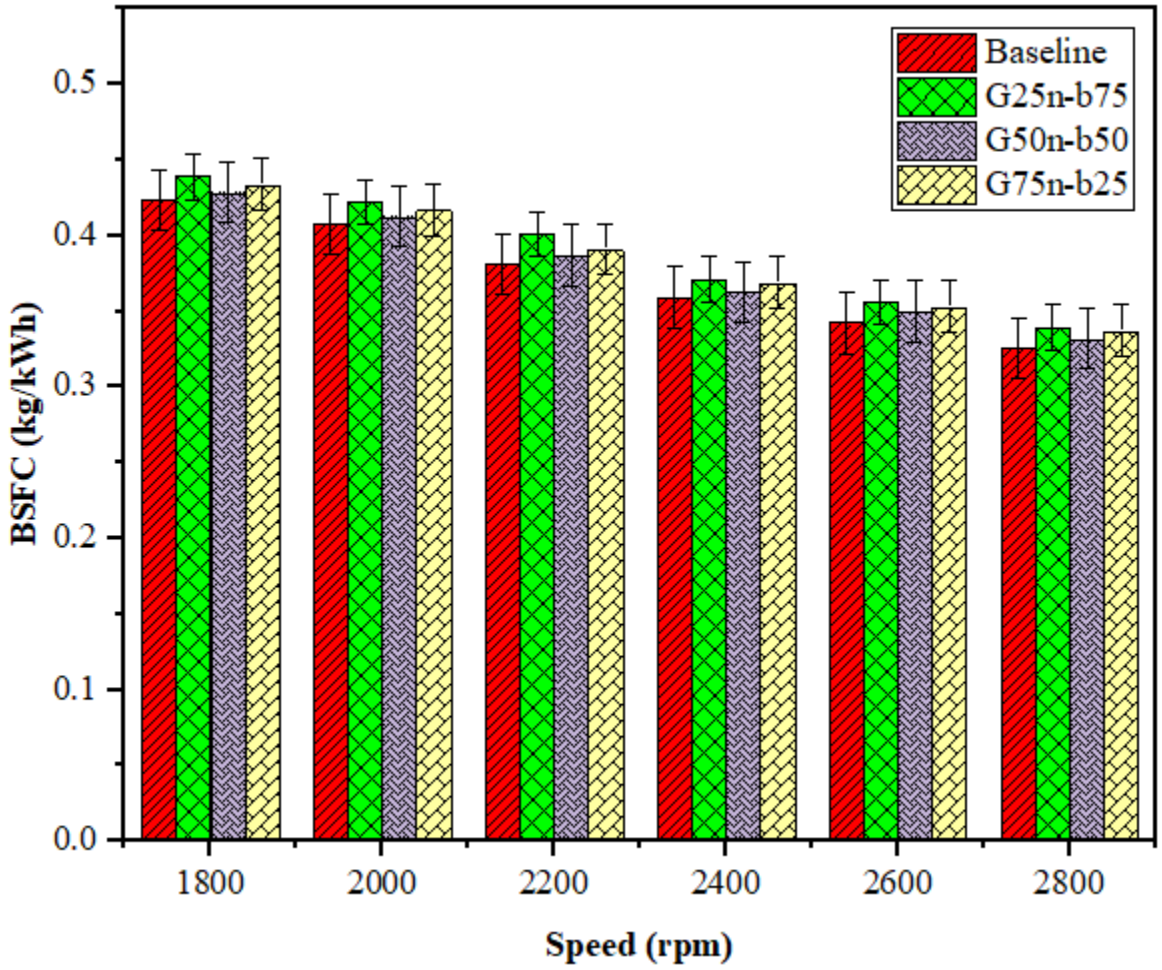

Figure 4.33 Brake specific fuel consumption of the engine

4.2.3. Emissions Analysis

4.2.3.1 Nitrogen oxides and Carbon dioxide emissions

Fig.4.34 illustrates the relationship between NOx emissions and engine speed for a baseline fuel and three distinct PI fuel blends. At an engine speed of 1800 rpm, the baseline fuel exhibits the highest NOx emissions at 83 ppm, while the B20+G25n-b75 blend shows the lowest emissions at 48 ppm. The B20+G50n-b50 and B20+G75n-b25 blends present intermediate emissions of 56 ppm

and 70 ppm, respectively. As the engine speed increases to 2800 rpm, there is a significant rise in NOx emissions for all fuel types, with the baseline fuel reaching a peak of 198 ppm. In comparison, the B20+G25n-b75, B20+G50n-b50, and B20+G75n-b25 blends record emissions of 150 ppm, 157 ppm, and 176 ppm, respectively. This trend indicates that the generation of NOx is heavily influenced by combustion temperature and the oxygen content in the fuel blends, as higher engine speeds result in elevated in-cylinder temperatures that promote NOx formation.

The B20+G25n-b75, B20+G50n-b50, and B20+G75n-b25 blends show average reductions in NOx emissions of approximately 36.5%, 26.7%, and 13.12%, respectively. The lower NOx emissions in blends with a higher n-butanol content align with previous research findings. This reduction in NOx can be attributed to the properties of n-butanol, which include a lower adiabatic flame temperature and a higher latent heat of vaporization, both of which contribute to a decrease in peak combustion temperatures (Sengupta et al., 2023).

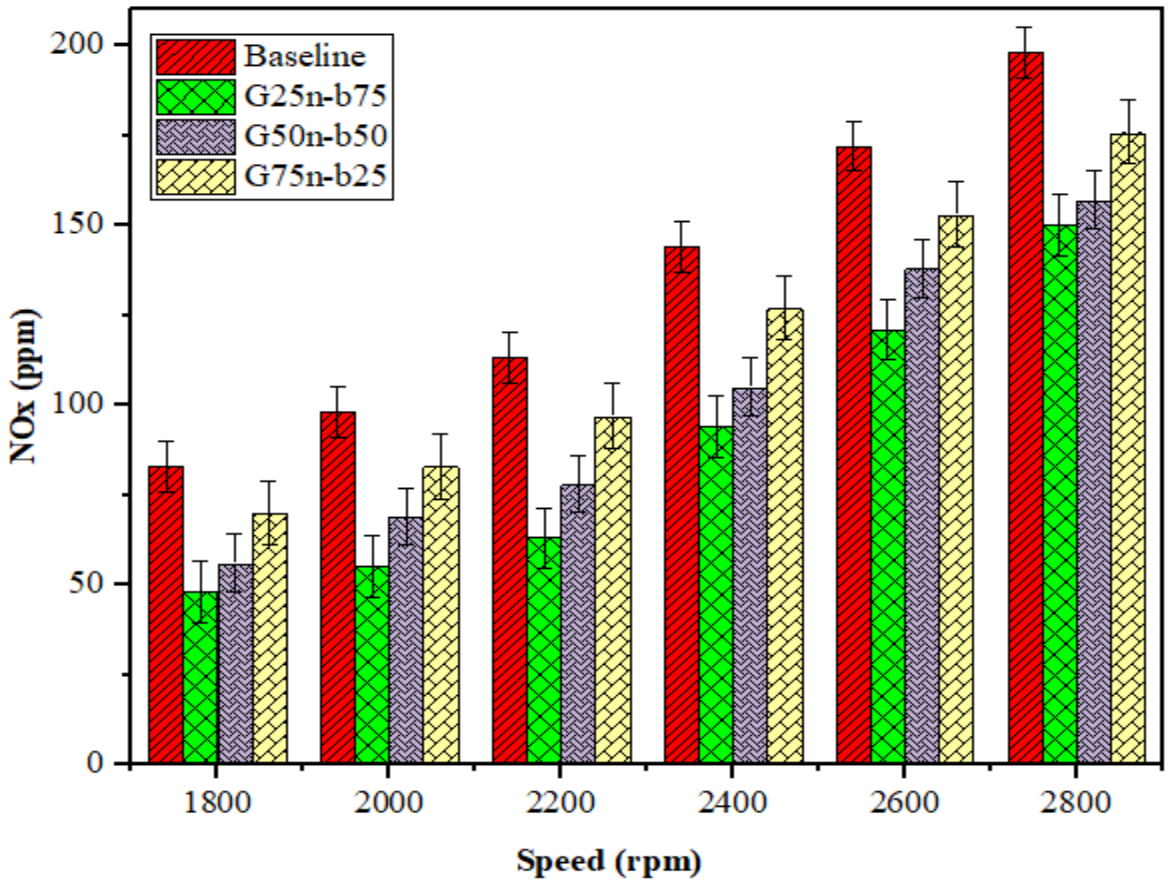

Figure 4.34 Nitrogen oxides emissions

Fig. 4.35 illustrates the relationship between CO_2 emissions and engine speeds for a baseline fuel and three distinct PI fuel blends. As the engine speed rises from 1800 rpm to 2800 rpm, a steady increase in CO_2 emissions is observed across all fuel types, indicating that higher speeds contribute to enhanced combustion efficiency. The baseline fuel exhibits the highest emissions, starting at 4.6 vol.% at 1800 rpm and increasing to 5.9 vol.% at 2800 rpm. In contrast, the B20+G25n-b75 blend shows the lowest emissions, ranging from 3.7 vol.% to 5.2 vol.% within the same speed range, followed by the B20+G75n-b25 and B20+G50n-b50 blends. The B20+G25n-b75, B20+G50n-b50, and B20+G75n-b25 blends demonstrate average reductions in CO_2 emissions of approximately 16.44%, 4.43%, and 10.28%, respectively. The reduced CO_2 emissions observed in RCCI mode with a higher proportion of n-butanol can be attributed to the oxygen content in n-butanol, which promotes more complete combustion.

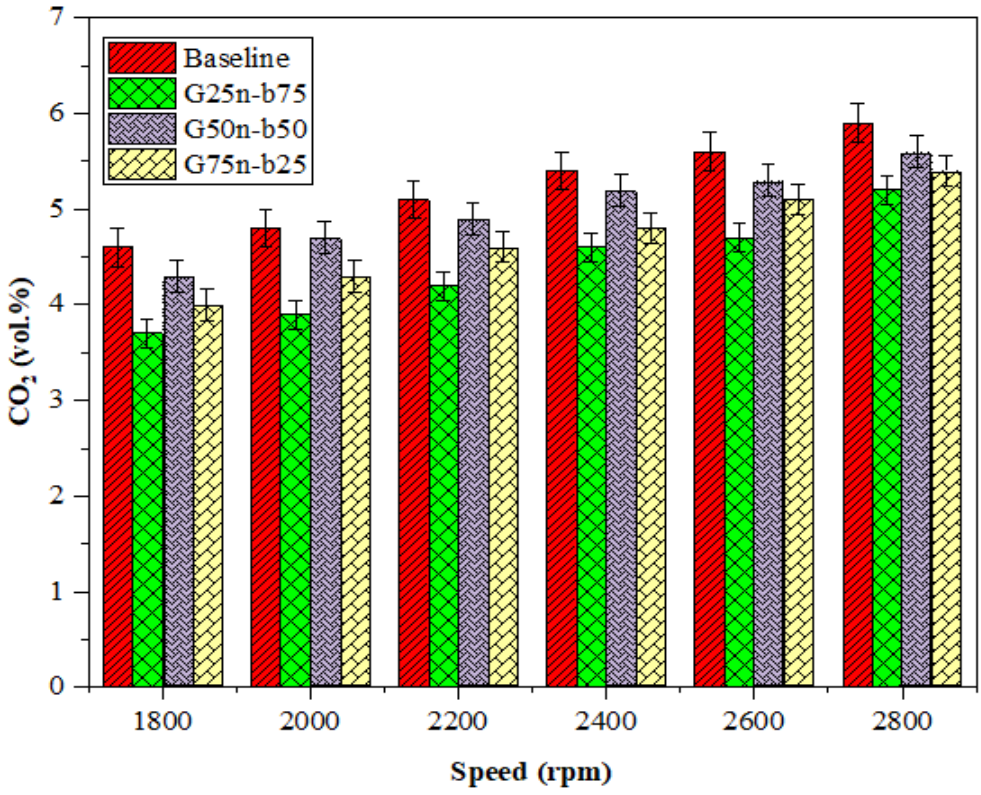

Figure 4.35 Carbon dioxide emission

4.2.3.2. Hydrocarbons and carbon monoxide emissions

Fig. 4.36 illustrates the relationship between hydrocarbon (HC) emissions and engine speed for the baseline fuel and three different port injection fuel blends. Across all fuel types, HC emissions

demonstrate a consistent increase as engine speed rises. At an engine speed of 1800 rpm, the baseline fuel records the lowest HC emissions at 19 ppm, whereas the B20+G25n-b75 blend shows the highest emissions at 23 ppm. As the engine speed escalates to 2800 rpm, HC emissions for all fuel types continue to rise, with the baseline fuel reaching 27 ppm and G75n-b25 peaking at 34 ppm. The B20+G25n-b75 and B20+G50n-b50 blends exhibit similar emission trends, with values ranging from 20-29 ppm and 22-32 ppm, respectively. The average increases in HC emissions for the B20+G25n-b75, B20+G50n-b50, and B20+G75n-b25 blends are approximately 21.69%, 15.86%, and 7.22%, respectively. These observations align with the findings of (Ganesan et al., 2020). The elevated HC emissions associated with n-butanol-rich blends can be explained by their higher latent heat of vaporization, which may result in incomplete combustion under all speeds. This situation underscores the balance between utilizing oxygenated fuel blends to improve combustion efficiency and the risk of increased unburned HC emissions due to the inherent properties of the fuel (Sun et al., 2021).

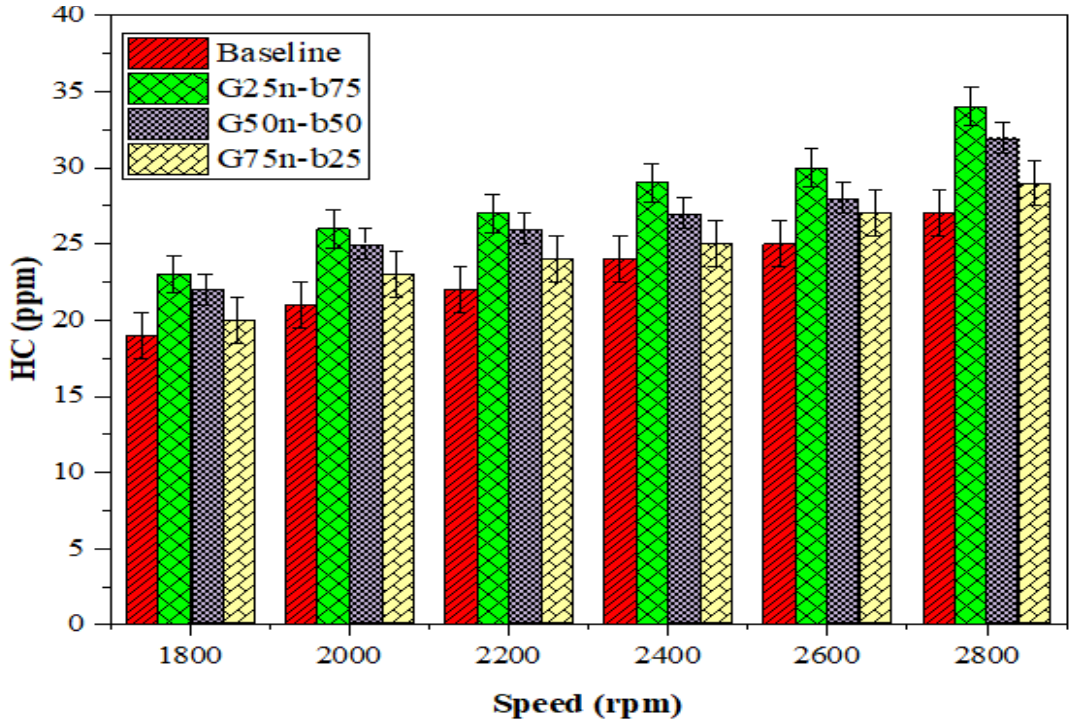

Figure 4.36 Hydrocarbons emission

Fig. 4.37 depicts the correlation between carbon monoxide (CO) emissions and engine speed for a baseline fuel alongside three distinct fuel blends utilized in port injection. At lower engine speeds, particularly at 1800 rpm, the baseline fuel exhibits the lowest CO emissions at 0.117 vol.%, while

the B20+G25n-b75 blend shows the highest emissions at 0.351 vol.%. As engine speed escalates, CO emissions for all fuel types also rise, reaching their maximum at 2800 rpm. At this peak, the baseline fuel records 0.874 vol.%, B20+G25n-b75 reaches 1.158 vol.%, B20+G50n-b50 shows 1.133 vol.%, and B20+G75n-b25 peaks at 1.126 vol.%. This trend suggests a direct relationship between CO emissions and engine speed, primarily attributed to incomplete oxidation during the rapid combustion process. The increased presence of n-butanol results in a reduction of charge temperature, which can be attributed to its high latent heat of vaporization. This property contributes to flame quenching during combustion, potentially impeding the complete oxidation of carbon compounds present in the fuel. As a result, this incomplete combustion may lead to heightened CO emissions (Han et al., 2021). Additionally, prior research has examined the impacts of various low and high reactivity fuel combinations in RCCI engines, and their findings have been compared with the results of the current study for validation, as detailed in Table 4.7.

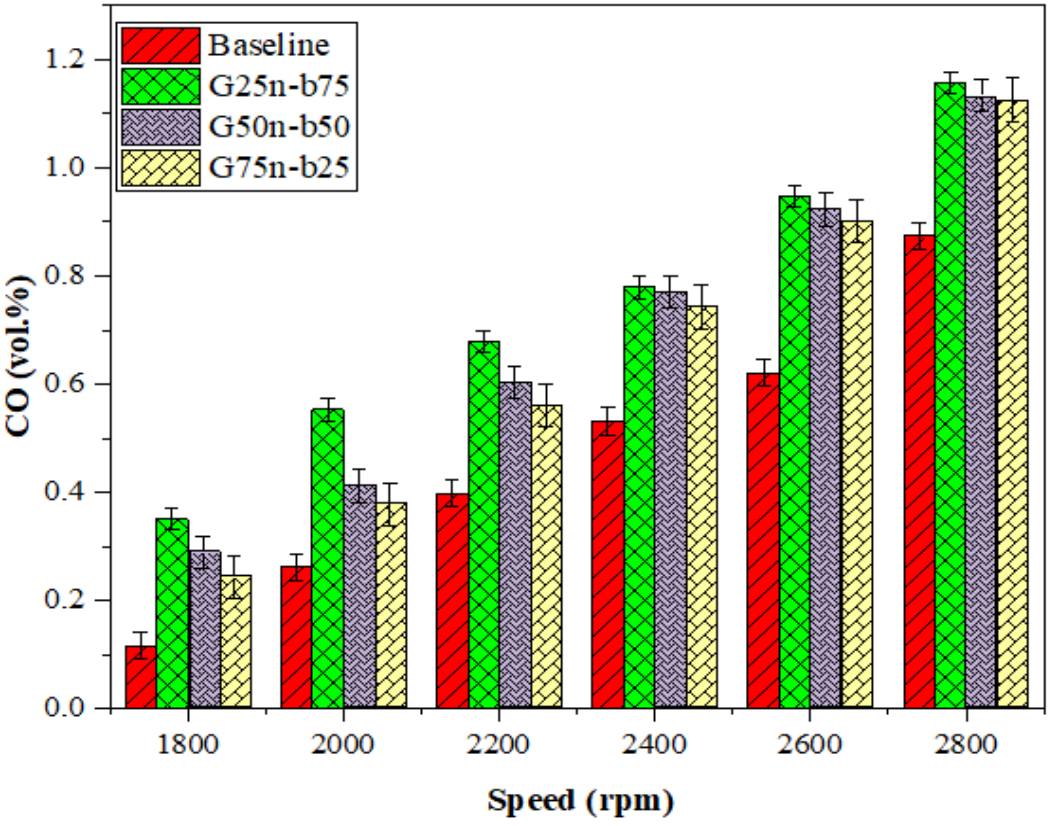

Figure 4.37 Carbon monoxide emission

Table 4.7 The comparison of previous studies on RCCI engines with the current study

Authors	**Fuel used (HRF/LRF)**	**Direct injection**	**Port injection**	**Results**
Wang et al., 2021	Methyl oleate/n-butanol	Methyl oleate/n-butanol blend	n-butanol	Peak CP increased by 15.26% , BSFC increased by 2.61%, NOx reduced by 18.40%, CO_2 reduced by 6.08%, HC increased by 18.22, CO increased by 41.31%
Zheng et al., 2018	Methyl ester/n-butanol	Methyl ester	n-butanol	Soot reduced by 4.3%, CO increased by 30.12% and HC increased by 22.68%
Harari et al., 2020	Biodiesel-diesel/gasoline	Biodiesel-diesel blend	gasoline	NOx reduced by 10.40%, , soot reduced by 5.22%, BSFC increased by 3.11%, CO increased by 46.92%, HC 19.36%
Ganesh et al., 2019	Diesel/iso-butanol	diesel	Iso-butanol	NOx reduced by 6.90%, and smoke reduced by 4.28%, CO increased by 22.16% and HC increased by 11.22%
Jagankumar et al., 2020	Diesel/gasoline	diesel	gasoline	BTE increased by 2.37%, BSFC increased by 3.11%, NOx reduced by 5.52%, , CO increased by 28.95%, smoke increased by 5.64%.

Wategave et al., 2021	Biodiesel-diesel/CNG	B20	CNG	NOx reduced by 7.71%, smoke reduced by 5.52%, , CO increased by 43.35%, HC increased by 22.73%
Habtamu et al., 2023	Diesel/ethanol-gasoline	diesel	Ethanol-gasoline blend	Peak CP increased by 24.86% , BSFC increased by 1.89%, NOx reduced by 20.73%, CO_2 reduced by 8.41%, HC increased by 12.15, CO increased by 39.06%
Current work	Biodiesel-diesel/gasoline-n-butanol	B20	gasoline-n-butanol blend	Peak CP increased by 20.4% , BSFC increased by 1.54%, NOx reduced by 25.44%, CO_2 reduced by 10.38%, HC increased by 14.92, CO increased by 35.37%

4.3. Optimization of performance and emissions of RCCI engine

4.3.1. Model analysis of response surface methodology

The foundation for a total of 13 experimental runs was established through a design matrix developed using the CCD of RSM. This investigation focused on two primary factors: speed (A) and the ratio of n-butanol to gasoline blend (B). The study intended to analyze the individual and interactive effects of these factors on the performance and emissions of an RCCI engine, employing RSM for this purpose. A quadratic polynomial model was utilized to define the numerical correlation between the output factors and the process factors. Furthermore, a mathematical formulation was established to conduct multiple regression analysis, which facilitated the creation of predictive models, as indicated in equations 4.1-4.7. To evaluate the correlations and ascertain the impact of the input variables on the response variables, the statistical technique of ANOVA was employed. The engine performance parameters, including BT, BP, and BSFC, as well as emission characteristics such as NOx, CO_2, CO, and HC, were obtained experimentally and are summarized in Table 4.8.

$$\text{BT (Nm)} = 4.92 - 0.00693A + 0.0658B - 0.000001A^2 - 0.000523B^2 - 0.000007AB \quad (4.1)$$

$$\text{BP(kW)} = 0.71 + 0.00161A + 0.01055B - 0.0000001A^2 - 0.000121B^2 - 0.0000001AB \quad (4.2)$$

$$\text{BSFC (kg/kWh)} = 0.304 + 0.00015A - 0.000859B - 0.0000001A^2 - 0.0000001B^2 - 0.0000001AB \quad (4.3)$$

$$CO_2\ \text{(vol)} = 31.32 - 0.02028A - 0.0853B + 0.000004A^2 + 0.000542B^2 + 0.00001AB \quad (4.4)$$

$$\text{CO (vol)} = 3.74 - 0.002027A + 0.00198B + 0.0000001A^2 - 0.000003B^2 + 0.000001AB \quad (4.5)$$

$$\text{HC (ppm)} = 233 - 0.165A - 0.647B + 0.000038A^2 + 0.01086B^2 - 0.0002AB \quad (4.6)$$

$$\text{NOx (ppm)} = 1165 - 1.307A - 2.679B + 0.000278A^2 + 0.00622B^2 + 0.0006AB \quad (4.7)$$

The assessment of the model's quality was conducted through various statistical parameters such as the F-value, P-value, R^2, and Adj-R^2. A favorable model fit is suggested by a higher Adj-R^2 value that is in close proximity to the R^2, particularly when the R^2 approaches 1. The outcomes of experiments can be contrasted to anticipated models using R^2. The R^2 for BT, BP, BSFC, CO_2, CO, NOx, and HC are 97.98%, 98.39%, 98.62%, 94.72%, 99.12%, 99.66% and 97.14%, respectively. These values, which are extremely near to 1, reflect a high level of accuracy when compared to

analytical results. The model's significance can be ascertained through the p-value. For a given model, a p-value < 0.05 shows statistically significant, indicating a divergence from the null hypothesis. Conversely, p-values exceeding 0.05 imply that the model lacks significance. Additionally, the ANOVA results reveal that higher F-values further support the significance of the model (Ramachandran et al., 2023). The results of the ANOVA concerning performance-related variables, including BP, BSFC, and BT, are detailed in Table 4.9, which assesses the statistical significance of each model term and interaction. Additionally, Table 4.10 presents the ANOVA findings related to emission characteristics, demonstrating the impact of the chosen factors on pollutants such as NOx, CO, HC, and CO_2. Moreover, Table 4.11 consolidates the diagnostic parameters employed to evaluate the adequacy and reliability of the constructed response surface models, featuring metrics such as the R^2, adjusted R^2, predicted R^2, lack-of-fit tests, and adequate precision. Collectively, these tables establish a thorough statistical basis for understanding the performance and emission characteristics of the RCCI engine under the specified operating conditions. The R^2 reflects both the accuracy and adequacy of the model. Furthermore, the disparity between the adj-R^2 and pred-R^2 values serves as an indicator of the model's consistency. The variability in data is demonstrated by the value of standard deviation (Std. Dev).

Normal probability plots of residuals serve as a tool for evaluating the extent to which the observed data conform to the assumption of normality. Such diagnostic plots are instrumental in confirming the distribution characteristics of the residuals present in the dataset. The validation of the residuals of BT, BP, BSFC, CO_2, NOx, HC, and CO are depicted in Fig. 4.38a-g, respectively, confirming that these residuals adhere to a normal distribution while also affirming the homogeneity required for ANOVA. Furthermore, the results of the ANOVA for the response variables indicate a robust correlation between the actual and predicted values, as illustrated in Fig. 4.39a-g. The data points are consistently distributed around the diagonal line, which implies that the model's predictions are unbiased and exhibit minimal error.

Table 4.7 Experimental matrix of RSM with the results of the responses

Run	Factors		Output Responses						
	A	B	BT	BP	BSFC	CO_2	NOx	CO	HC
1	2600	50	14.83	4.08	0.350	5.3	138	0.902	27
2	2600	85.3553	14.01	3.78	0.342	4.6	142	0.960	29
3	2600	50	14.81	4.07	0.351	5.2	136	0.903	26
4	2600	14.6447	14.34	4.04	0.345	4.9	157	1.017	30
5	2800	25	14.46	4.20	0.337	5.4	176	1.158	32
6	2600	50	14.85	4.06	0.349	5.3	140	0.904	27
7	2317.16	50	14.79	3.80	0.368	5.0	81	0.715	25
8	2800	75	14.15	4.09	0.339	5.2	150	1.133	34
9	2600	50	14.84	4.06	0.350	5.4	136	0.905	26
10	2400	75	14.51	3.79	0.371	4.6	94	0.771	27
11	2882.84	50	14.65	4.30	0.328	5.8	171	1.141	33
12	2400	25	14.68	3.89	0.369	4.8	127	0.779	29
13	2600	50	14.82	4.07	0.349	5.2	139	0.902	26

Table 4.8 ANOVA for engine performance

Source	BT		BP		BSFC	
	P – value	F – value	P – value	F – value	P – value	F – value
Model	0.00010	68.04	0.00010	323.77	0.00010	99.86
A-Speed	0.0010	27.47	0.00010	1413.37	0.00010	346.62
B- n-butanol ratio	0.00010	40.68	0.00010	194.74	0.00010	144.74
A^2	0.029	7.47	0.576	0.04	0.081	4.4
B^2	0.0001	269.92	0.0001	10.15	1.00	0.00
AB	0.224	1.78	0.855	0.04	0.095	3.72

Table 4.9 ANOVA for engine emissions

Source	CO_2		CO		HC		NOx	
	P-value	F-value	P-value	F-value	P-value	F-value	P-value	F-value
Model	0.0001	25.13	0.0001	158.39	0.00010	47.52	0.00010	406.28
A	0.0001	51.75	0.0001	772.58	0.00010	84.24	0.00010	1646.27
B	0.019	9.31	0.026	14.85	0.007	14.03	0.00010	218.78
A^2	0.008	13.25	0.085	4.03	0.033	7.00	0.00010	152.26
B^2	0.0001	56.70	0.715	0.14	0.0001	136.36	0.004	18.59
AB	0.427	0.71	0.807	0.06	0.233	1.70	0.04	6.36

Table 4. 10 Evaluation of ANOVA model

Parameter	BT	BP	Bsfc	CO	CO_2	HC	NOx
Std. Dev	0.0525	0.0264	0.00259	0.0138	0.1187	1.553	2.378
R^2	0.9798	0.9839	0.9862	0.9912	0.9472	0.9714	0.9966
Adj-R^2	0.9654	0.9724	0.9763	0.985	0.9095	0.9509	0.9941
Pred-R^2	0.8624	0.8909	0.9180	0.9379	0.6604	0.8235	0.9781

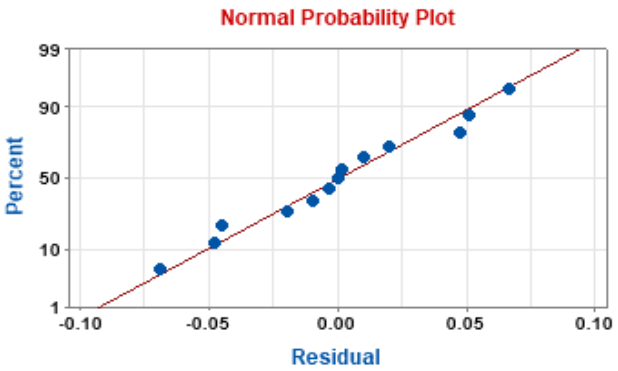

Normal probability plot for BT

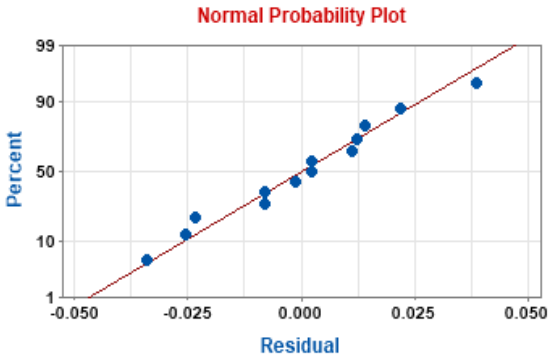

Normal probability plot for BP

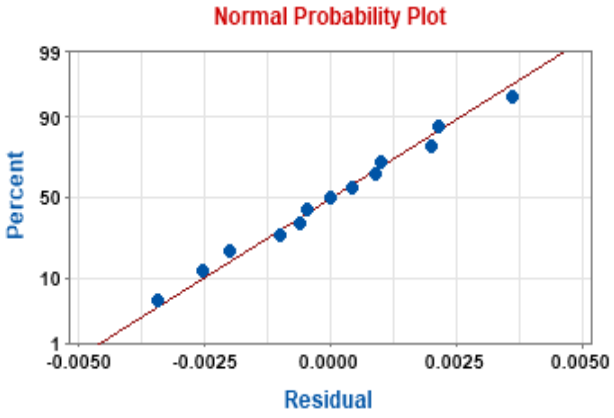

Normal probability plot for BSFC

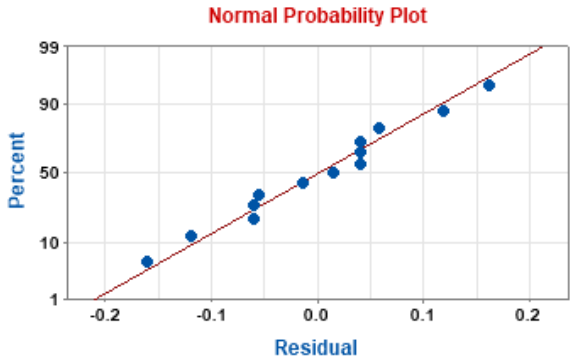

Normal probability plot for CO_2

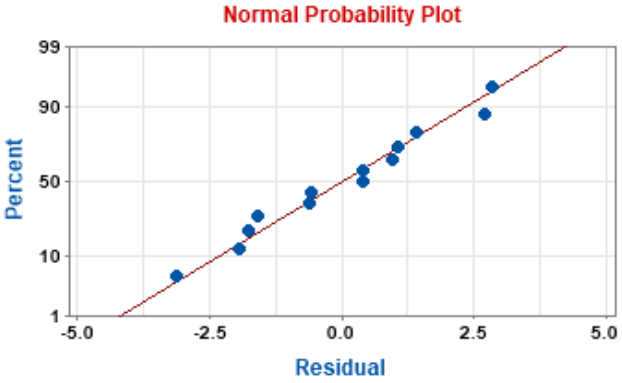

Normal probability plot for NOx

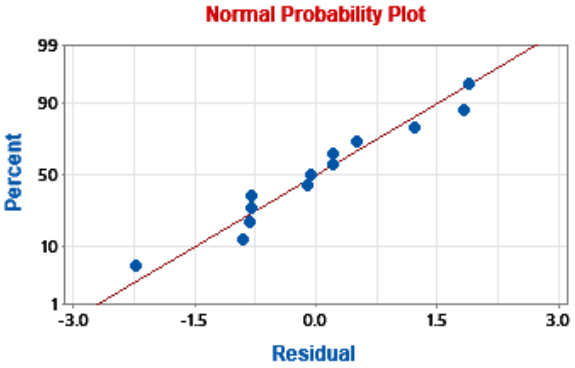

Normal probability plot for HC

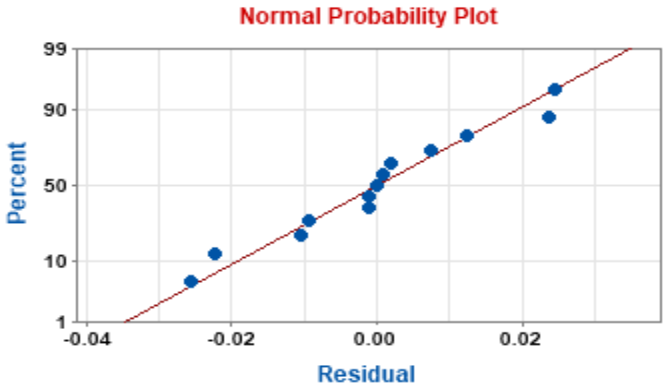

Normal probability plot for CO

Figure 4.38 Normal probability plot for engine performance and emission parameters

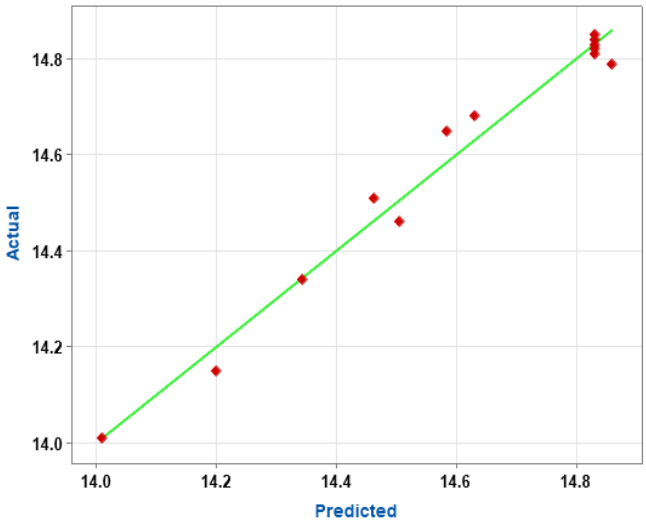

Predicted vs Actual data of BT

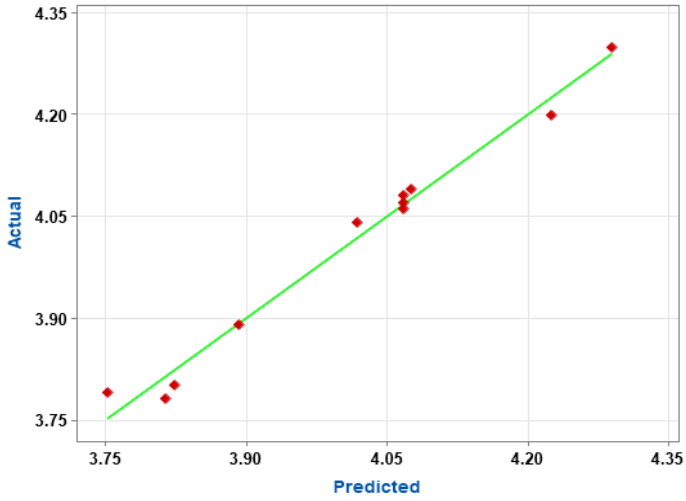

Predicted vs Actual data of BP

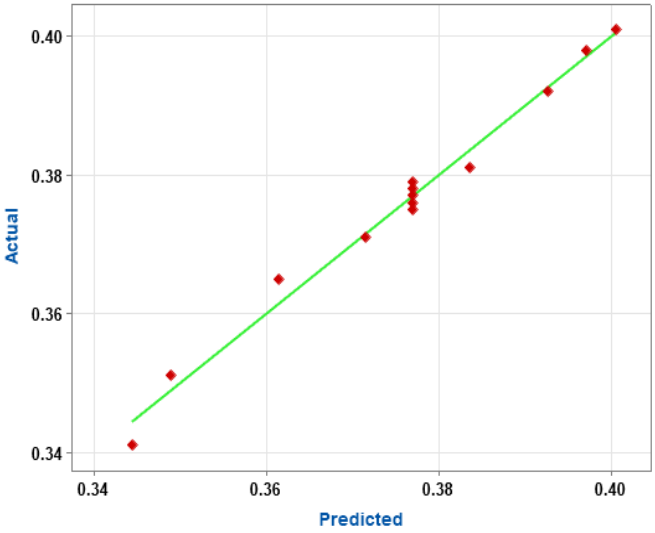

Predicted vs Actual data of BSFC

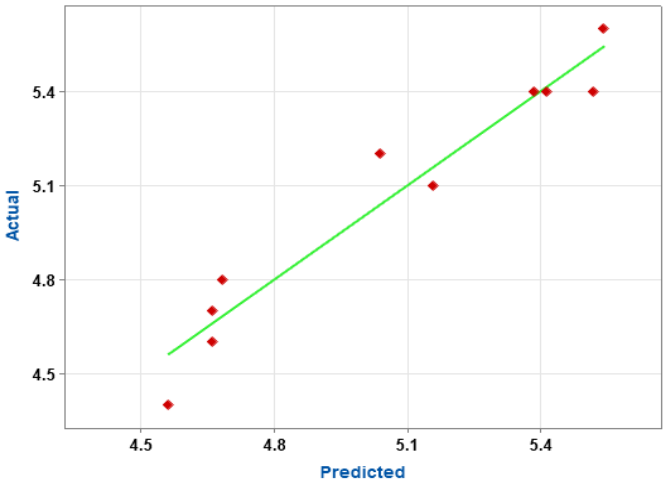

Predicted vs Actual data of CO_2

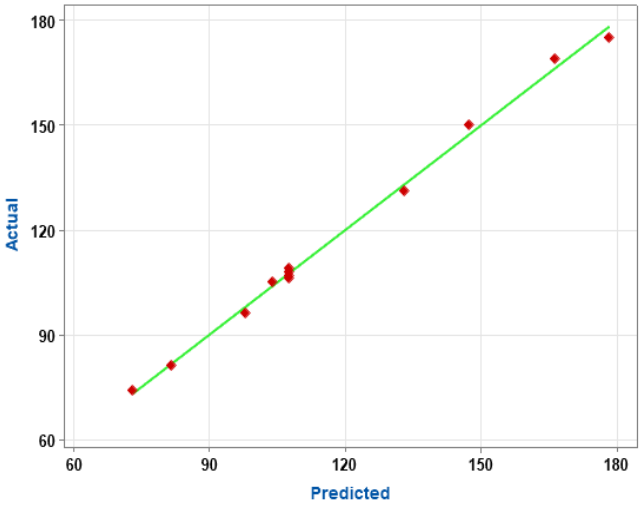

Predicted vs Actual data of NOx

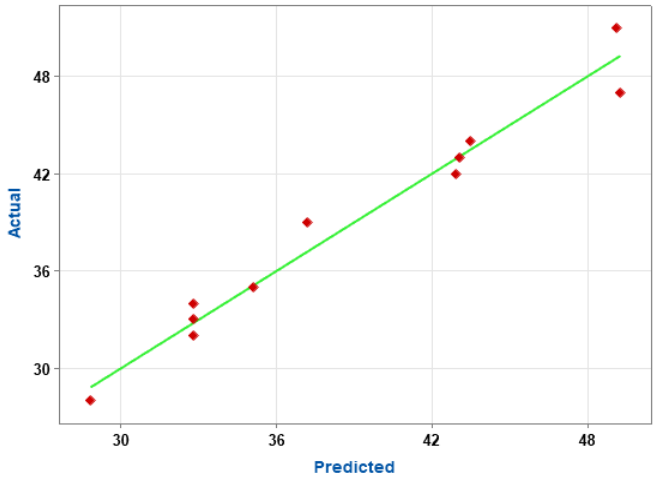

Predicted vs Actual data of HC

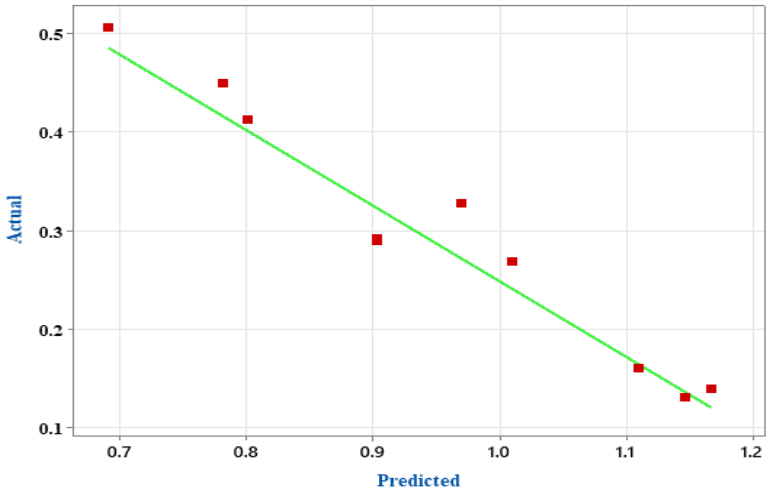

Predicted vs Actual data of CO

Figure 4.39 Predicted vs Actual data of engine performance and emission parameters

4.3.2. Optimization performance analysis

4.3.2.1. Brake Torque

The ANOVA analysis presented in Table 4.9, reveals that both A and B exert a considerable influence on the BT, with P-value of 0.001 and 0.0001, respectively, alongside notable F-values that suggest a significant effect. Furthermore, the term associated with B^2 demonstrates a high level of significance, with an F-value of 269.92 and a P-value of 0.0001. In contrast, the AB and A^2

terms appear to have a minimum impact on the overall response. The relationship between engine speed and n-butanol content on BT is further depicted in Fig.4.40 and Fig.4.41, which illustrates BT remains relatively stable across varying engine speeds, fluctuating between 14.01 Nm to 14.85 Nm with no extreme deviations. This stability indicates that n-butanol ratios up to 50% have a minimum detrimental impact on the torque output at tested engine speeds. For instance, at 2600rpm and 50% n-butanol, BT achieves a peak of 14.85 Nm, illustrating the blend's ability to maintain strong combustion efficiency. However, as the n-butanol ratio increases up to 85.35 % at the same speed, BT drops to 14.01 Nm because of minimum calorific value of n-butanol.

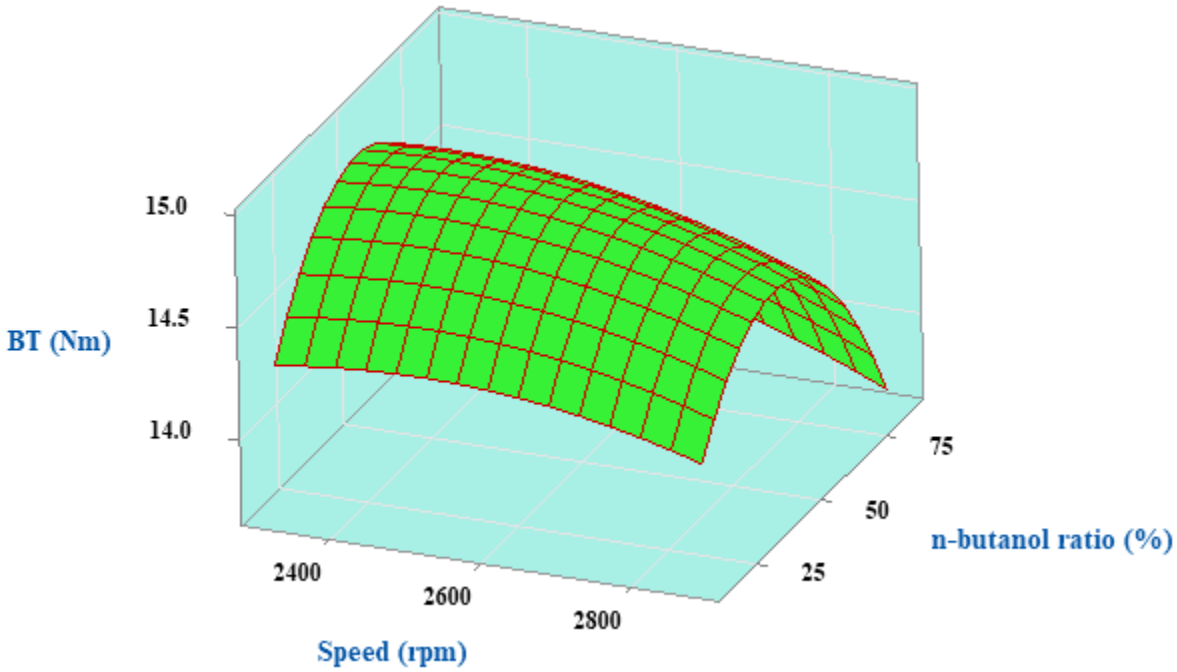

Figure 4.40 Surface plot of BT vs engine speed and n-butanol ratio

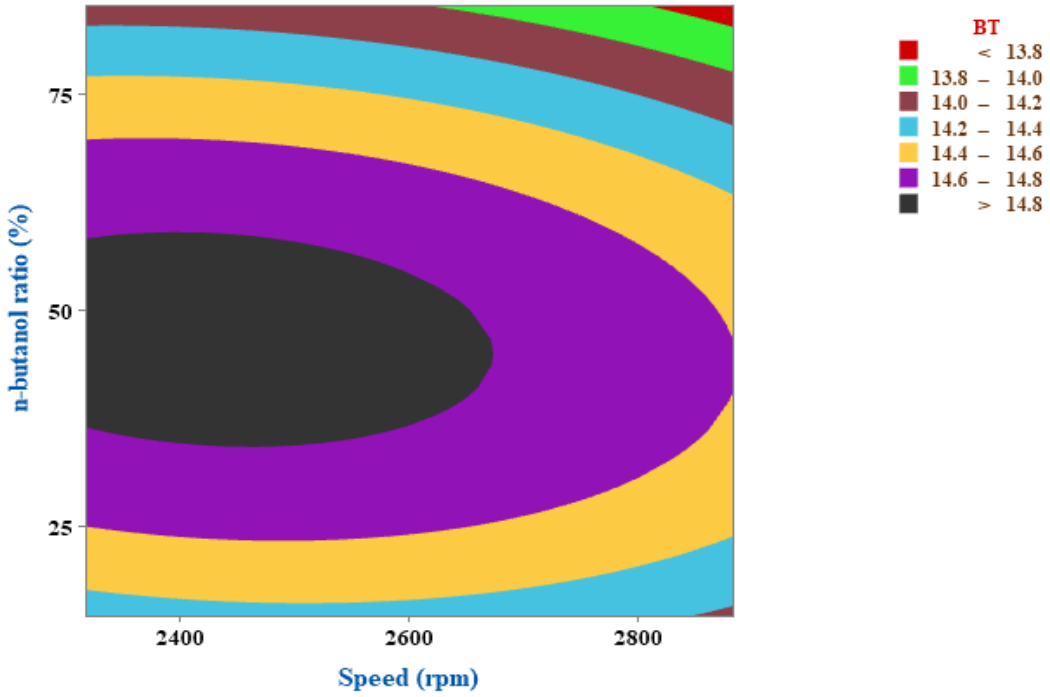

Figure 4.41 Contour plot of BT vs engine speed and n-butanol ratio

4.3.2.2. Brake Power

Table 4.9 illustrates that BP is markedly affected by factors A and B. This is supported by the highly significant P-values of 0.0001 for both variables, which suggest a minimal likelihood that the observed effects arise from random fluctuations. Furthermore, the associated F-values of 1413.37 for A and 194.74 for B highlight the extent of their impact on BP, with elevated F-values indicating more substantial contributions to the variation in response. Consequently, A exerts the most pronounced influence on BP, whereas the B also has a strong but comparatively smaller effect. The engine speed has the strongest impact on BP as higher speeds generally enhance BP by allowing more fuel combustion per unit time, though excessively high speeds could reduce efficiency due to increased friction and incomplete combustion. The n-butanol ratio affects BP as the result of its lower calorific value compared to conventional fuels, though its oxygen content can improve combustion efficiency. The term B^2 exhibits significance proved by an F-value of 10.15 and a P-value of 0.0001. Conversely, the terms A^2 and AB seem to exert a minimum influence on the BP. The relationship between engine speed and the n-butanol ratio on BP is illustrated in Fig.4.42 and Fig.4.43 as surface plot and contour plot, respectively. The findings suggested that BP generally rises with increasing engine speed, specifically between 2317 rpm

(3.80 kW) and 2883 rpm (4.30 kW). Additionally, as the n-butanol ratio increases, BP increases up to a certain point, then experiences a slight reduction due to the lower energy density of n-butanol; for instance, at 2800 rpm, BT drops from 4.20 kW at 25% of n-butanol to 4.09 kW at 75% n-butanol. The peak BP was achieved at 2883 rpm with 50% n-butanol content yielding a BP of 4.30 kW.

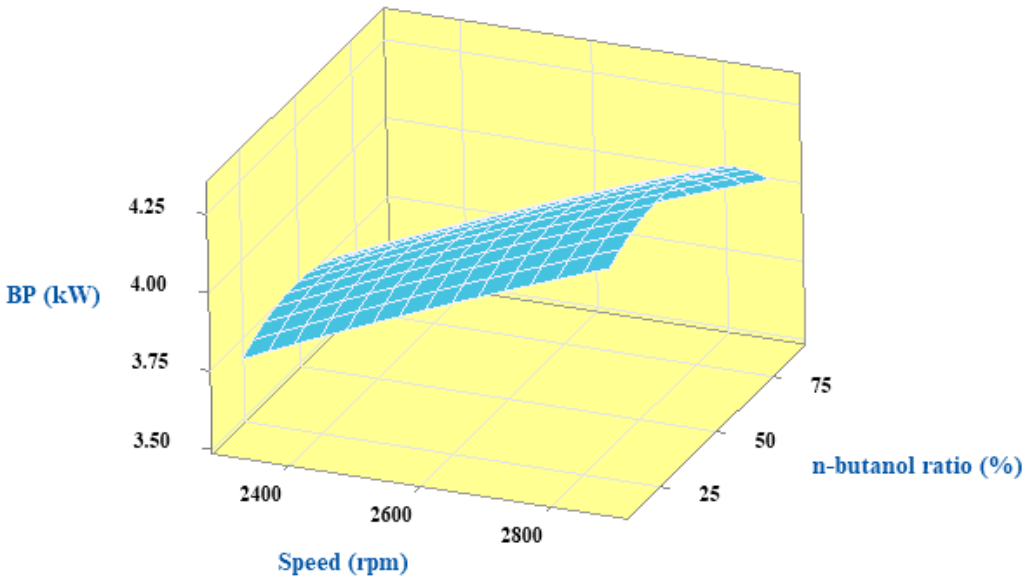

Figure 4.42 BP vs engine speed and n-butanol ratio surface plot

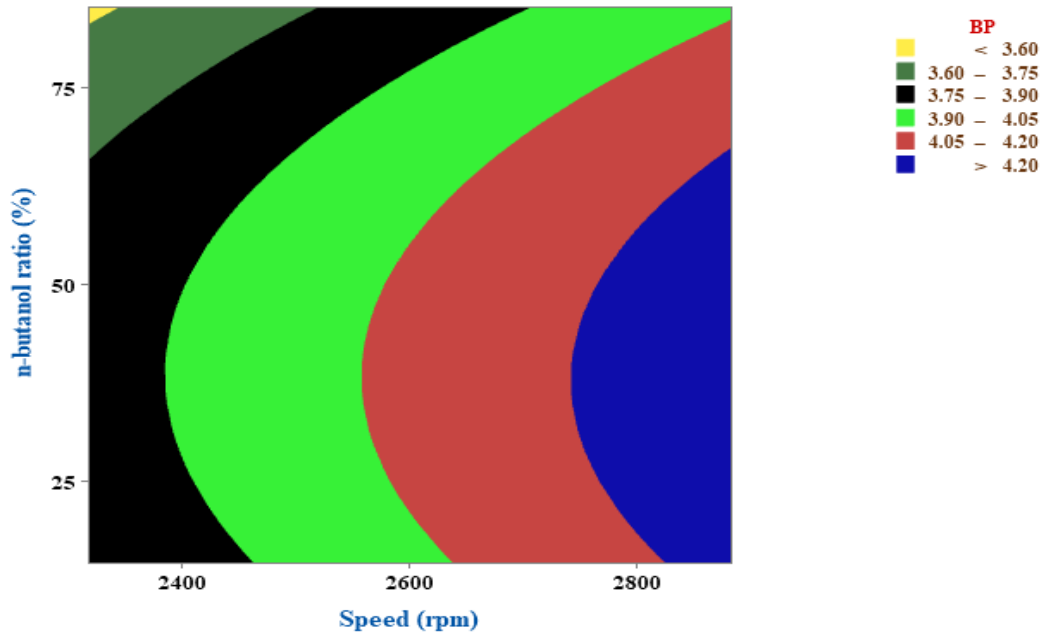

Figure 4.43 BP vs engine speed and n-butanol ratio contour plot

4.3.2.3. Brake specific energy consumption

Brake-specific energy consumption (BSFC) is a key engine parameter, defined as the amount of fuel consumed per unit of power generated over a specific period of time. This parameter is influenced by both the fuel's heating value and specific fuel consumption. The significance of this analysis becomes particularly evident when evaluating various fuels that possess distinct characteristics, including differing heating values and cetane number. The ANOVA results presented in Table 4.9 indicate that BSFC is notably affected by both A and B terms, underscoring their essential contributions to engine performance. Among these terms, A exerts the most substantial influence on BSFC, evidenced by a highly significant F-value of 346.62. The B term also plays a significant role in determining BSFC, with an F-value of 144.74, as an elevated ratio tends to raise fuel consumption as a result of the lower energy density of n-butanol. The quadratic term A^2 has negligible impact, while both quadratic term B^2 and interaction term AB are statistically insignificant. The interaction between engine speed and n-butanol ratio concerning BSFC is depicted in Fig.4.44 and Fig. 4.45. These plots reveal that BSFC increases with higher n-butanol content due to lower energy density, necessitating a greater fuel volume to generate the same power output. Conversely, higher engine speeds result in reduced fuel consumption to sustain the desired power levels. The lowest BSFC of 0.328 kg/kWh was attained at 2883 rpm with a G50n-b50 blend.

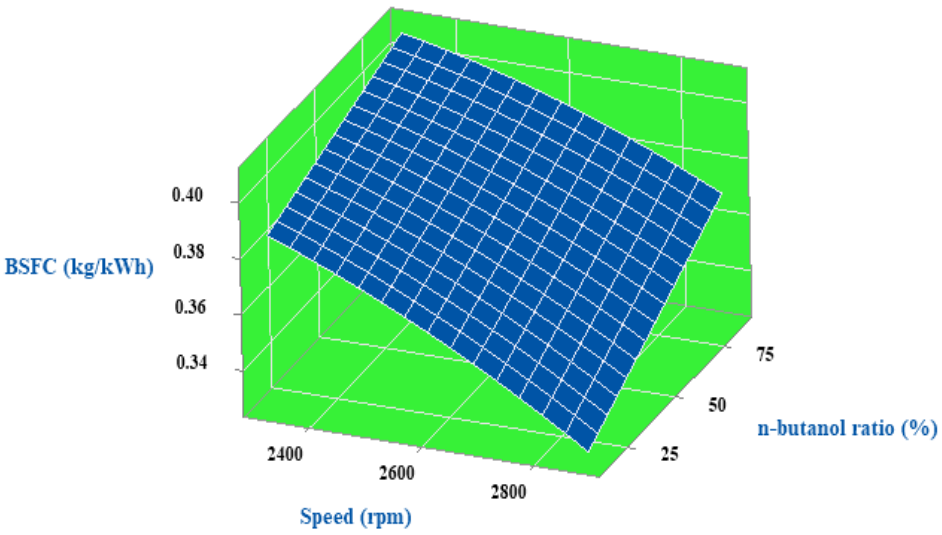

Figure 4.44 BSFC vs engine speed and n-butanol ratio surface plot

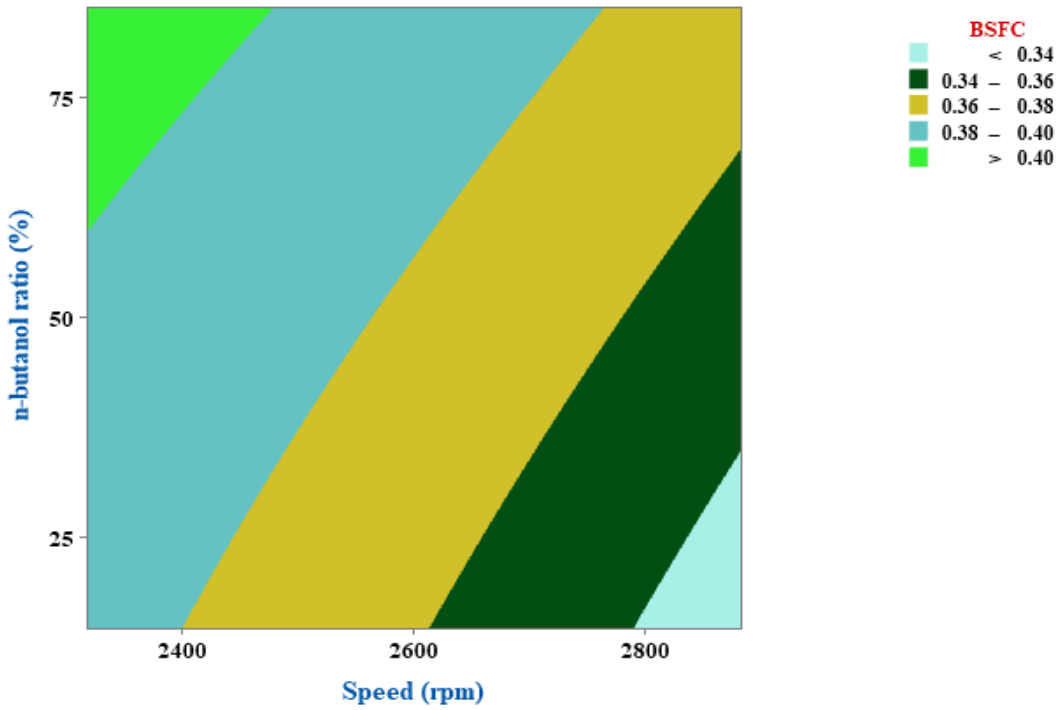

Figure 4.45 BSFC vs engine speed and n-butanol ratio contour plot

4.3.3. Optimization of emission analysis

4.3.3.1. Nitrogen oxides and carbon dioxide emissions

The ANOVA findings presented in Table 4.10 indicated that A and B terms play critical roles in influencing emissions of both NOx and CO_2. Specifically, A term exerts the most substantial impact on NOx with a highly significant F-value of 1646.47 and P-value of 0.0001. The B term also significantly affects NOx emissions, due to an F-value of 218.78 and a P-value of 0.0001. additionally, the quadratic terms A^2 and B^2 are significant, due to an F-value of 152.26 and 18.59, respectively. In terms of CO_2 emission, both the A term (P-value = 0.0001, F-value = 51.75) and the B term (P-value = 0.019 and F-value = 9.31) are again found to have substantial effects. The interaction term AB shows a minor significant influence on both NOx and CO_2 emissions.

Fig. 4.46 and Fig 4.47 depict the synergistic effects of engine speed and n-butanol content on NOx emissions. It observed that NOx level rises with increasing engine speeds, however, at lower speeds, emissions of NOx are mitigated as a result of a decrease in combustion temperature. Specifically, Fig.4.46 demonstrates that NOx decreases as the content of n-butanol increases (for instance, at 2400 rpm, the NOx level reduced from 127 ppm at 25% of n-butanol to 94 ppm at 75%

n-butanol). The reduction in NOx emissions can be ascribed to the significant latent vaporization associated with the low reactivity of n-butanol fuel. This property leads to lower cylinder temperature, thereby diminishing the production of NOx emissions (Lapuerta et al., 2018). Additionally, Fig.4.48 and Fig. 4.49 illustrate the interaction between engine speed and the content of n-butanol concerning CO_2 emission. It was observed that CO_2 emission rises with increasing speed; however, a high proportion of n-butanol leads to a reduction in emission. This reduction is likely attributable to the enhanced combustion efficiency provided by the oxygen content present in n-butanol. The lowest CO_2 emission level (4.6 %vol.) was attained at 2400 rpm with a G25n-b75 blend.

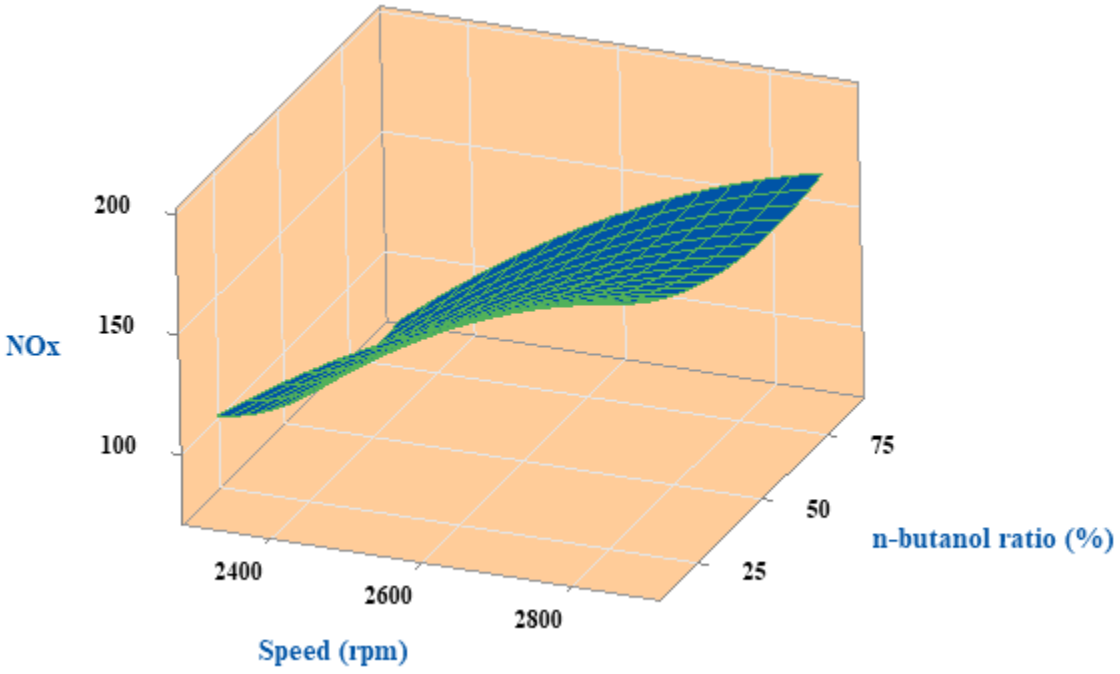

Figure 4.46 NOx vs engine speed and n-butanol ratio surface plot

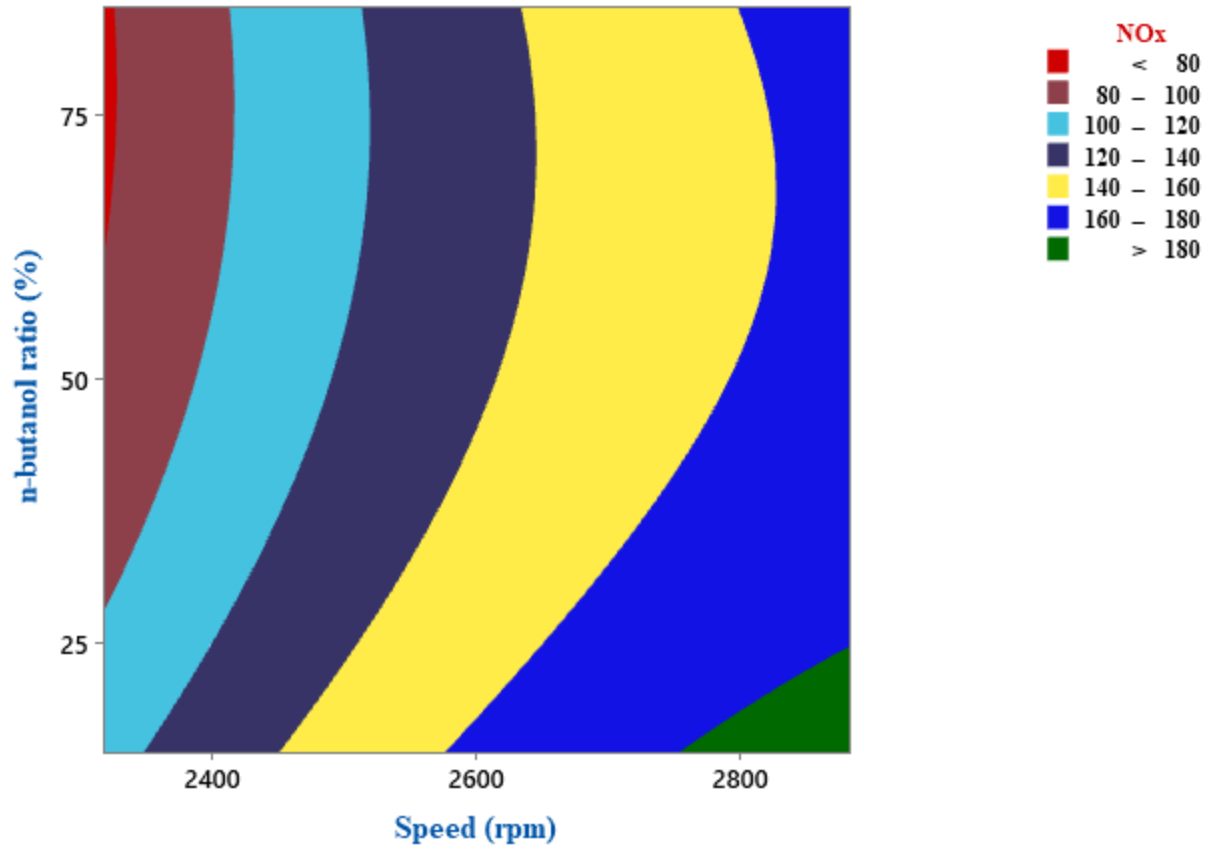

Figure 4.47 NOx vs engine speed and n-butanol ratio contour plot

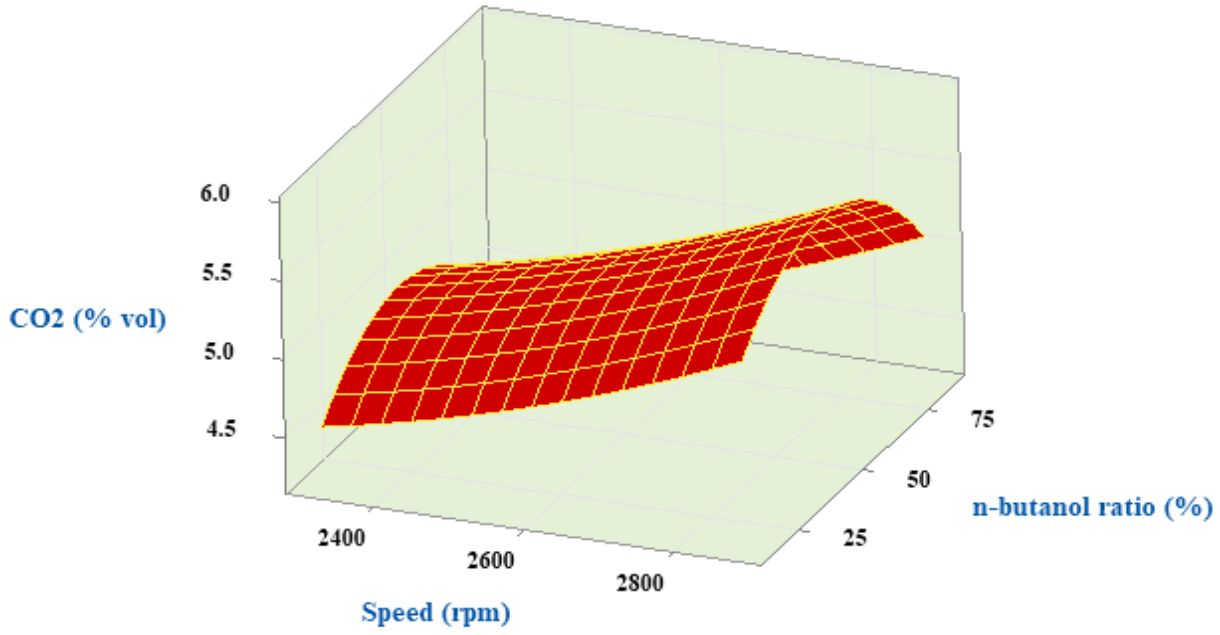

Figure 4.48 CO_2 vs engine speed and n-butanol ratio surface plot

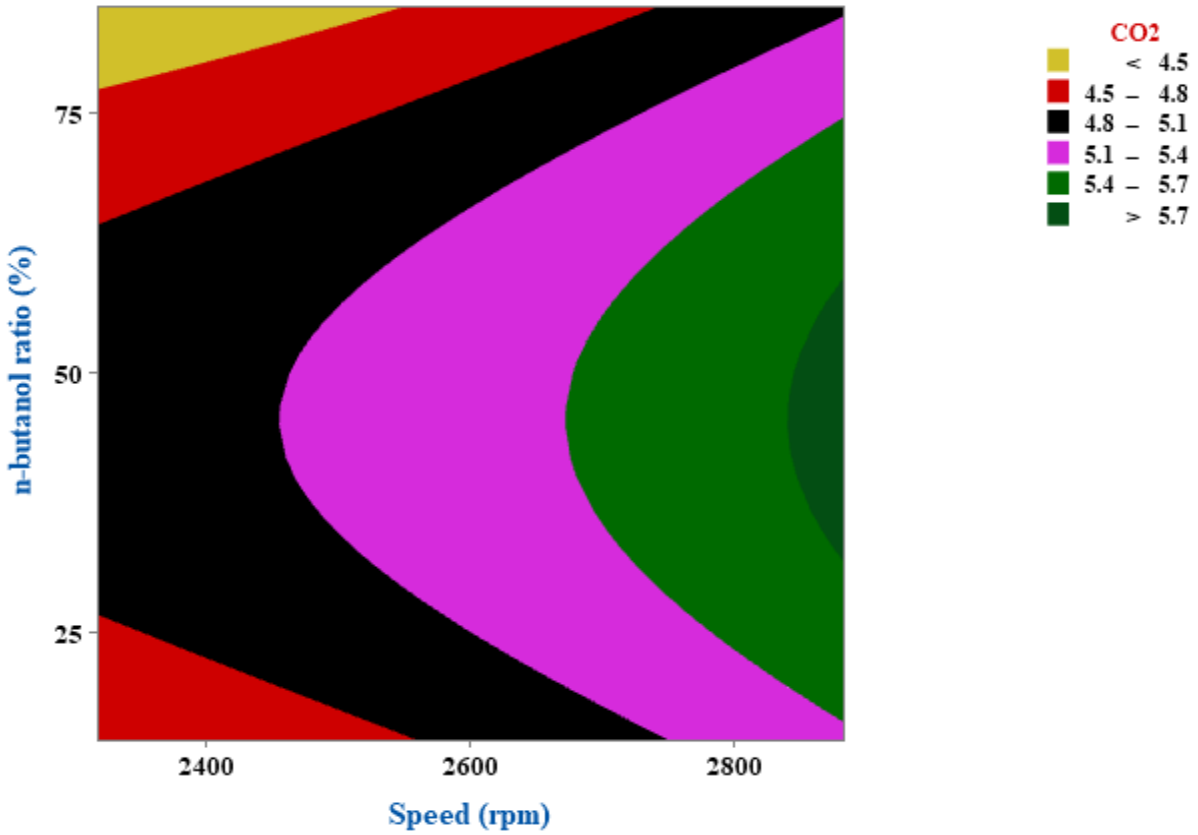

Figure 4.49 CO_2 vs engine speed and n-butanol ratio contour plot

4.3.3.2. Carbon monoxide and hydrocarbons emissions

The ANOVA analysis from Table 4.10 indicates that A term has the most significant influence on both HC and CO emissions, with P-values of 0.0001 and an F-value of 82.42 for HC and 585.46 for CO, indicating strong linear effects. In contrast, the B term shows a moderate influence on HC emissions, with an F-value (14.03) and a P-value (0.007), while its effect on CO emission is less, reflected in a P-value of 0.08 and an F-value of 4.19. notably, the quadratic term B^2 is more significant for HC, as shown by a P-value of 0.0001 and an F-value of 136.36, compared to CO, which has a P-value of 0.001 and an F-value of 33.61. Fig.4.50-Fig.4.53 demonstrate the influence of the input parameters, specifically engine speed and n-butanol concentration, on the emissions of CO and HC. Analysis of these figures reveals that both HC and CO emissions are at their lowest at minimum engine speeds; however, they increase significantly at higher speeds (for instance, CO emission rise from 0.715%vol. at 2317 rpm to 1.158% at 2800 rpm; while HC emissions increase from 25 ppm to 32 ppm). This trend indicates a tendency towards incomplete combustion at higher

speeds. Furthermore, the results from Fig.4.50 and Fig.4.52 shows a decrease in both CO and HC with enhancing levels of n-butanol up to certain point, then further increase of n-butanol increases both emissions (e.g., CO emission decrease from 0.779 % at 25% of n-butanol to 0.771 % at 75% of n-butanol; HC emissions decrease from 29 ppm at 25% of n-butanol to 27 ppm at 75% of n-butanol). This reduction can be attributed to the enhanced oxygen content in n-butanol, which facilitates more complete combustion. The lowest CO and HC emissions were attained at a speed of 2317 rpm and a fuel blend of G50n-b50, resulting in an emission of 0.715 %vol. for CO and 28 ppm for HC.

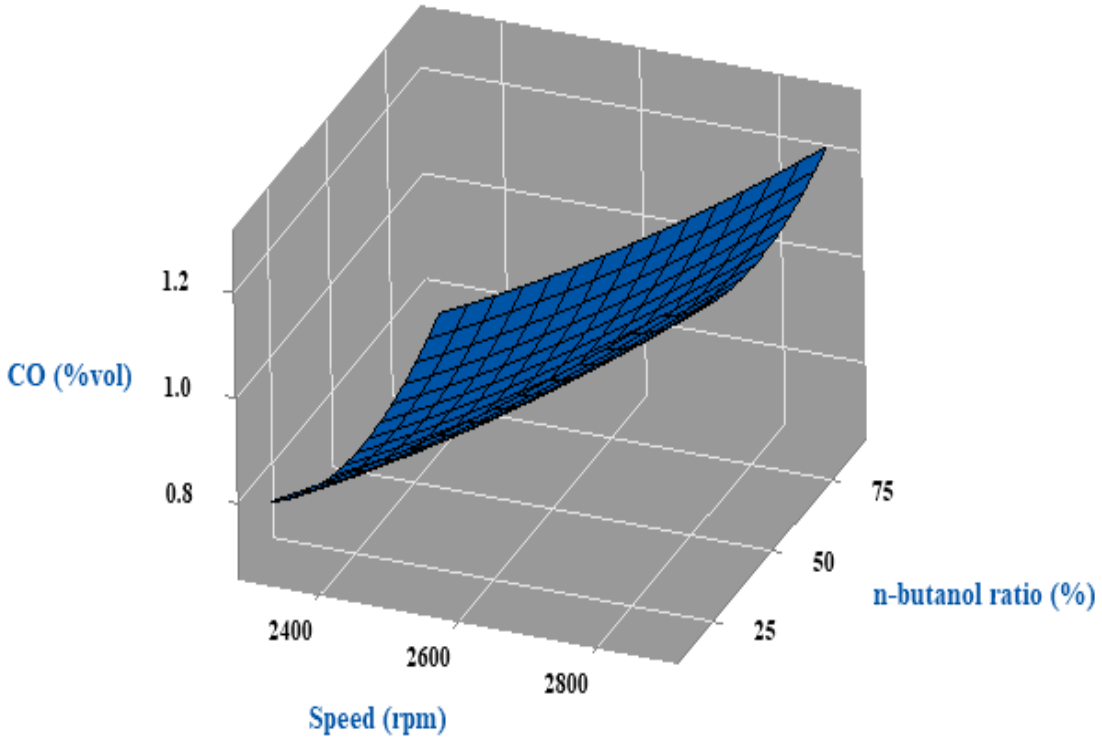

Figure 4.50 CO vs engine speed and n-butanol ratio surface plot

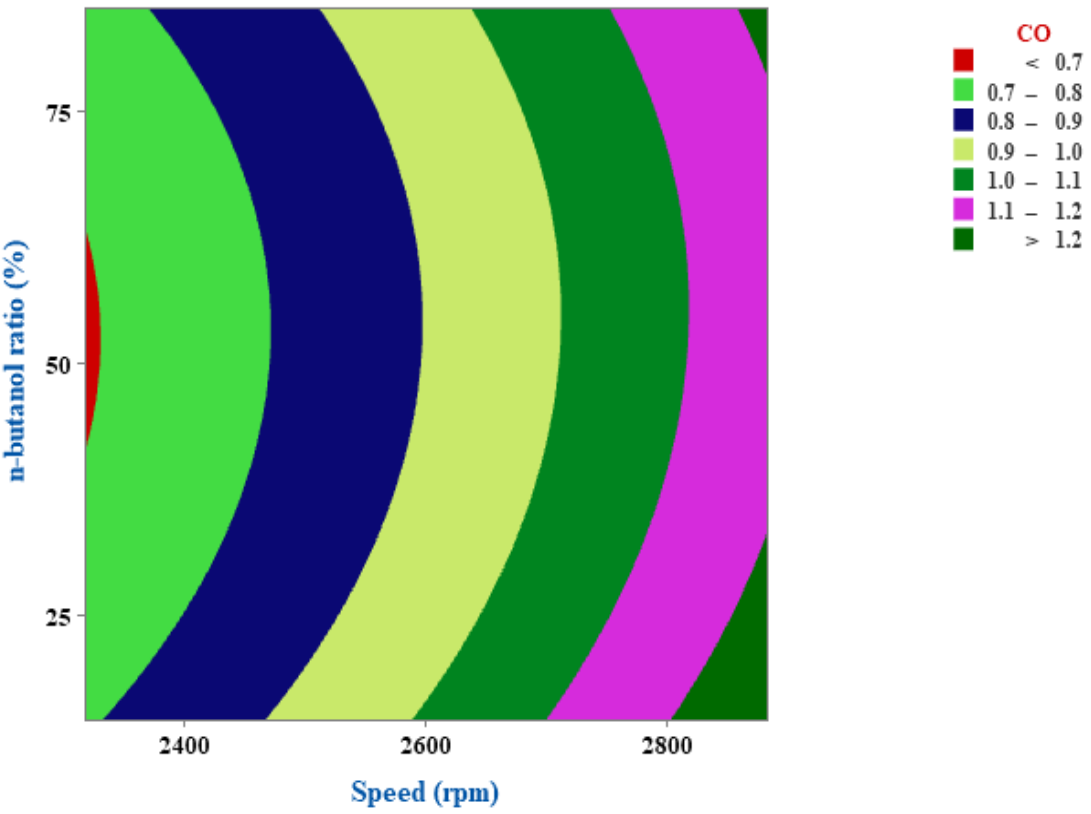

Figure 4.51 CO vs engine speed and n-butanol ratio contour plot

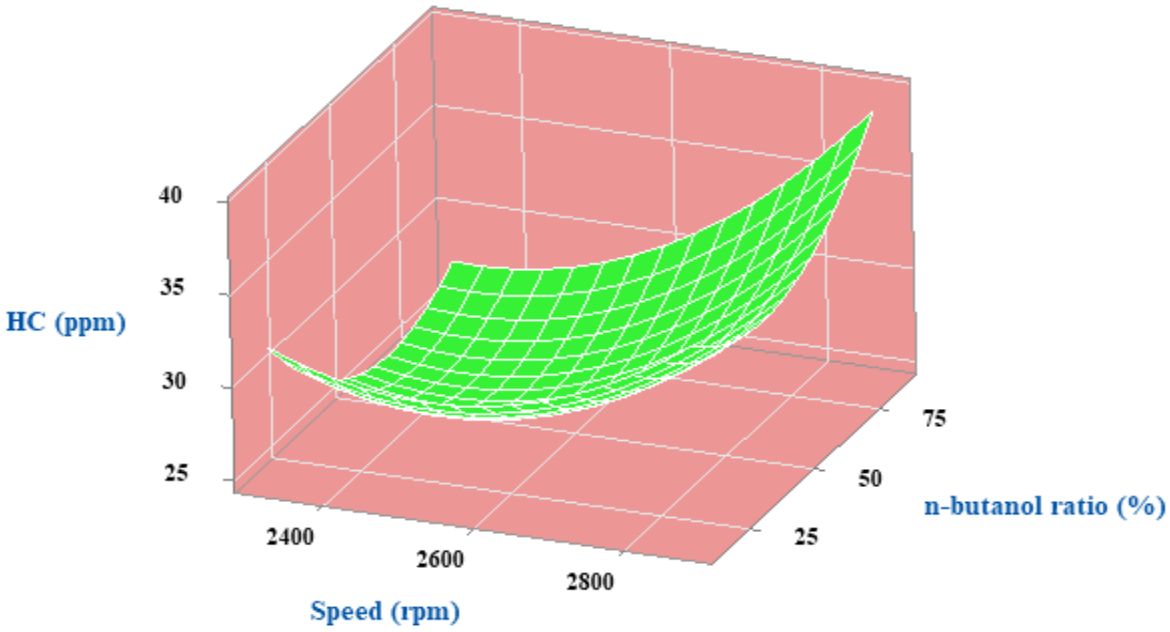

Figure 4.52 HC vs engine speed and n-butanol ratio surface plot

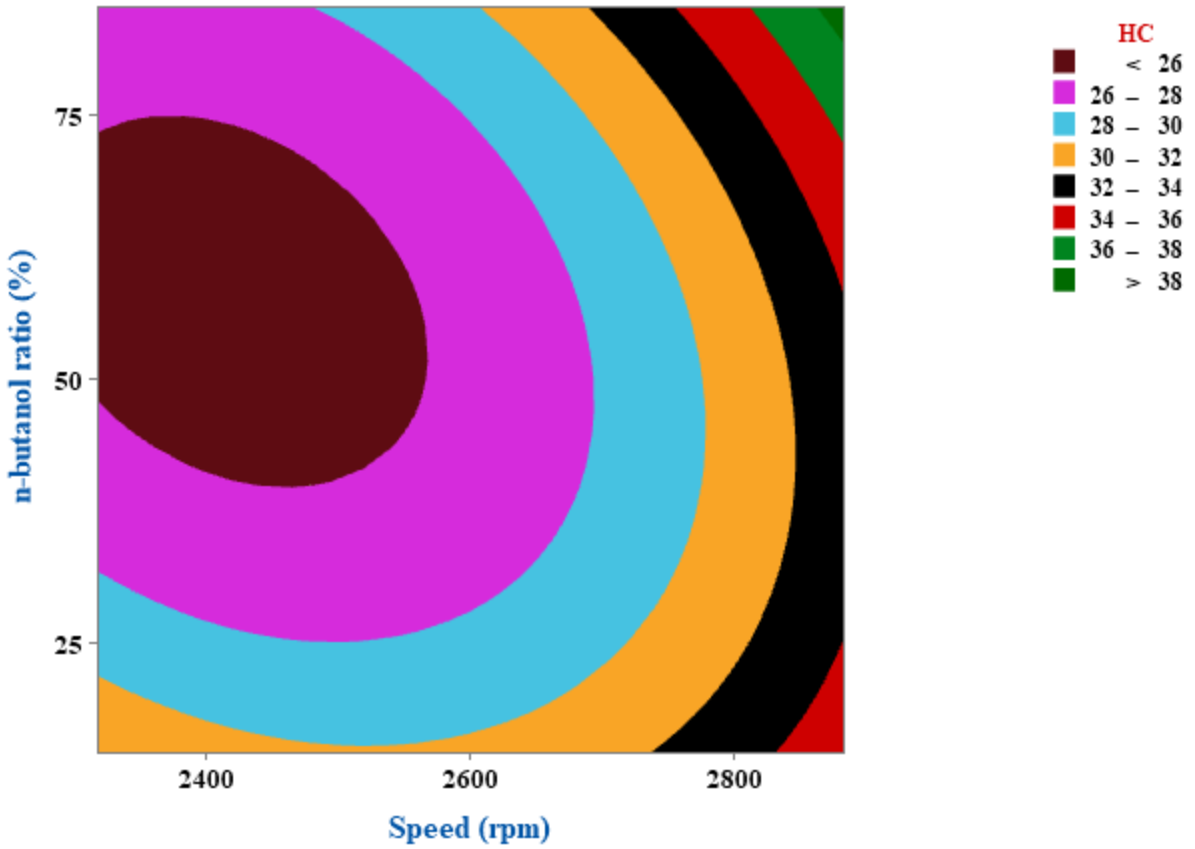

Figure 4.53 HC vs engine speed and n-butanol ratio contour plot

4.3.4. Response Surface Methodology Optimizer

In this study, a numerical optimization methodology was employed to increase the operational parameters of the engine. Using computational optimization with statistical software, the study focused on optimizing combinations of seven response variables in the context of an RCCI engine mode. The primary goal was to enhance engine performance while maintaining emissions at the lowest possible levels. During the numerical optimization, the criteria were set to maximize BP and BT, while reducing BSFC, CO, CO_2, HC, and NOx. Table 4.12 reveals the optimization setup utilized in the RSM analysis, showing the defined response limits and goals that guided the numerical search for the best operating condition. The table reveals that all performance-related outputs, brake torque, and brake power, were set to be maximized to meet the goal of improving engine effectiveness, while BSFC and all the emission parameters (NOx, CO_2, CO, and HC) were constrained with the goal of minimization in order to have cleaner combustion. The lower and upper bounds for each response were not restated but used to establish real constraints based on

the experimental range so that the optimizer searches within physically meaningful engine behavior. This configuration provided a balanced multi-objective framework that allowed the optimizer to identify an operating point that enhances performance while simultaneously reducing emissions. Using the RSM optimizer, the optimal operating conditions were found to be a 2523 engine speed and 51.78% n-butanol ratio. Under these conditions, the best response achieved was a BT of 14.85 Nm, a BP of 3.99 kW, a BSFC of 0.356 kg/kWh, a CO_2 emission of 5.17 %vol., a CO emission of 0.84 %vol, a NOx emission of 125 ppm, and an HC emission of 26 ppm. These RSM findings indicate that the performance and exhaust emissions parameters were significantly influenced by engine speed and n-butanol.

Table 4.11 Setup for optimization

Response	Lower limit	Upper limit	Goal
Brake torque (Nm)	14.01	14.85	Maximize
Brake power (kW)	3.78	4.30	Maximize
Brake specific fuel consumption (kg/kWh)	0.328	0.371	Minimize
Nitrogen oxides (ppm)	81	176	Minimize
Carbon dioxide (%vol.)	4.6	5.8	Minimize
Carbon monoxide (%vol.)	0.715	1.158	Minimize
Hydrocarbons (ppm)	24	34	Minimize

CHAPTER FIVE

CONCLUSION AND RECOMMENDATION

Conclusions

In this study, the production, optimization, and characterization of biodiesel derived from cottonseed oil were successfully achieved using transesterification process utilizing methanol and potassium hydroxide as a catalyst. The optimization of the process was conducted using RSM with a Box-Behnken design, which involved varying the ratios of methanol to oil, the concentration of the catalyst, and the duration of the reaction. The results of the ANOVA indicated that the methanol to oil ratio and catalyst concentration were the most influential variables, with the optimized conditions yielding 95.04% biodiesel, with an experimental validation yield of 94.80%, was achieved at the identified optimal operating conditions of a methanol-to-oil ratio of 1:6, a reaction time of 52.2 minutes, and a catalyst concentration of 0.985 wt.%. The produced biodiesel met ASTM and EN standards for key fuel properties. GC-MS analysis identified key FAMEs, confirming the fuel's composition.

Additionally, an experimental investigation was carried out on a Reactivity Controlled Compression Ignition (RCCI) engine using diesel-biodiesel blend (B20) as the high-reactivity fuel and blends of gasoline and n-butanol as the low-reactivity fuel. The implementation of the RCCI mode demonstrated significant enhancements in engine performance while simultaneously reducing harmful emissions in comparison to conventional diesel operation. Among the tested blends, the B20+G50n-b50 fuel blend achieved the highest cylinder pressure of 92.25 bar at 2800 rpm. Brake torque exhibited relative stability across all blends, with slight improvements observed at higher speeds for the B20+G50n-b50 blend. Furthermore, brake power was consistently higher for the RCCI fuels, particularly with the B20+G50n-b50 blend, although there was a slight increase in BSFC when operating in RCCI mode. The RCCI combustion strategy significantly influenced engine emissions, with the fuel blend ratio playing a crucial role. The B20+G25-nb75 blend achieved the lowest NOx and CO_2 emissions, with average reductions of approximately 36.5% and 16.44%, respectively, while CO and HC emissions were most effectively minimized using the B20+G75-nb25 blend. The B20+G50-nb50 and B20+G75-nb25 blends showed moderate reductions in NOx (approximately 26.7% and 13.12%) and CO_2 (approximately 4.43% and

10.28%) emissions. Corresponding average increases in HC emissions for the B20+G25-nb75, B20+G50-nb50, and B20+G75-nb25 blends were about 21.69%, 15.86%, and 7.22%, respectively.

The study also confirmed that RSM using a central composite design approaches were efficient in optimizing fuel blends and engine speeds. quadratic models developed from the experimental data demonstrated excellent predictive accuracy, with R^2 values exceeding 97% for all measured parameters. It was also observed that engine speed was the most influential factor on both performance and emissions, while the gasoline-n-butanol blend ratio had the greatest effect on brake torque. The study identified 2523 rpm engine speed and a 51.78% n-butanol ratio using RSM as the optimum operating conditions for RCCI mode.

Overall, the study highlights the effectiveness of biodiesel production from cottonseed oil and demonstrates the potential of RCCI engines using biodiesel and alcohol to enhance performance while lowering emissions, contributing to cleaner, more sustainable engine technologies.

Recommendations and Future Directions

The authors recommend that future research should build upon the results of this study to further advance the development and practical application of RCCI engine technology. Based on the findings, the following points are suggested for future investigation:

- Explore a wider range of gasoline/n-butanol and biodiesel/diesel blend ratios to comprehensively assess their effects on engine performance, combustion, and emissions, while efficiently guiding experiments using optimization and predictive tools such as Artificial Neural Networks (ANN), Genetic Algorithms, and factorial design to minimize the number of trials and obtain reliable predictive models.
- Extend experimental studies beyond steady-state conditions to include transient engine operation, variable loads, add dynamic driving cycles, which are essential real-world performance
- Prioritize research on the transient behavior of RCCI engines under various load conditions to address the gap between laboratory testing and real-driving scenarios, supporting compliance with modern emission standards.
- Limited long-term analysis of injector durability and deposit formation when using oxygenated alcohols and biodiesel blends at higher loads.

REFERENCES

Abdullahi, K., Ojonugwa, S. S., Yusuff, A. S., Umaru, M., Mohammed, I. A., Olutoye, M. A., & Aberuagba, F. (2023). Optimization of biodiesel production from Allamanda Seed Oil using design of experiment. *Fuel Communications*, *14*(December 2022), 100081. https://doi.org/10.1016/j.jfueco.2022.100081

Agarwal, A. K., Martínez, A. G., Kalwar, A., & Valera, H. (2022). Advanced Combustion for Sustainable Transport. Springer.

Agarwal, A. K., Singh, A. P., García, A., & Monsalve-Serrano, J. (2022). Challenges and opportunities for application of reactivity-controlled compression ignition combustion in commercially viable transport engines. *Progress in Energy and Combustion Science*, *93*, 101028. https://doi.org/10.1016/j.pecs.2022.101028.

Agu, C. M., Ani, K. A., Ani, O. N., Nnaji, P. C., Kadurumba, C. H., & Esonye, C. (2024). Application of efficient soft computing approaches for modeling methyl ester yield from Azadirachta Indica (Neem) seed oil: A comparative study of RSM, ANN and ANFIS. *Green Technologies and Sustainability*, *2*(1), 100057. https://doi.org/10.1016/j.grets.2023.100057

Agu, C. M., Orakwue, C. C., Menkiti, M. C., Agulanna, A. C., & Akaeme, F. C. (2022). RSM/ANN based modeling of methyl esters yield from Anacardium occidentale kernel oil by transesterification, for possible application as transformer fluid. *Current Research in Green and Sustainable Chemistry*, *5*(January), 100255. https://doi.org/10.1016/j.crgsc.2021.100255

Ahmad, A., Yadav, A. K., Singh, A., & Singh, D. K. (2024). A comprehensive machine learning-coupled response surface methodology approach for predictive modeling and optimization of biogas potential in anaerobic Co-digestion of organic waste. *Biomass and Bioenergy*, *180*, 106995. https://doi.org/10.1016/j.biombioe.2023.106995.

Ahmad, G., Imran, S., Farooq, M., Shah, A. N., Anwar, Z., Rehman, A. U., & Imran, M. (2023). Biodiesel Production from Waste Cooking Oil Using Extracted Catalyst from Plantain Banana Stem via RSM and ANN Optimization for Sustainable Development. *Sustainability (Switzerland)*, *15*(18). https://doi.org/10.3390/su151813599

Alhassan, F. H., Rashid, U., & Taufiq-Yap, Y. H. (2016). Optimization of simultaneous production

of waste cooking oil based-biodiesel using iron-manganese doped zirconia-supported molybdenum oxide nanoparticles catalyst. *Journal of Renewable and Sustainable Energy*, *8*(3). https://doi.org/10.1063/1.4953090

Amirthavalli, V., Warrier, A. R., & Gurunathan, B. (2022). Various methods of biodiesel production and types of catalysts. In *Biofuels and Bioenergy* (pp. 111–132). Elsevier. https://doi.org/10.1016/B978-0-323-85269-2.00020-4

Bajwa, W., Ikram, A., Malik, M. A. I., Razzaq, L., Khan, A. R., Latif, A., Hussain, F., & Qazi, A. (2024). Optimization of biodiesel yield from waste cooking oil and sesame oil using RSM and ANN techniques. *Heliyon*, *10*(15). https://doi.org/10.1016/j.heliyon.2024.e34804.

Balfas, R. N., Muhammad Syam, A., Muhammad, M., Setiawan, A., & Fithra, H. (2024). Characteristics of biodiesel produced from crude palm oil through non-alcohol synthesis route using dimethyl carbonate and immobilized eco-enzyme catalyst. *Energies*, *17*(7), 1551. https://doi.org/10.3390/en17071551.

Banga, S., & Pathak, V. V. (2023). Biodiesel production from waste cooking oil: a comprehensive review on the application of heterogenous catalysts. *Energy Nexus*, *10*, 100209. https://doi.org/10.1016/j.nexus.2023.100209.

Baral, N. R., & Shah, A. (2014). Microbial inhibitors: formation and effects on acetone-butanol-ethanol fermentation of lignocellulosic biomass. *Applied Microbiology and Biotechnology*, *98*, 9151–9172.

Begum, S., & Dahman, Y. (2015). Enhanced biobutanol production using novel clostridial fusants in simultaneous saccharification and fermentation of green renewable agriculture residues. *Biofuels, Bioproducts and Biorefining*, *9*(5), 529–544. https://doi.org/10.1002/bbb.1564.

Boichenko, S., Yakovlieva, A., Zubenko, S., & Shkilniuk, I. (2025). Physical, Chemical, and Performance Properties of Biodiesel Fuels: A Comparative Study of Lipid-Based Feedstocks. *Energies (19961073)*, *18*(16).

Bouaid, A., Iliuta, G., & Marchetti, J. M. (2024). Cold flow properties of biodiesel from waste cooking oil and a new improvement method. *Heliyon*, *10*(17). https://doi.org/10.1016/j.heliyon.2024.e36756.

Cai, Y., Jia, M., Li, Y., Li, H., Liu, Z., Ding, R., & Lu, X. (2024). Optimization of the full-load combustion schemes of n-butanol/biodiesel reactivity-controlled compression ignition (RCCI) toward high-efficiency and low-emission engines. *International Journal of Engine Research*, 14680874241278960. https://doi.org/10.1177/14680874241278960.

Cao, D. N., Hoang, A. T., Luu, H. Q., Bui, V. G., & Tran, T. T. H. (2024). Effects of injection pressure on the NOx and PM emission control of diesel engine: A review under the aspect of PCCI combustion condition. *Energy Sources, Part A: Recovery, Utilization, and Environmental Effects*, *46*(1), 7414–7431. https://doi.org/10.1080/15567036.2020.1754531.

Cardama, M., Cortez, A., Hosek, E., Krapp, A., Medimorec, N., & Yiu, A. (2023). *SLOCAT Transport, Climate and Sustainability Global Status Report*.

Charitha, V., Thirumalini, S., Prasad, M., & Srihari, S. (2019). Investigation on performance and emissions of RCCI dual fuel combustion on diesel - bio diesel in a light duty engine. *Renewable Energy*, *134*, 1081–1088. https://doi.org/10.1016/j.renene.2018.09.048

Chauhan, B. V., Sayyed, I., Vedrantam, A., Garg, A., Bharti, S., & Shukla, M. (2021). State of the art in low-temperature combustion technologies: HCCI, PCCI, and RCCI. In A. K. Agarwal, A. García Martínez, A. Kalwar & H. Valera (Eds.), Advanced Combustion for Sustainable Transport (pp. 95–139). Springer Singapore. https://doi.org/10.1007/978-981-16-8418-04.

Chozhavendhan, S., Singh, M. V. P., Fransila, B., Kumar, R. P., & Devi, G. K. (2020). A review on influencing parameters of biodiesel production and purification processes. *Current Research in Green and Sustainable Chemistry*, *1*, 1–6. https://doi.org/10.1016/j.crgsc.2020.04.002.

Clay, B., Reaction, C., & Shallsuku, P. (2023). Transesterification of Cotton Seed Oil to Biodiesel using Nanoparticles of Transesterification of Cotton Seed Oil to Biodiesel using Nanoparticles of Bentonite Clay Catalysed Reaction. *10*(August 2018), 92–116.

Couzin, H., Ioannou, A., & Seyboth, K. (2023). Renewables 2023 global status report. *REN21 Secretariat*, 11–13.

da Silva Trindade, W. R., & dos Santos, R. G. (2017). Review on the characteristics of butanol, its production and use as fuel in internal combustion engines. *Renewable and Sustainable Energy Reviews*, *69*, 642–651. https://doi.org/10.1016/j.rser.2016.11.213.

Dahham, R. Y., Wei, H., & Pan, J. (2022). Improving thermal efficiency of internal combustion engines: recent progress and remaining challenges. *Energies*, *15*(17), 6222. https://doi.org/10.3390/en15176222.

Dalha, I. B., Said, M. A., Abdul Karim, Z. A., & Mohammed, S. E. (2020). An experimental investigation on the influence of port injection at valve on combustion and emission characteristics of B5/biogas RCCI engine. *Applied Sciences (Switzerland)*, *10*(2). https://doi.org/10.3390/app10020452. https://doi.org/10.3390/app10020452.

Demisu, D. G. (2021). Factors affecting biodiesel production from non-edible vegetable oil via base-catalyzed transesterification process: synthesis. *Int. J. Sustain. Green Energy*, *10*(3), 85–91. doi: 10.11648/j.ijrse.20211003.11.

Dempsey, A. B. (2013). Dual-fuel reactivity controlled compression ignition (RCCI) with alternative fuels. The University Of Wisconsin-Madison.

Disassa, H. D., Ancha, V. R., & Nallamothu, R. B. (2023). Experimental study of triple fuel physiognomies on LDRCCI diesel engine combustion. *Results in Engineering*, *20*(x), 101451. https://doi.org/10.1016/j.rineng.2023.101451

Disassa, H. D., Ancha, V. R., Nallamothu, R. B., & Zeru, B. A. (2023). Experimental study on the effect of speed and port-injected fuel blend ratio on a reactivity-control compression ignition (RCCI) engine performance. *Energy Conversion and Management: X*, *20*(September), 100448. https://doi.org/10.1016/j.ecmx.2023.100448

Duan, H., Jia, M., Li, Y., & Wang, T. (2021). A comparative study on the performance of partially premixed combustion (PPC), reactivity-controlled compression ignition (RCCI), and RCCI with reverse reactivity stratification (R-RCCI) fueled with gasoline and polyoxymethylene dimethyl ethers (PODEn). *Fuel*, *298*(April), 120838. https://doi.org/10.1016/j.fuel.2021.120838

Duraisamy, G., Rangasamy, M., & Govindan, N. (2020). A comparative study on methanol/diesel and methanol/PODE dual fuel RCCI combustion in an automotive diesel engine. *Renewable Energy*, *145*, 542–556. https://doi.org/10.1016/j.renene.2019.06.044

Dwarshala, S. K. R., Rajakumar, S. S., Kummitha, O. R., Venkatesan, E. P., Veza, I., & Samuel,

O. D. (2023). A Review on Recent Developments of RCCI Engines Operated with Alternative Fuels. *Energies*, *16*(7). https://doi.org/10.3390/en16073192

Elango, R. K., Sathiasivan, K., Muthukumaran, C., Thangavelu, V., Rajesh, M., & Tamilarasan, K. (2019). Transesterification of castor oil for biodiesel production: Process optimization and characterization. *Microchemical Journal*, *145*, 1162–1168. https://doi.org/10.1016/j.microc.2018.12.039.

Elbanna, A. M., Cheng, X., Yang, C., Elkelawy, M., & Bastawissi, H. A.-E. (2023). Investigative research of diesel/ethanol advanced combustion strategies: A comparison of Premixed Charge Compression Ignition (PCCI) and Direct Dual Fuel Stratification (DDFS). *Fuel*, *345*, 128143. https://doi.org/10.1016/j.fuel.2023.128143.

Elkelawy, M., El Shenawy, E. A., Mohamed, S. A., Elarabi, M. M., & Bastawissi, H. A.-E. (2022). Impacts of using EGR and different DI-fuels on RCCI engine emissions, performance, and combustion characteristics. *Energy Conversion and Management: X*, *15*, 100236. https://doi.org/10.1016/j.ecmx.2022.100236.

Fakhari, A. H., Gharehghani, A., Salahi, M. M., Mahmoudzadeh Andwari, A., Mikulski, M., Hunicz, J., & Könnö, J. (2023). Numerical investigation of ammonia-diesel fuelled engine operated in RCCI mode. https://doi.org/10.4271/2023-24-0057.

Fan, J., Meng, X., Tian, J., Xing, C., Wang, C., & Wood, J. (2023). A review of transportation carbon emissions research using bibliometric analyses. *Journal of Traffic and Transportation Engineering (English Edition)*, *10*(5), 878–899. https://doi.org/10.1016/j.jtte.2023.09.002.

Feng, Z., Zhang, J., Gu, J., Leng, X., He, Z., & Nishida, K. (2025). Improving Biodiesel Atomization Performance in CI Engines: A Review of Spray Behavior, Droplet Impingement, and Advanced Techniques. *Processes*, *13*(8), 2527. https://doi.org/10.3390/pr13082527.

Feroskhan, M., & Gobinath, N. (2024). Experimental study of butanol blending in biogas-biodiesel fueled CI engine under dual fuel, RCCI and HCCI combustion modes. *Case Studies in Thermal Engineering*, *58*(April), 104349. https://doi.org/10.1016/j.csite.2024.104349

Fırat, M., Altun, Ş., Okcu, M., & Varol, Y. (2022). Experimental investigation on combustion and emission characteristics of reactivity controlled compression ignition engine powered with

iso-propanol/biodiesel blends. *Propulsion and Power Research*, *11*(2), 224–239. https://doi.org/10.1016/j.jppr.2022.04.003.

Gad, M. S., He, Z., El-Shafay, A. S., & El-Seesy, A. I. (2021). Combustion characteristics of a diesel engine running with Mandarin essential oil -diesel mixtures and propanol additive under different exhaust gas recirculation: Experimental investigation and numerical simulation. *Case Studies in Thermal Engineering*, *26*(February), 101100. https://doi.org/10.1016/j.csite.2021.101100

Ganesan, N., Masimalai, S., Ekambaram, P., & Selvaraju, K. (2020). Experimental Assessment of Effects of n-Butanol on Performance, Emission, and Combustion Characteristics of Mahua Oil Fueled Reactivity Controlled Compression Ignition (RCCI) Engine. *Emission Control Science and Technology*, *6*(3), 345–357. https://doi.org/10.1007/s40825-020-00163-1

Ganesh, D., Ayyappan, P. R., & Murugan, R. (2019). Experimental investigation of iso-butanol/diesel reactivity controlled compression ignition combustion in a non-road diesel engine. *Applied Energy*, *242*, 1307–1319. https://doi.org/10.1016/j.apenergy.2019.03.166.

García, A., Monsalve-Serrano, J., Villalta, D., & Guzmán-Mendoza, M. (2021). Methanol and OMEx as fuel candidates to fulfill the potential EURO VII emissions regulation under dual-mode dual-fuel combustion. *Fuel*, *287*(October). https://doi.org/10.1016/j.fuel.2020.119548

Gupta, S. K., & Anand, K. (2018). Experimental Investigations to reduce Unburned Emissions in Reactivity Controlled Compression Ignition through Fuel Modifications. *Applied Thermal Engineering*. https://doi.org/10.1016/j.applthermaleng.2018.10.036

Gupta, S. K., & Krishnasamy, A. (2024). A relative comparison of HCCI, PCCI, and RCCI combustion strategies: an alternative fuels perspective. *International Journal of Engine Research*, *25*(6), 1078–1092. https://doi.org/10.1177/14680874231216664.

Gwalwanshi, M., Kumar, R., & Kumar Chauhan, M. (2022). A review on butanol properties, production and its application in internal combustion engines. *Materials Today: Proceedings*, *62*(P12), 6573–6577. https://doi.org/10.1016/j.matpr.2022.04.573

Han, J., Bao, H., & Somers, L. M. T. (2021). Experimental investigation of reactivity controlled compression ignition with n-butanol/n-heptane in a heavy-duty diesel engine. *Applied*

Energy, *282*(PA), 116164. https://doi.org/10.1016/j.apenergy.2020.116164

Han, J., & Somers, B. (2020). Effects of butanol isomers on the combustion and emission characteristics of a heavy-duty engine in RCCI mode. SAE Technical Paper. https://doi.org/10.4271/2020-01-0307.

Hao, Q. (2023). A Review of Low Temperature Combustion Mode of Engine. *Trends in Renewable Energy*, *9*(2), 180–191. https://doi.org/10.17737/tre.2023.9.2.00160

Harari, P. A., Banapurmath, N. R., Yaliwal, V. S., Khan, T. M. Y., Soudagar, M. E. M., & Sajjan, A. M. (2020). Experimental studies on performance and emission characteristics of reactivity controlled compression ignition (RCCI) engine operated with gasoline and Thevetia Peruviana biodiesel. *Renewable Energy*, *160*, 865–875. https://doi.org/10.1016/j.renene.2020.07.009

Huang, H., Singh, V., & Qureshi, N. (2015). Butanol production from food waste: a novel process for producing sustainable energy and reducing environmental pollution. *Biotechnology for Biofuels*, *8*, 1–12. https://DOI 10.1186/s13068-015-0332-x.

Jagankumar, K. R., Prakash, N., Prasad, C., Shridhar, V. A., Singh, M. D., & Sathyamurthy, R. (2020). An experimental investigation on single cylinder RCCI engine fuelled with diesel/petrol. *Journal of Physics: Conference Series*, *1706*(1), 12200. https://doi:10.1088/1742-6596/1706/1/012200

Jimoh, A., Agbaji, E. B., Ajibola, V. O., & Uba, S. (2023a). Production of Methyl Ester from Used Cottonseed Oil Optimized Using Box Behnken Design Approach. *Advanced Journal of Chemistry, Section A*, *6*(1), 1–16. https://doi.org/10.22034/ajca.2023.359977.1327

Jimoh, A., Agbaji, E. B., Ajibola, V. O., & Uba, S. (2023b). Ptimization of the production of methyl ester from used cotton seed oil: A statistical approach using box-behnken design. *Chemical Review and Letters*, *6*(2), 183–212. https://doi.org/10.22034/crl.2023.359632.1179

Karchiyappan, T., & Karri, R. R. (2021). Process optimization and modeling of hydraulic fracturing process wastewater treatment using aerobic mixed microbial reactor via response surface methodology. In *Soft computing techniques in solid waste and wastewater management* (pp. 351–363). Elsevier. https://doi.org/10.1016/B978-0-12-824463-0.00023-9

Khandal, S. V., Banapurmath, N. R., & Gaitonde, V. N. (2019). Performance studies on homogeneous charge compression ignition (HCCI) engine powered with alternative fuels. *Renewable Energy*, *132*, 683–693. https://doi.org/10.1016/j.renene.2018.08.035

Lapuerta, M., Ballesteros, R., & Barba, J. (2017). Strategies to introduce n-butanol in gasoline blends. *Sustainability*, *9*(4), 589. https://doi.org/10.3390/su9040589.

Lapuerta, M., Hernández, J. J., Rodríguez-Fernández, J., Barba, J., Ramos, A., & Fernández-Rodríguez, D. (2018). Emission benefits from the use of n-butanol blends in a Euro 6 diesel engine. *International Journal of Engine Research*, *19*(10), 1099–1112. https://doi.org/10.1177/1468087417742578.

Li, J., Yang, W., & Zhou, D. (2017). Review on the management of RCCI engines. *Renewable and Sustainable Energy Reviews*, *69*(November 2016), 65–79. https://doi.org/10.1016/j.rser.2016.11.159

Li, T., Zhao, P., He, H., Wang, C., Zhang, H., Chen, Z., & Chen, H. (2025). Dual-fuel dual-direct injection: An efficient and clean combustion technology for diesel engines. *Journal of the Energy Institute*, 102006. https://doi.org/10.1016/j.joei.2025.102006.

Lin, Q., Tay, K. L., Yu, W., Yang, W., & Wang, Z. (2021). Effects of polyoxymethylene dimethyl ether 3 (PODE3) addition and injection pressure on combustion performance and particle size distributions in a diesel engine. *Fuel*, *283*(August 2020), 119347. https://doi.org/10.1016/j.fuel.2020.119347

Ma, W., Gao, S., Liu, H., & Li, D. (2024). The improvements of a diesel engine fueled with renewable and sustainable diesel/n-butanol/polyoxymethylene dimethyl ethers blended fuels at high altitudes. *Energy*, *289*, 130060. https://doi.org/10.1016/j.energy.2023.130060.

Malik, K., Capareda, S. C., Kamboj, B. R., Malik, S., Singh, K., Arya, S., & Bishnoi, D. K. (2024). Biofuels Production: A Review on Sustainable Alternatives to Traditional Fuels and Energy Sources. *Fuels*, *5*(2), 157–175. https://doi.org/10.3390/fuels5020010.

Mandari, V., & Devarai, S. K. (2022). Biodiesel production using homogeneous, heterogeneous, and enzyme catalysts via transesterification and esterification reactions: A critical review. *BioEnergy Research*, *15*(2), 935–961.

Maurya, R. K., & Akhil, N. (2017). Comparative study of the simulation ability of various recent hydrogen combustion mechanisms in HCCI engines using stochastic reactor model. *International Journal of Hydrogen Energy*, *42*(16), 11911–11925. https://doi.org/10.1016/j.ijhydene.2017.02.155

Mei, D., Yu, Q., Zhang, Z., Yue, S., & Tu, L. (2021). Effects of two pilot injection on combustion and emissions in a PCCI diesel engine. *Energies*, *14*(6), 1651. https://doi.org/10.3390/en14061651.

Mohammed Elbanna, A., Xiaobei, C., Can, Y., Elkelawy, M., Alm-Eldin Bastawissi, H., & Panchal, H. (2022). Fuel reactivity controlled compression ignition engine and potential strategies to extend the engine operating range: A comprehensive review. *Energy Conversion and Management: X*, *13*(November 2021), 100133. https://doi.org/10.1016/j.ecmx.2021.100133

Muhammad, G., Ngatcha, A. D. P., Lv, Y., Xiong, W., El-Badry, Y. A., Asmatulu, E., Xu, J., & Alam, M. A. (2022). Enhanced biodiesel production from wet microalgae biomass optimized via response surface methodology and artificial neural network. *Renewable Energy*, *184*, 753–764. https://doi.org/10.1016/j.renene.2021.11.091.

Naseef, H. H., & Tulaimat, R. H. (2025). Transesterification and esterification for biodiesel production: A comprehensive review of catalysts and palm oil feedstocks. *Energy Conversion and Management: X*, 100931. https://doi.org/10.1016/j.ecmx.2025.100931.

Neupane, D. (2022). Biofuels from Renewable Sources, a Potential Option for Biodiesel Production. *Bioengineering*, *10*(1), 29. https://doi.org/10.3390/bioengineering10010029.

Ngige, G. A., Ovuoraye, P. E., Igwegbe, C. A., Fetahi, E., Okeke, J. A., Yakubu, A. D., & Onyechi, P. C. (2023). RSM optimization and yield prediction for biodiesel produced from alkali-catalytic transesterification of pawpaw seed extract: Thermodynamics, kinetics, and Multiple Linear Regression analysis. *Digital Chemical Engineering*, *6*(May 2022). https://doi.org/10.1016/j.dche.2022.100066

Okcu, M., Varol, Y., Altun, Ş., & Fırat, M. (2021). Effects of isopropanol-butanol-ethanol (IBE) on combustion characteristics of a RCCI engine fueled by biodiesel fuel. *Sustainable Energy*

Technologies and Assessments, *47*(June). https://doi.org/10.1016/j.seta.2021.101443

Onukwuli, D. O., Emembolu, L. N., Ude, C. N., Aliozo, S. O., & Menkiti, M. C. (2017). Optimization of biodiesel production from refined cotton seed oil and its characterization. *Egyptian Journal of Petroleum*, *26*(1), 103–110. https://doi.org/10.1016/j.ejpe.2016.02.001

Pachiannan, T., Zhong, W., Rajkumar, S., He, Z., Leng, X., & Wang, Q. (2019). A literature review of fuel effects on performance and emission characteristics of low-temperature combustion strategies. *Applied Energy*, *251*(301), 113380. https://doi.org/10.1016/j.apenergy.2019.113380

Pan, S., Liu, X., Cai, K., Li, X., Han, W., & Li, B. (2020). Experimental study on combustion and emission characteristics of iso-butanol/diesel and gasoline/diesel RCCI in a heavy-duty engine under low loads. *Fuel*, *261*(October 2019), 116434. https://doi.org/10.1016/j.fuel.2019.116434

Park, H., Shim, E., & Bae, C. (2019). Injection strategy in natural gas–diesel dual-fuel premixed charge compression ignition combustion under low load conditions. *Engineering*, *5*(3), 548–557. https://doi.org/10.1016/j.eng.2019.03.005.

Pham, P. X., Nguyen, K. T., Pham, T. V, & Nguyen, V. H. (2020). Biodiesels manufactured from different feedstock: from fuel properties to fuel atomization and evaporation. *ACS Omega*, *5*(33), 20842–20853. https://dx.doi.org/10.1021/acsomega.0c02083.

Pradana, Y. S., Makertihartha, I. G. B. N., Indarto, A., Prakoso, T., & Soerawidjaja, T. H. (2024). A review of biodiesel cold flow properties and its improvement methods: towards sustainable biodiesel application. *Energies*, *17*(18), 4543. https://doi.org/10.3390/en17184543.

Rahman, S. M. A., Fattah, I. M. R., Ong, H. C., & Zamri, M. F. M. A. (2021). State-of-the-Art of Strategies to Reduce Exhaust Emissions from Diesel Engine Vehicles. Energies, 14(6), 1766. https://doi.org/10.3390/en14061766.

Rajendran, S., Dhairiyasamy, R., Jaganathan, S., Murugesan, S., Muthusamy, R., Periannan, S., Muniyappan, G., Jaganathan, B., Srinivasan, K., & Elangandhi, H. (2023). Effect of injection timing on combustion, emission and performance characteristics of safflower methyl ester in CI engine. *Results in Engineering*, *20*, 101599. https://doi.org/10.1016/j.rineng.2023.101599.

Ramachandran, E., Krishnaiah, R., Venkatesan, E. P., Shaik, S., Saleel, C. A., & Hussain, F. (2023). Investigation into the Ideal Concoction for Performance and Emissions Enhancement of Jatropha Biodiesel-Diesel with CuO Nanoparticles Using Response Surface Methodology. *ACS Omega*, *8*(42), 39067–39079. https://doi.org/10.1021/acsomega.3c03890.

Ramalingam, K., Kandasamy, M., Subbiah, G., Vellaiyan, S., Devarajan, Y., Chandran, D., & Raviadaran, R. (2024). Energy, environmental, and economic benefits of hydrogen-enriched biofuel using ammonium hydroxide in reactivity-controlled compression ignition engines. *Results in Engineering*, *24*, 103672. https://doi.org/10.1016/j.rineng.2024.103672.

Rameez, P. V, & Ibrahim, M. M. (2024). A comprehensive review on the utilization of hydrogen in low temperature combustion strategies: Combustion, performance and emission attributes. *Journal of the Energy Institute*, *113*, 101511. https://doi.org/10.1016/j.joei.2023.101511.

Rashed, M. M., Kalam, M. A., Masjuki, H. H., Rashedul, H. K., Ashraful, A. M., Shancita, I., & Ruhul, A. M. (2015). Stability of biodiesel, its improvement and the effect of antioxidant treated blends on engine performance and emission. *RSC Advances*, *5*(46), 36240–36261. https://doi.org/10.1039/C4RA14977G.

Razzaq, L., Abbas, M. M., Miran, S., Asghar, S., Nawaz, S., Soudagar, M. E. M., Shaukat, N., Veza, I., Khalil, S., Abdelrahman, A., & Kalam, M. A. (2022). Response Surface Methodology and Artificial Neural Networks-Based Yield Optimization of Biodiesel Sourced from Mixture of Palm and Cotton Seed Oil. *Sustainability (Switzerland)*, *14*(10). https://doi.org/10.3390/su14106130

Razzaq, L., Abbas, M. M., Waseem, A., Jauhar, T. A., Fayaz, H., Kalam, M. A., Soudagar, M. E. M., Silitonga, A. S., & Ishtiaq, U. (2023). Influence of varying concentrations of TiO2 nanoparticles and engine speed on the performance and emissions of diesel engine operated on waste cooking oil biodiesel blends using response surface methodology. *Heliyon*, *9*(7). https://doi.org/10.1016/j.heliyon.2023.e17758.

Riyadi, T. W. B., Spraggon, M., Herawan, S. G., Idris, M., Paristiawan, P. A., Putra, N. R., Silambarasan, R., & Veza, I. (2023). Biodiesel for HCCI engine: Prospects and challenges of sustainability biodiesel for energy transition. *Results in Engineering*, *17*, 100916. https://doi.org/10.1016/j.rineng.2023.100916.

Sakthivel, R., Ramesh, K., Mohamed Shameer, P., & Purnachandran, R. (2019). Experimental investigation on improvement of storage stability of bio-oil derived from intermediate pyrolysis of Calophyllum inophyllum seed cake. *Journal of the Energy Institute*, *92*(3), 768–782. https://doi.org/10.1016/j.joei.2018.02.006

Sambasivam, K. M., Kuppan, P., Laila, L. S., Shashirekha, V., Tamilarasan, K., & Abinandan, S. (2023). Kernel-Based Biodiesel Production from Non-Edible Oil Seeds: Techniques, Optimization, and Environmental Implications. *Energies*, *16*(22), 7589. https://doi.org/10.3390/en16227589.

Sánchez, F. Z., De Souza, O. M. R., Pradelle, R. N. C., Leal, S., Braga, C. V. T., & Loaiza, J. C. V. (2022). Effects of n-Butanol Compression Ignition of Ethanol by Rapid Compression Machine. *Journal Homepage: Http://Iieta. Org/Journals/Ijht*, *40*(5), 1115–1124.

Sarin, A., Sharma, N., Devgan, K., & Singh, M. (2021). Study of kinematic viscosity and density of biodiesels exposed to radiations. *Materials Today: Proceedings*, *46*, 5516–5522. https://doi.org/10.1016/j.matpr.2020.09.257.

Sattarzadeh, M., Ebrahimi, M., & Jazayeri, S. A. (2022). A detail study of a RCCI engine performance fueled with diesel fuel and natural gas blended with syngas with different compositions. *International Journal of Hydrogen Energy*, *47*(36), 16283–16296. https://doi.org/10.1016/j.ijhydene.2022.03.088.

Seal, S., Panda, A. K., Kumar, S., & Singh, R. K. (2015). Production and characterization of bio oil from cotton seed. *Environmental Progress & Sustainable Energy*, *34*(2), 542–547. https://doi.org/10.1002/ep.12011.

Selvan, S. S., Pandian, P. S., Subathira, A., & Saravanan, S. (2018). Comparison of response surface methodology (RSM) and artificial neural network (ANN) in optimization of aegle marmelos oil extraction for biodiesel production. *Arabian Journal for Science and Engineering*, *43*, 6119–6131. https://doi.org/10.1007/s13369-018-3272-5.

Sengupta, A., Biswas, S., & Banerjee, R. (2023). Performance-emission effect of n-butanol in Reactivity Controlled Compression Ignition regimes of biodiesel combustion. *Energy Sources, Part A: Recovery, Utilization, and Environmental Effects*, *45*(4), 11122–11141.

https://doi.org/10.1080/15567036.2023.2253746.

Shankar, A. A., Pentapati, P. R., & Prasad, R. K. (2017). Biodiesel synthesis from cottonseed oil using homogeneous alkali catalyst and using heterogeneous multi walled carbon nanotubes: Characterization and blending studies. *Egyptian Journal of Petroleum*, *26*(1), 125–133. https://doi.org/10.1016/j.ejpe.2016.04.001

Shim, E., Park, H., & Bae, C. (2020). Comparisons of advanced combustion technologies (HCCI, PCCI, and dual-fuel PCCI) on engine performance and emission characteristics in a heavy-duty diesel engine. *Fuel*, *262*, 116436. https://doi.org/10.1016/j.fuel.2019.116436.

Singh, A. P., Kumar, V., & Agarwal, A. K. (2020). Evaluation of comparative engine combustion, performance and emission characteristics of low temperature combustion (PCCI and RCCI) modes. *Applied Energy*, *278*, 115644. https://doi.org/10.1016/j.apenergy.2020.115644

Singh, D., Sharma, D., Soni, S. L., Sharma, S., Kumar Sharma, P., & Jhalani, A. (2020). A review on feedstocks, production processes, and yield for different generations of biodiesel. *Fuel*, *262*(July), 116553. https://doi.org/10.1016/j.fuel.2019.116553

Singh, D., Sharma, D., Soni, S. L., Sharma, S., & Kumari, D. (2019). Chemical compositions, properties, and standards for different generation biodiesels: A review. In *Fuel* (Vol. 253, pp. 60–71). Elsevier Ltd. https://doi.org/10.1016/j.fuel.2019.04.174

Srivatsa, C. V., Alam, S. S., Spickler, B., & Depcik, C. (2024). Effect of Exhaust Gas Recirculation on Combustion Characteristics of Ultra-Low-Sulfur Diesel in Conventional and PPCI Regimes for a High-Compression-Ratio Engine. *Energies*, *17*(16), 3950. https://doi.org/10.3390/en17163950.

Subramaniam, D., Murugesan, A., Avinash, A., & Kumaravel, A. (2013). Bio-diesel production and its engine characteristics—An expatiate view. *Renewable and Sustainable Energy Reviews*, *22*, 361–370. https://doi.org/10.1016/j.rser.2013.02.002.

Sun, W., Zhang, X., Guo, L., Sun, Y., Yan, Y., Li, J., Zhang, H., & Fu, D. (2021). Effects of Intake Components on Combustion and Emission Characteristics in an n-Butanol/Diesel Blend Fueled Engine. *ACS Omega*, *6*(24), 16129–16139. https://doi.org/10.1021/acsomega.1c02014

Thangaraj, B., & Solomon, P. R. (2020). Scope of biodiesel from oils of woody plants: a review. *Clean Energy*, *4*(2), 89–106. https://doi.org/10.1093/ce/zkaa006.

Vallinayagam, R., An, Y., S.Vedharaj, Sim, J., Chang, J., & Johansson, B. (2018). Naphtha vs. dieseline – The effect of fuel properties on combustion homogeneity in transition from CI combustion towards HCCI. *Fuel*, *224*(March), 451–460. https://doi.org/10.1016/j.fuel.2018.03.123

Venkatesan, H., John, G., & Sivamani, S. (2017). Cotton seed biodiesel as alternative fuel: Production and its characterization analysis using spectroscopic studies. *International Journal of Renewable Energy Research*, *7*(3), 1333–1339. https://doi.org/10.20508/ijrer.v7i3.6085.g7166

Veza, I., Spraggon, M., Fattah, I. M. R., & Idris, M. (2023). Response surface methodology (RSM) for optimizing engine performance and emissions fueled with biofuel: Review of RSM for sustainability energy transition. *Results in Engineering*, *18*, 101213. https://doi.org/10.1016/j.rineng.2023.101213.

Vilas Bôas, R. N., & Mendes, M. F. (2022). A review of biodiesel production from non-edible raw materials using the transesterification process with a focus on influence of feedstock composition and free fatty acids. *Journal of the Chilean Chemical Society*, *67*(1), 5433–5444.

Vinoth Arul Raj, J., Praveen Kumar, R., Vijayakumar, B., Gnansounou, E., & Bharathiraja, B. (2021). Modelling and process optimization for biodiesel production from Nannochloropsis salina using artificial neural network. *Bioresource Technology*, *329*(February), 124872. https://doi.org/10.1016/j.biortech.2021.124872

Wan Osman, W. N. A., Rosli, M. H., Mazli, W. N. A., & Samsuri, S. (2024). Comparative review of biodiesel production and purification. *Carbon Capture Science and Technology*, *13*(June), 100264. https://doi.org/10.1016/j.ccst.2024.100264

Wang, H., Liu, D., Ma, T., Tong, L., Zheng, Z., & Yao, M. (2019). Thermal efficiency improvement of PODE/Gasoline dual-fuel RCCI high load operation with EGR and air dilution. *Applied Thermal Engineering*, *159*, 113763. https://doi.org/10.1016/j.applthermaleng.2019.113763

Wang, X., Zhang, Q., Liu, F., Jin, Y., & Li, X. (2021). Experimental investigation on n-

butanol/methyl oleate dual fuel RCCI combustion in a single cylinder engine at high-load condition. *Scientific Reports*, *11*(1), 1–13. https://doi.org/10.1038/s41598-021-03693-y

Wategave, S. P., Banapurmath, N. R., Sawant, M. S., Soudagar, M. E. M., Mujtaba, M. A., Afzal, A., Basha, J. S., Alazwari, M. A., Safaei, M. R., & Elfasakhany, A. (2021). Clean combustion and emissions strategy using reactivity controlled compression ignition (RCCI) mode engine powered with CNG-Karanja biodiesel. *Journal of the Taiwan Institute of Chemical Engineers*, *124*, 116–131. https://doi.org/10.1016/j.jtice.2021.04.055.

Xu, G., Jia, M., Li, Y., Chang, Y., Liu, H., & Wang, T. (2019). Evaluation of variable compression ratio (VCR)and variable valve timing (VVT)strategies in a heavy-duty diesel engine with reactivity controlled compression ignition (RCCI)combustion under a wide load range. *Fuel*, *253*(January), 114–128. https://doi.org/10.1016/j.fuel.2019.05.020

Yusuff, A. S., Popoola, L. T., Adeniyi, D. O., & Olutoye, M. A. (2022). Coal fly ash supported ZnO catalyzed transesterification of Jatropha curcas oil: Optimization by response surface methodology. *Energy Conversion and Management: X*, *16*(September), 100302. https://doi.org/10.1016/j.ecmx.2022.100302

Zhao, W., Zhang, Y., Huang, G., He, Z., Qian, Y., & Lu, X. (2021). Experimental investigation on combustion and emission characteristics of butanol/biodiesel under blend fuel mode, dual fuel RCCI and ICCI modes. *Fuel*, *305*, 121590. https://doi.org/10.1016/j.fuel.2021.121590.

Zheng, Z., Xia, M., Liu, H., Shang, R., Ma, G., & Yao, M. (2018). Experimental study on combustion and emissions of n-butanol/biodiesel under both blended fuel mode and dual fuel RCCI mode. *Fuel*, *226*(March), 240–251. https://doi.org/10.1016/j.fuel.2018.03.151.

APPENDICES

Appendix A: Original research papers published from the results of study

Scientific African 28 (2025) e02665

Contents lists available at ScienceDirect

Scientific African

journal homepage: www.elsevier.com/locate/sciaf

Optimization of biodiesel production from cottonseed oil using response surface methodology and artificial neural network techniques

Negasa Tesfaye Tefera, Ramesh Babu Nallamothu, Getachew Alemayehu Lakew, Teshome Kumsa Kurse *

Department of Mechanical Engineering, Adama Science and Technology University, P.O.Box 1888, Adama, Ethiopia

www.nature.com/scientificreports

scientific reports

OPEN

Analysis of RCCI engine characteristics with n-butanol/ gasoline as low reactive fuel and biodiesel blend as high reactive fuel

Negasa Tesfaye Tefera, Ramesh Babu Nallamothu✉ & Getachew Alemayehu

Energy Conversion and Management: X 22 (2024) 100549

Contents lists available at ScienceDirect

Energy Conversion and Management: X

journal homepage: www.sciencedirect.com/journal/energy-conversion-and-management-x

Optimization, characterization, and GC-MS analysis of CSOME produced using alkali catalyzed transesterification

Negasa Tesfaye Tefera, Ramesh Babu Nallamothu *, Getachew Alemayehu, Yohannes Kefale

Department of Mechanical Engineering, Adama Science and Technology University, Adama, Ethiopia

Appendix B: Physicochemical properties of cottonseed oil

Acid value

The solution was maintained throughout the titration process until a color change to pink was observed. The acid value obtained using Eq. 3.10

Samples	Initial volume (mgKOH)	Volume of titration (mgKOH)
Sample (A)	0	0.345
Sample (B)	0	0.355
average		0.35

$$\text{Acid Value} = \frac{56.1 \times 0.1 \times 0.35}{5} = 0.3927$$

Iodine value

The endpoint of the titration was indicated by the transition of the pink color to colorless. The average iodine value obtained using Equation 3.12

sample	Initial Na_2SO_3 consumed	Final Na_2SO_3 used (mL)	V_b-V_S	Average
Sample (A)	0	23	20.6	20.175
Blank (A)	0	43.6		
Sample (B)	0	25	19.75	
Blank (B)	0	44.75		

$$\text{Iodine Value} = \frac{12.69 \times 0.1 \times (20.175)}{0.25} = 102.4$$

Saponification value

The saponification value was determined using the Eq. 3.11.

Sample	Initial amount of HCl used	Final amount HCl used (mL)	V_b-V_S	Average
Sample (A)	0	20	13.4	13.16
Blank (A)	0	33.4		
Sample (B)	0	25	12.92	
Blank (B)	0	37.9		

$$\text{Saponification Value} = \frac{56.1 \times 0.5 \times (13.16)}{2} = 184.6$$

Moisture content

The moisture content was determined using the Eq. 3.13.

Initial weight = 25 gm

Final wight = 24.9 gm

$$\text{Moisture content (\%)} = \frac{25 - 24.9}{25} \times 100\% = 0.04\%$$

Appendix C: Physicochemical properties of cottonseed biodiesel

Acid value

The solution was maintained throughout the titration process until a color change to pink was observed. The acid value obtained using Eq. 3.10

Samples	Initial volume (mgKOH)	Volume of titration (mgKOH)
Sample (A)	0	0.20
Sample (B)	0	0.19
average		0.195

$$\text{Acid Value} = \frac{56.1 \times 0.1 \times 0.195}{5} = 0.219$$

Iodine value

The endpoint of the titration was indicated by the transition of the pink color to colorless. The average iodine value obtained using Eq. 3.12

Sample	Initial Na_2SO_3 used (mL)	Final Na_2SO_3 used (mL)	V_b-V_S	average
Sample (A)	0	12	16.4	16.2
Blank (A)	0	28.4		
Sample (B)	0	35	16	
Blank (B)	0	51.4		

$$\text{Iodine Value} = \frac{12.69 \times 0.1 \times (16.2)}{0.25} = 82.23$$

Saponification value

The saponification value was determined using the Eq. 3.11.

Sample	Initial amount of HCl used (mL)	Final amount HCl used (mL)	V_b-V_S	average
Sample (A)	0	12	9.9	9.8
Blank (A)	0	21.9		
Sample (B)	0	25	9.7	
Blank (B)	0	34.7		

$$\text{Saponification Value} = \frac{56.1 \times 0.5 \times (9.7)}{2} = 137.45$$

Moisture content

The moisture content was determined using the Eq. 3.13.

Initial weight = 25 gm

Final wight = 24.9 gm

$$\text{Moisture content (\%)} = \frac{25 - 24.9}{25} \times 100\% = 0.04\%$$

Telefax 251-(0)11-551 29 38
251-(0)11-551 79 56
251-(0)11-554 19 05
Email - eth-petroleum@ethionet.et

Telephones:
P.B.X. (251) - 011-551 32 88
Direct: (251) - 011-551 00 45,
(251) - 011-552 60 30,
(251) - 011-554 19 04,
P.O.Box 3375
Addis Ababa - Ethiopia

የኢትዮጵያ ነዳጅ አቅራቢ ድርጅት
ETHIOPIAN PETROLEUM SUPPLY ENTERPRISE

Ref. No. 30601613.24/2016
ሕዳር 7 7 2016

የአዳማ ሳይንስና ቴክኖሎጂ ዩኒቨርስቲ
ለሜካኒካል፤ኬሚካል እና ማቴሪያልስ ኢንጂነሪንግ ት/ቤት
አዳማ

ጉዳዩ፡ የነዳጅ ምርመራ ውጤት ስለማሳወቅ

በህዳር 12/2016 ዓ.ም በቁጥር 7/2-1-1//7m80/38/73/16 በተጻፈ ደብዳቤ በተማሪ ነጋሳ ተስፋዬ የተዘጋጀ ሁለት (02) የባዮዲዝል እና የእሱ ድብልቅ ናሙና እንዲፈተሽላችሁ በጠየቃችሁት መሠረት የናሙናው ፍተሻ ውጤት በዚህ ሸኝ ደብዳቤ በ 01 ገጽ አባሪ በማድረግ የላክን መሆኑን በአክብሮት እንገልፃለን።

ከሠላምታ ጋር

ሰዩም አራጋው
የነዳጅ ጥራት ማረጋገጫ
አገልግሎት ኃላፊ

Company Name:		Document No: OF/EPSE/QAS/033	
	ETHIOPIAN PETROLEUM SUPPLY ENTERPRISE QUALITY ASSURANCE SERVICE	Page 1 of 1	

TITLE: CERTIFICATE OF TEST REPORT

Issue No.: 2	Date of Issue: August,2020
Prepared by: QT	Approved by: Tadesse H/Mariam

Sample Originator: ADAMA SCIENCE &TECHNOLOGY UNIVERSITY	**Request No:**7/2-1-1/7mgo/38/73/16
Sample Type: Bio-Diesel & its blends	**Analytical Method:** ASTM /IP/ISO.
Sample Number: 02	**Analytical Result:** Interpreted with stds.
Lab. Number: 2023- ADO-EXT-38	**Report No:** QA/0042/2023
Sample Submitted By: CUSTOMER	**Test date:** 02/12/2023
Date Submitted: 27/11/2023	**Issued Date:** 07/12/2023
Customer Address: ADAMA	**Telephone.** 0910-071529

S.N	Property	Test method ASTM	Limits	Test results of the sample		
				B100	B20	MU
1	Density@15°C, g/mL	D4052	Report	0.8837	0.8440	0.0003
	Density@20°C, g/mL	D4052	Report	0.8804	0.8405	0.0003
2	Kinematic viscosity @ 40 °c, mm^2/sec	D 445		4.4174	3.4731	0.0082
3	Calorific value, calc, BTU/LB	Calculated		19,216.70	19,574.0	

Liability:- Ethiopian Petroleum supply Enterprise, its Laboratory, its Servants or agents Shall not be held liable for any damages, loss, claims or expenses direct or indirect howsoever caused, arising in connection with the laboratory test carried out on **BIO-DIESEL**, sample submitted to it for analysis whether in tort or in contract, due to any act, omission or error of whatever nature, whether or not negligence and howsoever caused. Furthermore all expenses and implied warranties are specifically disclaimed. This test report shall not be reproduced or given to a third party without written approval of the **Petroleum Quality Assurance Service**.

Lab. Expert
Name- Thusla suet Barese
Signature-

Senior expert
Name-
Signature-

Quality Control Head
Name-
Signature-

Ethiopian Petroleum Supply Enterprise 1955 1966

PLEAS MAKE SURE THAT THIS IS THE CORRECT ISSUE BEFORE USE

Appendix D: Specifications of 100% Gasoline and Gasoil

Gasoline

S/N	Parameter	Test method	LIMITS (MAX/MIN)
1.	Density @15^{O}C	D 4052/1298	0.720-0.740
2.	10% volume recovered, ^{O}C	D 86	Max. 74
3.	50% volume recovered, ^{O}C	D 86	80-127
4.	90% volume recovered, ^{O}C	D 86	Max 190
5.	FBP, ^{O}C	D 86	Max 225
6.	Residue	D 86	Max 2
7.	Research octane number(RON)	D 2699	Min 92
8.	Total sulfur, %wt	D 4294	Max 0.001
9.	Reid vapor pressure, kPa	D 323	41-65
10.	Existence gum, mg/100ml	D 381	Max 4
11.	Copper strip corrosion 3 hrs @50 ^{O}C	D 130	Max no 1
12.	Doctor test	IP 30	Negative
13.	Lead content, g/l	IP 352	Max 0.013

Seyoum Aragaw
Petroleum Quality Assurance
Service Head

Gasoil

S/N	PARAMETER	TEST METHOD	LIMITS (MAX/MIN)
1.	Density @15^{O}C	D 4052/1298	0.820-0.860
2.	90% volume recovered, ^{O}C	D 86	Max. 362
3.	FBP, ^{O}C	D 86	Max 390
4.	Color	D 1500	Max 2
5.	Total sulfur, %wt	D 4294	Max 0.05
6.	Flash point, PMCC, ^{O}C	D 93	Min. 66
7.	Kinematic viscosity @ 40 ^{O}c	D 445	2.0-4.5
8.	Cloud point, ^{O}C	D 2500	Max +5
9.	Cetane index	D 976	Min 48
10.	Copper strip corrosion 3 hrs @100 ^{O}C	D 130	Max No. 1
11.	CCR ,%Wt	D 189	Max 0.2
12.	Ash , %Wt	D 482	Max 0.01
13.	Water and sediment, V/V %	D 2709	Max 0.05

Seyoum Aragaw
Petroleum Quality Assurance
Service Head

Appendix E: Engine setup Port injection system setup

Engine setup

Port injection system setup

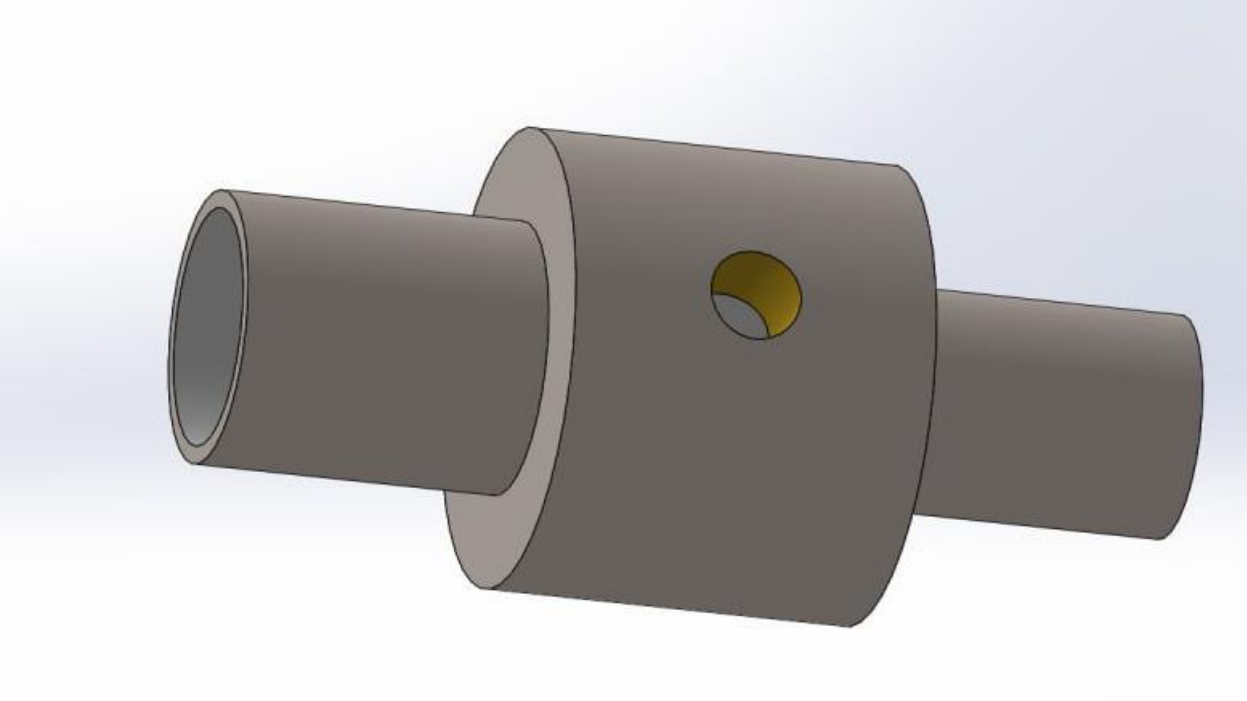

Injector mounting sleeve

Appendix F: Originality Declaration Form for Students

This form must be completed and signed for all works submitted to the University for Examination.

Name of student	Negasa Tesfaye Tefera
Id. No.	PGR/24596/14
Department	Mechanical engineering
College	Mechanical, Chemical, and Material Engineering
Course Title	Dissertation paper
Title of work / Assignment name	Effects of Gasoline-n-Butanol blend as Low Reactivity Fuel and Biodiesel-Diesel Blend as High Reactivity Fuel on the Performance and Emission Characteristics of RCCI Engine

DECLARATION

1. I understand what plagiarism is and I am aware of the university's policy in this regard.
2. I declare that this dissertation entitled **"Effects of Gasoline-n-Butanol blend as Low Reactivity Fuel and Biodiesel-Diesel Blend as High Reactivity Fuel on the Performance and Emission Characteristics of RCCI Engine"** research project is my original work and has not been submitted elsewhere for examination or award of a degree or publication. Wherever others' work or my own work has been utilized, it has been duly acknowledged and referenced in compliance with the university's requirements.
3. I have not sought or used the services of any professional agencies to produce this work.
4. I have not permitted, nor will I permit, anyone to plagiarize my work with the intention of presenting it as their own.
5. I am aware that making any false claims regarding this work will lead to disciplinary action in accordance with the university's Anti-Plagiarism Guidelines.

Signature _____

Date _____

24% Overall Similarity

The combined total of all matches, including overlapping sources, for each database.

Filtered from the Report

- Bibliography

Match Groups

- 731 Not Cited or Quoted 22%
  Matches with neither in-text citation nor quotation marks
- 89 Missing Quotations 2%
  Matches that are still very similar to source material
- 10 Missing Citation 0%
  Matches that have quotation marks, but no in-text citation
- 0 Cited and Quoted 0%
  Matches with in-text citation present, but no quotation marks

Top Sources

11% Internet sources
20% Publications
6% Submitted works (Student Papers)

Integrity Flags

0 Integrity Flags for Review

No suspicious text manipulations found.

Our system's algorithms look deeply at a document for any inconsistencies that would set it apart from a normal submission. If we notice something strange, we flag it for you to review.

A Flag is not necessarily an indicator of a problem. However, we'd recommend you focus your attention there for further review.